

Insights into the microbial reduction of pentavalent
and hexavalent uranium species by *Shewanella*
oneidensis MR-1

Présentée le 26 novembre 2021

Faculté de l'environnement naturel, architectural et construit
Laboratoire de microbiologie environnementale
Programme doctoral en génie civil et environnement

pour l'obtention du grade de Docteur ès Sciences

par

Margaux Camille Andréa MOLINAS

Acceptée sur proposition du jury

Prof. F. Golay, président du jury
Prof. R. Bernier-Latmani, directrice de thèse
Dr A. Plymale, rapporteur
Dr M. Edwards, rapporteur
Prof. A. Boghossian, rapporteuse

Acknowledgements

First of all, I would like to gratefully thank my committee members Ardemis Boghossian, Marcus Edwards and Andrew Plymale for accepting to review this thesis work.

Then I would like to thank Rizlan, my supervisor, who entrusted me this amazing thesis project. Rizlan, it was such an honor to collaborate with the admirable scientist that you are. For you, a problem always has a solution, you know how to turn things around to bring light on them. I found in you a rational, logical, steady, and brilliant mind. I am thankful that you encouraged me to push my limits over the past years. You have guided me on this rocky road, and you have taught me how to play science, how to enjoy small victories, how to apprehend tough questioning times. You are one of the persons who have contributed to who I am today. Merci Rizlan.

I would like to warmly thank my close collaborator Ash. Ash, it has been such a pleasure to work in your company and this work would not have been possible without your benevolent and strong support. I found in you the mentor to whom I could refer for any types of problems or questions. I truly benefited from your scientific experience, your sharp mind, and your rigor. I could not have dreamt best teammate for these U projects.

I would like also to affectionately thank Zezhen, my former labmate. I truly enjoyed having you around and sharing time with you, in the office, in the lab or elsewhere. You always had the words to sooth me in stressful times. Funny fact, you are the person with whom I have traveled the most during my PhD, namely to synchrotrons. I have wonderful memories of the times we spent together here in Lausanne or around Europe. We have built a sincere friendship, and I miss you a lot since you returned to China. I promise, I will come and visit you in China!

Also, this journey would not have been possible without the wonderful EML team! Thank you, Luca, for introducing me to Uranium and *Shewanella*! Thank you, Gabrielle, for having been such a cool and supportive officemate, still owe you a visit in Norway! Thank you, Karin, for your support and your help with the molecular biology! Merci Manon pour tous les chouettes moments de rire, pour ton énergie, de m'avoir fait découvrir le terrain, et de m'avoir aidé à surmonter ma frousse pour les araignées ! Barbora, merci pour ton aide sur la microscopie électronique ! Maria, merci pour toutes ces discussions relaxantes au détour de ton bureau ! Solenne, c'était génial de partager ces quelques années avec toi, et de déguster ces instants volés au labo ! Karen, gracias por tu escucha, tus consejos, el compartir, eres una hermosa persona y yo aprendí mucho sobre la vida gracias a ti ! Niels, thanks for cheering me up, making me laugh, sharing your inexhaustible good vibe! Tania, merci infiniment pour ton soutien, ta bienveillance, et ton délicieux soupçon d'extravagance! Edu, gràcies per la teva amistat, per escoltar-me i donar-me suport quan estava confós, gràcies pels bons moments d'escalada! Enfin, Colin, merci d'être un si chouette ami, merci de ton attention, ta présence et ton soutien, et surtout ces petits cafés au soleil...

I would like to thanks our collaborators, Marinella and Radmila! I am grateful for all the fruitful discussions that we had and for your scientific support on this project. Radmila, you were an awesome collaborator, I would not have gone that far without your precious help with some U(V) synthesis! Also, you are a beautiful person, and I hope we will have time to develop our friendship while you are around in Lausanne!

Many thanks also to the people from the CH C2 corridor, Lorenzo, Arnaud, Natalia, Tobias and Adrian. Always a pleasure to chat, have coffee, or aperos on Fridays! Merci Adrian, tu as été d'un grand soutien, j'ai adoré pouvoir prendre le temps de discuter maintes fois autour d'un café ou d'un déjeuner, des conversations sans fin mais toujours re motivantes et pleines de bienveillance ! On s'est vraiment tenu les coudes pour avancer dans nos doctorats respectifs !

I also met some fantastic people in Lausanne, and I would like to particularly thank Guillaume, Raphaël, Olivier, Antonin et Lucile.

Guillaume, on s'est suivi à Lausanne après avoir été à Chimie Paris ensemble. Toujours cool de se retrouver pour refaire le monde au détour d'un dîner, d'une soirée, et même pour aller grimper ces derniers temps ! Merci d'avoir été présent, je sais que je peux compter sur toi !

Raphaël, je suis ravie d'avoir fait ta connaissance, et te t'avoir pour ami ici. Tu as une énergie débordante, et c'est contagieux ! Merci de ta confiance, et merci de m'avoir tant écoutée : C'est toujours un plaisir de te retrouver ! A bientôt à Sisteron !

Oliver, je suis très heureuse d'avoir fait la connaissance d'une personne aussi riche que toi, j'adore ton esprit, tu me fais tellement rire ! Merci d'avoir été mon compagnon de bicyclette et de me faire reprendre goût au cyclisme, merci pour ces dîners et soirées au top, et merci de m'avoir communiqué ton enthousiasme et ton énergie ! À jamais ta DJ Margus !

Antonin, tu m'as récupérée en vrac, et tu m'as complètement remise sur pieds. Je t'en suis sincèrement reconnaissante. Aussi, tu es selon moi une personne incroyable, et ce que j'aime chez toi, c'est que tu aimes les gens, tu es fédérateur, généreux, vitalisant. Grâce à toi, j'ai pu aussi réfléchir profondément sur ce à quoi j'aspire, et quels chemins suivre ! Je sais que je peux compter sur toi.

Lucile, ma partenaire en crime pour la danse classique ! J'ai beaucoup aimé apprendre à te connaître et je suis toujours impatiente de te retrouver pour aller danser ! Tu m'as beaucoup touchée car tu es une belle personne, profonde et brillante. J'aime les détours de nos conversations, je les trouve toujours riches et instructives !

Un immense merci aux personnes qui ont partagé avec moi la collocation du 4 allée du Tilleul, Tao, Guillaume, Cyprien, Irène et Matteo. Matteo, incontra magnifico, sei molto stimolante, di una lucidità e intelligenza eccezionali. Puro piacere di interagire con te! È stato davvero divertente passare qualche mese rinchiuso con te durante la crisi del Covid, tra passeggiate, escursioni, cucina, canti, film que fanno ridere, conversazioni appassionate . E grazie per avermi fatto conoscere l'arrampicata! Puro piacere di interagire con te!

Tous les lundis et jeudis, sans faute, je rejoignais l'école de danse Igokat. J'y ai trouvé un environnement bienveillant et ressourçant. Un immense merci à toutes les danseuses et danseurs que je côtoie hebdomadairement, Dominique, Francesca, Claudine, Andréa, Sean et Lucile bien entendu. Merci à Laura et Marie-Hélène, pour tous ces cours plus entraînants les uns que les autres. Et surtout, Julie, tu m'as aidée à relâcher la pression tous les lundis soir avec tes exercices

de souplesses à ne plus pouvoir monter un escalier le lendemain, merci de ton écoute et ton soutien, ta présence est toujours réconfortante (même en position petite sirène sur le côté, retiré, développé).

Pierre, merci d'avoir été là pour moi, je te suis sincèrement reconnaissante.

Merci à ceux qui m'ont soutenu de loin, mais qui ont toujours été présents. Les filles Buli, Victoire, Laure et Maud, les retrouvailles à Paris, vos visites à Lausanne, les vacances en Indonésie, tant de moments qui m'ont aidés à me reconnecter et à me détendre. Merci pour ces belles et longues amitiés ! Alexandra, Quentin et Clément, je sais que je peux compter sur vous, même à distance, merci de votre soutien !

Ma chère Hélène, quelle rencontre hors norme ! Je n'oublierai jamais ces premiers cours de stretching où nous nous étirions mutuellement. Jamais à cet instant je n'aurais imaginé que nous allions vivre tant de moments ensemble. Tu es une personne magnifique et ta beauté a littéralement rayonné sur moi pendant ces quatre dernières années. Nous avons construit une belle amitié, une relation chaleureuse, ta bienveillance m'apaise. Tu as toujours été présente pour moi, et tu m'as soutenue à travers les moments d'allégresse aussi bien que lorsqu'un ciel nuageux épais engourdissait mon esprit. Chaque rendez-vous est un délice, et j'espère qu'il y en aura encore, encore et encore ! Merci du fond du cœur d'être ce que tu es et me permettre d'être ce que je suis.

Pierre, je te suis infiniment reconnaissante de m'avoir fait vibrer cette dernière année, qui n'avait rien d'une sinécure. Tu as intensifié les couleurs de mes journées, surligné les contours de mon âme, réhaussé les tons de ma personnalité et tu m'as aidée à préserver cette étincelle qui chaque jour me faisait faire quelques pas de plus vers le but. Nous avons partagé des moments de vie poignants, beaux, vrais et si humains, je les ai gravés. D'un côté plus pratique, grâce à toi j'ai maintenu un taux de globules rouges irréprochable pendant cette fin de thèse. La recette est simple, aller chatouiller les flans des montagnes gonflés d'eau cristalline tout l'hiver durant, et s'évader, en se promenant au détour des cimes de mes trois premiers 4000m alpins. Que de joie, de sérénité et d'émotions... Merci de ton soutien.

Mon Rom, je sais que tu es toujours là, je sais que je peux compter sur toi, merci pour cette forte présence. Je sais que peu importe ce que je traverse, ta porte est grande ouverte, je peux me glisser dans cet espace que nous avons entretenu depuis toutes ces années, et t'y retrouver pour partager avec toi des fragments de vie. Tu as été, et tu es pour moi un pilier. Tu as su me soutenir justement, grâce à ta sensibilité, ton écoute attentive, ton souci de mon bien-être. Tu tiens une place toute unique dans mon cœur et je suis fière d'avoir un frère comme toi.

Maman, Papa, vous m'avez transmis les outils nécessaires pour être libre de choisir, et j'ai choisi de cheminer ici à Lausanne pendant ces dernières années. Je suis si heureuse d'avoir pu faire ce choix. Il est impossible de résumer en quelques lignes combien je vous suis reconnaissante. Et votre soutien infaillible, votre patience sans borne pour démêler avec bienveillance aussi bien les nœuds professionnels que personnels. Toujours à l'écoute, toujours volontaires pour comprendre, même si ma science devait vous paraître être une jolie boîte noire. Maman, ton énergie, ta détermination, ta persévérance et ton enthousiasme m'ont toujours impressionnée, tu pétilles. Papa, ta force tranquille, ton optimisme intarissable, ton rire communicatif qui me fait toujours sourire jusqu'aux oreilles... j'aimerais avoir les épaules aussi solides que toi. Je me dis que vous avez aussi dû faire une thèse, tant vous m'avez accompagnée, merci !

Mamy, Papy, je vous dois tout. Vous m'avez tant appris, et je ne parle pas que de récolter les fruits, arracher les pommes de terre et les oignons, cueillir les asperges, tailler la vigne, planter des haricots, faire des poires au sirop, et rabattre des rideaux. Vous m'avez donné des valeurs et des vertus qui m'aident à avancer chaque jour. Je vous regarde émerveillée, je pense à vous, et vous me donnez de la force. J'ai toujours admiré votre assiduité au travail, votre rigueur, la façon dont vous mettez du cœur dans tout ce que vous entreprenez, votre dynamisme fougueux, vos valeurs de vie, votre grande générosité. Infiniment, merci, je vous dédie ce travail de thèse en reconnaissance.

« La vérité
n'est que la rectification d'une longue suite d'erreurs. »

Gaston Bachelard

« Pour l'instant, vivez les questions.
Peut-être un jour lointain,
entrerez-vous aussi,
peu à peu,
sans l'avoir remarqué
à l'intérieur de la réponse. »

Rainer Maria Rilke

« Q'une chose soit difficile
doit nous être une raison de plus pour l'entreprendre. »

Rainer Maria Rilke

À Marie et Daniel, mes grands-parents,
À Bruno, mon père.

Abstract

Decades of uranium-related activities such as ore mining, nuclear power generation, weapon manufacture, storage of nuclear wastes, have contributed to the release of U in the environment. U occurrence is concerning, since in surface environments, U is typically found in the U(VI) oxidation state, as uranyl, complexed with various ligands, and is highly soluble. Therefore, this toxic metal is likely to leech into soils and contaminate surface waters and groundwaters. In addition, owing to the long half-lives of the predominant isotopes ^{238}U and ^{235}U , U is considered as a persistent contaminant over geological timescales. For several decades, efforts have focused on the development of *in situ* remediation solutions to tackle U pollution in the subsurface, and limit its mobility.

With this aim, interest in the metabolic potential for U(VI)-respiration by dissimilatory metal-reducing bacteria (DMRB), such as *Shewanella oneidensis* MR-1, has seen a significant increase. This metabolically-versatile bacterium has been reported to reduce mobile U(VI) to typically insoluble crystalline and amorphous U(IV). The reduction of U(VI) in *S. oneidensis* MR-1 is coupled to the oxidation of an electron donor, which feeds electrons into an electron transport chain, extending from the cytoplasm to the outer-membrane of the cells.

The microbially mediated reduction of U(VI) to U(IV) is the result of a two-step process. It is assumed that one electron is first transferred to U(VI) to form a pentavalent U(V) intermediate, followed by the abiotic disproportionation of two U(V) atoms into U(IV) and U(VI). However, evidence for this mechanism is limited to experimental systems rich in carbonate, which permits the rapid disproportionation of U(V). Thus, it remains unclear whether a second, biologically-mediated, electron transfer to U(V) is possible under conditions in which disproportionation is limited. To explore this, a novel U(V)-dpaea complex, that is stable in water at pH 7, was utilized to investigate the second step of the reduction mechanism. Here, we observed that U(V) can be biologically reduced by an additional one-electron transfer, resulting in the accumulation of U(IV) without the need for disproportionation.

To improve our understanding of the molecular mechanism of U-dpaea reduction, we incubated mutant strains of *S. oneidensis* MR-1, lacking (i) only outer-membrane c-type cytochromes or (ii) all c-type cytochromes, with solid phase U(VI)-dpaea and aqueous U(V)-dpaea. We determined that U(VI)-dpaea reduction proceeds via the initial dissolution of the solid phase and that U(V)-dpaea reduction is mediated by outer-membrane c-type cytochromes. In particular, *in vitro* reactions between the purified outer-membrane c-type cytochrome MtrC and U(V)-dpaea demonstrated that MtrC can directly transfer electrons to U(V)-dpaea.

Finally, we sought to determine the factors that influence electron transfer kinetics between DMRB and U. To this end, we reacted U(VI) coordinated by various aminocarboxylate ligands with purified MtrC. Here, U speciation significantly impacted reduction rates and appeared to be related to the binding strength of the U-MtrC interaction, i.e., hydrogen bonding versus electrostatic.

All together, these findings provide further insights in the reduction mechanism of U by DMRB, and underline the importance of U speciation in controlling the pathway and rate of electron transfer.

Keywords

Pentavalent U(V), electron transfer, uranium reduction, disproportionation, *Shewanella oneidensis* MR-1, *c*-type cytochromes, MtrC, M₄-edge HR XANES, bioremediation.

Résumé

Au cours du siècle passé, les activités industrielles liées à l'Uranium telles que l'extraction minière, la mise au point d'armes atomiques, la production d'énergie nucléaire, ainsi que le stockage des déchets radioactifs, ont contribué à la contamination de l'environnement. La présence d'U dans les environnements surfaciques est préoccupante puisqu'il s'y trouve principalement sous la forme d'uranyle(VI), complexé à une variété de ligands, remarquablement soluble dans l'eau. Par conséquent, ce métal toxique peut aisément s'infiltrer dans les sols et contaminer les eaux de surface et les eaux souterraines. Par ailleurs, les deux isotopes naturels de l'uranium ^{238}U et ^{235}U , en raison de leurs longues demi-vies, font de cet élément un contaminant persistant à l'échelle des temps géologiques. Ainsi, au cours des dernières décennies, de nombreux travaux scientifiques ont porté sur l'étude et le développement de méthodes de remédiation *in situ*, afin de pallier la contamination du sous-sol en U, et également de limiter sa mobilité.

Dans ce cadre, un grand intérêt s'est porté sur le potentiel métabolique pour la respiration d'U(VI) des bactéries réductrices de métaux (DMRB), comme par exemple *Shewanella oneidensis* MR-1. Ce microorganisme au métabolisme versatile, peut réduire l'U(VI) mobile en une phase généralement insoluble d'U(IV), cristalline ou amorphe. La réduction de l'U(VI) par *S. oneidensis* MR-1 est couplée à l'oxydation d'un donneur d'électron. Les électrons ainsi générés circulent du cytoplasme à la membrane externe, via une chaîne de transport d'électrons constituées de cytochromes de type *c*.

Le transfert de deux électrons de la bactérie à l'U(VI) se produit en deux étapes. Il est supposé qu'un premier électron soit transféré à l'U(VI) pour former l'intermédiaire pentavalent, U(V), puis que deux atomes d'U(V) dismutent abiotiquement en U(VI) et U(IV). Cependant, ce mécanisme a été décrit expérimentalement dans des milieux riches en carbonates qui favorisent la dismutation spontanée de l'U(V). Ainsi, un second transfert d'électron biologique à l'U(V) serait envisageable dans des conditions limitant la dismutation. Afin de vérifier cette possibilité, un complexe d'uranyle(V) récemment synthétisé, l'U(V)-dpaea, stable dans l'eau à pH 7, a été utilisé pour explorer la deuxième étape du mécanisme de réduction. Nous avons ainsi établi que dans des conditions adéquates, l'U(V)-dpaea peut être biologiquement réduit par le transfert d'un électron supplémentaire, et qu'il ne dismute pas.

Afin de mieux appréhender le mécanisme de réduction de l'U-dpaea, nous avons incubé des souches mutantes de *S. oneidensis* MR-1, destituées (i) seulement des cytochromes de type *c* situés sur la membrane externe, ou (ii) de tous les cytochromes de type *c*, avec de l'U(VI)-dpaea solide et de l'U(V)-dpaea. Nous avons déterminé que la réduction de l'U(VI)-dpaea se produit via dissolution du solide, et que l'U(V)-dpaea est réduit par les cytochromes de type *c* de la membrane externe. Notamment, *in vitro*, la réaction du cytochrome de type *c* MtrC de la membrane externe avec de l'U(V)-dpaea, a prouvé que MtrC peut directement transférer des électrons à l'U(V)-dpaea.

Enfin, nous avons cherché à déterminer quels facteurs influencent la cinétique de transfert d'électrons entre l'U et les DMRB. Nous avons donc fait réagir différents complexes d'U aminocarboxylate en présence de MtrC. Nous avons

notamment observé que la nature du complexe d'U impacte la cinétique de réaction, et que le type d'interaction entre le complexe d'U et MtrC, de nature électrostatique ou via des liaisons hydrogènes, pourrait en être l'origine.

Pris ensemble, ces résultats apportent un nouvel aperçu du mécanisme de réduction de l'U par les DMRB. Ils soulignent que le mécanisme et la cinétique de transfert d'électron sont particulièrement sensibles à la nature des complexes d'U considérés.

Mots-clés

Uranium(V) pentavalent, transfert d'électrons, dismutation, *Shewanella oneidensis* MR-1, cytochromes *c*, MtrC, M₄-edge HR XANES, biorémediation.

Contents

Acknowledgements	vi
Abstract	xii
Keywords.....	xiii
Résumé	xiv
Mots-clés.....	xv
List of Figures.....	xix
List of Tables.....	21
Chapter 1 Introduction	23
1.1 Uranium: history, chemical and physical properties, and environmental behavior	23
1.1.1 Uranium history	23
1.1.2 Physicochemical properties of the metal U	24
1.1.3 Uranium in the environment.....	26
1.1.4 Pentavalent U(V)	26
1.2 Biologically mediated redox reactions of uranium in the environment	29
1.2.1 Biotransformation of uranium	29
1.2.2 Bioreduction of uranium	29
1.2.3 Reduction mechanism of U(VI): the pentavalent U(V) intermediate	31
1.2.4 Bioremediation.....	34
1.3 Electron transfer mechanism in <i>Shewanella oneidensis</i> MR-1	35
1.3.1 The versatile microorganism <i>S. oneidensis</i> MR-1	35
1.3.2 Electron transfer from the cytoplasm to the outer-membrane	36
1.4 Mechanism of electron transfer to electron acceptors in <i>S. oneidensis</i> MR-1	38
1.4.1 Direct or indirect transfer.....	38
1.4.2 Reduction of U by <i>c</i> -type cytochromes	39
1.4.3 Substrate-binding sites in <i>c</i> -type cytochromes from metal-reducing bacteria	40
1.5 Objectives of the thesis	41
1.5.1 Chapter 2: Biological reduction of a U(V)-organic ligand complex.....	42
1.5.2 Chapter 3: Role of <i>c</i> -type cytochromes in the reduction of U(VI)-dpaea and U(V)-dpaea complexes	42
1.5.3 Chapter 4: Speciation-dependent electron transfer from the <i>c</i> -type cytochrome MtrC to U(VI)-ligand complexes	42

1.6	References	23
Chapter 2	Biological reduction of a U(V)-organic ligand complex	53
	Abstract	54
2.1	Introduction	54
2.2	Experimental methods	56
2.2.1	Construction of the <i>ccmG</i> deletion mutant	56
2.2.2	Strain growth and conditions	56
2.2.3	Resting cell experiments	56
2.2.4	Ion-exchange chromatography	57
2.2.5	Uranium quantification	58
2.2.6	HR-XANES	58
2.2.7	Electron microscopy	58
2.3	Results	59
2.3.1	Reduction of U(VI)-dpaea	59
2.3.2	Reduction of U(V)-dpaea	63
2.4	Discussion	68
2.4.1	Mechanism of U(VI)-dpaea reduction	68
2.4.2	Thermodynamic considerations	68
2.4.3	Environmental relevance	69
2.5	Conclusion	70
2.6	References	71
Chapter 3	Mechanism of reduction of solid-phase U(VI)-dpaea and aqueous U(V)-dpaea complexes	75
	Abstract	76
3.1	Introduction	76
3.2	Experimental methods	78
3.2.1	Description of the <i>mtrC/omcA/mtrF</i> deletion mutant	78
3.2.2	Strains and growth conditions	78
3.2.3	Preparation of ferrihydrite and Fe(III)-citrate	78
3.2.4	Reduction experiments with ferrihydrite and Fe(III)-citrate	78
3.2.5	Reduction of U(VI)-dpaea	79
3.2.6	MtrC purification	79
3.2.7	Reduction of MtrC	79
3.2.8	Dialysis	80
3.2.9	Reaction of MtrC with U(V)-dpaea or U(IV)-citrate	80
3.3	Results	81
3.3.1	Mutant strains characterization with ferrihydrite and Fe(III)-citrate	81
3.3.2	Reduction of solid phase U(VI)-dpaea proceeds via dissolution followed by reduction	82

3.3.3	Role of <i>c</i> -type cytochromes in U(V)-dpaea reduction	84
3.4	Conclusion	91
3.5	References	93
Chapter 4	Speciation-dependent electron transfer from the <i>c</i>-type cytochrome MtrC to U(VI)-ligand complexes.....	97
	Abstract	98
4.1	Introduction	98
4.2	Experimental methods	100
4.2.1	MtrC purification and reduction	100
4.2.2	Preparation of the stock solutions	100
4.2.3	Kinetics of reaction.....	100
4.2.4	Binding tests.....	101
4.2.5	Uranium quantification	102
4.2.6	M ₄ -edge HR-XANES on U(VI)-carbonate reacted with reduced MtrC	102
4.3	Results	103
4.3.1	Kinetics of reduction	103
4.3.2	Binding of U complexed with NTA, EDTA, DTPA or carbonate to MtrC.....	109
4.3.3	Speciation of U during reaction of U(VI)-carbonate with reduced MtrC.....	112
4.4	Discussion	115
4.4.1	There is no obvious correlation between U-complex stability and reaction rate.	115
4.4.2	Interaction between MtrC and the soluble U substrates	116
4.5	Conclusion	117
4.6	Limits of the experimental study and outlooks	118
4.7	References	119
Chapter 5	Conclusion	124
5.1	Achieved results	124
5.2	Future development.....	126
Annexes.....	129
	Annex 1 – Supplementary information for chapter 2	130
	Annex 2 – Supplementary information for chapter 3	153
	Annex 3 – Supplementary information for chapter 4	155
Curriculum Vitae.....	157

List of Figures

Figure 1:1. Discovery of radioactivity.....	23
Figure 1:2. Fission and transmutation of U.....	25
Figure 1:3. U(V) structures.	27
Figure 1:4. First stable uranyl(V) complexes.	28
Figure 1:5. Cation-cation interaction between two uranyl(V) nuclei.....	28
Figure 1:6. U reduction product nature and localization.	30
Figure 1:7. Evidence of U(V) with various bacterial species.....	32
Figure 1:8. Mechanism of U(VI) reduction modeled by DFT calculations.	33
Figure 1:9. <i>S. oneidensis</i> MR-1 anaerobic metabolism.	35
Figure 1:10. Electron transfer chain in <i>S. oneidensis</i> MR-1 with U(VI) as the electron acceptor.	37
Figure 1:11. MtrC structure.	38
Figure 1:12. Proposed types of interaction between c-type cytochromes from DMRB bacteria.	41
Figure 2:1. Incubation of MR-1 cells with U(VI)-dpaea.	59
Figure 2:2. U M ₄ -edge HR-XANES spectra demonstrating reduction of (A) U(VI)-dpaea and (B) biologically-produced U(V)-dpaea	61
Figure 2:3. LCF fitting results (red) compared to the data (black) for the M ₄ -edge HERFD-XANES spectra obtained for supernatants from the reduction of U(VI)-dpaea A. 72h, B. 96h and a spectrum obtained for the solid phase C. at 150h. Panel D represents a spectrum obtained at 85h for the solid phase during the reduction of U(V)-dpaea.....	62
Figure 2:4. Aqueous and solid phase U concentration through time in incubations with <i>S. oneidensis</i> MR-1 and no-cell controls with (A) biologically-produced U(V)-dpaea (B) synthetic U(V)-dpaea.....	64
Figure 2:5. U oxidation state in the solid phase (cell pellet) and in the aqueous phase (supernatant) of (A) incubations with <i>S. oneidensis</i> MR-1 (B) and no-cell controls, in presence of 'biological' U(V)-dpaea.....	64
Figure 2:6. STEM images acquired on <i>S. oneidensis</i> MR-1 incubated with U(V)-dpaea for 3 months.	65
Figure 2:7. Aqueous U(V)-dpaea concentration (A) and cell viability (B) through time in incubations with <i>S. oneidensis</i> MR-1, the deletion mutant $\Delta ccmG$ and a no-cell control.	67
Figure 2:8. Reduction of solid phase U(VI)-dpaea (in red). U(VI)-dpaea is reduced to soluble U(V)-dpaea (in pink) by a one-electron transfer.	70
Figure 3:1. SDS-PAGE of purified recombinant MtrC isolated from $\Delta omcA$ strain LS331 of <i>S. oneidensis</i> MR-1.	80
Figure 3:2. Characterization of <i>S. oneidensis</i> mutant strains with Fe(III) substrates.	81
Figure 3:3. Incubation of MR-1, ΔOMC and $\Delta ccmG$ with U(VI)-dpaea.	83
Figure 3:4. Incubation of MR-1, ΔOMC and $\Delta ccmG$ with U(V)-dpaea.....	85
Figure 3:5. MtrC reacted with U(V)-dpaea.....	86
Figure 3:6. Timeline of the reaction between MtrC and U(V)-dpaea. Percentage of U(IV) obtained by ion exchange chromatography of the reaction between U(V)-dpaea and either oxidized (blue) or reduced (green) MtrC after 20s, 2h and 4h of reaction.....	87
Figure 3:7. MtrC reacted with U(IV)-citrate.	89

Figure 3:8. MtrC reacted with U(VI)-dpaea.....	90
Figure 3:9. Schematic representation of the evidenced mechanisms taking place in <i>S. oneidensis</i> MR-1 when incubated with solid phase U(VI)-dpaea (red) and aqueous U(V)-dpaea (pink).	92
Figure 4:1. Molecular structures of protonated aminocarboxylate ligands NTA, EDTA, and DTPA ...	104
Figure 4:2. Kinetics of reaction between MtrC and the U-ligands complexes.	106
Figure 4:3. Incubations of strain MR-1 cells with the U-ligand complexes.	108
Figure 4:4. Kinetics of reaction between strain MR-1 cells and the U-ligands complexes.....	109
Figure 4:5. Oxic binding tests. Distribution of U in the fractions recovered from 40kDa size-exclusion columns in the absence of protein or after reaction with oxidized MtrC.	110
Figure 4:6. Anoxic binding tests. Distribution of U in the fractions recovered from 40kDa size-exclusion columns under anoxic conditions.	112
Figure 4:7. U M ₄ -edge HR-XANES spectra of a time course reduction experiment between U(VI)-carbonate and reduced MtrC from 30s to 20min.	113
Figure 4:8. LCF fitting results (red) compared to the data (black) for the M4-edge HERFD-XANES spectra measured on the reaction mixture of U(VI)-carbonate and MtrC	114
Figure 4:9. Structure of some U(VI)-aminocarboxylate ligand complexes.....	115
Figure 4:10. Schematic representation of the factors which could influentiate electron transfer rate from MtrC to U(VI)-ligand complexes.....	118

List of Tables

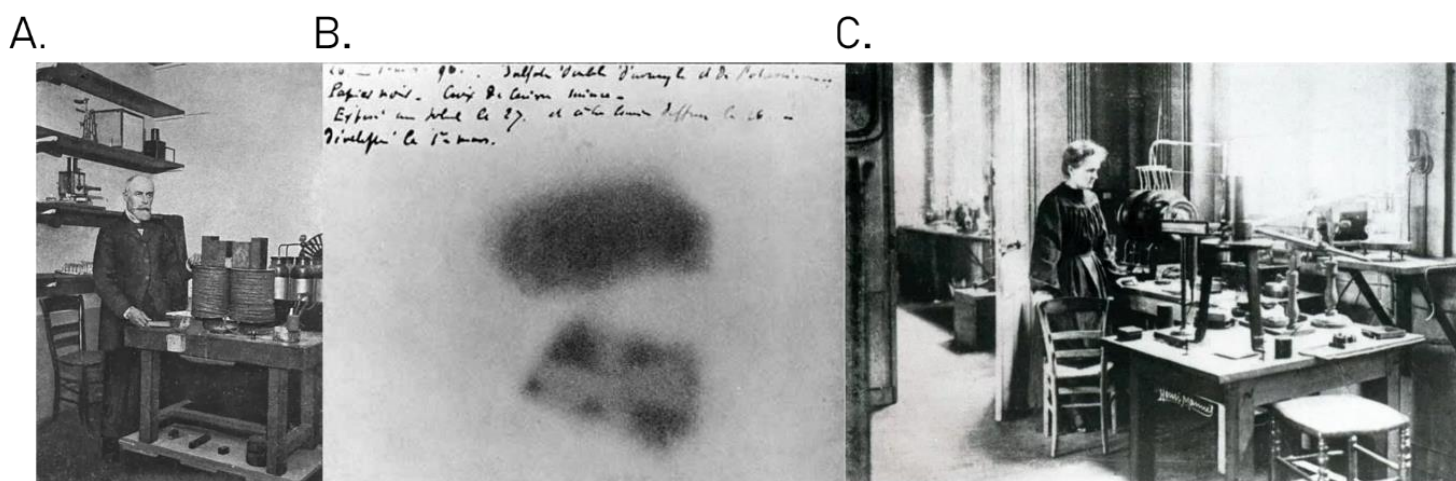
Table 2:1. U M_4 -edge main spectral features.	61
Table 2:2. LCF of the M_4 -edge HR-XANES spectra for samples described in Figure 2:2 and Figure S5 the text with the references U(VI)-dpaea, U(V)-dpaea, U(IV)-dpaea ₂	63
Table 3:1. Summary of the experimental results describing the reactions of U(V)-dpaea with either oxidized or reduced MtrC after 2 min.	87
Table 3:2. Summary of the experimental results describing the reactions of U(V)-dpaea with either oxidized or reduced MtrC over 4h..	88
Table 4:1. Average concentrations in U and MtrC, and their ratio for duplicate reactions between MtrC and U-ligand (ligand = NTA, EDTA, DTPA, carbonate) under oxic (MtrC oxidized) and reduced (MtrC reduced) conditions.	104
Table 4:2. U speciation calculated using Mineql for U(VI)-ligand complexes at pH 7.5, with 50mM NaCl, and 100mM HEPES.	104
Table 4:3. LogK of aqueous complexes of interest.	105
Table 4:4. Second-order rates for the kinetics of reactions between the U-ligand complex (ligand = NTA, EDTA, DTPA, carbonate) and MtrC, and MR-1.	107
Table 4:5. First-order rates for the kinetics reactions between the U-ligand complex (ligand = NTA, EDTA, DTPA, carbonate) and MtrC, and MR-1.....	108
Table 4:6. Concentrations in U and MtrC, and the ratio between them for the reactions between MtrC and U-ligand (ligand = NTA, EDTA, DTPA, carbonate) under oxic (MtrC oxidized) and reduced (MtrC reduced) conditions, in the whole reaction mixtures.	110
Table 4:7. Concentrations in U and MtrC, and the ratio between them for the reactions between MtrC and U-ligand (ligand = NTA, EDTA, DTPA, carbonate) under oxic (MtrC oxidized) and reduced (MtrC reduced) conditions, in the first fraction F1 eluted from the size-exclusion desalting columns.	111
Table 4:8. Percent of the total U recovered identified as U(VI) or U(IV) in both the first fraction F1 (in which MtrC elutes) and in the combined subsequent fractions F2 to F7 post reaction of reduced MtrC and the U-ligand complexes under reduced conditions.	111
Table 4:9. Average white line of the U M_4 -edge HR-XANES spectra.	114
Table 4:10. LCF of the M_4 -edge HR-XANES spectra for samples described in Figure 4.7 and Figure 4.8 using the references U(VI)-carbonate, U(V)-iodine, U(IV)O ₂	114

Chapter 1 Introduction

1.1 Uranium: history, chemical and physical properties, and environmental behavior

1.1.1 Uranium history

The German chemist Martin Klaproth discovered uranium (U) while analyzing pitchblende, a U oxide mineral, from the Joachimsthal silver mine, in Czech Republic in 1789. At that time, the phenomenon of radioactivity had not yet been brought to light. U was therefore used routinely as a coloring agent to give a yellow-green color to glass and orange, red or black tones to the glazes of ceramics. About a century later, in 1896, Henri Becquerel carried an experiment to investigate whether the radiations emitted from U were resulting from sunlight exposure (Figure 1.1.A.). He placed a white photographic plate with a U ore in a cupboard, away from any source of light. After developing the photographic plate, displaying fogged areas, he realized that the activity of U was independent from sunlight (Figure 1.1.B.).



(A) <http://scihi.org/henri-becquerel-and-radioactivity/>

(B) <https://timeline.web.cern.ch/becquerel-discovers-radioactivity>

(C) <https://www.franceculture.fr/emissions/lsd-la-serie-documentaire/quatre-femmes-de-science-44-marie-curie-le-radium-lestomac>

Figure 1.1: Discovery of radioactivity. A. Henri Becquerel in his laboratory; B. The photographic plate revealing the radiation of the U ore; C. Marie Curie in her laboratory.

This result was confirmed by Marie Curie, Henri Becquerel's doctoral student (Figure 1.1.C.), who worked on the characterization of the rays emitted by U. Only then was U recognized as a radioactive material. Following this discovery, Marie Curie investigated the radiation emitted by pitchblende. She found that the rays emitted by pitchblende were more intense than those of uranium. She hypothesized that other radioactive elements were contributing to the strong

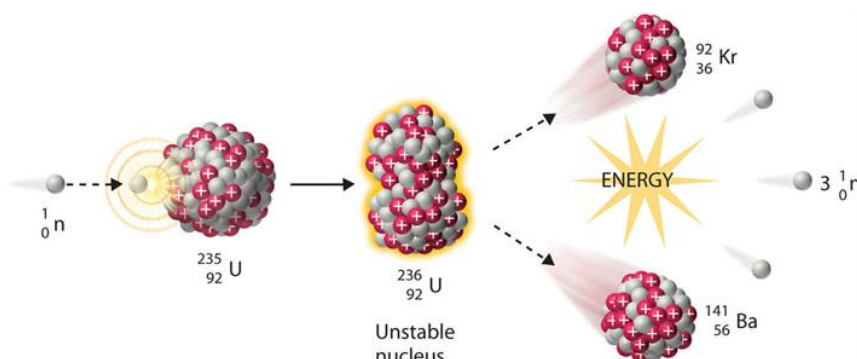
emission of pitchblende. Helped by her husband Pierre Curie and the chemist Gustave Bémont, she processed tons of uranium ore in order to isolate two new radioactive elements, named polonium and radium. Radium was thought to be beneficial for health and, as a result, a highly sought-after commodity at the beginning of the twentieth century. To meet the economic demand for radium, an intense uranium mining activity started in the early 1900s. Only after Hahn and Strassman discovered nuclear fission in 1938 did U chemistry and physics become leading research topics. All linked activities contributed to anthropogenic release of U in the environment.

1.1.2 Physicochemical properties of the metal U

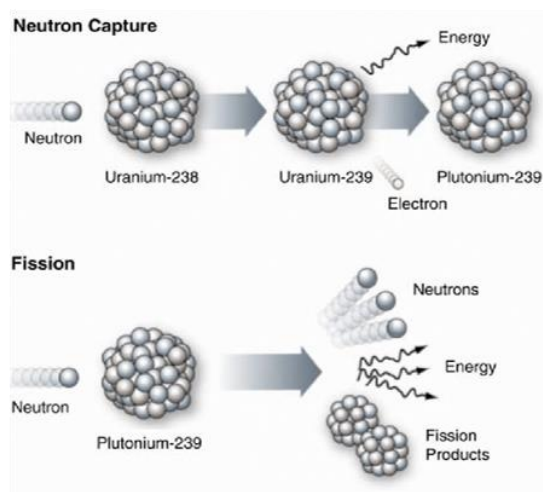
U is a radioactive and toxic metal belonging to the f-element series in the Mendeleyev periodic table, more precisely to the actinide elements. U occurs naturally in the terrestrial crust, with an average content of 4 mg/kg of crust¹, in the form of a variety of minerals in association with a wide-range of other elements (reactive non-metals, alkali metals, transition metals, metalloids, lanthanides, and other actinides). Among these minerals, uraninite (UO₂) is the most widespread along with pitchblende (mixed U oxides). The natural isotopes of U are ²³⁸U (99.28% abundance) and fissionable ²³⁵U (0.71%) as well as ²³⁴U (0.0054%) with respective half-lives of 4.47 billion years, 704 million years and 159 thousand years. In light of the slow decay of the most abundant natural isotopes ²³⁸U and ²³⁵U, U can be used as a marker to date geological processes. In addition, the natural isotopes ²³⁸U and ²³⁵U are commonly used for the production of nuclear energy. As ²³⁵U is fissile, it breaks down into two smaller nuclei upon impact by a neutron (Figure 1.2.A.). As for ²³⁸U, can be transmuted to plutonium 239 upon absorption of a neutron and can also undergo fission (Figure 1.2.B.).

Due to these properties, U is a key element to fuel nuclear energy, one viable alternative to coal, and a friendlier process regarding CO₂ emissions, although it leaves a heavy legacy of radioactive waste which must to be treated, confined and stored. However, permanent nuclear waste repositories are not yet operational but there is one repository under construction in Finland. In other countries, repositories are either in the permitting stage or being developed through scientific investigations. Because of its unusual radioactive properties, a great interest has arisen in U chemistry leading to the synthesis of various compounds whose structures, physicochemical and electronic properties were characterized. In these compounds, U is found in four oxidation states +III, +IV, +V, +VI, with +VI being the highest oxidation state as the electronic configuration of U is [Rn]5f³6d¹7s², hence six electrons in the valence orbitals.

A.

Fission of ^{235}U
<https://www.refletsdelaphysique.fr/articles/refdp/pdf/2016/03/refdp201650p30.pdf>

B.

Transmutation of ^{238}U

McGlynn et al. 2014

Figure 1:2. Fission and transmutation of U. A. Fission of ^{235}U ; B. Transmutation of ^{238}U in Plutonium 239 and subsequent fission of Plutonium 239.

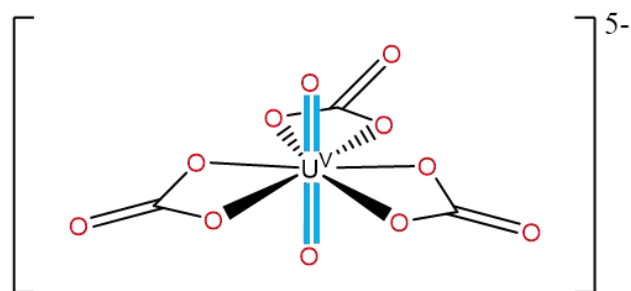
1.1.3 Uranium in the environment

Decades of U-related activities such as ore mining, processing for nuclear fuel and weapons, storage of nuclear waste, have contributed to the release of uranium to the environment. In water, soil, and sediments, U occurs in two principal oxidation states, +VI and +IV, i.e., U(VI) and U(IV). Their abundance and predominance in a specific subsurface setting depend on the chemical composition and the redox profile of subsurface sediments and groundwater. In oxygenated environments, the highest oxidation state, U(VI), prevails, and forms ionic complexes with hydroxo-, carbonato-, phosphato- functional groups^{1,2}, associates with humic substances such as fulvic acid, and complexes with organic matter². Hence, U(VI) is highly soluble and mobile in the subsurface, which facilitates its transport within the aquatic compartment of the subsurface. Nevertheless, in environments hosting reducing conditions, U(IV) predominates. In the absence of strong organic ligands, U(IV) forms stable solid phases, and thus has the propensity to immobilize U. The transition from U(VI) species to U(IV) species requires the transfer of two electrons to the U atom. Electron transfers in the environment are typically mediated by minerals phases^{3–9}, dissimilatory metal reducing bacteria (DMRB)^{10–19} or other microorganisms. Occulted by the two prevalent oxidation states U(VI) and U(IV), the environmental chemistry of pentavalent U(V) is scarcely documented. In fact, U(V) tends to spontaneously disproportionate to U(VI) and U(IV) in aqueous solution at circumneutral pH values²⁰, and further, it reacts rapidly with O₂ to undergo oxidation.

1.1.4 Pentavalent U(V)

The interest in U(V) compounds has several origins. In the mid-20th century, it was challenging to study this reactive oxidation state of U, given its high reactivity with oxygen and water²¹. Nowadays, the technical progresses achieved in the design of laboratory equipment permit conditions where U(V) persists. As a result, the study of U(V) chemistry has flourished²². The electronic configuration of U(V), [Rn]5f¹, with a single electron in the 5f orbital, makes it an amenable system to study f-orbital properties using spectroscopic, magnetic, or electron paramagnetic spectroscopy methods. In addition, the occurrence of U(V) in U systems is more frequent than initially thought. For instance, in spent nuclear fuel waste meant to be stored in deep geological repositories, a closer look to the U chemistry and oxidation states revealed that U(V) forms and persists. Indeed, U(V) mixed-oxide compounds emerge from successive disintegrations of U nucleus in spent nuclear fuels. Hence, local oxidation increases and triggers a rearrangement of UO₂ into U(V)-bearing mixed-oxides such as U₄O₉, U₃O₇, U₃O₈, and UO₃. Furthermore, U(V) was also observed in the structure of titanate ceramics, upon to stabilization of high-level nuclear waste prior to storage^{23,24}. In addition, the radiolysis of water, resulting in reactive radicals promoted surface oxidation of UO₂ to U(V) in stored spent fuels²⁵. Finally, a few geochemical studies have evidenced the presence of U(V) associated with environmental systems, related to biochemical transformations of the U(VI) moiety^{9,26–33}.

Until recently, most of the pentavalent U(V) chemistry was performed in non-aqueous media. Non-aqueous media chemistry was an attractive field, in particular for the development of efficient nuclear fuel reprocessing based on aqueous/organic separation³⁴. Two principal forms of U(V) exist. The uranyl(V) form has characteristic short axial dioxo bonds of about 1.9 Å, a shorter form of which is found in uranyl(VI) (1.8 Å) (Figure 1.3.A.). Compared to uranyl(V), the so-called uranate(V) has a more crystalline and symmetric structure, which lacks the short dioxo-uranyl bonds (Figure 1.3.B.). In uranate(V) the coordination number of uranium is lower or equal to 8.

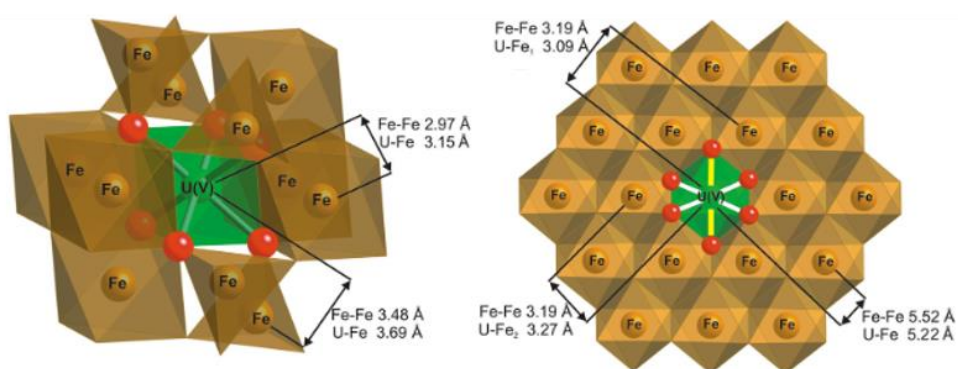


uranyl(V)

B.

magnetite

green rust



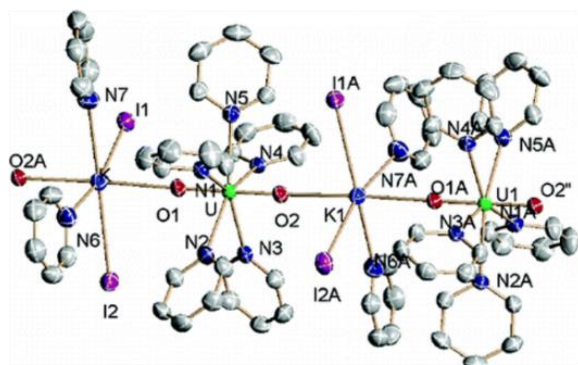
uranate(V)

Adapted from Roberts et al 2017

Figure 1:3. U(V) structures. A. Uranyl structure in the tri carbonato complex of U(V) $[U(V)O_2(CO_3)_3]^{5-}$ with the characteristic short dioxo bonds in blue, B. examples of uranate(V) structure incorporated in magnetite and green rust.

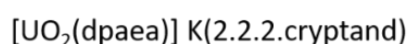
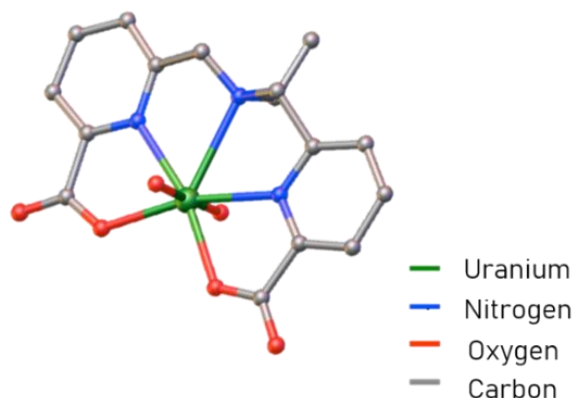
The first uranyl(V) complex was serendipitously identified in the early 2000s but the results were not reproducible. A few years later, the first reproducible uranyl(V) complex was synthesized in non-aqueous media and consisted of a linear polymeric complex of U(V)-iodide³⁵ (Figure 1.4.A.).

A.



Natrajan et al. 2006

B.



Adapted from Faizova et al. 2018

Figure 1:4. First stable uranyl(V) complexes. A. First uranyl(V) complex synthesized in a reproducible manner; B. first uranyl(V) complex stable in water at pH 7.

The low stability of uranyl(V) in water is due to cation-cation interactions (CCI) occurring between the U(V) atom and the oxygen atom of the dioxo bond of another U(V) atom (Figure 1.5). This phenomenon is particularly evident in U(V) because the single unpaired electron in the 5f orbitals provokes the lengthening of the dioxo bonds compared to that of U(VI). Hence the axial oxygens in U(V) are more Lewis basic, and amenable to interact with other U(V) atoms. Upon interaction, an electron is transferred between the two closer U(V) centers, leading to the disproportionation of U(V) to U(IV) and U(VI).

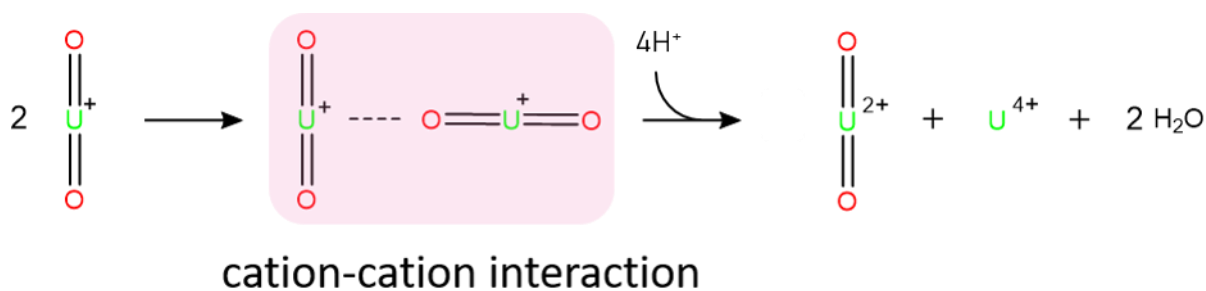


Figure 1:5. Cation-cation interaction between two uranyl(V) nuclei resulting in disproportionation in U(VI) and U(IV).

The protonation of U(V) was first thought to trigger its disproportionation³⁶, which is nowadays accepted as the consequence of CCI interactions^{37,38}. As the result of the propensity of U(V) to disproportionate, few studies have characterized uranyl(V) complexes in aqueous conditions. Until recently, only one uranyl(V) complex has been stabilized for over a period of a few days in water at a pH greater than 11³⁹. The tri-carbonato $[U(V)O_2(CO_3)_3]^{5-}$ was synthesized

electrochemically, and its structure was analyzed by extended x-ray absorption spectroscopy fine structure (EXAFS) and compared to that of $[\text{U(VI)}\text{O}_2(\text{CO}_3)_3]^{4-}$. U(VI) and U(V) displayed similar geometries, except that the bond lengths of both the axial and equatorial oxygens were longer in the U(V) complex (U(VI): 1.81 Å and 2.44 Å; U(V): 1.91 Å and 2.50 Å respectively). Recently, our collaborators at the group of complex chemistry at EPFL successfully synthesized a uranyl(V) complex stable in anaerobic aqueous medium at pH 7⁴⁰ (Figure 1.4.B.). Their strategy was to use a bulky aminocarboxylate ligand to saturate the equatorial plane of the U nucleus, hence preventing cation-cation interactions that lead to disproportionation. The ligand dpaea^{2-} ($\text{dpaeaH}_2 = \text{bis}(\text{pyridyl-6-methyl-2-carboxylate})\text{-ethylamine}$) is pentadentate and surrounds the equatorial plane. This recent finding suggests that other U(V) species may be stabilized in water in presence of appropriate organic ligands. In fact, another stable aqueous complex of U(V), U(V)-dpa (dpa = dipicolinic acid, found in bacterial endospores), was then characterized by the same group⁴¹. These results open new horizons to the environmental chemistry of U(V), for which stabilization can be achieved in aqueous media in presence of appropriate organic ligands.

1.2 Biologically mediated redox reactions of uranium in the environment

1.2.1 Biotransformation of uranium

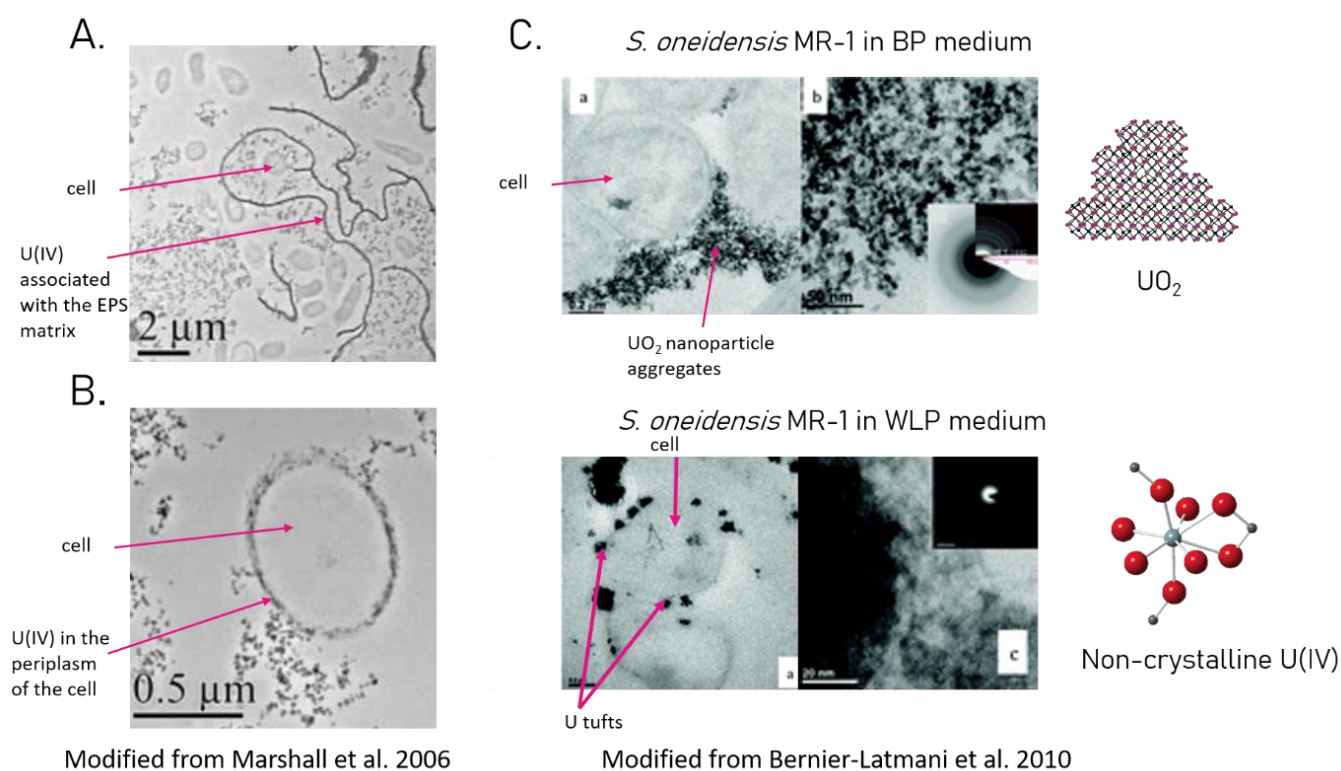
Microbial-U interaction in the environment have been broadly studied and are categorized in four main classes: bioreduction, biomineralization, biosorption and bioaccumulation. The underlying interest in these mechanisms resides in their ability to immobilize U in the subsurface. Hence, they are namely scrutinized for their potential in bioremediation processes of U contaminated sites. Bioreduction consists in the transfer of electrons from bacteria to U(VI), hence changing the oxidation state and consequently the chemistry of U. The biological reduction of U will be further discussed in the following paragraph. Regarding biomineralization, it consists in the precipitation of a mineral U phase at the surface of bacteria upon release of biologically produced ligands such as phosphate, carbonate, sulfate or hydroxide⁴²⁻⁴⁵. Biomineralization is often chosen as an alternative when U immobilization by reduction is not feasible. However, the biomineralization process also occurs after U reduction, namely resulting in crystalline U(IV) or non-crystalline U(IV) species^{13,14}. As for biosorption, it describes the sorption of a metal to the cell surface through functional moieties such as carboxylic, amino, phosphato, hydroxo, and sulfhydryl groups⁴⁶. Finally, U bioaccumulation refers to the intake of U inside the bacterial cells due to membrane permeability.

1.2.2 Bioreduction of uranium

Initially, the occurrence of insoluble U(IV) species, such as the uraninite crystal (UO_2) was believed to arise from abiotic U(VI) reduction⁴⁷⁻⁵⁰. However, it has been observed that extracts of *Micrococcus lactilyticus* could quantitatively reduce U(VI) in presence of H_2 ⁵¹. Following this discovery, Lovley et al.^{2,8} published the first work aiming at characterizing the microbial reduction of U(VI) by dissimilatory metal reducing bacteria (DMRB) such as *Geobacter metallireducens* GS-15 and *Shewanella putrefaciens*. To date, numerous studies have evidenced U(VI) reduction by microorganisms, such as *Cellulomonas* sp.¹⁸, *Clostridium* sp.^{19,52}, *Desulfovibrio* sp.^{11,53-56}, *Geobacter* sp.^{10,28,57}, and *Shewanella* sp.^{10,13,58,59}. The reduction of U(VI) by DMRB is coupled to the oxidation of an electron donor, often an organic carbon source such as lactate or acetate. Two electrons are provided from the microorganism to the external electron acceptor U(VI). The rate

of reduction and the final U(IV) species (soluble, crystalline or amorphous¹³) depend on the initial environmental conditions, i.e. pH and electrochemical potential E_H , the available electron donors, U speciation, and the microbial community. The most commonly reduced U species when pH values range from 5.0 to 8.5, and the carbonate concentration is low are carbonate-associated complexes, such as $(\text{UO}_2)_2(\text{OH})_3\text{CO}_3^-$, and hydroxyl complexes such as $\text{UO}_2(\text{OH})_3^-$. In the presence of higher carbonate concentrations, the bi-carbonato $[\text{U(VI)O}_2(\text{CO}_3)_2]^{2-}$ and tri-carbonato $[\text{U(VI)O}_2(\text{CO}_3)_3]^{4-}$ complexes form. In the presence of calcium in the groundwater, $\text{Ca}_2\text{UO}_2(\text{CO}_3)_3$ and $\text{CaUO}_2(\text{CO}_3)_3^{2-}$ occur, and render U reduction less amenable, probably due to a lower redox potential compared to the above-mentioned carbonate complexes⁶⁰ and a stronger complexation constant. For example, the logK of $\text{Ca}_2\text{UO}_2(\text{CO}_3)_3$ has a logK of 30.55 ± 0.25 ⁶¹, whereas that of $[\text{U(VI)O}_2(\text{CO}_3)_3]^{4-}$ is 16.94 ± 0.12 ⁶². In addition, U(VI) can form organic complexes with ligands such as oxalate, malonate, citrate, or the aminocarboxylate ligands NTA and EDTA, for which bioreduction has been observed^{63–65}. In most cases, upon reduction, U(IV) precipitates at the surface of the bacterial cells, in association with the extra polymeric substance if any, or inside the periplasm of the cells^{17,33,53,66} (Figure 1.6). However, in organic-rich environments, for instance in presence of the previously listed ligands, U(IV) is more soluble and remains in the aqueous phase.

Figure 1:6. U reduction product nature and localization. TEM images from cell suspensions of *S. oneidensis* MR-1 incubated with uranyl(VI)-acetate



showing the location of the precipitated U(IV) product A. in association with the EPS matrix and B. inside the periplasm of the cells. C. Difference in the crystallinity of U(IV) products upon U(VI) reduction by *S. oneidensis* MR-1 depending on the incubation conditions. Top part shows crystalline UO₂ precipitated at the cell surface, bottom part shows amorphous U(IV) phases, called non-crystalline U(IV), often associated with phosphate groups.

1.2.3 Reduction mechanism of U(VI): the pentavalent U(V) intermediate

1.2.3.1 First step: one electron transfer from U(VI) to U(V) species

Two electrons need to be transferred from the bacteria to U(VI) to form U(IV). It has been evidenced, experimentally, by Renshaw et al. that a first one electron transfer occurs, and U(VI) is reduced to a pentavalent U(V) intermediate²⁸. In that work, they performed EXAFS, at the L₃-edge of U, on whole cells and supernatants of *Geobacter sulfurreducens* cultures inoculated with U(VI)-carbonate over 24h. The authors observed a progressive change in the U structure over-time by examining the d_{axial}(U(VI)-O), d_{axial}(U(V)-O) and d_{equatorial}(U(VI,V)-O) features in the Fourier transforms of the EXAFS signals (Figure 1.7.A.). These data suggest that uranyl(V) started to form starting at 2h of incubation, with the highest abundance after about 4h. In fact, after 4h of incubation, they observed the stretching in the U-O dioxo bond compared to that of the uranyl(VI) in both the whole cell culture and the culture supernatant. The bond length of one dioxo oxygen increased from 1.8Å to 1.91Å in the whole culture and from 1.8Å to 1.92 Å in the culture supernatant. These bond lengths correspond to that measured in the [U(V)O₂(CO₃)₃]⁵⁻ reference. Further, density functional theory (DFT) calculations of uranyl(VI) reduction by the periplasmic c-type cytochrome PpcA of *G. sulfurreducens*⁶⁷ support the mechanism proposed by Renshaw et al.²⁸. According to the calculations, two uranyl(VI) centers bind to a carboxylic residue in the active site of PpcA, and intermediate U(V)-bearing complexes U(VI)-U(V) and U(V)-U(V) form via two consecutive one-electron transfers. In addition, the occurrence of U(V) in bacterial systems using laser fluorescence spectroscopy was reported in a microbial biofilm and recently in *G. sulfurreducens*. In the work of Grossman et al., nanoparticles of U(V) were detected in a multi-species biofilm incubated with aqueous U(VI)²⁹. They identified the nanoparticles using confocal laser microscopy and using a wavelength of 408nm. Some nanoparticles had an emitted fluorescence ranging from 415nm to 475 nm, characteristic of U(V) species. Jones et al. followed the evolution of the intensity of the fluorescence emittance at 525nm, characteristic of the uranyl(VI)-O bond, in *G. sulfurreducens* cultures incubated with aqueous U(VI)-acetate³⁰. They obtained a saw-tooth profile, where the decreases in intensity were interpreted as reduction of U(VI) to U(V), which does not fluoresce at 525nm. Finally, recently Vettese et al. and Molinas et al. reported the occurrence of U(V) species identified in *S. oneidensis* MR-1 cultures by U M₄-edge high resolution x-ray absorption near edge spectroscopy (HR-XANES). In the work of Vettese et al., U(V) was identified in both cell suspensions and cell pellet after 4.5h of incubation with U(VI) carbonate (Figure 1.7.B.). They report that the U(V) species persisted up to 120.5h in association with the cells. However, the speciation of U(V) remains unclear as they could interpret their M₄-edge data either using a uranate(V) or uranyl(V) standard. Also, Molinas et al. observed that the reduction of solid phase U(VI)-dpaea by *S. oneidensis* MR-1 results in the formation of uranyl(V)-dpaea in the supernatant of the cultures, starting at the early stages of incubation and remaining stable for a few days.

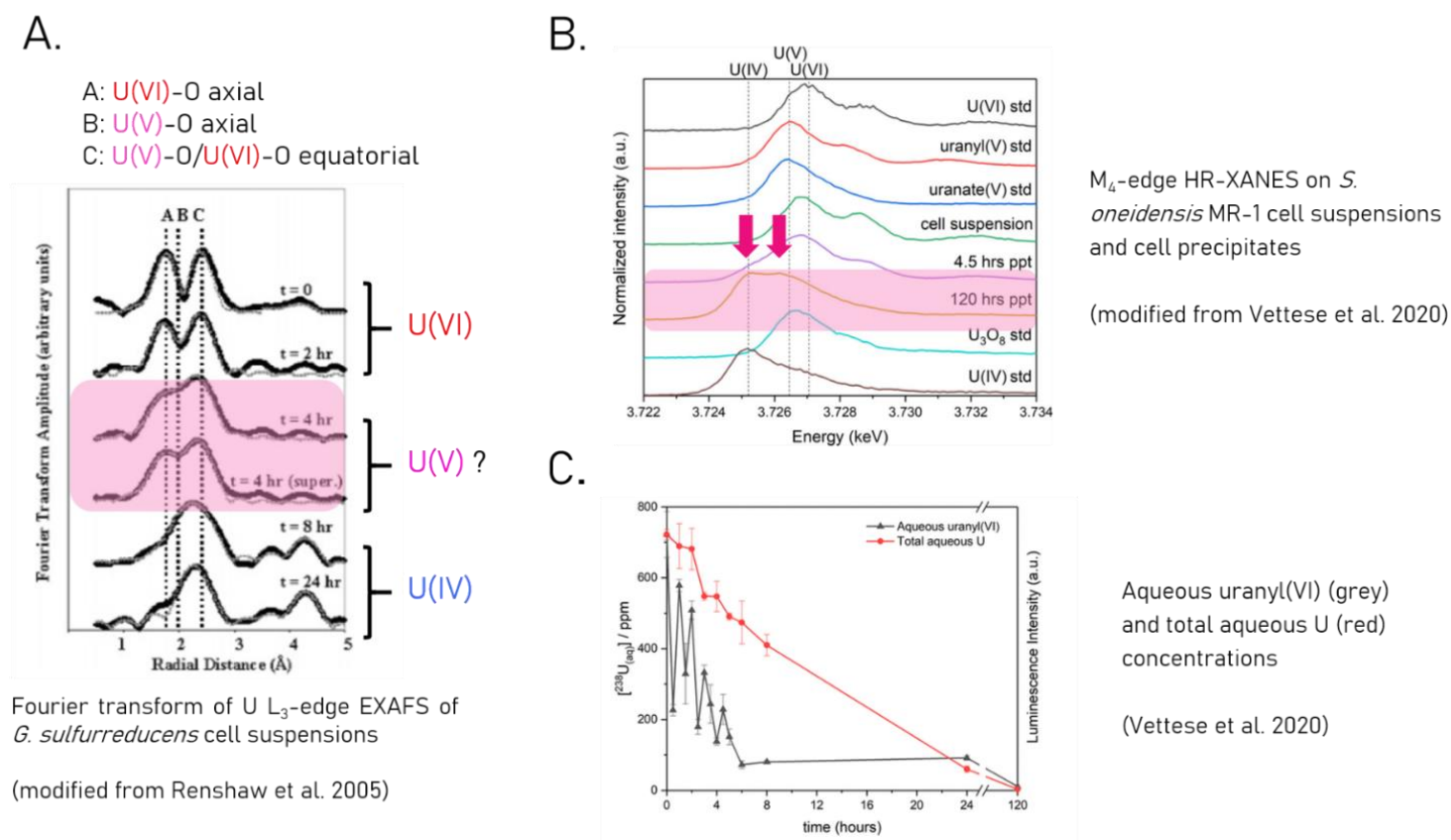


Figure 1:7. Evidence of U(V) with various bacterial species. A. EXAFS spectra of *G. sulfurreducens* cell suspensions and supernatants over 24h. B. M_4 -edge HR-XANES of cell suspensions and a cell pellet. Contribution from U(V) is clearly evidenced in the 120h cell pellet. The two arrows indicate (from left to right) the contribution from U(IV) and from U(V). C. Aqueous concentration of uranyl(VI) (grey) and total U (red) measured by luminescence spectroscopy. The aqueous uranyl(VI) concentration displays the saw-tooth profile believed to account for successive reduction of U(VI) to U(V) and subsequent disproportionation of U(V).

1.2.3.2 Second step: disproportionation or additional one electron transfer?

The fate of uranyl(V) species was first assessed by Renshaw et al., by investigating the ability of *G. sulfurreducens* to reduce stable neptunium(V), a proxy for U(V)²⁸. They argued that thermodynamically, if U(V) can be biologically reduced, then Np(V) should. Over 218h, the aqueous concentration of Np(V)O₂⁺ dropped by about 13%, in the culture with and without electron donor, and of about 10% in dead cell cultures. The aqueous Np phase was still in the Np(V)O₂⁺ form after 218h, however the cell pellets were not analyzed for Np speciation. Thus, the authors concluded that as *G. sulfurreducens* did not reduce Np(V), U(V) would not be either, and therefore U(V) would disproportionate to form U(IV) species. Likewise, Sundararajan et al. calculations concur to invoke the disproportionation of the two uranyl(V) moieties bound to PpcA⁶⁷ (Figure 1.8). Such observations were later supported experimentally by Jones et al., and more recently by Vettese et al.^{31,34}. In fact, they observed that the fluorescence intensity of uranyl(VI) in *G. sulfurreducens* and *S. oneidensis* MR-1 cultures respectively, displayed a saw-tooth profile (Figure 1.7.C.). They proposed that the repeated increases in intensity may correspond to U(V) disproportionation to U(VI) and U(IV), consequently leading to an increase

of the intensity detected for U(VI). Nonetheless, the latter investigations were performed using a carbonate-rich buffer, which promotes the disproportionation of U(V) at neutral pH³⁶.

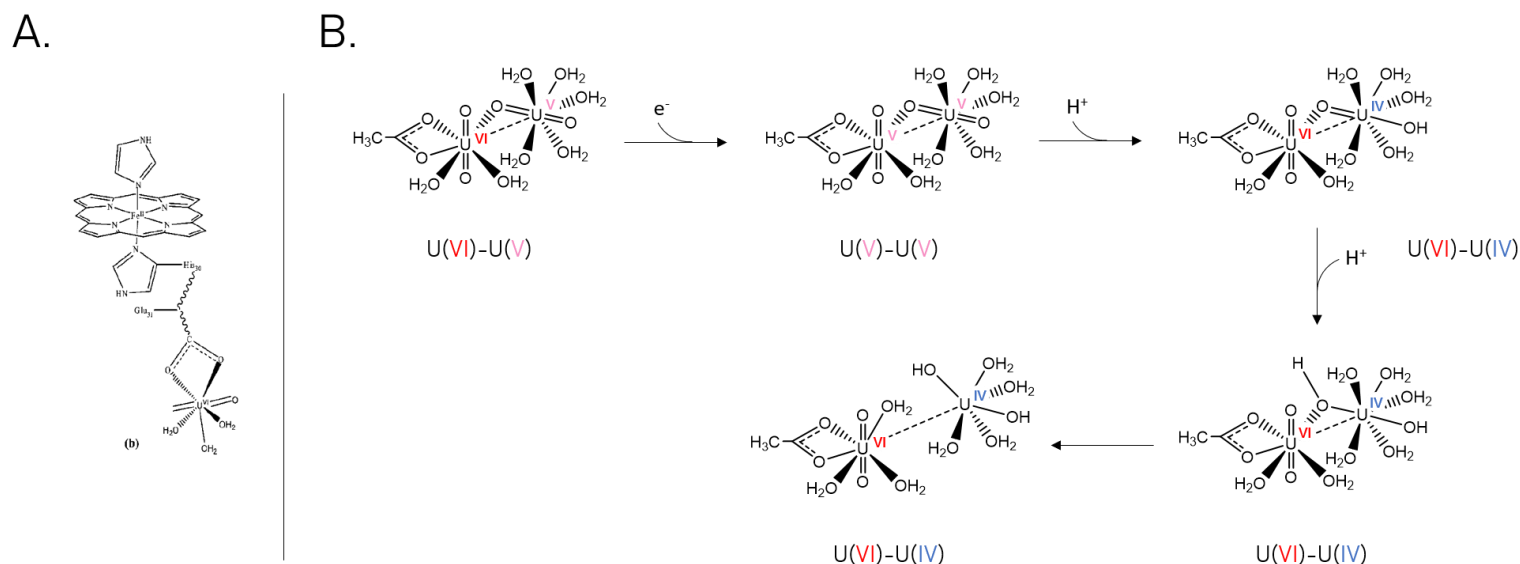


Figure 1:8. Mechanism of U(VI) reduction modeled by DFT calculations. A. Binding site of uranyl(VI) to a glutamate residue close to heme 1 of PpcA, B. modeled mechanism of U(VI) reduction to a U(V)-U(V) bound to PpcA, and disproportionation of U(V) to U(VI) and U(IV).

1.2.3.3 Biological reduction of Np(V) and Pu(V)

Identically to U, higher oxidation states of Np and Pu are soluble and mobile in the subsurface, whereas lower oxidation states have the tendency to form solid phases. Regarding Np, as mentioned in the previous paragraph, Renshaw et al. did not observe reduction of Np(V) by *G. sulfurreducens*. However, Icopini et al. proved that *S. oneidensis* MR-1 could reduce both, free Np(V) and complexed Np(V) to citrate, whereas *G. metallireducens* could only reduce Np(V)-citrate⁶⁸. Furthermore, Lloyd et al. coupled two microorganisms to reduce and precipitate Np(V)⁶⁹. In the later study, *Shewanella putrefaciens* reduced Np(V) to Np(IV) species, subsequently precipitated into insoluble Np(IV) phases by *Citrobacter* sp.. Also, a sulfate-reducing consortium exhibited reducing activity toward Np(V)⁷⁰. As for Pu reduction, both Pu(VI) and Pu(V) were reduced by *G. metallireducens* and *S. oneidensis* MR-1, as nanoparticles of Pu(IV) associated with the cell surface were observed by transmission electron microscopy⁷¹. Pu(IV) can be further reduced to Pu(III), which is more soluble, but its reductive mobilization depends in the initial Pu(IV) species. In fact, Boukhalfa et al. demonstrated that an amorphous phase of Pu(IV) could be partially reduced to Pu(III) by *S. oneidensis* MR-1 but not by *G. metallireducens*. However, a Pu(IV)-EDTA complex was rapidly converted to Pu(III) by both bacteria⁷². The differences observed between the different microorganisms may be related to the difference in electron donor, i.e. lactate for *Shewanella* species and acetate for *Geobacter* species. Lactate forms stronger complexes with free radionuclides, and may lower their toxicity for the microorganism.

1.2.4 Bioremediation

Ultimately, the efforts in understanding the molecular mechanism of U reduction are aimed at providing better strategies to efficiently mitigate U contamination in the subsurface. Previously, the most commonly used methods were pump-and-treat of the aquifer, or flushing the groundwater until aqueous U concentration reached acceptable levels. These techniques were often set up over long periods of time and had limited efficiency. The alternative of using microorganisms was investigated on several contaminated sites, in the US, for instance at the well-studied Oak Ridge site in Tennessee, or Rifle site in Colorado. Bioremediation includes techniques using biosorption, biomineralization and bio-immobilization, often by reduction. Multiple laboratory tests were performed on contaminated groundwater to evaluate the possibility of up-scaling bioreduction to contaminated sites. U(VI) can successfully be removed from contaminated groundwater, as Lovley et al. demonstrated, incubating *Desulfivibrio desulfuricans* with groundwaters originated from a former mining site, and from the Hanford site in Washington⁷³. However, in the field, many parameters influence the ability of microorganisms to reduce U(VI), i.e., the presence of other electron acceptors such as oxygen, Fe(III), NO₃⁻ or SO₄²⁻, the E_H-pH conditions, the in-situ microbial community, the type of electron donors, the hydrology of the site, etc. In practice, the indigenous microbial communities are stimulated by the injection of an electron donor in the contaminated aquifer. Then, the concentrations of U are monitored overtime, along with the type of metabolism established and the associated microbial communities. Each site needs specific tuning depending on the local conditions in order to set-up efficient remediation strategies. For instance, at the Oak Ridge site, Madden et al. investigated several selected electron donors to stimulate the microbial communities, such as methanol, ethanol, glucose⁷⁴. They showed that glucose and methanol were more favorable for U reduction, but all three donors stimulated predominantly bacteria from the *Geobacter* sp.. Moreover, at the Rifle site, Anderson et al. attempted to use acetate as an electron donor in the contaminated area⁷⁵. During the nine first days, the concentration in U(VI) decreased in the groundwater as Fe(II) concentrations increased, pointing to the reduction of U(VI) coupled to that of Fe(III). In the following 50 days of acetate injection, sulfate was depleted and some U was remobilized. A switch was observed in the microbial community from *Geobacter* sp. to sulfate-reducing bacteria. Two additional experiments were run at Rifle and reported by Williams et al.⁷⁶. Injections of acetate were set-up two successive summers, lasting 31 and 110 days, respectively. The dominant metabolisms were iron reduction and sulfate reduction, respectively. As Anderson et al. observed, with the sulfate reduction, U concentrations increased in the groundwater, but were successfully lowered back down by increasing the concentration of acetate injected. Some bacteria from the *Geobacter* sp. were still active with higher acetate concentration during the sulfate-reducing phase. Another example of fine-tuning of the conditions was the concomitant removal of U(VI) and technetium(VII) studied by Istok et al. on a field with unusually high concentrations of NO₃⁻⁷⁷. Upon donor injection, removal of NO₃⁻ and Tc(VII) occurred in parallel, however, U concentrations were stable. Addition of electron donor allowed iron-reducing condition to set-in with *Geobacter* sp., and fostered U removal. These examples prove that bioreduction is a successful bio-immobilization process, and encourage further studies on the mechanism of U reduction in order to pinpoint the mechanistic steps and the associated chemistry of the intermediates.

1.3 Electron transfer mechanism in *Shewanella oneidensis* MR-1

Henceforth in this thesis, the focus will be on the microorganism *S. oneidensis* MR-1, model microorganism for this work. *S. oneidensis* MR-1 is a well characterized metal-reducing bacteria, fast-growing, and there are efficient genomic tools to develop mutant strains to investigate the pathways of U reduction.

1.3.1 The versatile microorganism *S. oneidensis* MR-1

S. oneidensis MR-1 belongs to the *Shewanella* genus, which describes about 70 species of mostly facultative anaerobes, Gram-negative, non-fermentative γ -Proteobacteria. These rod-shaped microorganisms are found in many aquatic environments, and can adapt to various ecosystems⁷⁸, including fresh and saline water, shallow or deep marine sediments, ice-cold⁷⁹ or equatorial climates, but also polluted areas. They are known in the food industry for being associated with spoiled food. In fact, the *Shewanella* gender was first identified in putrid butter by Derby et Hammer in 1931⁸⁰. The strain *S. oneidensis* MR-1 (Figure 1.9.A.) was discovered in 1988 in Lake Oneida (New York State) and was reported by Nealson et al. as a manganese oxide reducer⁸¹.

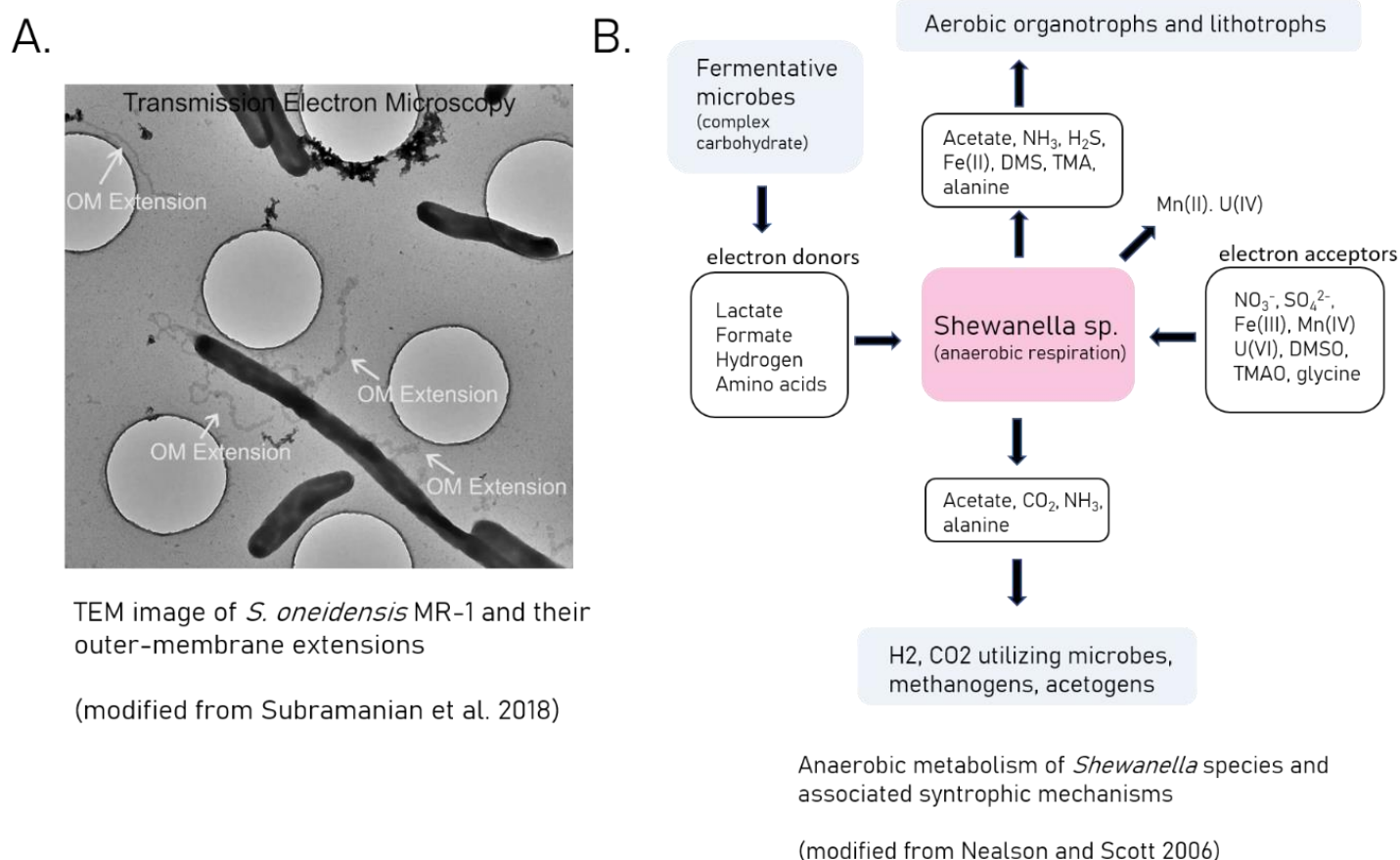


Figure 1:9. *S. oneidensis* MR-1 anaerobic metabolism. A. TEM image of *S. oneidensis* MR-1 showing its membrane extension extending in the extra-cellular medium. B. Anaerobic respiration of *Shewanella* sp. and possible interactions with other microbial communities.

S. oneidensis is limited in the type of carbon source it can use. It grows with simple molecules such as lactate, formate, formate combined to H₂, and amino acids. Under aerobic conditions, it uses the tricarboxylic acid (TCA) cycle⁸², whereas under anaerobic conditions, the oxidation of the carbon source is coupled to the reduction of a variety of electron acceptors (NO₃⁻, SO₄²⁻, Fe(III), Mn(IV), U(VI),...) ⁷⁸ (Figure 1.9.B.). Nowadays, *S. oneidensis* MR-1 is often used as a model organism for lab-based environmental studies, in field remediation campaigns, but also applied to microbial fuel cells studies⁸³.

1.3.2 Electron transfer from the cytoplasm to the outer-membrane

1.3.2.1 Up to MtrA

The carbon source, lactate for instance, is oxidized in the cytoplasm of the cells, resulting in the reduction of electron carriers such as NAD⁺ or FAD⁺, that initiate the electron flow. NADH and FADH are in turn oxidized by the inner membrane menaquinone pool, i.e., the quinone (Q) is reduced to quinol (QH₂). QH₂ is oxidized by the dehydrogenase CymA, a tetraheme *c*-type cytochrome anchored in the inner membrane. Then, CymA redirects electrons to periplasmic multi-heme *c*-type cytochromes⁸⁴. The most abundant periplasmic *c*-type cytochromes are the fumarate reductase FccA and the small tetraheme *c*-type cytochrome STC. Both can receive electrons from CymA^{85–87} and shuttle them across the periplasm to the outer-membrane (Figure 1.10). Other periplasmic *c*-type cytochromes are likely also involved in this electron transfer.

1.3.2.2 MtrA to MtrC-OmcA

From the periplasm, the electrons enter the MtrCAB porin complex embedded in the outer-membrane, linking the periplasm to the extracellular medium (Figure 1.10). MtrCAB is composed of the two decaheme *c*-type cytochromes MtrA and MtrC. MtrA faces the inside of the cells, and MtrC is exposed at the surface of the cells. MtrA is inserted inside into a β -barrel porin protein MtrB and MtrC sits on the top⁸⁸. This porin-complex facilitates electron transfer from the periplasm to the cell surface via direct heme-heme contact between MtrA and MtrC^{89–92}. An additional *c*-type cytochrome OmcA is co-expressed with the MtrCAB operon and locates at the surface of the cells in close interaction with MtrC^{17,91,93}. OmcA was proposed to form a 1:2 MtrC/OmcA complex with MtrC^{85,93}, but was not found in association with the crystal structure of MtrCAB⁸⁸, suggesting a weak interaction. MtrC and OmcA are terminal reductases which can transfer electrons to extracellular electron acceptors^{17,91,93}. The MtrCAB complex spans a window of reduction potentials from 0 to - 400 mV versus the standard hydrogen electrode (SHE) and thus, have the ability to receive electrons from the periplasm and transfer them to a wide range of electron acceptors⁹¹. A paralogous porin complex also exists in *S. oneidensis* MR-1, MtrFDE: MtrF is the homologue of MtrC, MtrD that of MtrA, and MtrE that of MtrB.

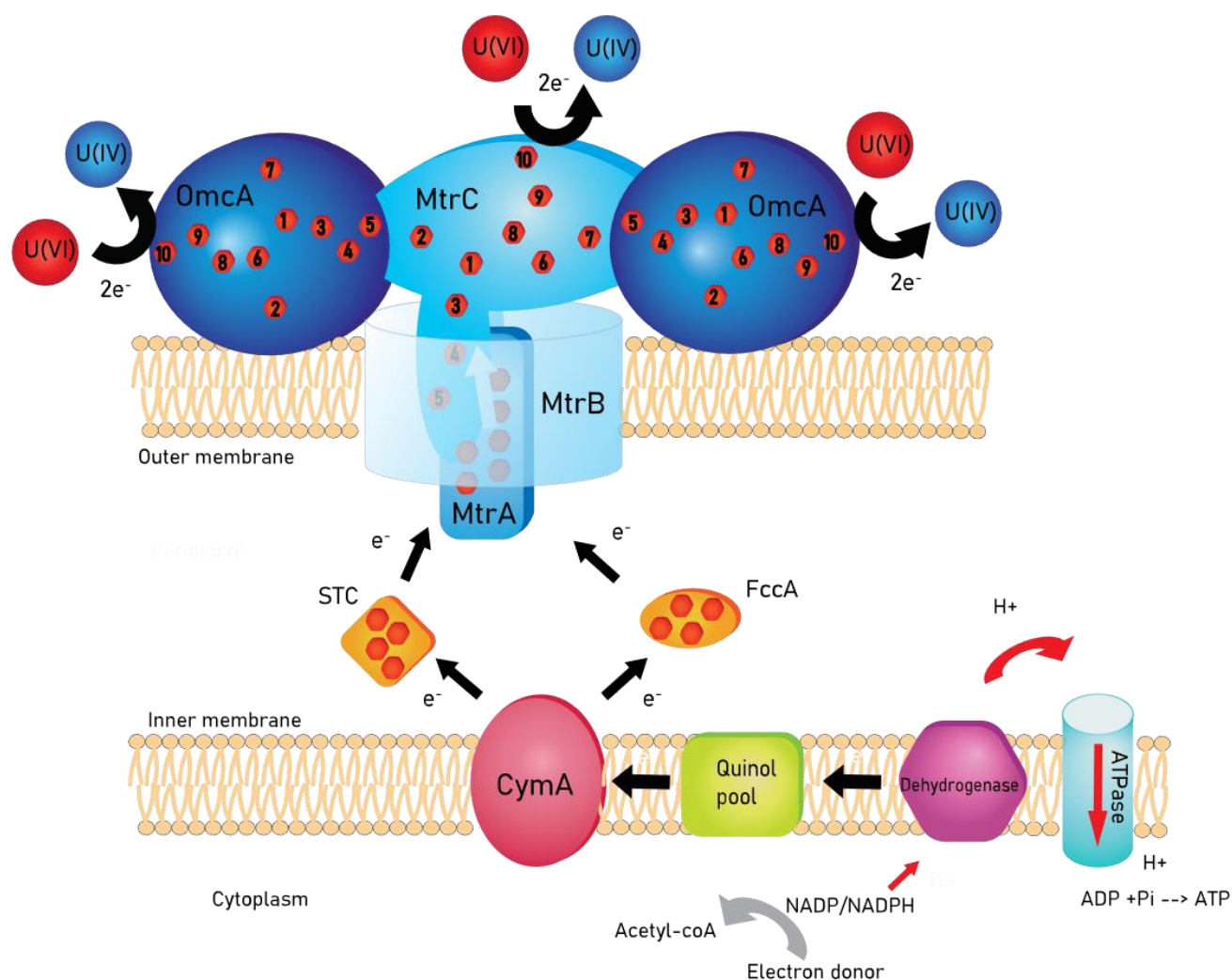
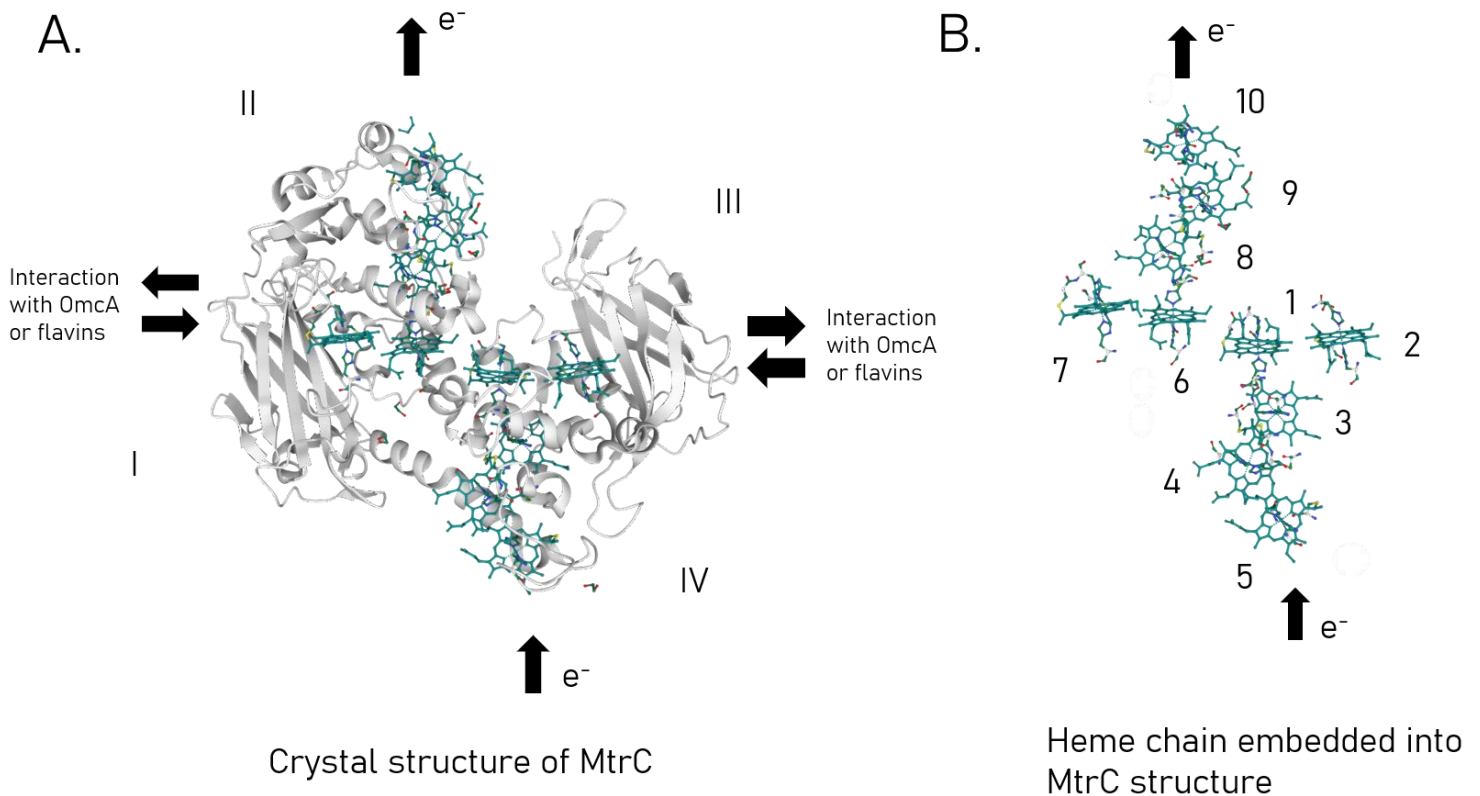


Figure 1:10. Electron transfer chain in *S. oneidensis* MR-1 with U(VI) as the electron acceptor.

1.3.2.3 The outer-membrane decaheme *c*-type cytochromes

Among the four outer-membrane *c*-type cytochromes in *S. oneidensis* MR-1, MtrC, MtrF, and OmcA, MtrC and OmcA are the most studied because of their major contribution to the metal reduction mechanism. MtrC and OmcA have common characteristics which are essential for metal reduction. The structure of MtrC was resolved at a resolution of 1.8Å⁹⁴ and that of OmcA at 2.7Å⁹⁵. MtrC is about 90 Å × 60 Å × 40 Å, and its size suggests that it is mostly exposed on the cell surface⁹⁴. The heme-binding motif CXXCH in the protein are highly conserved^{96,97,98}. Each cytochrome is made up of four domains: two heme-domains (hemes 1 to 5 and 6 to 10) forming a cross-like arrangement, and two β-barrel domains which scaffold the two pentaheme domains. In MtrC, hemes 5 and 10 are exposed at opposite ends of the structure suggesting that they may be sites for electron exchange with electron donors and acceptors (Figure 1.11.A. and B.). Hemes 2 and 7 are oriented towards the β-barrel domains, and could be binding sites for proteins or electron shuttles such as flavins^{97,99} (Figure 1.11.A. and B.).



Drawing extracted from Consurf with the PDB ID 4LM8 from Edwards et al. 2015

Figure 1:11. MtrC structure. A. Crystal structure of MtrC, showing electron entrance and exit, interaction sites with other protein or electron shuttle, when associated to the MtrCAB porin complex. B. Heme chain embedded in MtrC structure. The electrons flow from heme 5 to heme 10, or 2 and 7.

1.4 Mechanism of electron transfer to electron acceptors in *S. oneidensis* MR-1

We will now focus on the mechanism of electron transfer in *S. oneidensis* MR-1.

1.4.1 Direct or indirect transfer

The electron transfer occurs between the outer-membrane *c*-type cytochromes and the extracellular environment. In *S. oneidensis* MR-1, electrons are carried through a chain of *c*-type cytochromes from the cytoplasm to the outer-membrane of the cells. Once the electron has reached the outer-membrane of the cells, three possible mechanisms have been suggested. Either, (i) there is direct contact between the outer-membrane cytochromes and the extracellular electron acceptor, (ii) bacteria secrete reduced low-molecular weight shuttles (e.g., flavins or AQDS) to provide the electron acceptor with electrons, or (iii) the transfer occurs through bacteria conductive pili, or nanowires, for instance in *G. sulfurreducens*. In *S. oneidensis* MR-1, membrane extensions mimic the role of conductive pili by extending into the extracellular medium.

1.4.1.1 Direct contact

MtrC and OmcA are key mediators of electron transfer, as *S. oneidensis* MR-1 mutants lacking MtrC and OmcA were severely impaired in Fe(III) reduction^{100,101}, but also partially impaired in U(VI) reduction¹⁷. In addition, *in vitro*, purified

reduced MtrC and OmcA were oxidized by Fe(III)-chelated soluble species^{102,103}, suggesting that electrons are directly delivered from the outer-membrane *c*-type cytochromes. Indeed, Ross et al. investigated the reduction rates by stopped-flow spectrometry of three soluble complexes of Fe(III), Fe(III)-NTA, Fe(III)-EDTA and Fe(III)-citrate and compared those to whole cells kinetics¹⁰³. In that work, both MtrC and OmcA were re-oxidized upon interaction with the Fe(III) soluble complexes, implying electron transfer by direct contact. Reduction rates were similar to those observed by Wang et al.¹⁰⁴. In addition, Ross et al. probed the reduction of the insoluble iron oxide goethite, and concluded that MtrC and OmcA can directly reduce solid phase iron¹⁰³. Furthermore, experiments carried out using proteoliposomes have evidenced that direct electron transfer is possible between the MtrCAB complex and soluble Fe(III) or insoluble Fe(III) oxides^{89, 91, 105, 106}. In those experiments, the MtrCAB porin complex was inserted in the membrane of proteoliposomes filled with methyl viologen, an electron carrier and color redox indicator¹⁰⁵. Upon exposure to electron acceptors, reduced MV inside the proteoliposomes turned blue, suggesting that electrons were flowing out of the proteoliposomes to reduce soluble Fe(III)⁹¹, or the insoluble Fe(III) phases goethite, lepidocrocite and hematite⁸⁹. Hence these studies support the role of the outer-membrane *c*-type cytochromes MtrC and OmcA in transferring electrons directly to electron acceptors.

1.4.1.2 Indirect electron transfer mediated by soluble electron shuttles

Hartshorne et al. and White et al. demonstrated that the rate of reduction of soluble Fe(III) species by purified MtrC or OmcA is slower than that of the whole cells, suggesting that electron transfer may be enhanced by additional components in the cells^{89,107}. When a biofilm of *S. oneidensis* MR-1 was grown on a carbon electrode, an electron flow was detected, by measuring a current. Upon replacement of the initial medium, the current decreased suggesting that soluble electron transfer mediators secreted were responsible for most of the electron transfer. These mediators were identified to be flavins molecules¹⁰⁸. Okamoto et al. confirmed that the presence of flavin molecules enhances the rate of electron transfer to a tin oxide electrode. Moreover, they demonstrated that flavins interact with outer-membrane cytochromes, as an unstable intermediate of the flavin was identified, probably in association with MtrC or OmcA¹⁰⁹. Furthermore, using proteoliposomes, Wang et al. proposed that the flavin FMN can behave either as a co-factor of the MtrCAB complex, or as an electron free shuttle¹¹⁰. Finally, in Kotloski et al., the *bfe* gene coding for the bacterial flavin adenine dinucleotide exporter was deleted from *S. oneidensis* MR-1. The strain was impaired in the reduction of several iron oxides, and recovered its function when flavins were added to the bioreactor¹¹¹.

1.4.1.3 Membrane extension

S. oneidensis MR-1 produces membrane extensions which extend into the extracellular environment. They were most recently imaged by cryo-tomography¹¹² (Figure 1.9.A.). These membrane extensions are made of a succession of vesicles which are coated with the outer-membrane *c*-type cytochromes where electron transfer can take place, both by direct or indirect contact as presented above.

1.4.2 Reduction of U by *c*-type cytochromes

The MtrCAB-OmcA complex involved in Fe(III) reduction was also shown to play a key role in U reduction. A mutant lacking all *c*-type cytochromes was incubated with U(VI)-carbonate and shown to be impaired in U reduction. Mutants lacking the outer-membrane *c*-type cytochromes MtrC, OmcA, or both were partially impaired¹⁷. In addition, *in vitro*

experiment reacting purified MtrC or OmcA with uranyl(VI)-citrate were conducted and the redox status of the protein hemes followed by stop-flow spectrophotometry¹⁷. MtrC could reduce U(VI) as its hemes were being re-oxidized upon reaction, whereas OmcA could not, even if the mutant strain of *S. oneidensis* MR-1 lacking OmcA was deficient with respect to U(VI) reduction. Furthermore, DNA microarray analysis was performed to examine the gene expression profile of *S. oneidensis* MR-1 during U(VI) reduction¹¹³. 121 genes were upregulated while U(VI) was reduced belonging to two main categories: cytochromes and stress proteins. Genes encoding cytochromes and other electron transport proteins corresponded to putative cytochromes, cytochrome synthesis proteins, reductases and proteins involved in reduction of other electron donors. Namely, genes encoding for proteins involved in Fe(III) electron transport chain, *mtrC*, *mtrB*, *mtrA*, and *omcA* were upregulated, confirming the activity of MtrC and OmcA towards U reduction. As for flavins, Cherkouk et al. observed that riboflavins were not involved in U(VI) reduction although they enhanced reduction rate of Tc(VII), Np(V) and Pu(IV)¹¹⁴. Nevertheless, cyclic voltammetry tests using riboflavin, FMN and FAD showed that flavins chemically reduce U(VI)¹¹⁵

1.4.3 Substrate-binding sites in c-type cytochromes from metal-reducing bacteria

If the involvement of c-type cytochromes in the reduction of soluble metal complexes and insoluble mineral phases was extensively studied, it is still not clear whether MtrC or OmcA have a dedicated binding site for these electron acceptors. In addition, the type of interaction existing between the protein and the substrates is poorly documented. Investigations of binding to iron oxides (Fe₂O₃), using phage display technology led to the identification of possible binding motifs in MtrC and OmcA¹¹⁶. Interestingly, the amino acid sequences of the identified binding motifs were spotted in the sequence of MtrC (Ser-Pro-Ser) and OmcA (Thr-Pro-Ser) close to the terminal heme 10. Molecular dynamics studies revealed that the serine residues involved in these sequences form hydrogen bonds with hematite mineral¹¹⁶(Figure 1.12.A.). These results support those of Kerisit et al., who performed molecular dynamic simulations on the binding of the small tetraheme c-type cytochrome STC and hematite surface¹¹⁷. Most of the mineral-protein interactions found involved binding of a solvent-exposed heme. Most likely the heme binds to the mineral surface with the propionate functional groups of the heme or the carboxylic groups of the residues of amino acid, such as glutamate and aspartate, via hydrogen bonds¹¹⁷. In addition, Fukushima et al. proposed that MtrF can interact electrostatically with the negatively charged hematite surface, via a positively charged patch near hemes 6 and 7 (Figure 1.12.B.). They performed protease foot-printing analysis on MtrF reacted with hematite nanoparticles. When reconstituting the protein sequence, they noticed that some regions were missing, probably corresponding to sites the protease could not access because they were obstructed by iron particles. Additionally, binding to U(VI) was investigated computationally by a single study. Sundararajan et al. looked for a U binding site in the periplasmic tetraheme c-type cytochrome PpcA from *G. sulfurreducens*⁶⁷ (Figure 1.12.C.). According to the calculations, U(VI) binds to the glutamate 31 residue of PpcA, in close vicinity to heme 1. Overall, these studies of potential binding sites suggest that c-type cytochromes are extremely versatile proteins which can interact electrostatically, via hydrogen bonds, or covalent bonds with a variety of substrates.

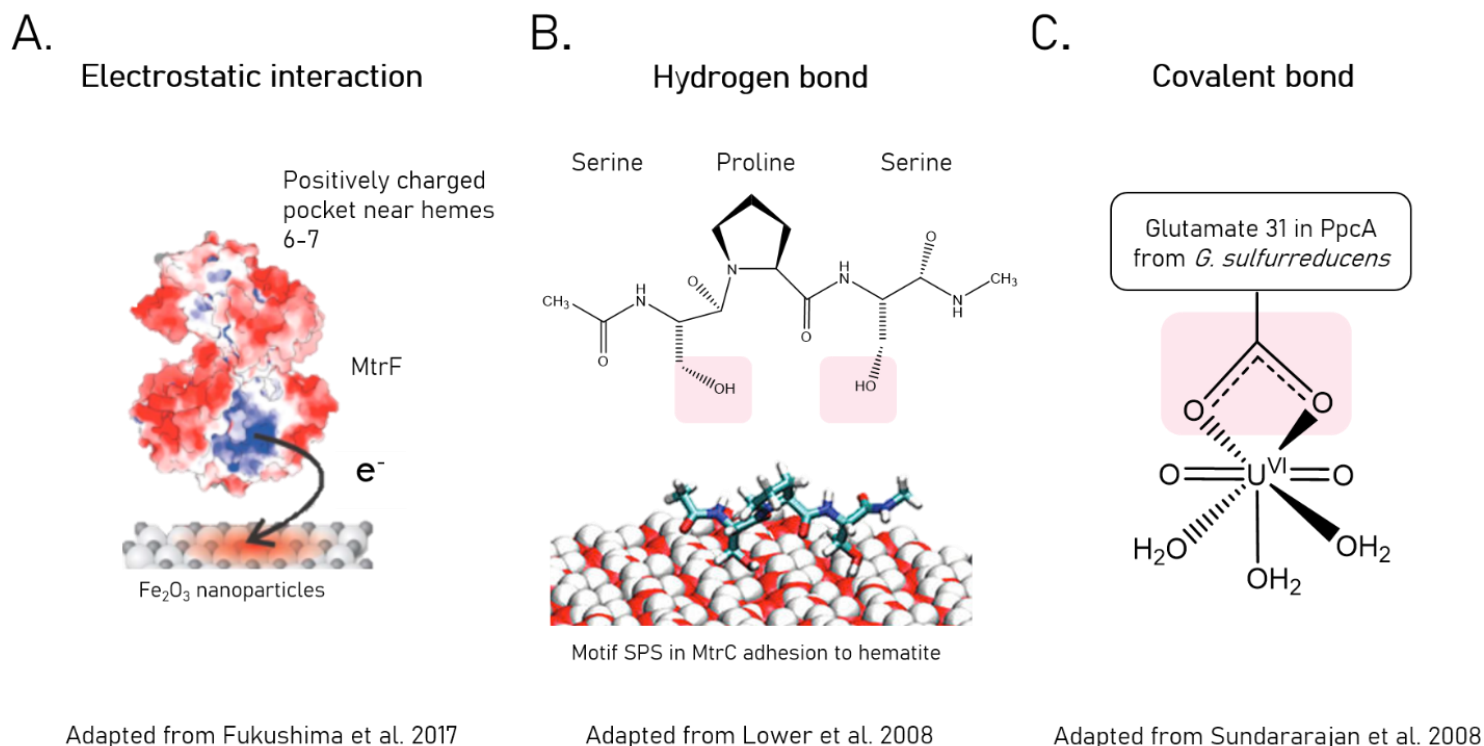


Figure 1:12. Proposed types of interaction between *c*-type cytochromes from DMRB bacteria. A. Electrostatic interaction between MtrF and nanoparticles of iron oxide; B. Hydrogen bonds between MtrC and the surface of hematite; C. Covalent bonds formed between PpcA and uranyl(VI).

1.5 Objectives of the thesis

The uranium biological reduction pathway(s) have been extensively studied, using a variety of metal-reducing bacteria, as it has proven to be an efficient method to remediate contaminated sites, and also provides insights into the redox cycle of U on Earth. However, the mechanism of reduction remains only partially understood. The transformation of a wide range of U(VI) complexes to U(IV) species was well-characterized, but the mechanistic steps were not yet deciphered. Recent studies suggest that U(V) forms as an intermediate, and it was proposed that as U(V) is unstable in water under environmental conditions, as it likely disproportionates to U(VI) and U(IV). Yet, direct experimental evidence accounting for U(V) disproportionation upon biological reduction of U(VI) are limited.

This work aims at investigating the mechanistic steps of U(VI) and U(V) reduction bound to an organic ligand, at both the cell and the enzymatic level. In fact, we found out, through a collaboration with the Group of Complex Chemistry at EPFL, that an aminocarboxylate ligand, dpaea, could stabilize U(V) in water at pH 7.5. This class of ligands is ubiquitous in the environment and could be potential stabilizers for U(V). We chose to focus on the DMRB *S. oneidensis* MR-1 and its outer-membrane *c*-type cytochrome MtrC. On the one hand, at the cellular level, we are interested in studying the formation of U(V) and its subsequent transformation to U(IV), in presence of the dpaea ligand. On the other hand, at the enzymatic level, we seek to investigate the role of *c*-type cytochromes in the transformation of U(V) to U(IV). In addition, we intend to explore the parameters which control the interaction between MtrC and U, using a series of

aminocarboxylate ligands (NTA, EDTA and DTPA). Hence this thesis was conceived in three main parts: (i) Chapter 2 exposes the mechanistic steps of U(VI)-dpaea and U(V)-dpaea reduction by *S. oneidensis* MR-1; (ii) Chapter 3 focuses on the role of *c*-type cytochromes in the reduction of solid phase U(VI)-dpaea and aqueous U(V)-dpaea, in particular that of MtrC; and (iii) Chapter 4 provides an insight in the molecular underpinnings of U(VI) reduction by the *c*-type cytochrome MtrC. A fifth chapter highlights the take-away messages and the future outlooks of this project.

1.5.1 Chapter 2: Biological reduction of a U(V)-organic ligand complex

In this chapter, our goal was to follow the reduction of solid phase U(VI)-dpaea to U(IV) species. In particular, we aimed at identifying whether U(V)-dpaea formed and how it was further transformed to U(IV) species. We demonstrated that *S. oneidensis* MR-1 can reduce U(VI)-dpaea to U(V)-dpaea, and that U(V)-dpaea can be biologically reduced to U(IV) via an additional active one-electron transfer from the bacteria to the U complex. Hence, we gave direct experimental evidence here for the transformation of a U(V) complex to U(IV), and ultimately showed that U(V)-ligand can be reduced and does not necessarily undergo disproportionation.

1.5.2 Chapter 3: Role of *c*-type cytochromes in the reduction of U(VI)-dpaea and U(V)-dpaea complexes

Here, we worked with both whole cells and the purified enzyme MtrC. We first investigated the reduction of solid phase U(VI)-dpaea and U(V)-dpaea using the wild-type strain and two mutant strains of *S. oneidensis* MR-1. The mutant strains lacked either the outer-membrane *c*-type cytochromes or either all *c*-type cytochromes. We observed that solid phase U(VI)-dpaea reduction proceeds via dissolution of the solid, followed by reduction of the soluble U(VI), and that U(V)-dpaea reduction relies on *c*-type cytochromes, in particular the outer-membrane cytochromes. We then used a simplified system consisting of the isolated *c*-type cytochrome MtrC to further investigate the transformation of U(V) to U(IV). We showed that MtrC can directly transfer electrons to U(V)-dpaea, and therefore bolstered the previous finding underlying that U(V)-dpaea undergoes biological reduction by a one-electron transfer, and not disproportionation.

1.5.3 Chapter 4: Speciation-dependent electron transfer from the *c*-type cytochrome MtrC to U(VI)-ligand complexes

In this last experimental chapter, we sought to provide insights in the kinetics of reaction and the interaction between the *c*-type cytochrome MtrC of *S. oneidensis* MR-1 with soluble U(VI) substrates. To this end, we followed the kinetics of reduction of four U(VI) complexes, U(VI)-NTA, U(VI)-EDTA, U(VI)-DTPA and U(VI)-carbonate by both strain MR-1 cells and purified MtrC. We additionally probed the binding extent with both MtrC oxidized and MtrC reduced. With MtrC oxidized, we aimed at evaluating the binding extent of the U(VI) complexes, and with reduced MtrC to quantify the binding of the U(IV) product of reduction. Eventually, we performed M₄-edge-XANES on reduced MtrC reacted with U(VI)-carbonate to follow the reduction over 20min. Our results suggest that the rate of reduction is speciation dependent with both, strain MR-1 cells and MtrC. In particular with MtrC, two clusters of reaction rates were observed. We proposed to correlate these to the nature of the interaction between MtrC and the soluble U(VI) substrates. Hence, we suggest that faster rates could be explained by weak electrostatic binding of the U substrates to MtrC, and slower rates

by stronger binding via hydrogen bonds. As for strain MR-1, we reported here reduction rates of U(VI) bound to NTA, EDTA and DTPA.

1.6 References

- (1) Ribera, D.; Labrot, F.; Tisnerat, G.; Narbonne, J. F. Uranium in the Environment: Occurrence, Transfer, and Biological Effects. *Rev. Environ. Contam. Toxicol.* **1996**, *146*, 53–89.
- (2) Markich, S. J. Uranium Speciation and Bioavailability in Aquatic Systems: An Overview. *ScientificWorldJournal* **2002**, *2*, 707–729. <https://doi.org/10.1100/tsw.2002.130>.
- (3) Veeramani, H.; Alessi, D. S.; Suvorova, E. I.; Lezama-Pacheco, J. S.; Stubbs, J. E.; Sharp, J. O.; Dippon, U.; Kappler, A.; Bargar, J. R.; Bernier-Latmani, R. Products of Abiotic U(VI) Reduction by Biogenic Magnetite and Vivianite. *Geochim. Cosmochim. Acta* **2011**, *75* (9), 2512–2528. <https://doi.org/10.1016/j.gca.2011.02.024>.
- (4) Veeramani, H.; Scheinost, A. C.; Monsegue, N.; Qafoku, N. P.; Kukkadapu, R.; Newville, M.; Lanzirrotti, A.; Pruden, A.; Murayama, M.; Hochella, M. F. Abiotic Reductive Immobilization of U(VI) by Biogenic Mackinawite. *Environ. Sci. Technol.* **2013**, *47* (5), 2361–2369. <https://doi.org/10.1021/es304025x>.
- (5) Scott, T. B.; Allen, G. C.; Heard, P. J.; Randell, M. G. Reduction of U(VI) to U(IV) on the Surface of Magnetite. *Geochim. Cosmochim. Acta* **2005**, *69* (24), 5639–5646. <https://doi.org/10.1016/j.gca.2005.07.003>.
- (6) O'Loughlin, E. J.; Kelly, S. D.; Cook, R. E.; Csencsits, R.; Kemner, K. M. Reduction of Uranium(VI) by Mixed Iron(II)/Iron(III) Hydroxide (Green Rust): Formation of UO₂ Nanoparticles. *Environ. Sci. Technol.* **2003**, *37* (4), 721–727. <https://doi.org/10.1021/es0208409>.
- (7) Yuan; Ilton; S, E.; Antonio; R, M.; Li; Cook; Becker, U. Electrochemical and Spectroscopic Evidence on the One-Electron Reduction of U(VI) to U(V) on Magnetite. *ResearchGate* **2015**, *49* (10). <https://doi.org/10.1021/acs.est.5b00025>.
- (8) Yuan, K.; Renock, D.; Ewing, R. C.; Becker, U. Uranium Reduction on Magnetite: Probing for Pentavalent Uranium Using Electrochemical Methods. *Geochim. Cosmochim. Acta* **2015**, *156*, 194–206. <https://doi.org/10.1016/j.gca.2015.02.014>.
- (9) Ilton, E. S.; Pacheco, J. S. L.; Bargar, J. R.; Shi, Z.; Liu, J.; Kovarik, L.; Engelhard, M. H.; Felmy, A. R. Reduction of U(VI) Incorporated in the Structure of Hematite. *Environ. Sci. Technol.* **2012**, *46* (17), 9428–9436. <https://doi.org/10.1021/es3015502>.
- (10) Lovley, D. R.; Phillips, E. J. P.; Gorby, Y. A.; Landa, E. R. Microbial Reduction of Uranium. *Nature* **1991**, *350* (6317), 413–416. <https://doi.org/10.1038/350413a0>.
- (11) Lovley, D. R.; Roden, E. E.; Phillips, E. J. P.; Woodward, J. C. Enzymatic Iron and Uranium Reduction by Sulfate-Reducing Bacteria. *Mar. Geol.* **1993**, *113* (1–2), 13.
- (12) Burgos, W. D.; McDonough, J. T.; Senko, J. M.; Zhang, G.; Dohnalkova, A. C.; Kelly, S. D.; Gorby, Y.; Kemner, K. M. Characterization of Uraninite Nanoparticles Produced by *Shewanella Oneidensis* MR-1. *Geochim. Cosmochim. Acta* **2008**, *72* (20), 4901–4915. <https://doi.org/10.1016/j.gca.2008.07.016>.

- (13) Bernier-Latmani, R.; Veeramani, H.; Vecchia, E. D.; Junier, P.; Lezama-Pacheco, J. S.; Suvorova, E. I.; Sharp, J. O.; Wigginton, N. S.; Bargar, J. R. Non-Uraninite Products of Microbial U(VI) Reduction. *Environ. Sci. Technol.* **2010**, *44* (24), 9456–9462. <https://doi.org/10.1021/es101675a>.
- (14) Alessi, D. S.; Lezama-Pacheco, J. S.; Stubbs, J. E.; Janousch, M.; Bargar, J. R.; Persson, P.; Bernier-Latmani, R. The Product of Microbial Uranium Reduction Includes Multiple Species with U(IV)–Phosphate Coordination. *Geochim. Cosmochim. Acta* **2014**, *131*, 115–127. <https://doi.org/10.1016/j.gca.2014.01.005>.
- (15) Lloyd, J. R.; Chesnes, J.; Glasauer, S.; Bunker, D. J.; Livens, F. R.; Lovley, D. R. Reduction of Actinides and Fission Products by Fe(III)-Reducing Bacteria. *Geomicrobiol. J.* **2002**, *19* (1), 103–120. <https://doi.org/10.1080/014904502317246200>.
- (16) Gorby, Y. A.; Lovley, D. R. Electron Transport in the Dissimilatory Iron Reducer, GS-15. *Appl. Environ. Microbiol.* **1991**, *57* (3), 867–870.
- (17) Marshall, M. J.; Beliaev, A. S.; Dohnalkova, A. C.; Kennedy, D. W.; Shi, L.; Wang, Z.; Boyanov, M. I.; Lai, B.; Kemner, K. M.; McLean, J. S.; Reed, S. B.; Culley, D. E.; Bailey, V. L.; Simonson, C. J.; Saffarini, D. A.; Romine, M. F.; Zachara, J. M.; Fredrickson, J. K. C-Type Cytochrome-Dependent Formation of U(IV) Nanoparticles by *Shewanella Oneidensis*. *PLoS Biol.* **2006**, *4* (8). <https://doi.org/10.1371/journal.pbio.0040268>.
- (18) Sani, R. K.; Peyton, B. M.; Smith, W. A.; Apel, W. A.; Petersen, J. N. Dissimilatory Reduction of Cr(VI), Fe(III), and U(VI) by *Cellulomonas* Isolates. *Appl. Microbiol. Biotechnol.* **2002**, *60* (1–2), 192–199. <https://doi.org/10.1007/s00253-002-1069-6>.
- (19) Francis, A. J.; Dodge, C. J.; Lu, Fulong.; Halada, G. P.; Clayton, C. R. XPS and XANES Studies of Uranium Reduction by *Clostridium* Sp. *Environ. Sci. Technol.* **1994**, *28* (4), 636–639. <https://doi.org/10.1021/es00053a016>.
- (20) Morss, L. R.; Edelstein, N. M.; Fuger, J. *The Chemistry of the Actinide and Transactinide Elements*; 2011. <https://doi.org/10.1007/978-94-007-0211-0>.
- (21) Selbin, J.; Ortego, J. D. Chemistry of Uranium (V). *Chem. Rev.* **1969**, *69* (5), 657–671. <https://doi.org/10.1021/cr60261a004>.
- (22) Graves, C. R.; Kiplinger, J. L. Pentavalent Uranium Chemistry—Synthetic Pursuit of a Rare Oxidation State. *Chem. Commun.* **2009**, No. 26, 3831–3853. <https://doi.org/10.1039/B902969A>.
- (23) Fortner, J. A.; Kropf, A. J.; Finch, R. J.; Bakel, A. J.; Hash, M. C.; Chamberlain, D. B. Crystal Chemistry of Uranium (V) and Plutonium (IV) in a Titanate Ceramic for Disposition of Surplus Fissile Material. *J. Nucl. Mater.* **2002**, *304* (1), 56–62. [https://doi.org/10.1016/S0022-3115\(02\)00870-X](https://doi.org/10.1016/S0022-3115(02)00870-X).
- (24) Van den Berghe, S.; Laval, J.-P.; Gaudreau, B.; Terryn, H.; Verwerft, M. XPS Investigations on Cesium Uranates: Mixed Valency Behaviour of Uranium. *J. Nucl. Mater.* **2000**, *277* (1), 28–36. [https://doi.org/10.1016/S0022-3115\(99\)00146-4](https://doi.org/10.1016/S0022-3115(99)00146-4).
- (25) Santos, B. G.; Nesbitt, H. W.; Noël, J. J.; Shoesmith, D. W. X-Ray Photoelectron Spectroscopy Study of Anodically Oxidized SIMFUEL Surfaces. *Electrochimica Acta* **2004**, *49* (11), 1863–1873. <https://doi.org/10.1016/j.electacta.2003.12.016>.
- (26) Roberts, H. E.; Morris, K.; Law, G. T. W.; Mosselmans, J. F. W.; Bots, P.; Kvashnina, K.; Shaw, S. Uranium(V) Incorporation Mechanisms and Stability in Fe(II)/Fe(III) (Oxyhydr)Oxides. *Environ. Sci. Technol. Lett.* **2017**, *4* (10), 421–426. <https://doi.org/10.1021/acs.estlett.7b00348>.

- (27) Ilton, E. S.; Haiduc, A.; Cahill, C. L.; Felmy, A. R. Mica Surfaces Stabilize Pentavalent Uranium. *Inorg. Chem.* **2005**, *44* (9), 2986–2988. <https://doi.org/10.1021/ic0487272>.
- (28) Renshaw, J. C.; Butchins, L. J. C.; Livens, F. R.; May, I.; Charnock, J. M.; Lloyd, J. R. Bioreduction of Uranium: Environmental Implications of a Pentavalent Intermediate. *ResearchGate* **2005**, *39* (15), 5657–5660. <https://doi.org/10.1021/es048232b>.
- (29) Großmann, K.; Arnold, T.; Krawczyk-Bärsch, E.; Diessner, S.; Wobus, A.; Bernhard, G.; Krawietz, R. Identification of Fluorescent U(V) and U(VI) Microparticles in a Multispecies Biofilm by Confocal Laser Scanning Microscopy and Fluorescence Spectroscopy. *Environ. Sci. Technol.* **2007**, *41* (18), 6498–6504. <https://doi.org/10.1021/es0710609>.
- (30) Jones, D. L.; Andrews, M. B.; Swinburne, A. N.; Botchway, S. W.; Ward, A. D.; Lloyd, J. R.; Natrajan, L. S. Fluorescence Spectroscopy and Microscopy as Tools for Monitoring Redox Transformations of Uranium in Biological Systems. *Chem. Sci.* **2015**, *6* (9), 5133–5138. <https://doi.org/10.1039/C5SC00661A>.
- (31) Vettese, G. F.; Morris, K.; Natrajan, L. S.; Shaw, S.; Vitova, T.; Galanzew, J.; Jones, D. L.; Lloyd, J. R. Multiple Lines of Evidence Identify U(V) as a Key Intermediate during U(VI) Reduction by *Shewanella Oneidensis* MR1. *Environ. Sci. Technol.* **2020**. <https://doi.org/10.1021/acs.est.9b05285>.
- (32) Molinas, M.; Faizova, R.; Brown, A.; Galanzew, J.; Schacherl, B.; Bartova, B.; Meibom, K. L.; Vitova, T.; Mazzanti, M.; Bernier-Latmani, R. Biological Reduction of a U(V)–Organic Ligand Complex. *Environ. Sci. Technol.* **2021**, *55* (8), 4753–4761. <https://doi.org/10.1021/acs.est.0c06633>.
- (33) Lloyd, J. R.; Leang, C.; Hodges Myerson, A. L.; Coppi, M. V.; Cuifo, S.; Methe, B.; Sandler, S. J.; Lovley, D. R. Biochemical and Genetic Characterization of PpcA, a Periplasmic c-Type Cytochrome in *Geobacter Sulfurreducens*. *Biochem. J.* **2003**, *369* (Pt 1), 153–161. <https://doi.org/10.1042/BJ20020597>.
- (34) Jones, M. B.; Gaunt, A. J. Recent Developments in Synthesis and Structural Chemistry of Nonaqueous Actinide Complexes. *Chem. Rev.* **2013**, *113* (2), 1137–1198. <https://doi.org/10.1021/cr300198m>.
- (35) Natrajan, L.; Burdet, F.; Pécaut, J.; Mazzanti, M. Synthesis and Structure of a Stable Pentavalent-Uranyl Coordination Polymer. *J. Am. Chem. Soc.* **2006**, *128* (22), 7152–7153. <https://doi.org/10.1021/ja0609809>.
- (36) Kern, D. M. H.; Orlemann, E. F. The Potential of the Uranium (V), Uranium (VI) Couple and the Kinetics of Uranium (V) Disproportionation in Perchlorate Media. *J. Am. Chem. Soc.* **1949**, *71* (6), 2102–2106. <https://doi.org/10.1021/ja01174a055>.
- (37) Ekstrom, A. Kinetics and Mechanism of the Disproportionation of Uranium(V). *Inorg. Chem.* **1974**, *13* (9), 2237–2241. <https://doi.org/10.1021/ic50139a035>.
- (38) Steele, H.; Taylor, R. J. A Theoretical Study of the Inner-Sphere Disproportionation Reaction Mechanism of the Pentavalent Actinyl Ions. *Inorg. Chem.* **2007**, *46* (16), 6311–6318. <https://doi.org/10.1021/ic070235c>.
- (39) Ikeda, A.; Hennig, C.; Tsushima, S.; Takao, K.; Ikeda, Y.; Scheinost, A. C.; Bernhard, G. Comparative Study of Uranyl(VI) and -V Carbonato Complexes in an Aqueous Solution. *Inorg. Chem.* **2007**, *46* (10), 4212–4219. <https://doi.org/10.1021/ic070051y>.
- (40) Faizova, R.; Scopelliti, R.; Chauvin, A.-S.; Mazzanti, M. Synthesis and Characterization of a Water Stable Uranyl(V) Complex. *J. Am. Chem. Soc.* **2018**, *140* (42), 13554–13557. <https://doi.org/10.1021/jacs.8b07885>.

- (41) Faizova, R.; Fadaei-Tirani, F.; Bernier-Latmani, R.; Mazzanti, M. Ligand-Supported Facile Conversion of Uranyl(VI) into Uranium(IV) in Organic and Aqueous Media. *Angew. Chem.* **2020**, *132* (17), 6822–6825. <https://doi.org/10.1002/ange.201916334>.
- (42) Macaskie, L. E.; Bonthron, K. M.; Rouch, D. A. Phosphatase-Mediated Heavy Metal Accumulation by a *Citrobacter* Sp. and Related Enterobacteria. *FEMS Microbiol. Lett.* **1994**, *121* (2), 141–146. <https://doi.org/10.1111/j.1574-6968.1994.tb07090.x>.
- (43) Beazley, M. J.; Martinez, R. J.; Sobecky, P. A.; Webb, S. M.; Taillefert, M. Uranium Biomineralization as a Result of Bacterial Phosphatase Activity: Insights from Bacterial Isolates from a Contaminated Subsurface. *Environ. Sci. Technol.* **2007**, *41* (16), 5701–5707. <https://doi.org/10.1021/es070567g>.
- (44) Beazley, M. J.; Martinez, R. J.; Sobecky, P. A.; Webb, S. M.; Taillefert, M. Nonreductive Biomineralization of Uranium(VI) Phosphate Via Microbial Phosphatase Activity in Anaerobic Conditions. *Geomicrobiol. J.* **2009**, *26* (7), 431–441. <https://doi.org/10.1080/01490450903060780>.
- (45) Shelobolina, E. S.; Konishi, H.; Xu, H.; Roden, E. E. U(VI) Sequestration in Hydroxyapatite Produced by Microbial Glycerol 3-Phosphate Metabolism. *Appl. Environ. Microbiol.* **2009**, *75* (18), 5773–5778. <https://doi.org/10.1128/AEM.00628-09>.
- (46) Beveridge, T. J.; Murray, R. G. Sites of Metal Deposition in the Cell Wall of *Bacillus Subtilis*. *J. Bacteriol.* **1980**, *141* (2), 876–887. <https://doi.org/10.1128/jb.141.2.876-887.1980>.
- (47) Jensen, M. L. Sulfur Isotopes and the Origin of Sandstone-Type Uranium Deposits [Colorado Plateau and Wyoming]. *Econ. Geol.* **1958**, *53* (5), 598–616. <https://doi.org/10.2113/gsecongeo.53.5.598>.
- (48) Hostetler, P. B.; Garrels, R. M. Transportation and Precipitation of Uranium and Vanadium at Low Temperatures, with Special Reference to Sandstone-Type Uranium Deposits. *Econ. Geol.* **1962**, *57* (2), 137–167. <https://doi.org/10.2113/gsecongeo.57.2.137>.
- (49) Langmuir, D. Uranium Solution-Mineral Equilibria at Low Temperatures with Applications to Sedimentary Ore Deposits. *Geochim. Cosmochim. Acta* **1978**, *42* (6, Part A), 547–569. [https://doi.org/10.1016/0016-7037\(78\)90001-7](https://doi.org/10.1016/0016-7037(78)90001-7).
- (50) Maynard, J. B. *Geochemistry of Sedimentary Ore Deposits*; Springer-Verlag: New York, 1983. <https://doi.org/10.1007/978-1-4613-9493-8>.
- (51) Woolfolk, C. A.; Whiteley, H. R. REDUCTION OF INORGANIC COMPOUNDS WITH MOLECULAR HYDROGEN BY MICROCOCCUS LACTILYTICUS I. *J. Bacteriol.* **1962**, *84* (4), 647–658.
- (52) Finneran, K. T.; Housewright, M. E.; Lovley, D. R. Multiple Influences of Nitrate on Uranium Solubility during Bioremediation of Uranium-Contaminated Subsurface Sediments. *Environ. Microbiol.* **2002**, *4* (9), 510–516. <https://doi.org/10.1046/j.1462-2920.2002.00317.x>.
- (53) Lovley, D. R.; Phillips, E. J. Reduction of Uranium by *Desulfovibrio Desulfuricans*. *Appl. Environ. Microbiol.* **1992**, *58* (3), 850–856. <https://doi.org/10.1128/aem.58.3.850-856.1992>.
- (54) Payne, R. B.; Gentry, D. M.; Rapp-Giles, B. J.; Casalot, L.; Wall, J. D. Uranium Reduction by *Desulfovibrio Desulfuricans* Strain G20 and a Cytochrome C3 Mutant. *Appl. Environ. Microbiol.* **2002**, *68* (6), 3129–3132. <https://doi.org/10.1128/AEM.68.6.3129-3132.2002>.

- (55) Pietzsch, K.; Babel, W. A Sulfate-Reducing Bacterium That Can Detoxify U(VI) and Obtain Energy via Nitrate Reduction. *J. Basic Microbiol.* **2003**, *43* (4), 348–361. <https://doi.org/10.1002/jobm.200390038>.
- (56) Pietzsch, K.; Hard, B. C.; Babel, W. A Desulfovibrio Sp. Capable of Growing by Reducing U(VI). *J. Basic Microbiol.* **1999**, *39* (5–6), 365–372. [https://doi.org/10.1002/\(SICI\)1521-4028\(199912\)39:5/6<365::AID-JOBM365>3.0.CO;2-C](https://doi.org/10.1002/(SICI)1521-4028(199912)39:5/6<365::AID-JOBM365>3.0.CO;2-C).
- (57) Jeon, B.-H.; Kelly, S. D.; Kemner, K. M.; Barnett, M. O.; Burgos, W. D.; Dempsey, B. A.; Roden, E. E. Microbial Reduction of U(VI) at the Solid–Water Interface. *Environ. Sci. Technol.* **2004**, *38* (21), 5649–5655. <https://doi.org/10.1021/es0496120>.
- (58) Caccavo, F.; Blakemore, R. P.; Lovley, D. R. A Hydrogen-Oxidizing, Fe(III)-Reducing Microorganism from the Great Bay Estuary, New Hampshire. *Appl. Environ. Microbiol.* **1992**, *58* (10), 3211–3216.
- (59) Truex, M. J.; Peyton, B. M.; Valentine, N. B.; Gorby, Y. A. Kinetics of U(VI) Reduction by a Dissimilatory Fe(III)-Reducing Bacterium under Non-Growth Conditions. *Biotechnol. Bioeng.* **1997**, *55* (3), 490–496. [https://doi.org/10.1002/\(SICI\)1097-0290\(19970805\)55:3<490::AID-BIT4>3.0.CO;2-7](https://doi.org/10.1002/(SICI)1097-0290(19970805)55:3<490::AID-BIT4>3.0.CO;2-7).
- (60) Butler, J. E.; Kaufmann, F.; Coppi, M. V.; Núñez, C.; Lovley, D. R. MacA, a Diheme c-Type Cytochrome Involved in Fe(III) Reduction by *Geobacter Sulfurreducens*. *J. Bacteriol.* **2004**, *186* (12), 4042–4045. <https://doi.org/10.1128/JB.186.12.4042-4045.2004>.
- (61) Bernhard, G.; Geipel, G.; Reich, T.; Brendler, V.; Amayri, S.; Nitsche, H. Uranyl(VI) Carbonate Complex Formation: Validation of the $\text{Ca}_2\text{UO}_2(\text{CO}_3)_3(\text{Aq.})$ Species. *Radiochim. Acta* **2001**, *89* (8), 511–518. <https://doi.org/10.1524/ract.2001.89.8.511>.
- (62) Grenthe, I.; Fuger, J.; Lemire, R. J.; Muller, A. B.; Nguyen-Trung Cregu, C.; Wanner, H. Chemical Thermodynamics of Uranium. **1992**.
- (63) Ganesh, R.; Robinson, K. G.; Chu, L.; Kucsmas, D.; Reed, G. D. Reductive Precipitation of Uranium by *Desulfovibrio Desulfuricans*: Evaluation of Cocontaminant Effects and Selective Removal. *Water Res.* **1999**, *33* (16), 3447–3458. [https://doi.org/10.1016/S0043-1354\(99\)00024-X](https://doi.org/10.1016/S0043-1354(99)00024-X).
- (64) Dodge, C. J.; Francis, A. J. Biotransformation of Binary and Ternary Citric Acid Complexes of Iron and Uranium. *Environ. Sci. Technol.* **1997**, *31* (11), 3062–3067. <https://doi.org/10.1021/es961058+>.
- (65) Suzuki, Y.; Tanaka, K.; Kozai, N.; Ohnuki, T. Effects of Citrate, NTA, and EDTA on the Reduction of U(VI) by *Shewanella Putrefaciens*. *Geomicrobiol. J.* **2010**, *27* (3), 245–250. <https://doi.org/10.1080/01490450903456764>.
- (66) Liu, C.; Gorby, Y. A.; Zachara, J. M.; Fredrickson, J. K.; Brown, C. F. Reduction Kinetics of Fe(III), Co(III), U(VI), Cr(VI), and Tc(VII) in Cultures of Dissimilatory Metal-Reducing Bacteria. *Biotechnol. Bioeng.* **2002**, *80* (6), 637–649. <https://doi.org/10.1002/bit.10430>.
- (67) Sundararajan, M.; Campbell, A. J.; Hillier, I. H. Catalytic Cycles for the Reduction of $[\text{UO}_2]^{2+}$ by Cytochrome C7 Proteins Proposed from DFT Calculations. *J. Phys. Chem. A* **2008**, *112* (19), 4451–4457. <https://doi.org/10.1021/jp800209p>.
- (68) Icopini, G. A.; Boukhalfa, H.; Neu, M. P. Biological Reduction of Np(V) and Np(V) Citrate by Metal-Reducing Bacteria. *Environ. Sci. Technol.* **2007**, *41* (8), 2764–2769. <https://doi.org/10.1021/es0618550>.

- (69) Lloyd, J. R.; Yong, P.; Macaskie, L. E. Biological Reduction and Removal of Np(V) by Two Microorganisms. *Environ. Sci. Technol.* **2000**, *34* (7), 1297–1301. <https://doi.org/10.1021/es990394y>.
- (70) Rittmann, B. E.; Banaszak, J. E.; Reed, D. T. Reduction of Np(V) and Precipitation of Np(IV) by an Anaerobic Microbial Consortium. *Biodegradation* **2002**, *13* (5), 329–342. <https://doi.org/10.1023/A:1022382627690>.
- (71) Icopini, G. A.; Lack, J. G.; Hersman, L. E.; Neu, M. P.; Boukhalfa, H. Plutonium(V/VI) Reduction by the Metal-Reducing Bacteria *Geobacter Metallireducens* GS-15 and *Shewanella Oneidensis* MR-1. *Appl. Environ. Microbiol.* **2009**, *75* (11), 3641–3647. <https://doi.org/10.1128/AEM.00022-09>.
- (72) Boukhalfa, H.; Icopini, G. A.; Reilly, S. D.; Neu, M. P. Plutonium(IV) Reduction by the Metal-Reducing Bacteria *Geobacter Metallireducens* GS15 and *Shewanella Oneidensis* MR1. *Appl. Environ. Microbiol.* **2007**, *73* (18), 5897–5903. <https://doi.org/10.1128/AEM.00747-07>.
- (73) Lovley, D. R.; Phillips, E. J. P. Bioremediation of Uranium Contamination with Enzymatic Uranium Reduction. *Environ. Sci. Technol.* **1992**, *26* (11), 2228–2234. <https://doi.org/10.1021/es00035a023>.
- (74) Madden, A. S.; Palumbo, A. V.; Ravel, B.; Vishnivetskaya, T. A.; Phelps, T. J.; Schadt, C. W.; Brandt, C. C. Donor-Dependent Extent of Uranium Reduction for Bioremediation of Contaminated Sediment Microcosms. *J. Environ. Qual.* **2009**, *38* (1), 53–60. <https://doi.org/10.2134/jeq2008.0071>.
- (75) Anderson, R. T.; Vronis, H. A.; Ortiz-Bernad, I.; Resch, C. T.; Long, P. E.; Dayvault, R.; Karp, K.; Marutzky, S.; Metzler, D. R.; Peacock, A.; White, D. C.; Lowe, M.; Lovley, D. R. Stimulating the in Situ Activity of *Geobacter* Species to Remove Uranium from the Groundwater of a Uranium-Contaminated Aquifer. *Appl. Environ. Microbiol.* **2003**, *69* (10), 5884–5891.
- (76) Williams, K. H.; Bargar, J. R.; Lloyd, J. R.; Lovley, D. R. Bioremediation of Uranium-Contaminated Groundwater: A Systems Approach to Subsurface Biogeochemistry. *Curr. Opin. Biotechnol.* **2013**, *24* (3), 489–497. <https://doi.org/10.1016/j.copbio.2012.10.008>.
- (77) Istok, J. D.; Senko, J. M.; Krumholz, L. R.; Watson, D.; Bogle, M. A.; Peacock, A.; Chang, Y.-J.; White, D. C. In Situ Bioreduction of Technetium and Uranium in a Nitrate-Contaminated Aquifer. *Environ. Sci. Technol.* **2004**, *38* (2), 468–475. <https://doi.org/10.1021/es034639p>.
- (78) Nealson, K. H.; Scott, J. Ecophysiology of the Genus *Shewanella*. In *The Prokaryotes: A Handbook on the Biology of Bacteria Volume 6: Proteobacteria: Gamma Subclass*; Dworkin, M., Falkow, S., Rosenberg, E., Schleifer, K.-H., Stackebrandt, E., Eds.; Springer: New York, NY, 2006; pp 1133–1151. https://doi.org/10.1007/0-387-30746-X_45.
- (79) Brown, M. V.; Bowman, J. P. A Molecular Phylogenetic Survey of Sea-Ice Microbial Communities (SIMCO). *FEMS Microbiol. Ecol.* **2001**, *35* (3), 267–275. <https://doi.org/10.1111/j.1574-6941.2001.tb00812.x>.
- (80) Derby, H. A.; Hammer, B. W. *Bacteriology of Butter. IV, IV*; Agricultural Experiment Station, Iowa State College of Agriculture and Mechanic Arts: Ames, Iowa, 1931.
- (81) Myers, C. R.; Nealson, K. H. Microbial Reduction of Manganese Oxides: Interactions with Iron and Sulfur. *Geochim. Cosmochim. Acta* **1988**, *52* (11), 2727–2732. [https://doi.org/10.1016/0016-7037\(88\)90041-5](https://doi.org/10.1016/0016-7037(88)90041-5).
- (82) Scott, J. H.; Nealson, K. H. A Biochemical Study of the Intermediary Carbon Metabolism of *Shewanella Putrefaciens*. *J. Bacteriol.* **1994**, *176* (11), 3408–3411. <https://doi.org/10.1128/jb.176.11.3408-3411.1994>.

- (83) Gorby, Y. A.; Yanina, S.; McLean, J. S.; Rosso, K. M.; Moyles, D.; Dohnalkova, A.; Beveridge, T. J.; Chang, I. S.; Kim, B. H.; Kim, K. S.; Culley, D. E.; Reed, S. B.; Romine, M. F.; Saffarini, D. A.; Hill, E. A.; Shi, L.; Elias, D. A.; Kennedy, D. W.; Pinchuk, G.; Watanabe, K.; Ishii, S.; Logan, B.; Nealson, K. H.; Fredrickson, J. K. Electrically Conductive Bacterial Nanowires Produced by *Shewanella Oneidensis* Strain MR-1 and Other Microorganisms. *Proc. Natl. Acad. Sci. U. S. A.* **2006**, *103* (30), 11358–11363. <https://doi.org/10.1073/pnas.0604517103>.
- (84) Marritt, S. J.; Lowe, T. G.; Bye, J.; McMillan, D. G. G.; Shi, L.; Fredrickson, J.; Zachara, J.; Richardson, D. J.; Cheesman, M. R.; Jeuken, L. J. C.; Butt, J. N. A Functional Description of CymA, an Electron-Transfer Hub Supporting Anaerobic Respiratory Flexibility in *Shewanella*. *Biochem. J.* **2012**, *444* (3), 465–474. <https://doi.org/10.1042/BJ20120197>.
- (85) Ross, D. E.; Ruebush, S. S.; Brantley, S. L.; Hartshorne, R. S.; Clarke, T. A.; Richardson, D. J.; Tien, M. Characterization of Protein-Protein Interactions Involved in Iron Reduction by *Shewanella Oneidensis* MR-1. *Appl. Environ. Microbiol.* **2007**, *73* (18), 5797–5808. <https://doi.org/10.1128/AEM.00146-07>.
- (86) Schuetz, B.; Schicklberger, M.; Kuermann, J.; Spormann, A. M.; Gescher, J. Periplasmic Electron Transfer via the C-Type Cytochromes MtrA and FccA of *Shewanella Oneidensis* MR-1. *Appl. Environ. Microbiol.* **2009**, *75* (24), 7789–7796. <https://doi.org/10.1128/AEM.01834-09>.
- (87) Myers, J. M.; Myers, C. R. Role of the Tetraheme Cytochrome CymA in Anaerobic Electron Transport in Cells of *Shewanella Putrefaciens* MR-1 with Normal Levels of Menaquinone. *J. Bacteriol.* **2000**, *182* (1), 67–75.
- (88) Edwards, M. J.; White, G. F.; Butt, J. N.; Richardson, D. J.; Clarke, T. A. The Crystal Structure of a Biological Insulated Transmembrane Molecular Wire. *Cell* **2020**, *181* (3), 665–673.e10. <https://doi.org/10.1016/j.cell.2020.03.032>.
- (89) White, G. F.; Shi, Z.; Shi, L.; Wang, Z.; Dohnalkova, A. C.; Marshall, M. J.; Fredrickson, J. K.; Zachara, J. M.; Butt, J. N.; Richardson, D. J.; Clarke, T. A. Rapid Electron Exchange between Surface-Exposed Bacterial Cytochromes and Fe(III) Minerals. *Proc. Natl. Acad. Sci. U. S. A.* **2013**, *110* (16), 6346–6351. <https://doi.org/10.1073/pnas.1220074110>.
- (90) Richardson, D. J.; Edwards, M. J.; White, G. F.; Baiden, N.; Hartshorne, R. S.; Fredrickson, J.; Shi, L.; Zachara, J.; Gates, A. J.; Butt, J. N.; Clarke, T. A. Exploring the Biochemistry at the Extracellular Redox Frontier of Bacterial Mineral Fe(III) Respiration. *Biochem. Soc. Trans.* **2012**, *40* (3), 493–500. <https://doi.org/10.1042/BST20120018>.
- (91) Hartshorne, R. S.; Reardon, C. L.; Ross, D.; Nuester, J.; Clarke, T. A.; Gates, A. J.; Mills, P. C.; Fredrickson, J. K.; Zachara, J. M.; Shi, L.; Beliaev, A. S.; Marshall, M. J.; Tien, M.; Brantley, S.; Butt, J. N.; Richardson, D. J. Characterization of an Electron Conduit between Bacteria and the Extracellular Environment. *Proc. Natl. Acad. Sci.* **2009**, *106* (52), 22169–22174. <https://doi.org/10.1073/pnas.0900086106>.
- (92) Shi, L.; Squier, T. C.; Zachara, J. M.; Fredrickson, J. K. Respiration of Metal (Hydr)Oxides by *Shewanella* and *Geobacter*: A Key Role for Multiheme c-Type Cytochromes. *Mol. Microbiol.* **2007**, *65* (1), 12–20. <https://doi.org/10.1111/j.1365-2958.2007.05783.x>.
- (93) Shi, L.; Chen, B.; Wang, Z.; Elias, D. A.; Mayer, M. U.; Gorby, Y. A.; Ni, S.; Lower, B. H.; Kennedy, D. W.; Wunschel, D. S.; Mottaz, H. M.; Marshall, M. J.; Hill, E. A.; Beliaev, A. S.; Zachara, J. M.; Fredrickson, J. K.; Squier, T. C. Isolation of a High-Affinity Functional Protein Complex between OmcA and MtrC: Two Outer Membrane

- Decaheme c-Type Cytochromes of *Shewanella Oneidensis* MR-1. *J. Bacteriol.* **2006**, *188* (13), 4705–4714. <https://doi.org/10.1128/JB.01966-05>.
- (94) Edwards, M. J.; White, G. F.; Norman, M.; Tome-Fernandez, A.; Ainsworth, E.; Shi, L.; Fredrickson, J. K.; Zachara, J. M.; Butt, J. N.; Richardson, D. J.; Clarke, T. A. Redox Linked Flavin Sites in Extracellular Decaheme Proteins Involved in Microbe-Mineral Electron Transfer. *Sci. Rep.* **2015**, *5*, 11677. <https://doi.org/10.1038/srep11677>.
- (95) Edwards, M. J.; Baiden, N. A.; Johs, A.; Tomanicek, S. J.; Liang, L.; Shi, L.; Fredrickson, J. K.; Zachara, J. M.; Gates, A. J.; Butt, J. N.; Richardson, D. J.; Clarke, T. A. The X-Ray Crystal Structure of *Shewanella Oneidensis* OmcA Reveals New Insight at the Microbe–Mineral Interface. *FEBS Lett.* **2014**, *588* (10), 1886–1890. <https://doi.org/10.1016/j.febslet.2014.04.013>.
- (96) Edwards, M. J.; Fredrickson, J. K.; Zachara, J. M.; Richardson, D. J.; Clarke, T. A. Analysis of Structural MtrC Models Based on Homology with the Crystal Structure of MtrF. *Biochem. Soc. Trans.* **2012**, *40* (6), 1181–1185. <https://doi.org/10.1042/BST20120132>.
- (97) Edwards, M. J.; Baiden, N. A.; Johs, A.; Tomanicek, S. J.; Liang, L.; Shi, L.; Fredrickson, J. K.; Zachara, J. M.; Gates, A. J.; Butt, J. N.; Richardson, D. J.; Clarke, T. A. The X-Ray Crystal Structure of *Shewanella Oneidensis* OmcA Reveals New Insight at the Microbe–Mineral Interface. *FEBS Lett.* **2014**, *588* (10), 1886–1890. <https://doi.org/10.1016/j.febslet.2014.04.013>.
- (98) Clarke, T. A.; Edwards, M. J.; Gates, A. J.; Hall, A.; White, G. F.; Bradley, J.; Reardon, C. L.; Shi, L.; Beliaev, A. S.; Marshall, M. J.; Wang, Z.; Watmough, N. J.; Fredrickson, J. K.; Zachara, J. M.; Butt, J. N.; Richardson, D. J. Structure of a Bacterial Cell Surface Decaheme Electron Conduit. *Proc. Natl. Acad. Sci. U. S. A.* **2011**, *108* (23), 9384–9389. <https://doi.org/10.1073/pnas.1017200108>.
- (99) Clarke, T. A.; Edwards, M. J.; Gates, A. J.; Hall, A.; White, G. F.; Bradley, J.; Reardon, C. L.; Shi, L.; Beliaev, A. S.; Marshall, M. J.; Wang, Z.; Watmough, N. J.; Fredrickson, J. K.; Zachara, J. M.; Butt, J. N.; Richardson, D. J. Structure of a Bacterial Cell Surface Decaheme Electron Conduit. *Proc. Natl. Acad. Sci. U. S. A.* **2011**, *108* (23), 9384–9389. <https://doi.org/10.1073/pnas.1017200108>.
- (100) Coursolle, D.; Gralnick, J. A. Modularity of the Mtr Respiratory Pathway of *Shewanella Oneidensis* Strain MR-1. *Mol. Microbiol.* **2010**, *77* (4), 995–1008. <https://doi.org/10.1111/j.1365-2958.2010.07266.x>.
- (101) Reardon, C. L.; Dohnalkova, A. C.; Nachimuthu, P.; Kennedy, D. W.; Saffarini, D. A.; Arey, B. W.; Shi, L.; Wang, Z.; Moore, D.; McLean, J. S.; Moyles, D.; Marshall, M. J.; Zachara, J. M.; Fredrickson, J. K.; Beliaev, A. S. Role of Outer-Membrane Cytochromes MtrC and OmcA in the Biomineralization of Ferrihydrite by *Shewanella Oneidensis* MR-1. *Geobiology* **2010**, *8* (1), 56–68. <https://doi.org/10.1111/j.1472-4669.2009.00226.x>.
- (102) Clarke, T. A.; Holley, T.; Hartshorne, R. S.; Fredrickson, J. K.; Zachara, J. M.; Shi, L.; Richardson, D. J. The Role of Multihaem Cytochromes in the Respiration of Nitrite in *Escherichia Coli* and Fe(III) in *Shewanella Oneidensis*. *Biochem. Soc. Trans.* **2008**, *36* (5), 1005–1010. <https://doi.org/10.1042/BST0361005>.
- (103) Ross, D. E.; Brantley, S. L.; Tien, M. Kinetic Characterization of OmcA and MtrC, Terminal Reductases Involved in Respiratory Electron Transfer for Dissimilatory Iron Reduction in *Shewanella Oneidensis* MR-1. *Appl. Environ. Microbiol.* **2009**, *75* (16), 5218–5226. <https://doi.org/10.1128/AEM.00544-09>.
- (104) Wang, Z.; Liu, C.; Wang, X.; Marshall, M. J.; Zachara, J. M.; Rosso, K. M.; Dupuis, M.; Fredrickson, J. K.; Heald, S.; Shi, L. Kinetics of Reduction of Fe(III) Complexes by Outer Membrane Cytochromes MtrC and OmcA of

- Shewanella Oneidensis MR-1. *Appl. Environ. Microbiol.* **2008**, *74* (21), 6746–6755. <https://doi.org/10.1128/AEM.01454-08>.
- (105) White, G. F.; Shi, Z.; Shi, L.; Dohnalkova, A. C.; Fredrickson, J. K.; Zachara, J. M.; Butt, J. N.; Richardson, D. J.; Clarke, T. A. Development of a Proteoliposome Model to Probe Transmembrane Electron-Transfer Reactions. *Biochem. Soc. Trans.* **2012**, *40* (6), 1257–1260. <https://doi.org/10.1042/BST20120116>.
- (106) Liu, Y.; Wang, Z.; Liu, J.; Levar, C.; Edwards, M. J.; Babauta, J. T.; Kennedy, D. W.; Shi, Z.; Beyenal, H.; Bond, D. R.; Clarke, T. A.; Butt, J. N.; Richardson, D. J.; Rosso, K. M.; Zachara, J. M.; Fredrickson, J. K.; Shi, L. A Trans-Outer Membrane Porin-Cytochrome Protein Complex for Extracellular Electron Transfer by *Geobacter Sulfurreducens* PCA. *Environ. Microbiol. Rep.* **2014**, *6* (6), 776–785. <https://doi.org/10.1111/1758-2229.12204>.
- (107) Hartshorne, R. S.; Reardon, C. L.; Ross, D.; Nuester, J.; Clarke, T. A.; Gates, A. J.; Mills, P. C.; Fredrickson, J. K.; Zachara, J. M.; Shi, L.; Beliaev, A. S.; Marshall, M. J.; Tien, M.; Brantley, S.; Butt, J. N.; Richardson, D. J. Characterization of an Electron Conduit between Bacteria and the Extracellular Environment. *Proc. Natl. Acad. Sci. U. S. A.* **2009**, *106* (52), 22169–22174. <https://doi.org/10.1073/pnas.0900086106>.
- (108) Marsili, E.; Baron, D. B.; Shikhare, I. D.; Coursolle, D.; Gralnick, J. A.; Bond, D. R. *Shewanella* Secretes Flavins That Mediate Extracellular Electron Transfer. *Proc. Natl. Acad. Sci. U. S. A.* **2008**, *105* (10), 3968–3973. <https://doi.org/10.1073/pnas.0710525105>.
- (109) Okamoto, A.; Hashimoto, K.; Neelson, K. H.; Nakamura, R. Rate Enhancement of Bacterial Extracellular Electron Transport Involves Bound Flavin Semiquinones. *Proc. Natl. Acad. Sci. U. S. A.* **2013**, *110* (19), 7856–7861. <https://doi.org/10.1073/pnas.1220823110>.
- (110) Wang, Z.; Shi, Z.; Shi, L.; White, G. F.; Richardson, D. J.; Clarke, T. A.; Fredrickson, J. K.; Zachara, J. M. Effects of Soluble Flavin on Heterogeneous Electron Transfer between Surface-Exposed Bacterial Cytochromes and Iron Oxides. *Geochim. Cosmochim. Acta* **2015**, *163*, 299–310. <https://doi.org/10.1016/j.gca.2015.03.039>.
- (111) Kotloski, N. J.; Gralnick, J. A. Flavin Electron Shuttles Dominate Extracellular Electron Transfer by *Shewanella Oneidensis*. *mBio* **2013**, *4* (1), e00553-12. <https://doi.org/10.1128/mBio.00553-12>.
- (112) Subramanian, P.; Pirbadian, S.; El-Naggar, M. Y.; Jensen, G. J. Ultrastructure of *Shewanella Oneidensis* MR-1 Nanowires Revealed by Electron Cryotomography. *Proc. Natl. Acad. Sci. U. S. A.* **2018**, *115* (14), E3246–E3255. <https://doi.org/10.1073/pnas.1718810115>.
- (113) Bencheikh-Latmani, R.; Williams, S. M.; Haucke, L.; Criddle, C. S.; Wu, L.; Zhou, J.; Tebo, B. M. Global Transcriptional Profiling of *Shewanella Oneidensis* MR-1 during Cr(VI) and U(VI) Reduction. *Appl. Environ. Microbiol.* **2005**, *71* (11), 7453–7460. <https://doi.org/10.1128/AEM.71.11.7453-7460.2005>.
- (114) Cherkouk, A.; Law, G. T. W.; Rizoulis, A.; Law, K.; Renshaw, J. C.; Morris, K.; Livens, F. R.; Lloyd, J. R. Influence of Riboflavin on the Reduction of Radionuclides by *Shewanella Oneidensis* MR-1. *Dalton Trans.* **2016**, *45* (12), 5030–5037. <https://doi.org/10.1039/C4DT02929A>.
- (115) Yamasaki, S.; Tanaka, K.; Kozai, N.; Ohnuki, T. Effect of Flavin Compounds on Uranium(VI) Reduction- Kinetic Study Using Electrochemical Methods with UV-Vis Spectroscopy. *Appl. Geochem.* **2017**, *78*, 279–286. <https://doi.org/10.1016/j.apgeochem.2017.01.014>.

- (116) Lower, B. H.; Lins, R. D.; Oestreicher, Z.; Straatsma, T. P.; Hochella, M. F.; Shi, L.; Lower, S. K. In Vitro Evolution of a Peptide with a Hematite Binding Motif That May Constitute a Natural Metal-Oxide Binding Archetype. *Environ. Sci. Technol.* **2008**, *42* (10), 3821–3827.
- (117) Kerisit, S.; Rosso, K. M.; Dupuis, M.; Valiev, M. Molecular Computational Investigation of Electron-Transfer Kinetics Across Cytochrome–Iron Oxide Interfaces. *J. Phys. Chem. C* **2007**, *111* (30), 11363–11375. <https://doi.org/10.1021/jp072060y>.

Chapter 2 Biological reduction of a U(V)-organic ligand complex

Chapter 2 studies the biological reduction of U(VI)-dpaea and U(V)-dpaea by the microorganism *Shewanella oneidensis* MR-1. The U-dpaea complexes were used as models to simulate the behaviour of similar U-aminocarboxylate ligands which could be found in the environment.

This work is published in Environmental Science and Technology as follows:

Molinas, M.; Faizova, R.; Brown, A.; Galanzew, J.; Schacherl, B.; Bartova, B.; Meibom, K. L.; Vitova, T.; Mazzanti, M.; BernierLatmani, R. Biological Reduction of a U(V)–Organic Ligand Complex. *Environ. Sci. Technol.* **2021**, 55 (8), 4753–4761. <https://doi.org/10.1021/acs.est.0c06633>.

Author Contributions :

The manuscript was written through contributions from all authors. RBL and MMA conceived of the research. MMo performed all the experiments with support from RF who synthesized the U-dpaea complexes, AB, who developed the ion-exchange chromatography method, BB, who performed the STEM analysis, and TV, JG, and BS who assisted with the HR-XANES measurements. All authors gave their approval for the final version of the manuscript.

Abstract

Metal-reducing microorganisms such as *Shewanella oneidensis* MR-1 reduce highly soluble species of hexavalent uranyl (U(VI)) to less mobile tetravalent uranium (U(IV)) compounds. The biologically-mediated immobilization of U(VI) is being considered for the remediation of U contamination. However, the mechanistic underpinnings of biological U(VI) reduction remain unresolved. It has become clear that a first electron transfer occurs to form pentavalent (U(V)) intermediates, but it has not been definitively established whether a second one-electron transfer can occur or if disproportionation of U(V) is required. Here, we utilize the unusual properties of dpaea²⁻ ((dpaeaH₂=Bis(pyridyl-6-methyl-2-carboxylate)-ethylamine)), a ligand forming a stable soluble aqueous complex with U(V), and investigate the reduction of U(VI)-dpaea and U(V)-dpaea by *S. oneidensis* MR-1. We establish U speciation through time by separating U(VI) from U(IV) by ion exchange chromatography and characterize the reaction end-products using U M₄-edge High Resolution X-ray Absorption Near-Edge Structure (HR-XANES) spectroscopy. We document the reduction of solid phase U(VI)-dpaea to aqueous U(V)-dpaea but, most importantly, demonstrate that of U(V)-dpaea to U(IV). This work establishes the potential for biological reduction of U(V) bound to a stabilizing ligand. Thus, further work is warranted to investigate the possible persistence of U(V)-organic complexes followed by their bioreduction in environmental systems.

2.1 Introduction

The environmental behavior of uranium (U) is driven by its redox chemistry. In its oxidized cationic form, U(VI) (UO₂²⁺), it is highly soluble and mobile when forming stable complexes with appropriate ligands (e.g., carbonate)^{1,2}, whereas in its reduced form, U(IV), it tends to precipitate as crystalline U oxides¹⁰ or in an amorphous U phase¹³. These physicochemical properties have been proposed for the remediation of U-contaminated areas by immobilizing U as U(IV)¹¹⁷. The transition from U(VI) to U(IV) occurs via the transfer of 2 electrons by a microorganism^{10,13,11,19,17,118}, such as dissimilatory metal-reducing bacteria (DMBR) *Geobacter sulfurreducens*¹⁰ or *Shewanella oneidensis* MR-1^{13,17,118}, or a reduced mineral phase, such as ferrous iron-bearing minerals^{3,4,6,119}. In both mineral and biological cases, a pentavalent U(V) intermediate has been shown to form following a one-electron transfer to the U(VI) moiety^{9,7,120,26,28,29–31,121}. Furthermore, U(V) appears to persist under certain environmentally-relevant conditions^{9,7}, however it remains challenging to detect it, due to its sensitivity to oxidation and its ability to undergo rapid disproportionation to U(VI) and U(IV), through the interaction of two uranyl(V) cations (i.e., cation-cation interaction, CCI)³⁸.

If the biological formation of U(V) has been documented repeatedly as the result of a one-electron transfer from bacteria to U(VI), the transformation of U(V) to U(IV) has yet to be clarified. Indeed, it has been suggested in multiple studies that uranyl(V) forms and disproportionates to uranyl(VI) ion and a U(IV) species^{28,29–31,121}. In those studies, U(VI) reduction was monitored in a carbonate-rich buffer in the presence of *Geobacter sulfurreducens*^{28,30}, *Shewanella oneidensis* MR-1³¹ or a microbial biofilm²⁹. Direct experimental evidence of uranyl(V) arose from EXAFS analysis of the incubation supernatants of *G. sulfurreducens*²⁸, and recently from M₄-edge HR-XANES on cell suspensions of *S. oneidensis* MR-1³¹. As for the second step of the biological reduction, these studies support the disproportionation of uranyl(V), which leads to U(VI) and U(IV). In fact, Renshaw et al. justify uranyl(V) disproportionation in their system by substituting stable Np(V) to U(V) in their experiment and reporting its lack of reduction²⁸. By analogy, the authors conclude that U(V) would not

either, and thus that U(V) disproportionates to form U(IV). Such observations were later supported by Jones et al.³⁰ and more recently by Vettese et al.³¹, who report a saw-tooth profile for uranyl(VI) fluorescence in cell suspensions of *G. sulfurreducens* and *S. oneidensis* MR-1, respectively^{30,31}. The repeated increases in the U(VI) fluorescence intensity, forming the saw-tooth profile, are interpreted as U(V) disproportionation releasing uranyl(VI).

However, these experiments were conducted in carbonate-rich buffer^{28,31} in which the disproportionation of U(V) is rapid at circumneutral pH¹²². In the environment, biological U(VI) reduction often occurs in organic-rich environments^{123,124}. In light of the fact that other pentavalent actinides, such as Np(V) and Pu(V), are reduced to Np(IV)⁶⁷ and Pu(IV)⁷⁰ by *S. oneidensis*, stabilization of U(V) by organic ligands may allow the direct biological reduction of U(V) to U(IV).

In order to fully characterize the mechanism of biological transformation of U(V) to U(IV), we sought direct evidence of the biological reduction of U(V) by *S. oneidensis* MR-1, using an original approach—the stabilization of soluble U(V) with the novel ligand, dpaea²⁻ (dpaeaH₂=Bis(pyridyl-6-methyl-2-carboxylate)-ethylamine). Dpaea belongs to the class of aminocarboxylate ligands, characterized by one or more nitrogen atom(s) bonded to a carboxylic group via a carbon atom. These ligands have the propensity to chelate metal ions (such as Fe³⁺, Cu²⁺, Zn²⁺)¹²⁵. Dpaea contains the pyridinecarboxylate metal-binding groups also found in dipicolinic acid. Aminocarboxylate ligands are found naturally in the environment. In fact, they are produced as dipicolinic acid in bacterial endospores¹²⁶, or nicotianamide in gramineous plants¹²⁷. In addition, because of their chelation potential, they are applied to remediate metal-contaminated sites (for instance ethylenediaminetetraacetic (EDTA), nitrilotriacetic acid (NTA), ethylenediamine-*N,N'*-disuccinic acid (EEDS))¹²⁸, or support radionuclide extraction in nuclear wastes (for instance, diethylenetriaminepentaacetic acid DTPA)^{129,130,131,132}.

The two goals of this work were to confirm that U(V) forms as a pathway intermediate in the presence of complexing ligands such as dpaea and to establish whether U(V)-dpaea undergoes further biological reduction to U(IV). We would like to note that direct reduction of the U(V)-dpaea complex by chemical reagents has been recently observed by some of the authors in both organic solvents and in water-affording monometallic ([U^{IV}(dpaea)(OBpin)₂(py)] and trimetallic ([Na(H₂O)₅U(dpaea)]₃(μ-O)₂(μ-OH)(μ₃-SO₃))] complexes, respectively⁴¹. Previously reported complexes of dpaea with uranium include U(VI)-dpaea ([UO₂(dpaea)]), U(V)-dpaea ([K(2.2.2.crypt)][UO₂(dpaea)]), U(IV)-dpaea (U(dpaea)₂)^{40,41} and the trinuclear uranium(IV) μ-oxo/hydroxo bridged cluster [Na(H₂O)₅U(dpaea)]₃(μ-O)₂(μ-OH)(μ₃-SO₃)] obtained from the chemical reduction of U(VI)- and U(V)-dpaea in water. The U(V)-dpaea complex is stable and soluble in water at pH 7, allowing for the persistence of the ordinarily transient pentavalent species⁴⁰. Here, we monitored U oxidation state through time using a combination of spectroscopic, spectrophotometric, and separation techniques. We report the reduction of U(VI)-dpaea to uranyl(V)-dpaea, and observe the further reduction to a solid-phase, non-crystalline U(IV) product. Hence, we suggest that the biological reduction of U(VI)-dpaea occurs via two successive one-electron transfers, rather than via disproportionation of the U(V)-dpaea intermediate. The reaction proceeds as follows: (i) U(VI)-dpaea_(s) to U(V)-dpaea_(aq), and then (ii) U(V)-dpaea_(aq) to non-crystalline U(IV) and organic complexes of U(IV)_(s).

2.2 Experimental methods

2.2.1 Construction of the *ccmG* deletion mutant

Regions flanking *ccmG* (SO_0267) in *S. oneidensis* MR-1 were amplified by PCR with primers *ccmG_5'O/ccmG_5'I* and *ccmG_3'I/ccmG_3'O* (table S1), fused by overlap extension PCR and cloned into suicide plasmid pMQS [2]. Overnight cultures of *S. oneidensis* MR-1 and *Escherichia coli* WM3064 with the plasmid pMQS-*ccmG*, carrying the *ccmG* deletion construct (table S2) were mixed and incubated on LB agar with diaminopimelic acid (DAP). Next, *S. oneidensis* colonies with a single crossover plasmid insertion were selected on LB agar supplemented with 50 µg/mL kanamycin (without DAP). Individual colonies were streaked on LB with kanamycin, and then grown in LB devoid of NaCl followed by incubation on LB agar plates (without NaCl) supplemented with 10% sucrose to select for a second crossover event. Colonies were then streaked in parallel on LB agar plates with kanamycin and LB with sucrose, and kanamycin sensitive and sucrose resistant colonies were tested by PCR using primers *ccmG_FO/ccmG_RO* (table S1). Colonies containing a deletion of *ccmG* were identified by the size of the PCR product and a deletion was further indicated by the white color of the colonies compared to the reddish color of the WT strain. The PCR product of the mutant strain used was additionally sequenced to confirm the deletion of *ccmG*.

2.2.2 Strain growth and conditions

To grow *Shewanella oneidensis* MR-1 and $\Delta ccmG$, a liquid pre-culture was started from a frozen stock (-80°C) and grown overnight in Luria-Bertani (LB) medium at 30°C in a shaking incubator (140 rpm). An aliquot of this pre-culture was further inoculated in fresh LB with a starting OD₆₀₀ of 0.1. When the culture reached an OD₆₀₀ of 2 (mid- to late-exponential phase), the cells were harvested by centrifugation at 9,610 ×g for 10 minutes at room temperature, and washed three times anoxically with modified Widdel low phosphate (WLP) medium at pH 7.3, prior to amendment with U. The modified WLP medium lacked bicarbonate and phosphate to prevent their complexation of U (Table S3).

2.2.3 Resting cell experiments

2.2.3.1 Reduction of U(VI)-dpaea

All manipulations were performed inside a nitrogen-atmosphere anaerobic chamber (MBraun, Germany), with O₂ < 0.1 ppm. *S. oneidensis* MR-1 was incubated, under non-growth conditions, in anoxic modified WLP medium (Table S3) in the presence of solid phase U(VI)-dpaea ([UO₂(dpaea)] MW = 583 g.mol⁻¹) at an equivalent aqueous concentrations of 2.5 mM, and synthesized as previously described⁴⁰, along with 20 mM of lactate as the electron donor. The starting OD₆₀₀ of the incubations was measured to be 1. The incubations were maintained in the dark at room temperature, inside the anaerobic chamber. At several time points, an entire culture was sacrificed for analysis purposes. Solid phase U was separated by centrifugation (10 minutes at 12,100 ×g) and the supernatant was further filtered through 0.2 µm PTFE filters (Whatman, Maidstone, United Kingdom). Aliquots of the filtered supernatant were saved for U concentration determination and for HR-XANES measurements. In the latter case, the supernatant and the solid phase were instantaneously frozen in the glovebox with a cold trap filled with liquid nitrogen. Both solid and aqueous phases were also retained for further separation by ion exchange chromatography, as described below.

2.2.3.2 Reduction of U(V)-dpaea

As U(V) is highly sensitive to oxidation, all materials were left at least 24 hours under vacuum prior to entering the anoxic chamber, and allowed to equilibrate for 2-3 days under anoxic conditions before use. Regarding the preparation of the cells, in addition to the three washes in modified anoxic WLP, 10 min cycles of vacuum followed by nitrogen injection were done (in the headspace of a 10 mL anaerobic glass vial). Two sets of experiments were performed. The first set (called 'biological'), used as a starting material U(V)-dpaea biologically produced via reduction of U(VI)-dpaea with *S. oneidensis* MR-1 (described above). The supernatant of the culture incubated with U(VI)-dpaea was recovered by filtration through 0.2 μm filters. As U(VI)-dpaea is insoluble, the majority of U in solution was expected (and later confirmed) to be U(V)-dpaea. The second set (called 'synthetic') used synthetic U(V)-dpaea prepared as previously described ($[(\text{K}(\text{2.2.2.cryptand}))[\text{UO}_2(\text{dpaea})]]$ MW = 998.93 g.mol⁻¹)⁴⁰. For both starting materials, *S. oneidensis* MR-1 was incubated with soluble U(V)-dpaea and 20 mM lactate. The initial concentration of U in the 'biological' set was 50 μM (corresponding to about 100 μg of U(V)-dpaea) and in the 'synthetic' set, 30 μM (corresponding to 60 μg of U(V)-dpaea). Both types of systems were incubated for 41 days in the glovebox, in the dark.

All experiments were conducted in duplicate and a no-cell control experiment was performed in parallel. The no-cell control experiment consisted of U(V)-dpaea, either 'biological' or 'synthetic', in modified WLP anoxic media (identical to the one used for the cells) in the presence of 20 mM lactate. At specific times, entire cultures were sacrificed from each 'biological' and 'synthetic' U(V)-dpaea incubations, and associated no-cell or inactive cell controls (where relevant), followed by separation of U(VI) and U(IV) by ion exchange chromatography. Confirmatory UV-vis characterization was performed in selected cases (Text S1 and Figure S1).

Additionally, experiments were conducted with a control consisting of a deletion mutant lacking one gene from the maturation system of the c-type cytochrome pool, ΔccmG (Text S2, Figure S2, Tables S1 and S2).

In order to analyze the end-product of reduction by U M₄-edge HR-XANES spectroscopy, solid phase U was recovered by centrifugation after 4 days of incubation of *S. oneidensis* MR-1 with 400 μM biologically produced U(V)-dpaea and stored frozen until analysis.

2.2.4 Ion-exchange chromatography

Ion exchange chromatography was performed to resolve the U oxidation state in both the solid and aqueous phases as a function of time, for both the U(VI) and U(V) reduction experiments described in the previous sections. Separation was achieved with Dowex 1 \times 8 powder (100-200 mesh; chloride form) packed in polypropylene chromatography columns (Poly-Prep®, Bio-Rad, Hercules, California, United-States) inside the anaerobic chamber. The Dowex resin is a strongly basic cationic resin which allows the separation of U(VI) from U(IV) in an HCl-acidified sample^{133,134}. For U(VI) reduction experiments, aqueous phases (supernatants) were collected and diluted in anoxic HCl to a final concentration of 4.5M HCl, and solid phases (cell pellets) were digested in 4.5M HCl. After digestion, samples were loaded onto resin slurry-packed columns that were pre-treated with 4.5 M HCl. The U(IV) fraction was eluted first in about 30 mL of anoxic 4.5M HCl (15 bed volumes), followed by elution of the U(VI) fraction in 0.1M HCl, again in approximately 15 bed volumes of eluent. All separations were performed in analytical grade HCl.

2.2.5 Uranium quantification

U concentration was measured by Inductively Coupled Plasma Mass Spectrometry (ICP-MS, Perkin-Elmer ELAN DRC 2) for both filtered supernatants and samples eluted from the ion exchange chromatography test. Dilutions to a range of 1 to 10 ppb of U were performed in a matrix of 1% HNO₃ prior to analysis. All samples were measured in technical duplicates. Measurement and standard deviation values for the ion-exchange chromatography results are gathered in Table S4 for all measurement U concentration was measured by Inductively Coupled Plasma Mass Spectrometry (ICP-MS, Perkin-Elmer ELAN DRC 2) for both filtered supernatants and samples eluted from the ion exchange chromatography test. Dilutions to a range of 1 to 10 ppb of U were performed in a matrix of 1% HNO₃ prior to analysis. All samples were measured in technical duplicates. Measurement and standard deviation values for the ion-exchange chromatography results are gathered in Table S4 for all measurements.

2.2.6 HR-XANES

U M₄-edge (3.726 keV) HR-XANES was used to elucidate the oxidation state of U in selected samples. Spectra were collected at the station for actinide science (ACT) at the CAT-ACT beamline at the Karlsruhe Research Accelerator (KARA), Karlsruhe, Germany. The CAT-ACT beamline is equipped with a Johann type X-ray emission spectrometer¹³⁵. The incident beam was monochromatized by a Si(111) double crystal monochromator (DCM) and focused onto the sample to a spot size of about 500 µm x 500 µm. The X-ray emission spectrometer consists of four Si (110) crystals with 1 m bending radius and a single diode VITUS silicon drift detector (Ketek, Germany), which together with the sample are arranged in a vertical Rowland circle geometry. A UO₂ reference was used to calibrate the spectra. The main absorption maximum was set to 3.275 keV. The sample cells were placed in an inert gas cell and were constantly flushed with He, maintaining anoxic conditions. The X-ray spectrometer was inside a He flushed box in order to minimize intensity loss due to absorption or scattering of photons. Wet pastes and liquid samples were loaded into the sample holder in an anaerobic chamber, frozen immediately and stored on dry ice until the measurements. Regarding data processing, normalization and linear combination fits (LCF) were performed using the ATHENA software¹³⁶. The spectra obtained for the wet pastes and the liquids were modeled using the references U(VI)-dpaea, U(V)-dpaea and U(IV)-dpaea₂, for which spectra were also collected and analyzed in the same manner. The goodness of fit was evaluated with two statistical parameters, the R-factor and the reduced χ^2 , which were minimized by the fitting algorithm.

2.2.7 Electron microscopy

The solid phase U(IV) product associated with the biomass of a 3-month-old incubation was collected by centrifugation (10 minutes at 12,100 ×g) in a N₂ atmosphere. The pellet was resuspended in 100 µL anoxic 100% ethanol. 2 µL of this mixture were loaded onto an ultra-thin carbon grid (Electron Microscopy Sciences CF200-CU-UL; 200 µm square mesh; 3-4 nm carbon foil; copper grid; silicon free) and allowed to dry in an anoxic chamber for 5 min. The grid was exposed for about 1 min to the ambient atmosphere when mounted on the microscope holder. The samples were first analyzed by Bright Field 9 STEM to describe the morphology of U, and then by energy dispersive x-ray spectroscopy (EDS) to identify the predominant elements in association with U. The high-resolution TEM (HR-TEM) mode was used to probe the crystallinity of the U(IV) product by recording Selected Area Electron Diffraction (SAED) patterns on the U morphologies of interest. The analysis was performed with a beam energy of 200 keV and a beam current of 1 nA.

2.3 Results

2.3.1 Reduction of U(VI)-dpaea

2.3.1.1 Transformation of U(VI)-dpaea by *S. oneidensis* MR-1

U(VI) reduction by strain MR-1 has been studied extensively^{10,13,17,118,31}. Here, in contrast to most previous studies, we considered the reduction of solid phase U(VI), in the form of U(VI)-dpaea. In fact, we expected that the reduction of U(VI)-dpaea would result in the formation of the soluble U(V)-dpaea complex⁴⁰, effectively reductively mobilizing U. Therefore, we monitored U concentration in the incubation supernatants through time by ICP-MS. As illustrated in Figure 2:1.A., we observed an increase in the U concentration in the culture supernatants, up to 1.9 mM (corresponding to 75% of total U) after 96h of incubation. The no-cell control experiments showed a low U concentration in solution (50 μ M, corresponding to 2% of total U in this experiment) due to the low solubility of the U(VI)-dpaea complex (Figure S3). Thus, we propose that solid phase U(VI)-dpaea was being transformed by *S. oneidensis* MR-1, forming soluble U species. In addition, we noticed that the aqueous phase turned pink.

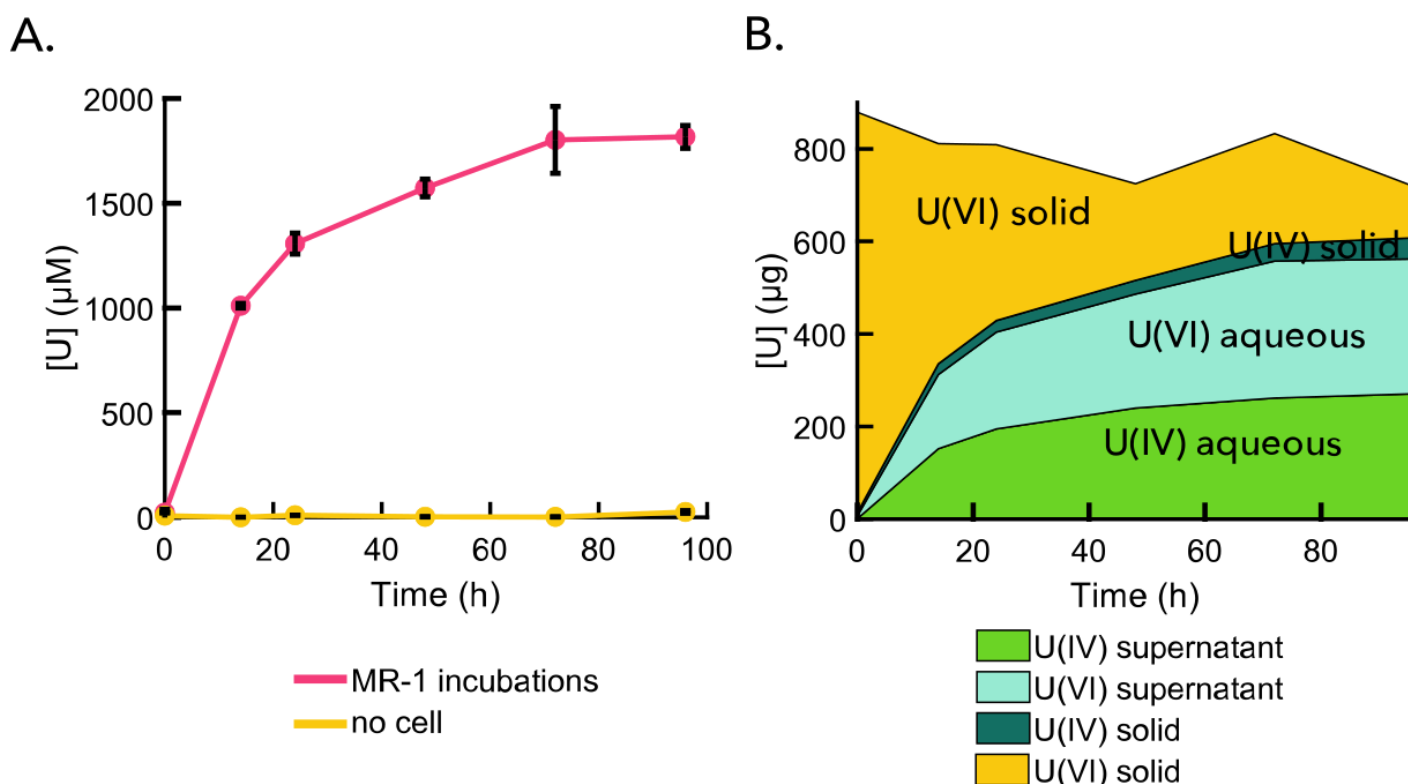


Figure 2:1. Incubation of MR-1 cells with U(VI)-dpaea. A. U concentration in the incubation supernatants (pink dots) and in no-cell controls (yellow dots), measured from 0 to 96h of incubation with U(VI)-dpaea (in duplicates). B. U speciation in the solid phase and in the aqueous phase of the incubations (in μ g). The U(VI) and U(IV) fractions were obtained by ion exchange chromatography.

Therefore, we attempted to follow the reaction by UV-vis spectroscopy (Figure S1.A.). UV-vis spectra of the aqueous phase were collected at 0h, 24h and 72h. At 0h, we did not detect any light-absorbing compound. However, after 24h and 72h, light absorbance was detected and the spectra showed a broad line with a maximum at 460nm. By comparing this spectrum with the reference spectra of U(V)-dpaea under identical conditions, we hypothesized that U(V)-dpaea was formed in the aqueous phase of the incubations.

2.3.1.2 Ion exchange chromatography of U(VI) and U(IV)

In order to further confirm our hypothesis that the soluble U product that accumulated in the aqueous phase was pentavalent U, we performed ion exchange chromatography. For each time point, we were able to delineate the contribution of U(VI) and U(IV) as shown in Figure 2:1.B and Table S4. As the amount of solid phase U(VI)-dpaea decreased, we observed the formation of a small amount of solid phase U(IV), and increasing U(VI) and U(IV) in the aqueous phase. The ion exchange chromatography separation cannot directly identify U(V), because the samples are acidified prior to loading onto the column. Acid treatment is known to disproportionate uranyl(V) and to produce equal proportions of U(VI) and U(IV)¹²². We observed that, at all incubation times analyzed, aqueous U(VI) and U(IV) were distributed in the supernatants at a contribution of 55% and 45%, respectively, suggesting that U(V)-dpaea formed and accumulated in the supernatant. The slight excess of aqueous U(VI) (corresponding to 50 μ M U) was attributed to the solubility (albeit low) of U(VI)-dpaea (Figure S3).

To confirm that the obtained ratio of U(VI) and U(IV) is a proxy for U(V)-dpaea, we eluted a preparation of 600 μ M synthetic U(V)-dpaea under similar conditions. After acidification and separation, U concentrations in the U(VI) and U(IV) fractions were 294.6 μ M and 294.4 μ M, respectively. This test confirmed that a 1:1 U(VI)/U(IV) ratio obtained after ion exchange chromatography separation, corresponds to U(V).

2.3.1.3 M₄-edge HR-XANES

To provide further evidence for the oxidation state of U in the aqueous and solid phases, we collected M₄-edge HR-XANES spectra. Late time points were selected in order to ensure that a sufficiently high concentration of U had accumulated in the aqueous phase to allow the acquisition of spectra with high signal to noise ratio (Figure 2:2). The energy positions of the first intense absorption peak of the spectra of the U(IV)-dpaea, U(V)-dpaea and U(VI)-dpaea references shift to higher energies in the order U(IV), U(V), U(VI) (Figure 2:2.A.). The energy positions of the spectral features are listed in Table 2:1. The spectra of U(VI)-dpaea and U(V)-dpaea displayed shapes typical for uranyl(VI) (UO₂²⁺) and uranyl(V), respectively^{137,138}. The spectra obtained for the supernatants (aqueous phase) collected after 72h and 96h of incubation (Figure 2:2.A.) resembled closely that of U(V)-dpaea, which confirms the ion exchange chromatography results (Figure 2:2:1.). The spectra of the samples feature two intense peaks with maxima at 3.7258 keV and 3.7272 keV for the 72-hour sample and at 3.7260 keV and 3.7272 keV for the 96-hour sample. In comparison, the U(V)-dpaea standard exhibits peak maxima of those peaks at 3.7258 keV and 3.7271 keV (Table 2:1.).

Sample	white line (keV)	2nd peak (keV)	3rd peak (keV)
Standards			
U(IV)-dpaea ₂	3.7253	-	-
U(V)-dpaea	3.7258	3.7271	3.7297
U(VI)-dpaea	3.7268	3.7288	3.7328
U(VI)-dpaea reduction			
Aqueous phase 72h	3.7260	3.7272	3.7297
Aqueous phase 96h	3.7258	3.7272	3.7298
Solid phase 150h	3.7268	3.7289	3.7326
U(V)-dpaea reduction			
Cell pellet 85h	3.7257	-	-

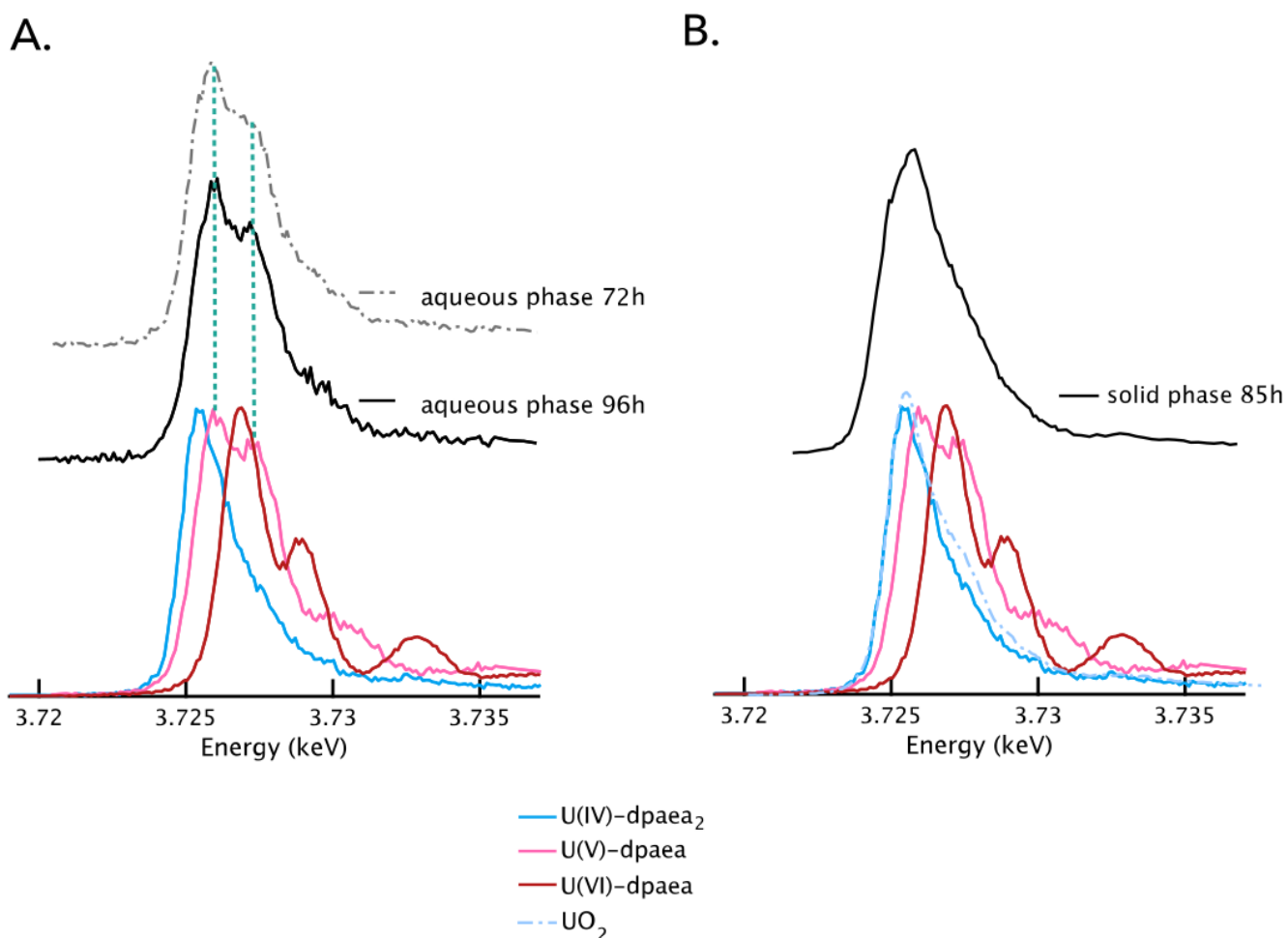
Table 2:1. U M₄-edge main spectral features measured in this study.

Figure 2:2. U M₄-edge HR-XANES spectra demonstrating reduction of (A) U(VI)-dpaea and (B) biologically-produced U(V)-dpaea. The references U(VI)-dpaea (in red), U(V)-dpaea (in pink) and U(IV)-dpaea₂ (in blue) are presented in both panels. The spectra obtained for UO₂ is shown as a dashed line. U(IV)-dpaea₂ was used as a reference and likely does not fully characterize the U(IV) phases present. In addition to the references, the spectra obtained for (A) the aqueous phase after 72h and 96h of incubation, and for (B) the solid phase (cell pellet) collected after 85h of incubation of *S. oneidensis* MR-1 with U(V)-dpaea are presented.

Moreover, linear combination fits (LCF) (Figure 2:2:3. and S4) revealed that both supernatants contained more than 80% U(V), as reported in Table 2:2.. Furthermore, the split peak at 3.7258-3.7260 keV to 3.7272 keV in both the uranyl(V) standard and the samples (Figure 2:2:3.) indicated the presence of uranyl(V) rather than uranate(V)^{120,137}. Qualitative analysis of M4 XANES data show that the U solid phase collected after 150 h (Figure S4) is mainly composed of U(VI)-dpaea with small contributions of U(IV) and possibly U(V) (Table 2:2.). We interpret this result as the contribution of residual solid phase U(VI) combined with a small amount of precipitated U(IV). We attribute the presence of U(V) in the solid phase to the sorption of soluble U(V)-dpaea on the cells or the surface of U(VI)-dpaea.

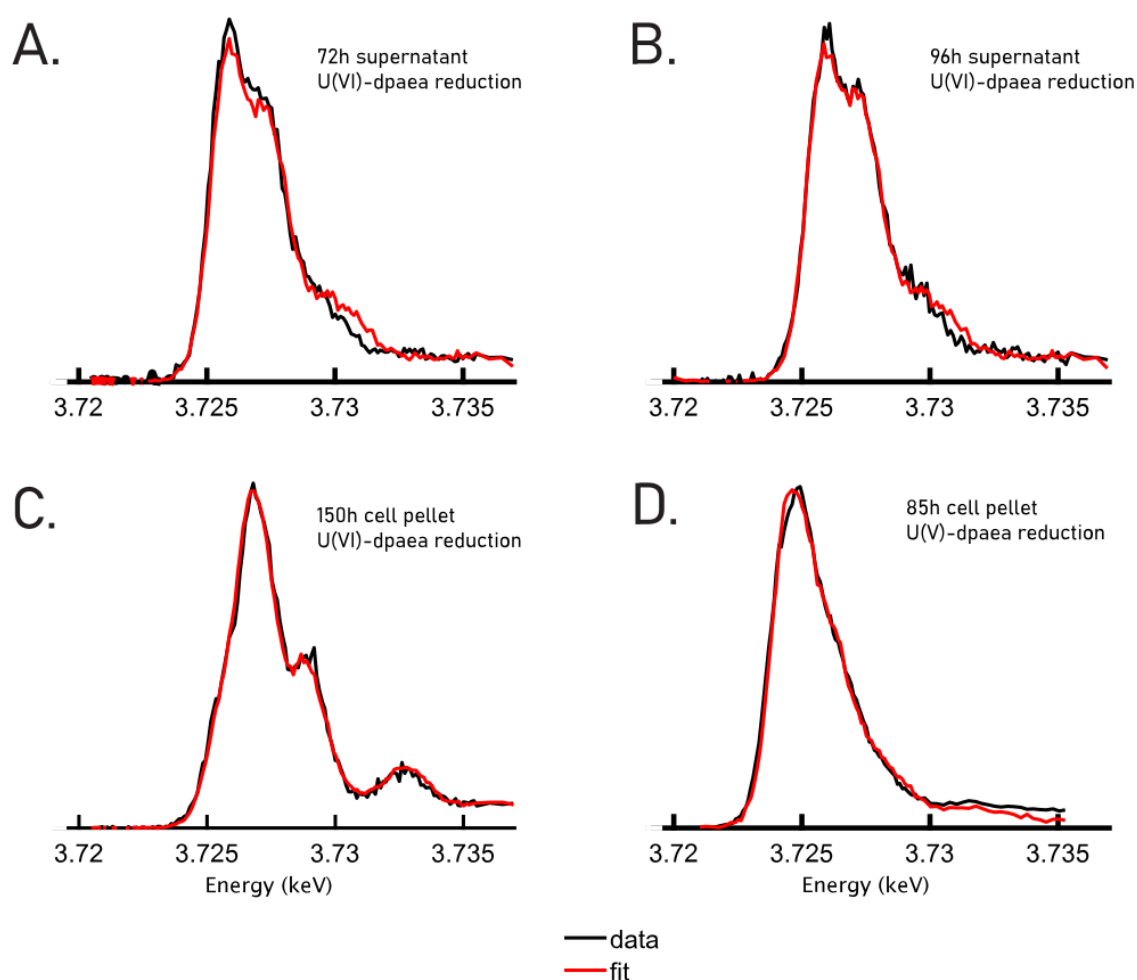


Figure 2:3. LCF fitting results (red) compared to the data (black) for the M4-edge HERFD-XANES spectra obtained for supernatants from the reduction of U(VI)-dpaea A. 72h, B. 96h and a spectrum obtained for the solid phase C. at 150h. Panel D represents a spectrum obtained at 85h for the solid phase during the reduction of U(V)-dpaea.

Sample	% U(VI)-dpaea	% U(V)-dpaea	% U(IV)-dpaea	R factor	Reduced χ^2
--------	---------------	--------------	---------------	----------	------------------

U(VI)-dpaea reduction					
Aqueous phase 72h	0	81.5 ± 2.2	18.5 ± 3.1	0.0103	0.2131
Aqueous phase 96h	3.7 ± 2.5	85.5 ± 1.7	10.8 ± 1.1	0.0061	0.1196
Solid phase 150h	74 ± 1.4	17.9 ± 2.1	13.1 ± 1.4	0.0064	0.0955
U(V)-dpaea reduction					
Solid phase 85h	3.9 ± 3.8	7.4 ± 2.3	89 ± 3	0.0061	0.2170

Table 2:2. LCF of the M4-edge HR-XANES spectra for samples described in Figure 2:2 and Figure S5 the text with the references U(VI)-dpaea, U(V)-dpaea, U(IV)-dpaea₂. We interpret these figures as supportive indicators for the presence of a given U oxidation state, providing qualitative information about the distribution of the oxidation U states in the samples. The error bars are derived from the linear combination fit algorithm.

2.3.2 Reduction of U(V)-dpaea

In order to probe whether biological reduction of U(V)-dpaea occurred in these experiments, we performed two additional bio-reduction experiments with U(V)-dpaea as the starting substrate. The first, utilizing biologically-generated U(V)-dpaea, was performed to establish the continuity of the reduction mechanism from U(VI) to U(IV). The second, utilizing chemically synthesized U(V)-dpaea, was performed in order to systematically uncouple the second electron transfer (U(V) to U(IV)) from the first (U(VI) to U(V)).

For this set of experiments, we validated the ion-exchange chromatography by testing it on decreasing U(V)-dpaea concentrations (from 220 µM to 4.2 µM). We noticed that the U(VI)/U(IV) ratio obtained after separation of U(V)-dpaea was dependent on the initial U(V)-dpaea concentration in solution, before acid treatment (Figure S6). Therefore, the results of the U(V)-dpaea reduction experiments, presented in the sections below, were corrected after establishing the relationship between initial [U(V)-dpaea] and the percentage of U in the U(IV) fraction (Figure S7). We also evaluated that the dpaea ligand does not have an effect on chromatography elution (Figure S8). The details of this correction factor are reported in the Supplementary information (Text S3).

2.3.2.1 Reduction of biologically produced U(V)-dpaea

Aqueous U concentrations were monitored in incubations of *S. oneidensis* with biogenic U(V)-dpaea over up to 312 hours (13 days). Over this experimental time, we showed that the cell number decreased but remained greater than a thousand cells/mL (experimental method described in Text S2, and results in Figure S9). Whilst the concentration of aqueous U remained constant at around 50 µM in the controls without cells over the duration of the experiment, aqueous U in the biological incubations decreased steadily down to 30 µM (Figure 2:4.A.). In addition, as U(V)-dpaea was removed from the aqueous phase, a concomitant increase in solid-associated U was observed (Figure 2:4.A.). In contrast, we did not observe the formation of a solid phase in the abiotic controls. Ion exchange chromatography of the solid phases recovered from the incubations revealed that they are composed of U(IV) (Figure 2:5.A.).

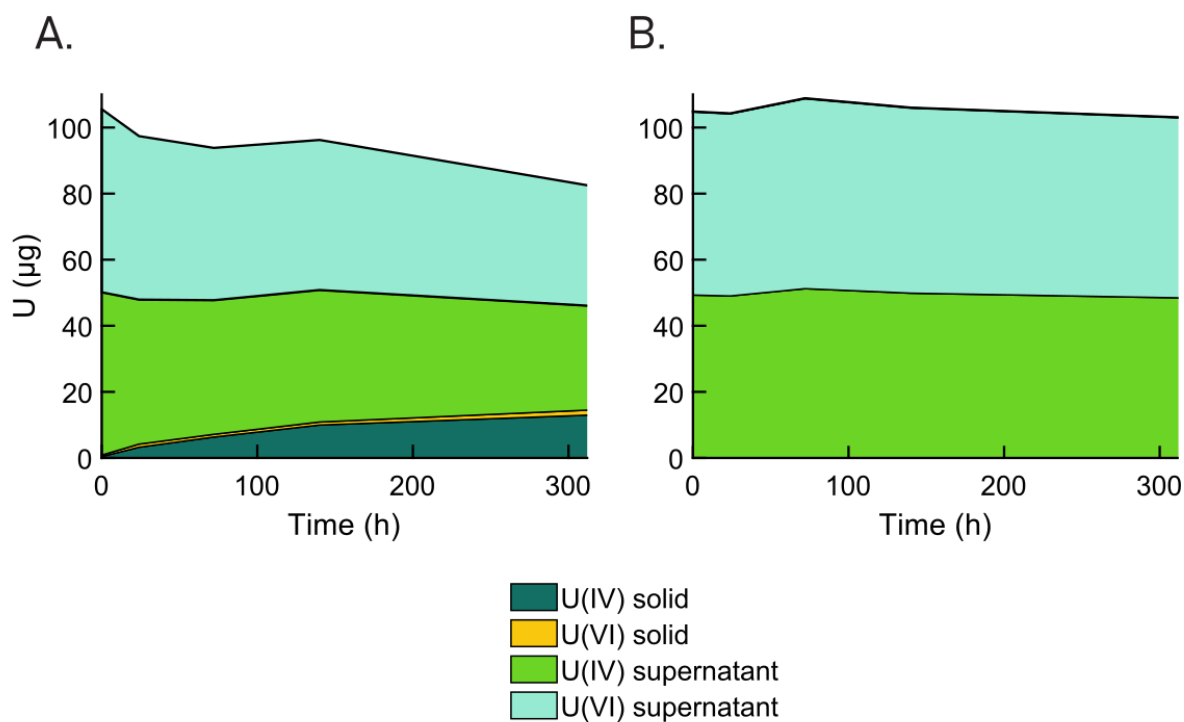


Figure 2:4. Aqueous and solid phase U concentration through time in incubations with *S. oneidensis* MR-1 and no-cell controls with (A) biologically-produced U(V)-dpaea (B) synthetic U(V)-dpaea.

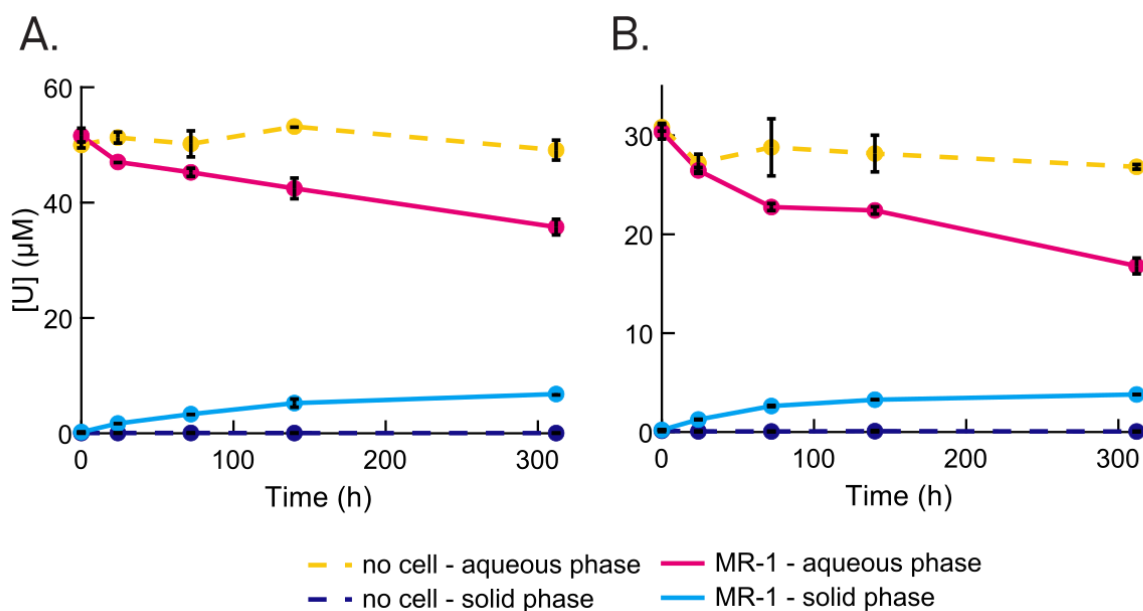


Figure 2:5. U oxidation state in the solid phase (cell pellet) and in the aqueous phase (supernatant) of (A) incubations with *S. oneidensis* MR-1 (B) and no-cell controls, in presence of 'biological' U(V)-dpaea. The U(VI) and U(IV) fractions were obtained by ion exchange chromatography. The ion exchange chromatography separation cannot directly identify U(V), because the samples are acidified prior to loading onto the column. Acid treatment is known to disproportionate uranyl(V) and to produce equal proportions of U(VI) and U(IV). Therefore, here the equal proportions observed for U(VI) and U(IV) in the supernatant are a proxy for U(V) (result demonstrated by U $M_{4,5}$ -edge HR-XANES).

We further substantiate U speciation in the solid phase using $M_{4\text{-edge}}$ HR-XANES (Figure 2:2.B.). The spectra collected for the solid phase U recovered after 85h of incubation showed a single peak at 3.7257 keV (Table 2:1.), similar to the U(IV)-dpaea₂ standard, and LCF suggests a composition of ~90% U(IV) with a small contribution of U(V), most likely in a uranate configuration (Figure 2:3.D and Table 2:2.).

To better delineate the nature of the U(IV) product, samples of the cell pellet recovered after 3 months of incubation were analyzed by TEM. We pinpointed two major morphologies of the U(IV) product which are represented in Figure 2:6.. The first morphology corresponds to small aggregates of U, smaller than 200nm, distributed at the surface of the bacteria (Figure 2:6. A-C.), and the second exhibits U-bearing clusters larger than 1 μm associated with biomass (Figure 2:6. D-F.). EDS spectra of the two types of U morphology showed the predominance of U and O for both types but only significant contributions of N (Figure S10). SAED diffraction patterns also acquired on both morphologies display diffuse rings, suggesting that both are non-crystalline (Figures S11 and S12). We propose that the type 1 morphology corresponds to U(IV)-dpaea₂ (a sparingly soluble complex with an equilibrium solubility of 10 μM , Figure S3) and type 2 to non-crystalline U(IV) typically expected in U(VI) reduction by bacteria¹³. EXAFS analysis is needed to determine definitively the structure of the end product.

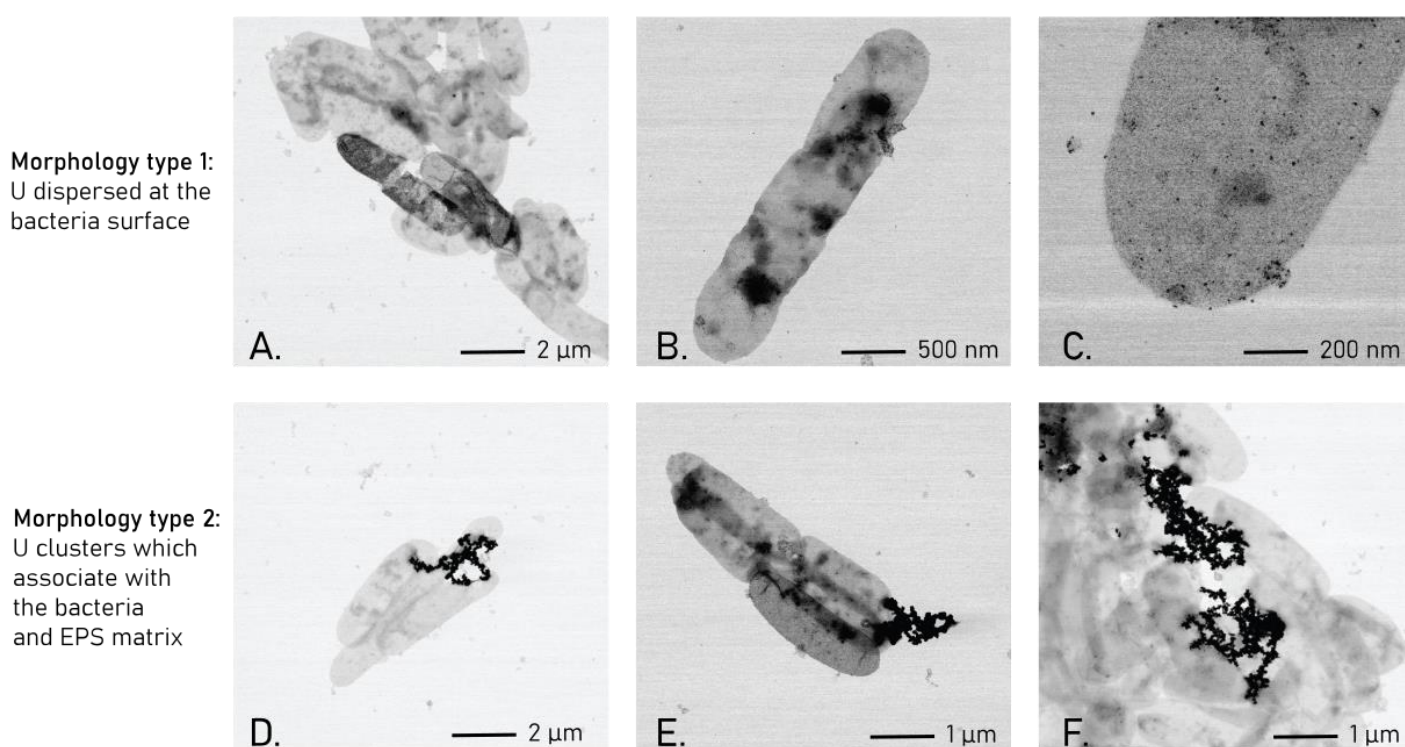


Figure 2:6. STEM images acquired on *S. oneidensis* MR-1 incubated with U(V)-dpaea for 3 months. We mainly observed two types of uranium morphologies. A, B and C describe morphology type 1 corresponding to U aggregates smaller than 200nm dispersed at the surface of the bacteria. D, E and F show morphology type 2, in which U forms larger (> 1 microns or μm) clusters in association with the bacterial cells

2.3.2.2 Reduction of synthetic U(V)-dpaea

We observed similar results when the same experiment was conducted with synthetic U(V)-dpaea. Indeed, U remained stable in the no-cell controls at around 27 μM (Figure 2:4.B.). In contrast, the amount of U in solution decreased steadily in the culture supernatants down to 13 μM , with the concomitant formation of a solid phase (Figure 2:4.B). Ion exchange chromatography separation of the acid-solubilized solid phase also showed the predominance of solid U(IV) (Figure S12). Furthermore, UV-vis spectroscopy of the aqueous phase showed (i) stability of U(V)-dpaea in the aqueous phase in the absence of cells and (ii) a slight decrease in the absorbance for incubations with cells further supporting that U(V)-dpaea was transformed by the bacteria (Figure S1.B.). Cell viability was monitored over 30 days (Figure S9), and shown to decrease, as expected, but to remain above 10^3 cells/mL.

2.3.2.3 Reduction is the dominant mechanism

In order to confirm that the solid phase U(IV) observed in the incubations of *S. oneidensis* MR-1 with U(V)-dpaea was the product of an active reduction mechanism, we probed the ability of a *ccmG* deletion mutant to carry out the reduction. The ΔccmG mutant lacks a key gene involved in the maturation of *c*-type cytochromes, and therefore is devoid of these proteins. Hence, in an experiment similar to the one described above, we incubated ΔccmG cells, MR-1 wild type (WT) cells, and a no-cell control with 550 μM synthetic U(V)-dpaea. As expected, ΔccmG cells did not transform U(V)-dpaea over 336h (14 days) (Figure 2:7.A.), whereas we observed a 20% decrease in the concentration of U(V)-dpaea in the incubations with MR-1 WT cells and a 2.5% decrease for the no-cell control. Cell viability showed similar trends in both ΔccmG and WT incubations (Figure 2:7.B). This finding suggests that the presence of *c*-type cytochromes is required for U(V)-dpaea reduction. Additionally, we can exclude disproportionation as a significant contributor to U(V)-dpaea reduction. This is because U(V)-dpaea reduction does not occur in the presence of the ΔccmG mutant. Furthermore, the complex is stable in the absence of cells (no-cell control), or in presence of inactivated cells (Text S4 and S5, Figure S14, S15 and S16). In contrast, we observed the substantial decrease in the concentration of U(V)-dpaea in the presence of active cells, providing evidence for microbial U(V)-dpaea reduction. These results concur to demonstrate that U(V)-dpaea can be actively reduced by strain MR-1 cells via an electron transfer flow likely mediated by *c*-type cytochromes.

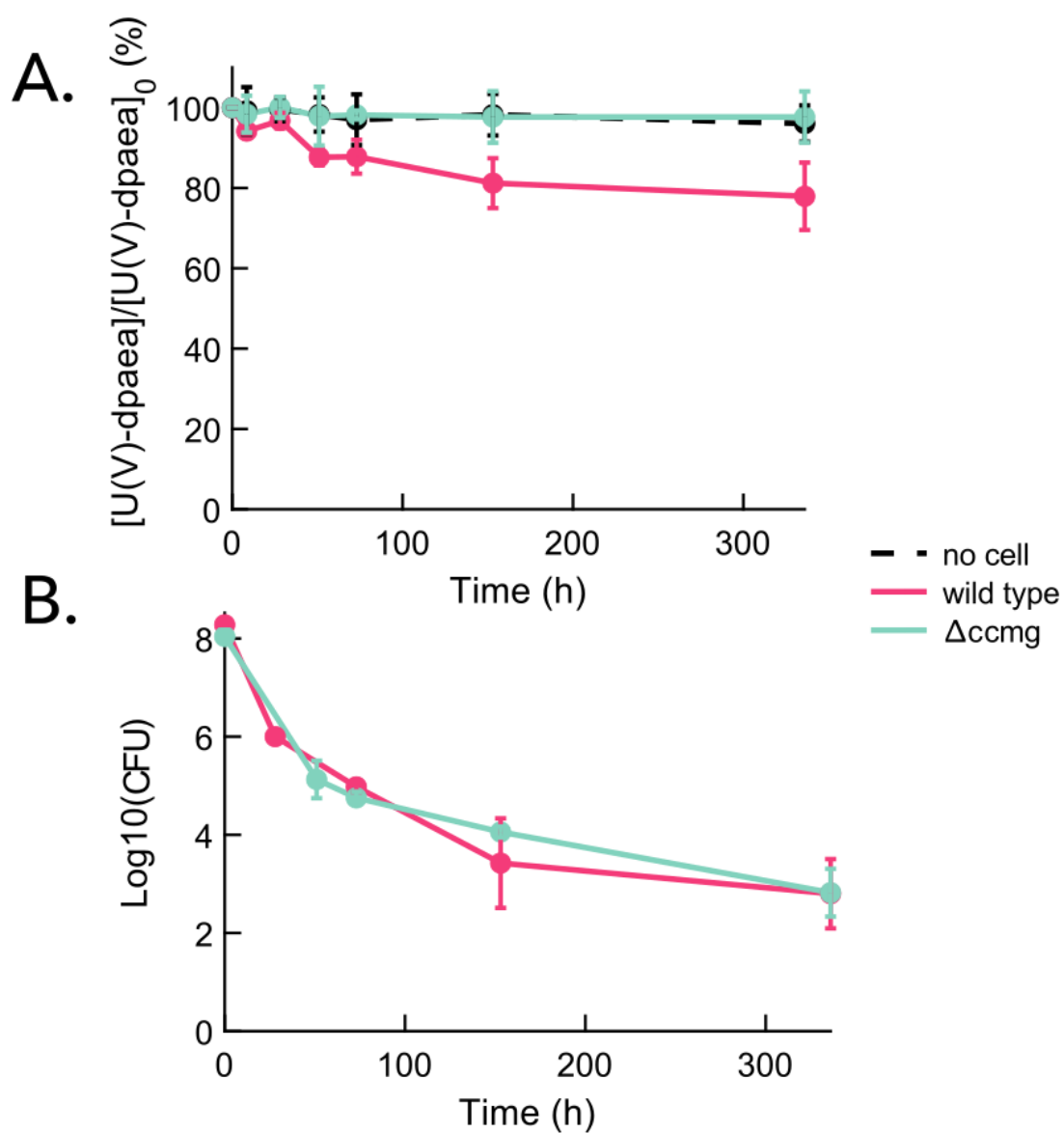


Figure 2:7. Aqueous U(V)-dpaea concentration (A) and cell viability (B) through time in incubations with *S. oneidensis* MR-1, the deletion mutant ΔccmG and a no-cell control.

2.4 Discussion

2.4.1 Mechanism of U(VI)-dpaea reduction

We report that *S. oneidensis* MR-1 can reduce solid phase U(VI)-dpaea to uranyl(V)-dpaea by a one-electron transfer. U(V)-dpaea is released in the culture supernatant and remains stable over the duration of the experiment. The use of the dpaea ligand to coordinate and stabilize U(V) in water at pH 7 allowed for the accumulation of this intermediate in solution. Our results are congruent with the Renshaw et al. and others^{28,30,31}, where a transient uranyl(V) species was proposed to form in *Geobacter sulfurreducens* cell suspensions after 4 h of incubation. However, additionally, our system evidenced the biological reduction of U(V)-dpaea by an additional one-electron transfer. Clearly, the enhanced stability of U(V) afforded by the dpaea ligand extends the half-life of U(V) in solution, allowing this process to take place. The significance of the results lies in the demonstration that *S. oneidensis* MR-1 cells are able to actively reduce U(V)-dpaea. This finding is consistent with the reduction of Np(V) and Pu(V) by the same organism^{67,70}. It is conceivable that the same would occur for U(V) organic complexes provided that they persist sufficiently long for biological reduction to preempt disproportionation.

Thus, the molecular mechanism of U(VI)-dpaea reduction is distinct from that described by Sundararajan et al. for $[U(VI)O_2(H_2O)_5]^{2+}$ ⁶⁶. They assumed that a transient U(V) species formed after the transfer of two electrons from the *c*-type cytochrome PpcA of *Geobacter sulfurreducens* to the associated U(VI)-U(VI) dimer. In the proposed scenario, a U(V)-U(V) dimer is formed and disproportionates to U(VI) and U(IV). In this work, it is unlikely that such a dimer can form because of the bulky pentadentate ligand dpaea. In fact, the dpaea ligand obstructs the equatorial plane of the U atom, preventing CCI and thus, disproportionation. Therefore, we suggest that electron transfer involved a monomer U(VI)-dpaea. Once U(V)-dpaea was formed in the supernatant, it remained stable until further reduction occurred. Spontaneous disproportionation was excluded since the structure was found to be stable up to three months in water at pH=7⁴⁰. Moreover, [U(V)-dpaea] remained unchanged in the no-cell controls over the course of our assays.

The reduction of water stable U(V)-dpaea to U(IV) implies that structural changes took place, namely the cleavage of the two uranyl di-oxo bonds. The process may be facilitated by the functionalization of one of the uranyl oxygen atoms¹³⁹ by hydrogen binding with an enzymatic residue of the outer-membrane cytochromes MtrC or OmcA. Also, the second reduction step exhibited slower kinetics than the first, with half-lives of 984 hours (41 days) and 528 hours (22 days) for the 'biological' and 'synthetic' U(V)-dpaea respectively, compared to 20 h for U(VI)-dpaea reduction to U(V)-dpaea. The differences observed in the half-lives of 'biological' or 'synthetic' could be attributed to the initial concentration of U(V)-dpaea in the incubations (60 μ M for the 'biological' and 30 μ M for the 'synthetic'). It could also be that some residual metabolites remained in the medium of 'biological' U(V)-dpaea and inhibited the reaction by interacting with the cell surface.

2.4.2 Thermodynamic considerations

The MtrCAB protein complex in *S. oneidensis* MR-1 spans potentials from 0 to -400 mV (against the standard hydrogen electrode (SHE))⁹⁰, and therefore accesses a large range of redox substrates. The reduction potential of U(VI)-dpaea/U(V)-dpaea was -312 mV (SHE)⁴¹, thus, the first reduction step of U(VI) to U(V), lies within the reduction

potentials accessible to the MtrCAB complex. It suggests that a one-electron reduction of U(VI)-dpaea by MtrC/OmcA would be energetically favorable.

Regarding the second reduction step from U(V)-dpaea to U(IV), there is no reported redox potential for the U(V)-dpaea/U(IV) in aqueous medium. Indeed, the absence of a redox wave on the cyclic voltammogram of U(V)-dpaea associated with the transition of U(V) to U(IV) may be explained by the slow kinetics of electron transfer or by significant structural rearrangements⁴¹. However, dithionite, which is the reduced product in the sulfite/dithionite couple ($\text{HSO}_3^{2-}/\text{S}_2\text{O}_4^{2-}$), with an electrochemical potential of -660mV against SHE at pH 7, was shown experimentally to reduce U(V)-dpaea to U(IV) in an aqueous solution buffered at pH 7 with HEPES⁴¹. This observation implies that the redox potential of U(V)-dpaea/U(IV) could be accessible by MtrC/OmcA and a one-electron reduction of U(V)-dpaea to U(IV), energetically favorable.

2.4.3 Environmental relevance

In this work, the dpaea ligand was a powerful tool to characterize the reduction mechanism of U reduction and to trap the pentavalent species. This is an approach that allowed the elucidation of whether biological U(V) reduction was possible in the presence of organic ligands closely related to dipicolinic acid. With this point now resolved, it opens the door for investigations with more environmentally relevant ligands.

Bulky ligands and ligands that can bind metal ions with a high number of donor atoms may contribute to slowing down the disproportionation, by preventing CCI between two uranium nuclei. The dpaea ligand displays significant steric effects around the U nucleus because of the aromatic rings occupying the equatorial plane of the complex. In addition, this ligand is pentadentate and therefore occupies five coordination sites at the metal center, which prevents disproportionation^{140,141}. In contrast, smaller ligands or ligands with a coordination number lower than 3 may allow CCI and consequently disproportionation¹⁴².

We expect that other polydentate ligands, with similar properties as dpaea, may stabilize uranyl(V) sufficiently to allow the reduction of the U(V) species. For instance, we could envision other aminocarboxylate ligands such as EDTA, NTA, or DTPA (used to extract radionuclides in the process of radioactive waste treatment¹²⁹) may behave similarly. In addition, fulvic and humic acids, abundant in organic rich soils, have numerous carboxylic and hydroxyl functional groups and are additional candidates to stabilize uranyl(V) in the subsurface.

Additional work, with the abovementioned ligands and in natural sediments, is needed to investigate these hypotheses. Moreover, the dpaea system could be a valuable system to interrogate the isotopic signature associated with a single one-electron transfer step and how it impacts the overall isotopic fractionation of biological U reduction.

2.5 Conclusion

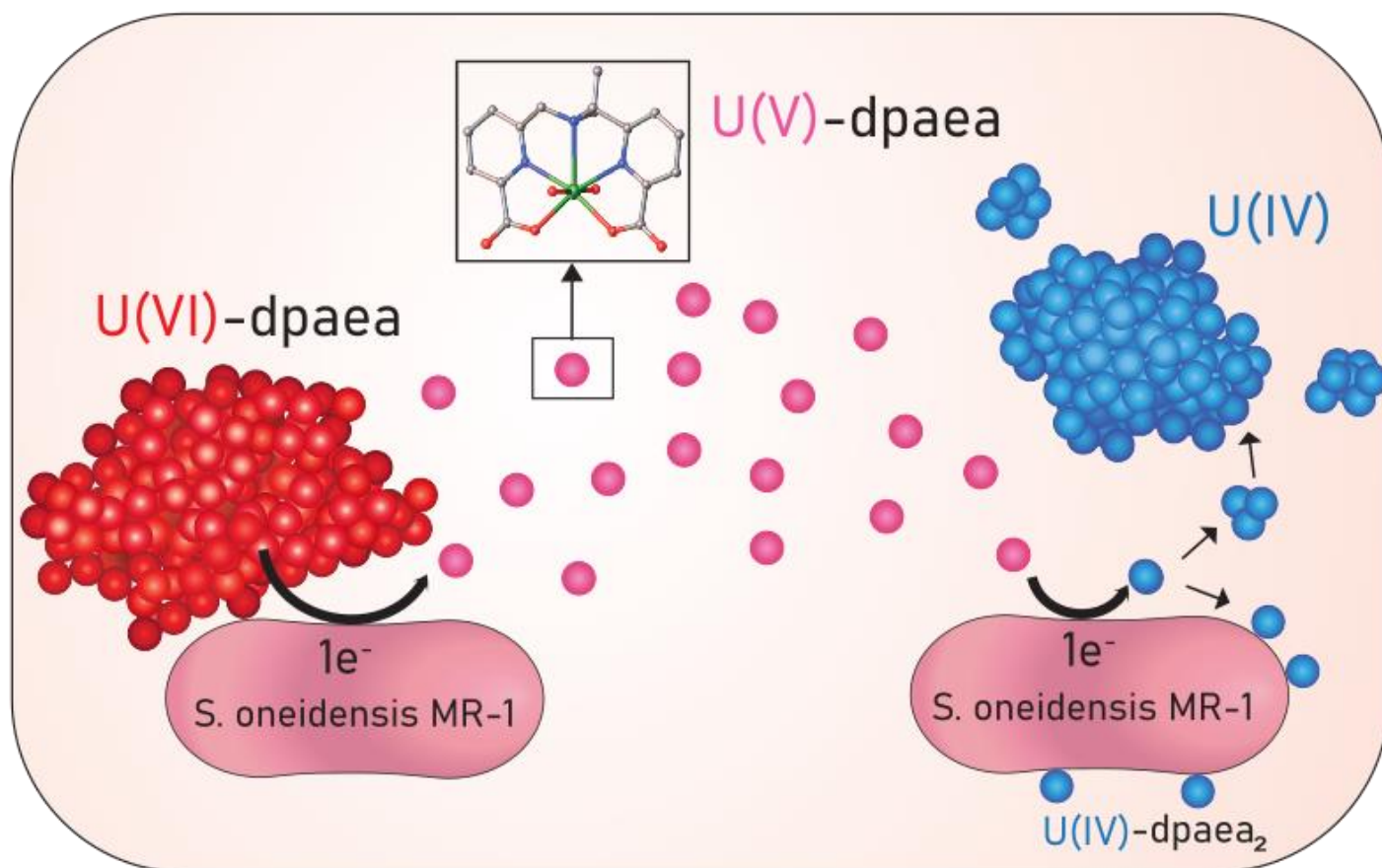


Figure 2:8. Reduction of solid phase U(VI)-dpaea (in red). U(VI)-dpaea is reduced to soluble U(V)-dpaea (in pink) by a one-electron transfer. U(V)-dpaea is released to the culture medium, and further reduced to amorphous U(IV) and organic complexes of U(IV), (in blue) by an additional one-electron transfer.

In this first chapter, we investigated the mechanistic steps of U(VI)-dpaea reduction by *S. oneidensis* MR-1: We demonstrated that U(VI)-dpaea is reduced via two single successive electron transfers: (i) solid U(VI)-dpaea to aqueous U(V)-dpaea, (ii) U(V)-dpaea to U(IV) species (Figure 2:8.).

2.6 References

- (1) Ribera, D.; Labrot, F.; Tisnerat, G.; Narbonne, J. F. Uranium in the Environment: Occurrence, Transfer, and Biological Effects. *Rev. Environ. Contam. Toxicol.* **1996**, *146*, 53–89.
- (2) Markich, S. J. Uranium Speciation and Bioavailability in Aquatic Systems: An Overview. *ScientificWorldJournal* **2002**, *2*, 707–729. <https://doi.org/10.1100/tsw.2002.130>.
- (3) Lovley, D. R.; Phillips, E. J. P.; Gorby, Y. A.; Landa, E. R. Microbial Reduction of Uranium. *Nature* **1991**, *350* (6317), 413–416. <https://doi.org/10.1038/350413a0>.
- (4) Bernier-Latmani, R.; Veeramani, H.; Vecchia, E. D.; Junier, P.; Lezama-Pacheco, J. S.; Suvorova, E. I.; Sharp, J. O.; Wigginton, N. S.; Bargar, J. R. Non-Uraninite Products of Microbial U(VI) Reduction. *Environ. Sci. Technol.* **2010**, *44* (24), 9456–9462. <https://doi.org/10.1021/es101675a>.
- (5) Barton, L. L.; Choudhury, K.; Thomson, B. M.; Steenhoudt, K.; Groffman, A. R. Bacterial Reduction of Soluble Uranium: The First Step of in Situ Immobilization of Uranium. *Radioact. Waste Manag. Environ. Restor.* **1996**, *20* (2–3), 141–151.
- (6) Lovley, D. R.; Roden, E. E.; Phillips, E. J. P.; Woodward, J. C. Enzymatic Iron and Uranium Reduction by Sulfate-Reducing Bacteria. *Mar. Geol.* **1993**, *113* (1–2), 13.
- (7) Francis, A. J.; Dodge, C. J.; Lu, Fulong.; Halada, G. P.; Clayton, C. R. XPS and XANES Studies of Uranium Reduction by *Clostridium* Sp. *Environ. Sci. Technol.* **1994**, *28* (4), 636–639. <https://doi.org/10.1021/es00053a016>.
- (8) Marshall, M. J.; Beliaev, A. S.; Dohnalkova, A. C.; Kennedy, D. W.; Shi, L.; Wang, Z.; Boyanov, M. I.; Lai, B.; Kemner, K. M.; McLean, J. S.; Reed, S. B.; Culley, D. E.; Bailey, V. L.; Simonson, C. J.; Saffarini, D. A.; Romine, M. F.; Zachara, J. M.; Fredrickson, J. K. C-Type Cytochrome-Dependent Formation of U(IV) Nanoparticles by *Shewanella Oneidensis*. *PLoS Biol.* **2006**, *4* (8). <https://doi.org/10.1371/journal.pbio.0040268>.
- (9) Bargar, J. R.; Bernier-Latmani, R.; Giammar, D. E.; Tebo, B. M. Biogenic Uraninite Nanoparticles and Their Importance for Uranium Remediation. *Elements* **2008**, *4* (6), 407–412. <https://doi.org/10.2113/gselements.4.6.407>.
- (10) Veeramani, H.; Alessi, D. S.; Suvorova, E. I.; Lezama-Pacheco, J. S.; Stubbs, J. E.; Sharp, J. O.; Dippon, U.; Kappler, A.; Bargar, J. R.; Bernier-Latmani, R. Products of Abiotic U(VI) Reduction by Biogenic Magnetite and Vivianite. *Geochim. Cosmochim. Acta* **2011**, *75* (9), 2512–2528. <https://doi.org/10.1016/j.gca.2011.02.024>.
- (11) Veeramani, H.; Scheinost, A. C.; Monsegue, N.; Qafoku, N. P.; Kukkadapu, R.; Newville, M.; Lanzirotti, A.; Pruden, A.; Murayama, M.; Hochella, M. F. Abiotic Reductive Immobilization of U(VI) by Biogenic Mackinawite. *Environ. Sci. Technol.* **2013**, *47* (5), 2361–2369. <https://doi.org/10.1021/es304025x>.
- (12) O'Loughlin, E. J.; Kelly, S. D.; Cook, R. E.; Csencsits, R.; Kemner, K. M. Reduction of Uranium(VI) by Mixed Iron(II)/Iron(III) Hydroxide (Green Rust): Formation of UO₂ Nanoparticles. *Environ. Sci. Technol.* **2003**, *37* (4), 721–727. <https://doi.org/10.1021/es0208409>.
- (13) Scott, T. B.; Allen, G. C.; Heard, P. J.; Randell, M. G. Reduction of U(VI) to U(IV) on the Surface of Magnetite. *Geochim. Cosmochim. Acta* **2005**, *69* (24), 5639–5646. <https://doi.org/10.1016/j.gca.2005.07.003>.

- (14) Ilton, E. S.; Pacheco, J. S. L.; Bargar, J. R.; Shi, Z.; Liu, J.; Kovarik, L.; Engelhard, M. H.; Felmy, A. R. Reduction of U(VI) Incorporated in the Structure of Hematite. *Environ. Sci. Technol.* **2012**, *46* (17), 9428–9436. <https://doi.org/10.1021/es3015502>.
- (15) Yuan; Ilton; S, E.; Antonio; R, M.; Li; Cook; Becker, U. Electrochemical and Spectroscopic Evidence on the One-Electron Reduction of U(VI) to U(V) on Magnetite. *ResearchGate* **2015**, *49* (10). <https://doi.org/10.1021/acs.est.5b00025>.
- (16) Pidchenko, I.; Kvashnina, K. O.; Yokosawa, T.; Finck, N.; Bahl, S.; Schild, D.; Polly, R.; Bohnert, E.; Rossberg, A.; Göttlicher, J.; Dardenne, K.; Rothe, J.; Schäfer, T.; Geckeis, H.; Vitova, T. Uranium Redox Transformations after U(VI) Coprecipitation with Magnetite Nanoparticles. *Environ. Sci. Technol.* **2017**, *51* (4), 2217–2225. <https://doi.org/10.1021/acs.est.6b04035>.
- (17) Roberts, H. E.; Morris, K.; Law, G. T. W.; Mosselmans, J. F. W.; Bots, P.; Kvashnina, K.; Shaw, S. Uranium(V) Incorporation Mechanisms and Stability in Fe(II)/Fe(III) (Oxyhydr)Oxides. *Environ. Sci. Technol. Lett.* **2017**, *4* (10), 421–426. <https://doi.org/10.1021/acs.estlett.7b00348>.
- (18) Renshaw, J. C.; Butchins, L. J. C.; Livens, F. R.; May, I.; Charnock, J. M.; Lloyd, J. R. Bioreduction of Uranium: Environmental Implications of a Pentavalent Intermediate. *ResearchGate* **2005**, *39* (15), 5657–5660. <https://doi.org/10.1021/es048232b>.
- (19) Großmann, K.; Arnold, T.; Krawczyk-Bärsch, E.; Diessner, S.; Wobus, A.; Bernhard, G.; Krawietz, R. Identification of Fluorescent U(V) and U(VI) Microparticles in a Multispecies Biofilm by Confocal Laser Scanning Microscopy and Fluorescence Spectroscopy. *Environ. Sci. Technol.* **2007**, *41* (18), 6498–6504. <https://doi.org/10.1021/es0710609>.
- (20) Sundararajan, M.; Campbell, A. J.; Hillier, I. H. Catalytic Cycles for the Reduction of [UO₂]²⁺ by Cytochrome C7 Proteins Proposed from DFT Calculations. *J. Phys. Chem. A* **2008**, *112* (19), 4451–4457. <https://doi.org/10.1021/jp800209p>.
- (21) Jones, D. L.; Andrews, M. B.; Swinburne, A. N.; Botchway, S. W.; Ward, A. D.; Lloyd, J. R.; Natrajan, L. S. Fluorescence Spectroscopy and Microscopy as Tools for Monitoring Redox Transformations of Uranium in Biological Systems. *Chem. Sci.* **2015**, *6* (9), 5133–5138. <https://doi.org/10.1039/C5SC00661A>.
- (22) Vettese, G. F.; Morris, K.; Natrajan, L. S.; Shaw, S.; Vitova, T.; Galanzew, J.; Jones, D. L.; Lloyd, J. R. Multiple Lines of Evidence Identify U(V) as a Key Intermediate during U(VI) Reduction by *Shewanella Oneidensis* MR1. *Environ. Sci. Technol.* **2020**. <https://doi.org/10.1021/acs.est.9b05285>.
- (23) Steele, H.; Taylor, R. J. A Theoretical Study of the Inner-Sphere Disproportionation Reaction Mechanism of the Pentavalent Actinyl Ions. *Inorg. Chem.* **2007**, *46* (16), 6311–6318. <https://doi.org/10.1021/ic070235c>.
- (24) Kern, D. M. H.; Orlemann, E. F. The Potential of the Uranium (V), Uranium (VI) Couple and the Kinetics of Uranium (V) Disproportionation in Perchlorate Media. *J. Am. Chem. Soc.* **1949**, *71* (6), 2102–2106. <https://doi.org/10.1021/ja01174a055>.
- (25) Wang, Y.; Frutschi, M.; Suvorova, E.; Phrommavanh, V.; Descostes, M.; Osman, A. A. A.; Geipel, G.; Bernier-Latmani, R. Mobile Uranium(IV)-Bearing Colloids in a Mining-Impacted Wetland. *Nat. Commun.* **2013**, *4*, ncomms3942. <https://doi.org/10.1038/ncomms3942>.

- (26) Bhattacharyya, A.; Campbell, K. M.; Kelly, S. D.; Roebbert, Y.; Weyer, S.; Bernier-Latmani, R.; Borch, T. Biogenic Non-Crystalline U (IV) Revealed as Major Component in Uranium Ore Deposits. *Nat. Commun.* **2017**, *8* (1), 15538. <https://doi.org/10.1038/ncomms15538>.
- (27) Icopini, G. A.; Boukhalfa, H.; Neu, M. P. Biological Reduction of Np(V) and Np(V) Citrate by Metal-Reducing Bacteria. *Environ. Sci. Technol.* **2007**, *41* (8), 2764–2769. <https://doi.org/10.1021/es0618550>.
- (28) Icopini, G. A.; Lack, J. G.; Hersman, L. E.; Neu, M. P.; Boukhalfa, H. Plutonium(V/VI) Reduction by the Metal-Reducing Bacteria *Geobacter Metallireducens* GS-15 and *Shewanella Oneidensis* MR-1. *Appl. Environ. Microbiol.* **2009**, *75* (11), 3641–3647. <https://doi.org/10.1128/AEM.00022-09>.
- (29) Nowack, B. Environmental Chemistry of Aminopolycarboxylate Chelating Agents. *Environ. Sci. Technol.* **2002**, *36* (19), 4009–4016. <https://doi.org/10.1021/es025683s>.
- (30) Setlow, B.; Atluri, S.; Kitchel, R.; Koziol-Dube, K.; Setlow, P. Role of Dipicolinic Acid in Resistance and Stability of Spores of *Bacillus Subtilis* with or without DNA-Protective α/β -Type Small Acid-Soluble Proteins. *J. Bacteriol.* **2006**, *188* (11), 3740–3747. <https://doi.org/10.1128/JB.00212-06>.
- (31) Takahashi, M.; Terada, Y.; Nakai, I.; Nakanishi, H.; Yoshimura, E.; Mori, S.; Nishizawa, N. K. Role of Nicotianamine in the Intracellular Delivery of Metals and Plant Reproductive Development. *Plant Cell* **2003**, *15* (6), 1263–1280. <https://doi.org/10.1105/tpc.010256>.
- (32) Tandy, S.; Bossart, K.; Mueller, R.; Ritschel, J.; Hauser, L.; Schulin, R.; Nowack, B. Extraction of Heavy Metals from Soils Using Biodegradable Chelating Agents. *Environ. Sci. Technol.* **2004**, *38* (3), 937–944. <https://doi.org/10.1021/es0348750>.
- (33) Nowack, B.; VanBriesen, J. M. Chelating Agents in the Environment. In *Biogeochemistry of Chelating Agents*; ACS Symposium Series; American Chemical Society, 2005; Vol. 910, pp 1–18. <https://doi.org/10.1021/bk-2005-0910.ch001>.
- (34) Deblonde, G. J.-P. (ORCID:0000000208258714); Kelley, M. P. (ORCID:0000000151969821); Su, J. (ORCID:0000000268952150); Batista, E. R.; Yang, P. (ORCID:0000000347262860); Booth, C. H. (ORCID:0000000168270080); Abergel, R. J. (ORCID:0000000239068761). Spectroscopic and Computational Characterization of Diethylenetriaminepentaacetic Acid/Transplutonium Chelates: Evidencing Heterogeneity in the Heavy Actinide(III) Series. *Angew. Chem. Int. Ed.* **2018**, *57* (17). <https://doi.org/10.1002/anie.201709183>.
- (35) Brown, M. A.; Paulenova, A.; Gelis, A. V. Aqueous Complexation of Thorium(IV), Uranium(IV), Neptunium(IV), Plutonium(III/IV), and Cerium(III/IV) with DTPA. *Inorg. Chem.* **2012**, *51* (14), 7741–7748. <https://doi.org/10.1021/ic300757k>.
- (36) Lapka, J. L.; Paulenova, A.; Alyapyshev, M. Y.; Babain, V. A.; Herbst, R. S.; Law, J. D. Extraction of Uranium(VI) with Diamides of Dipicolinic Acid from Nitric Acid Solutions. *Radiochim. Acta* **2009**, *97* (6), 291–296. <https://doi.org/10.1524/ract.2009.1588>.
- (37) Faizova, R.; Fadaei-Tirani, F.; Bernier-Latmani, R.; Mazzanti, M. Ligand-Supported Facile Conversion of Uranyl(VI) into Uranium(IV) in Organic and Aqueous Media. *Angew. Chem.* **2020**, *132* (17), 6822–6825. <https://doi.org/10.1002/ange.201916334>.
- (38) Faizova, R.; Scopelliti, R.; Chauvin, A.-S.; Mazzanti, M. Synthesis and Characterization of a Water Stable Uranyl(V) Complex. *J. Am. Chem. Soc.* **2018**, *140* (42), 13554–13557. <https://doi.org/10.1021/jacs.8b07885>.

- (39) Stoliker, D. L.; Kaviani, N.; Kent, D. B.; Davis, J. A. Evaluating Ion Exchange Resin Efficiency and Oxidative Capacity for the Separation of Uranium(IV) and Uranium(VI). *Geochem. Trans.* **2013**, *14* (1), 1. <https://doi.org/10.1186/1467-4866-14-1>.
- (40) Wang, X.; Johnson, T. M.; Lundstrom, C. C. Isotope Fractionation during Oxidation of Tetravalent Uranium by Dissolved Oxygen. *Geochim. Cosmochim. Acta* **2015**, *150*, 160–170. <https://doi.org/10.1016/j.gca.2014.12.007>.
- (41) Zimina, A.; Dardenne, K.; Denecke, M. A.; Doronkin, D. E.; Huttel, E.; Lichtenberg, H.; Mangold, S.; Pruessmann, T.; Rothe, J.; Spangenberg, Th.; Steininger, R.; Vitova, T.; Geckeis, H.; Grunwaldt, J.-D. CAT-ACT—A New Highly Versatile x-Ray Spectroscopy Beamline for Catalysis and Radionuclide Science at the KIT Synchrotron Light Facility ANKA. *Rev. Sci. Instrum.* **2017**, *88* (11), 113113. <https://doi.org/10.1063/1.4999928>.
- (42) Ravel, B.; Newville, M. ATHENA, ARTEMIS, HEPHAESTUS: Data Analysis for X-Ray Absorption Spectroscopy Using IFEFFIT. *J. Synchrotron Radiat.* **2005**, *12* (Pt 4), 537–541. <https://doi.org/10.1107/S0909049505012719>.
- (43) Zegke, M.; Zhang, X.; Pidchenko, I.; Hlina, J. A.; Lord, R. M.; Purkis, J.; Nichol, G. S.; Magnani, N.; Schreckenbach, G.; Vitova, T.; Love, J. B.; Arnold, P. L. Differential Uranyl(V) Oxo-Group Bonding between the Uranium and Metal Cations from Groups 1, 2, 4, and 12; a High Energy Resolution X-Ray Absorption, Computational, and Synthetic Study. *Chem. Sci.* **2019**. <https://doi.org/10.1039/C8SC05717F>.
- (44) Vitova, T.; Denecke, M. A.; Göttlicher, J.; Jorissen, K.; Kas, J. J.; Kvashnina, K.; Prüßmann, T.; Rehr, J. J.; Rothe, J. Actinide and Lanthanide Speciation with High-Energy Resolution X-Ray Techniques. *J. Phys. Conf. Ser.* **2013**, *430*, 012117. <https://doi.org/10.1088/1742-6596/430/1/012117>.
- (45) Sundararajan, M.; Campbell, A. J.; Hillier, I. H. Catalytic Cycles for the Reduction of [UO₂]²⁺ by Cytochrome C7 Proteins Proposed from DFT Calculations. *J. Phys. Chem. A* **2008**, *112* (19), 4451–4457. <https://doi.org/10.1021/jp800209p>.
- (46) Schnaars, D. D.; Wu, G.; Hayton, T. W. Reduction of Pentavalent Uranyl to U(IV) Facilitated by Oxo Functionalization. *J. Am. Chem. Soc.* **2009**, *131* (48), 17532–17533. <https://doi.org/10.1021/ja906880d>.
- (47) Hartshorne, R. S.; Reardon, C. L.; Ross, D.; Nuester, J.; Clarke, T. A.; Gates, A. J.; Mills, P. C.; Fredrickson, J. K.; Zachara, J. M.; Shi, L.; Beliaev, A. S.; Marshall, M. J.; Tien, M.; Brantley, S.; Butt, J. N.; Richardson, D. J. Characterization of an Electron Conduit between Bacteria and the Extracellular Environment. *Proc. Natl. Acad. Sci.* **2009**, *106* (52), 22169–22174. <https://doi.org/10.1073/pnas.0900086106>.
- (48) Ikeda, A.; Hennig, C.; Tsushima, S.; Takao, K.; Ikeda, Y.; Scheinost, A. C.; Bernhard, G. Comparative Study of Uranyl(VI) and -(V) Carbonato Complexes in an Aqueous Solution. *Inorg. Chem.* **2007**, *46* (10), 4212–4219. <https://doi.org/10.1021/ic070051y>.
- (49) Mougél, V.; Pécaut, J.; Mazzanti, M. New Polynuclear U(IV)–U(V) Complexes from U(IV) Mediated Uranyl(V) Disproportionation. *Chem. Commun.* **2011**, *48* (6), 868–870. <https://doi.org/10.1039/C1CC16646H>.
- (50) Nocton, G.; Horeglad, P.; Pécaut, J.; Mazzanti, M. Polynuclear Cation–Cation Complexes of Pentavalent Uranyl: Relating Stability and Magnetic Properties to Structure. *J. Am. Chem. Soc.* **2008**, *130* (49), 16633–16645. <https://doi.org/10.1021/ja804766r>.

Chapter 3 Mechanism of reduction of solid-phase U(VI)-dpaea and aqueous U(V)-dpaea complexes

Chapter 3 follows up on findings from chapter 2 and provides insights into the biological reduction of U(VI)-dpaea and U(V)-dpaea by the microorganism *S. oneidensis* MR-1 and the purified multiheme outer-membrane c-type cytochrome MtrC of *S. oneidensis* MR-1.

This work is intended for publication.

Author Contributions:

Margaux Molinas, Karin Meibom Lederballe, Radmila Faizova, Ashley Brown, Marinella Mazzanti, Rizlan Bernier-Latmani.

The manuscript was written through contributions from all authors. RBL and MMA conceived of the research. MMo performed the experiments, RF synthesized the U-dpaea complexes, KLM prepared the deletion mutants, AB developed the ion-exchange chromatography method. All authors gave their approval for the final version of the manuscript.

Abstract

The biological reduction of soluble U(VI) complexes to form immobile U(IV) species has been used to remediate contaminated sites. Recent studies have confirmed that the reduction mechanism proceeds via a one electron transfer forming pentavalent U(V) species, believed then to readily disproportionate. Nonetheless, biologically-formed U(V) persisted in aqueous solution at pH 7 in the presence of a stabilizing aminocarboxylate ligand, dpaea²⁻ (dpaeaH₂=bis(pyridyl-6-methyl-2-carboxylate)-ethylamine). In addition, it is well established that multiheme *c*-type cytochromes (MHC) are key mediators of electron transfer to aqueous phase U(VI) complexes in *Shewanella oneidensis* MR-1. Hence, we aim at exploring the role of MHC in the reduction of U(V)-dpaea to U(IV) species, and at establishing the mechanism of solid phase U(VI)-dpaea reduction. To that end, we investigated U-dpaea reduction by two deletion mutant strains of *S. oneidensis* MR-1, lacking either all or only outer-membrane MHC, or by the purified outer-membrane MHC MtrC. Our results suggest that (i) solid phase U(VI)-dpaea reduction occurs via dissolution followed by reduction by outer-membrane and periplasmic *c*-type cytochromes; and (ii) MtrC can directly transfer electrons to U(V)-dpaea to form U(IV) species, underscoring the involvement of MHC in the reduction of this pentavalent U species.

3.1 Introduction

Uranium (U) contamination in the subsurface, resulting from past or present anthropogenic activities such as mining, ore processing, and the production of weapons-grade U can be remediated biologically⁷². To that end, subsurface microorganisms are stimulated to immobilize the highly mobile hexavalent U (U(VI)) species to less mobile tetravalent U (U(IV)) species^{1,2,10,13}. U(VI) and U(IV) are the most abundant oxidation states of U in the subsurface.

The biological reduction of metals and metalloids by *Shewanella oneidensis* MR-1 is an anaerobic process by which electrons, released upon oxidation of the electron donor, feed an electron transfer chain, consisting of a sequence of *c*-type cytochromes¹⁶ linking the cytoplasm to the extracellular environment. Thus, electrons from the cytoplasm are delivered to a periplasmic pool of *c*-type cytochromes, and then shuttled across the periplasm to, for instance, the *c*-type cytochrome chain MtrA-MtrC, part of the MtrCAB porin complex embedded in the outer-membrane. The decaheme *c*-type cytochromes MtrC and OmcA, located on the outer membrane of the cells and its finger-like extensions¹¹¹, are terminal reductases that deliver electrons to extracellular electron acceptors^{16,143,90,104}, or to secreted flavin shuttles that mediate electron transfer^{109,93,113,108}.

The role of multiheme *c*-type cytochromes (MHC) in the reduction of aqueous U(VI) was studied both experimentally by Marshall et al.¹⁷, and theoretically by Sundadarajan¹²¹. Marshall et al. investigated a collection of *S. oneidensis* MR-1 mutants to determine which *c*-type cytochromes were involved in the reduction of aqueous U(VI)-carbonate species. The mutant lacking all *c*-type cytochromes ($\Delta ccmC$) lost the ability to reduce U(VI), underscoring the key role of these proteins in U(VI) reduction. Moreover, single outer-membrane MHC deletion mutants $\Delta mtrC$ and $\Delta omcA$, but also the double cytochrome deletion mutant $\Delta mtrC\text{-}omcA$ displayed slower reduction rates as compared to wild type (WT) MR-1. Such results suggest that both MtrC and OmcA are involved in electron transfer to aqueous phase U(VI)-carbonate. Additionally, using purified MtrC and OmcA, they observed that MtrC, but not OmcA, could transfer electrons to U(VI)-citrate. However, the fact that single and double outer-membrane MHC deletion mutants could still reduce U(VI)-

carbonate hinted at periplasmic MHC-mediated electron transfer. Furthermore, Sundararajan et al. studied the mechanism of aqueous uranyl(VI) reduction by the *c*-type cytochrome PpcA of *G. sulfurreducens* using density functional theory (DFT) calculations⁶⁶. According to their model, a single electron transfer is expected to occur from PpcA to U(VI), producing U(V), followed by the spontaneously disproportionation of two U(V) to U(VI) and U(IV).

However, recent studies have revealed the persistence of an aqueous pentavalent U (U(V))-organic ligand complex at circumneutral pH values under laboratory conditions^{40,32}. The ligand in question, dpaea²⁻ (dpaeaH₂=bis(pyridyl-6-methyl-2-carboxylate)-ethylamine), is synthetic, but belongs to the family of aminocarboxylate ligands. These ligands occur in the environment either naturally, for instance, dipicolinic acid in bacterial endospores^{126,127}, or as a consequence of human-related activities such as metal chelation in remediation processes¹⁴⁴, radionuclide extraction in nuclear wastes^{131,132}, or additives in detergents^{145,146}. We have recently demonstrated the biological reduction of U(V)-dpaea by *S. oneidensis* MR-1, suggesting that upon stabilization of U(V), its biological reduction is possible. In fact, the reduction of U(VI)-dpaea occurs via two single successive electron transfers: (i) solid phase U(VI)-dpaea is reduced to soluble U(V)-dpaea, and (ii) U(V)-dpaea to solid-phase U(IV) species, such as U(IV)-dpaea₂, and non-crystalline U(IV)³².

While the reduction of aqueous U(VI) species has been abundantly documented, there is limited information about solid phase U(VI) reduction. A kinetic model was developed to characterize the reduction of the mineral sodium boltwoodite (NaUO₂SiO₃OH·1.5 H₂O), and indicated that the dissolution of solid U(VI) precedes its reduction¹⁴⁷. A similar result was observed with hydrogen uranyl phosphate crystals, for which dissolution was the first step¹⁴⁸. In addition, we recently showed that in the presence a strong organic ligand, which favour the stabilization of U(V), solid phase U(VI)-dpaea was mobilized to aqueous U(V)-dpaea. The mobilization of solid phase U(VI) may be of concern in contaminated areas, hence a topic

Additionally, while the role of MHC in U(V) reduction has been exemplified in our previous work by showing the absence of reduction of U(V) by a $\Delta ccmG$ mutant (lacking *c*-type cytochromes), it is unclear whether outer-membrane or periplasmic and cytoplasmic MHC are involved. In this context, we sought to probe the implication of outer-membrane *c*-type cytochromes in solid phase U(VI)-dpaea reduction to U(V)-dpaea, as well as in the subsequent electron transfer from U(V)-dpaea to U(IV) species. We investigated the mechanism of reduction of U(VI)-dpaea and U(V)-dpaea at the cellular level by constructing a deletion mutant strain lacking the outer-membrane *c*-type cytochromes MtrC, OmcA and MtrF (strain $\Delta mtrC/omcA/mtrF$). At the molecular level, we investigated the reaction between the purified *c*-type cytochrome MtrC and solid/aqueous phase U(VI)-dpaea or aqueous phase U(V)-dpaea. We established that solid phase U(VI)-dpaea reduction proceeds via dissolution prior to reduction to U(V)-dpaea by periplasmic and outer-membrane *c*-type cytochromes. Additionally, purified MtrC reduced U(V)-dpaea to U(IV) species efficiently, implying that this outer-membrane *c*-type cytochrome can be involved in the reduction of U(V)-dpaea.

3.2 Experimental methods

3.2.1 Description of the *mtrC/omcA/mtrF* deletion mutant

Regions flanking *mtrF* (SO_1780) in *Shewanella oneidensis* $\Delta omcA\Delta mtrC$ ¹⁷ were amplified by PCR with primers *mtrF*_5'O/*mtrF*_5'I and *mtrF*_3'I(DD)/*mtrF*_3'O(DD) (Table S1), fused by overlap extension PCR and cloned into suicide plasmid pMQS¹⁴⁹. The resulting plasmid, pMQS-*mtrF*(DD), was introduced into *Shewanella oneidensis* $\Delta omcA\Delta mtrC$ by conjugation from *E. coli* strain WM3064. Colonies with single crossover plasmid insertions were selected on LB agar plates containing kanamycin, purified once on agar plates with kanamycin and resistant colonies were subsequently grown overnight in LB (containing no NaCl) without antibiotic. Double crossover mutants were selected on LB agar plates (containing no NaCl) supplemented with 10% sucrose. Sucrose resistant and kanamycin sensitive colonies were checked by colony PCR for gene deletion using primers flanking the deleted region (*mtrF*_FO + *mtrF*_RO(DD)) (Table S1). Selected clones were purified, genomic DNA isolated, and the region containing the deleted gene was amplified by PCR and the deletion verified by Sanger sequencing (Table S2). Henceforth, for simplicity, the $\Delta mtrC/omcA/mtrF$ deletion mutant will be referred as ΔOMC . 'OMC' stands for outer-membrane c-type cytochromes.

3.2.2 Strains and growth conditions

In addition to WT *S. oneidensis* MR-1 and the newly generated mutant, ΔOMC , this study also includes the previously generated $\Delta ccmG$ deletion mutant³². The three strains were first incubated in a liquid pre-culture started from a frozen stock (-80°C) and grown overnight in Luria-Bertani (LB) medium at 30°C in a shaking incubator (140 rpm). An aliquot of this pre-culture was further inoculated in fresh LB with a starting OD₆₀₀ of 0.1. When the culture reached an OD₆₀₀ of 2 (mid- to late-exponential phase), the cells were harvested by centrifugation at 9,610 ×g for 10 minutes at room temperature (Avanti J-26 XP, Beckman, Brea, California, US), and washed three times anoxically with modified Widdel low phosphate (WLP) medium at pH 7.3, prior to amendment of U. The modified WLP medium lacked bicarbonate and phosphate to prevent their complexation of U³²

3.2.3 Preparation of ferrihydrite and Fe(III)-citrate

Fresh ferrihydrite was prepared by titrating 0.5M Fe(III)-Cl with 10M NaOH until the pH value reached 7. After 30 minutes of equilibration, the precipitate was centrifuged and washed 5 times with deionized water (8,000 g, 10 min). A Fe(III)-citrate stock solution was prepared by dissolving Fe(III)-citrate ($M_w = 245.95\text{g/mol}$) in deionized water and adjusting the pH value to 7 with 10M NaOH. The obtained solution was filter-sterilized with 0.2 μm filters. The final iron concentrations in both the ferrihydrite and Fe(III)-citrate solutions were measured by ICP-OES after digestion of an aliquot in 4.5M HCl. The suspension and solution were both stored at 4°C, wrapped in aluminum foil until use.

3.2.4 Reduction experiments with ferrihydrite and Fe(III)-citrate

All the experiments described in the following paragraph were performed inside a nitrogen-atmosphere anaerobic chamber (MBraun, Germany), with O₂ < 0.1 ppm. *S. oneidensis* MR-1, ΔOMC and $\Delta ccmG$ were prepared as described above. They were incubated, in addition to a no-cell control, under non-growth conditions in a WLP modified medium³² supplemented with 20 mM lactate, as the electron donor, and with 5 mM anoxic ferrihydrite or Fe(III)-citrate as electron

acceptors. The starting OD₆₀₀ of the incubations was calculated to be 1. The incubations were maintained in the dark at room temperature, inside the anaerobic chamber. Fe(II) was measured by the ferrozine assay and cell viability was followed by streaking an aliquot of culture on LB agar plates. Each experimental condition was set up in duplicate.

3.2.5 Reduction of U(VI)-dpaea

S. oneidensis MR-1, Δ OMC, and Δ ccmG were incubated, under non-growth conditions, in anoxic modified WLP medium in the presence of solid phase U(VI)-dpaea ([UO₂(dpaea)] MW = 583 g.mol⁻¹) at an equivalent aqueous concentrations of 2 mM, synthesized as previously described⁴⁰, along with 20 mM of lactate as the electron donor. The starting OD₆₀₀ of the incubations was measured to be 1. The incubations were maintained in the dark at room temperature, inside the anaerobic chamber. At several time points, aliquots of the incubations were filtered through 0.2 μ m PTFE filters (Whatman, Maidstone, United Kingdom). Similarly, the three abovementioned strains were incubated on aqueous phase U(VI)-dpaea obtained by filtering suspensions of solid phase U(VI)-dpaea in modified WLP medium supplemented with 20 mM lactate through a 0.2 μ m PTFE filter in order to remove the solid phase. The experimental details are similar to those described for the solid phase U(VI)-dpaea experimental set up. Each experimental condition was set up in duplicate. U was quantified by ICP-MS (ICP-MS 7900, Agilent, Santa Clara, California, US) as described in the Experimental methods in chapter 1.

3.2.6 MtrC purification

Recombinant protein MtrC was expressed in the double mutant Δ omc Δ mtrC strain of *S. oneidensis* MR-1 LS331, kindly provided by Liang Shi³⁷. 0.1 mM L-arabinose-induced culture supernatant was collected by centrifugation. To facilitate purification, the Ni²⁺-NTA sepharose resin (Bio-rad) was added directly to the culture supernatant to a ratio of 8 mL of resin per liter of supernatant. To allow the resin to bind, bottles containing MtrC and the resin were rotationally shaken for 3 hours at 4°C. The resin was recovered by sedimentation and loaded onto a column for protein purification. The protein was entirely eluted in a buffer made of 40 mM imidazole in 20 mM HEPES and 150 mM NaCl at pH 7.5. Imidazole was washed by two successive dialysis steps. The protein was concentrated using ultrafiltration membranes. Following elution and concentration, the purified MtrC migrated as a single band on an SDS-PAGE gel with an apparent mass of 75 kDa (Figure 3:1). The protein concentration was evaluated by bicinchoninic acid assay (Pierce™BCA Protein Assay Kit, ThermoFisher Scientific, Waltham MA USA).

3.2.7 Reduction of MtrC

In an MBraun glovebox, the purified protein was reduced using sodium dithionite (Na₂S₂O₄). Sodium dithionite was added gradually, until the hemes were fully reduced. Their redox status was monitored by UV-vis spectrophotometry (UV-2501P, Shimadzu, Kyoto Japan) in a wavelength range of 500 nm to 580 nm. An anaerobic quartz cuvette (Msscientific, Berlin, Germany) was used for this purpose. Reduced MtrC is characterized by two peaks at 522 nm and 552 nm (β and α Soret absorption peaks), whereas oxidized MtrC displays a maximum at 530 in this spectral region.

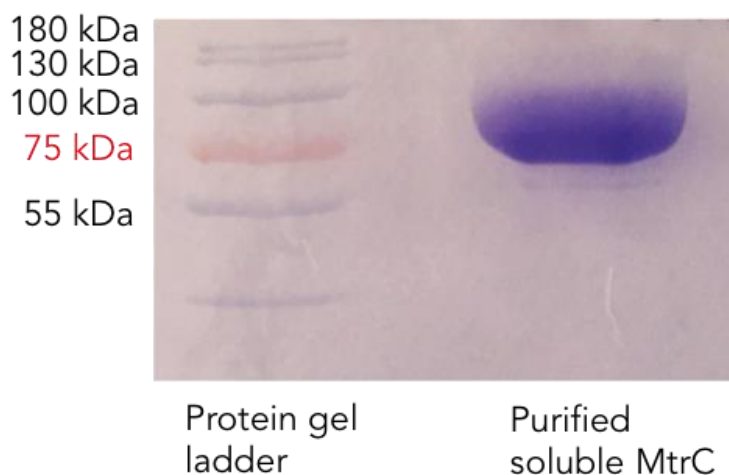


Figure 3:1. SDS-PAGE of purified recombinant MtrC isolated from $\Delta omcA/mtrC$ strain LS331 of *S. oneidensis* MR-1.

3.2.8 Dialysis

In order to remove the potential excess of sodium dithionite, which could react with U, the reduced protein was dialyzed for about 18h using dialysis cassettes (Side-A-Lizer[®], ThermoFisher Scientific, Waltham MA USA) in the glovebox. The buffer (buffer A) used was composed of 100mM HEPES and 50mM NaCl, and the pH was adjusted to a value of 7.5. The redox status of the hemes was probed after dialysis in order to ensure that they were still fully reduced. The concentration was measured again with the BCA assay. To ensure that dialysis effectively removed excess sodium dithionite from the protein solution, the same volume of sodium dithionite as that used to reduce the cytochromes was mixed to buffer A in a similar ratio. The mixture of sodium dithionite in buffer A was dialyzed following the method described above. After dialysis, the mixture was reacted with U(V)-dpaea. We did not observe reduction of U(V)-dpaea, suggesting that the dialysis was efficient enough to remove excess reducing agent. The functionality of reduced and dialyzed MtrC was tested using U(VI)-carbonate and U(VI)-citrate. MtrC reduced both substrates to an extent of 60% and 64%, respectively, after 30 seconds (data not shown).

3.2.9 Reaction of MtrC with U(V)-dpaea or U(IV)-citrate

In the glovebox, five reactions were initiated as follows: (i) U(V)-dpaea in buffer A; (ii) U(V)-dpaea in buffer A with oxidized MtrC, (iii) U(V)-dpaea in buffer A with reduced MtrC, (iv) U(IV)-citrate in buffer A, (v) U(IV)-citrate in buffer A with oxidized MtrC. Reactions (i) and (iv) served to control the initial oxidation state of U, and in the case of U(V)-dpaea, to assess its stability over the experimental time. U(V)-dpaea powder was resuspended in buffer A to a concentration of 300 μ M. Aqueous U(IV)-citrate (200 μ M) was obtained from the reduction of U(VI)-citrate by *S. oneidensis* MR-1. Both oxidized and reduced MtrC were prepared at a concentration of 300 μ M. The reactions were initiated by mixing equal volumes of U and MtrC in buffer A ((ii), (iii), and (v)), or U and buffer A ((i) and (iv)). Timepoints were collected by removing an aliquot from the reaction mixture, and immediately loading it onto an ion-exchange chromatography resin to separate U(VI) from U(IV). The heme redox status was probed before and after reaction by UV-vis spectrophotometry to evaluate how they were influenced by U. U was quantified in both U(IV) and U(VI) fraction by ICP-MS as described in the Experimental methods in chapter 1.

3.3 Results

3.3.1 Mutant strains characterization with ferrihydrite and Fe(III)-citrate

In order to characterize the Δ OMC and Δ ccmG strains, the strains were incubated with two Fe(III) substrates: (i) ferrihydrite (solid phase Fe(III)) or (ii) Fe(III)-citrate (aqueous phase Fe(III)). As expected, no significant ferrihydrite reduction was observed with either Δ OMC or Δ ccmG in the first 48h, whereas in the WT incubations, the Fe(II) concentration reached 758.6 μ M (Figure 3:2.A.). However, we noticed some reduction after 72h as the Fe(II) concentrations in Δ OMC and Δ ccmG incubations increased from 143.1 μ M to 223.2 μ M and from 138.1 to 367.7 μ M, respectively (Figure 3:2.A.). We attribute this late reduction activity to cell death (Figure 3:2.C), lysis, and the subsequent release of intracellular reducing agents. With Fe(III)-citrate, we observed rapid Fe(III) reduction in the incubations with the WT, with the reaction reaching completion after 4h (Figure 3:2.B.). In contrast, in the incubations with Δ OMC, the Fe(II) concentration increased slowly but steadily to 4.12mM (Figure 3:2.B.). In contrast, Δ ccmG was fully impaired in its capacity to reduce Fe(III)-citrate in the first 24h, but a steady increase in Fe(II) concentration was observed subsequently (Figure 3:2.B.).

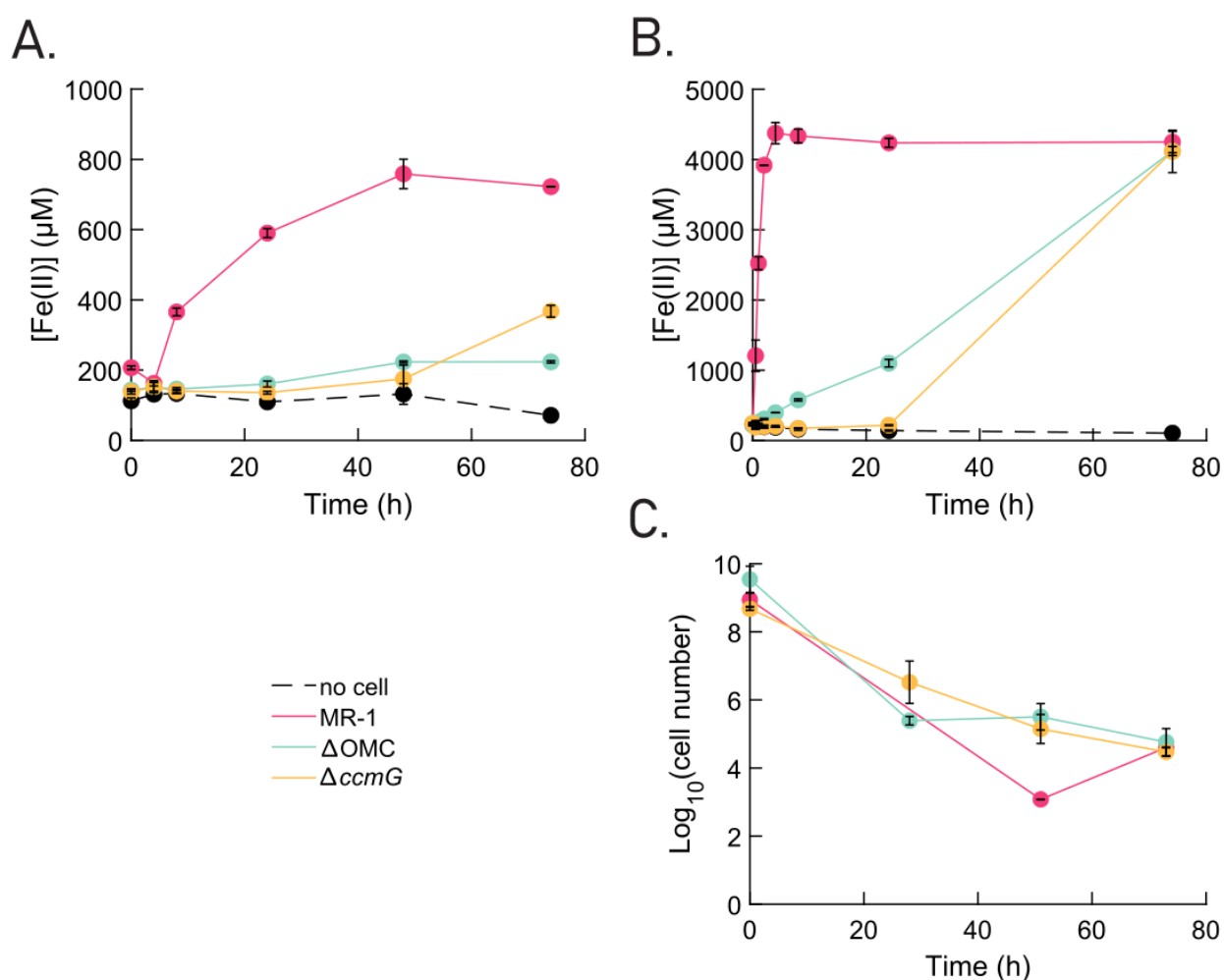


Figure 3:2. Characterization of *S. oneidensis* mutant strains with Fe(III) substrates. A. and B. Fe(II) concentration in the incubation supernatants of MR-1 (pink dots), Δ OMC (blue dots), Δ ccmG (yellow dots) and a no-cell control (black dots) from 0 to 72h of incubation with A. ferrihydrite, and B. Fe(III)-citrate. C. cell viability of MR-1, Δ OMC and Δ ccmG over time in incubations with Fe(III)-citrate.

The ability of Δ OMC to reduce soluble Fe(III)-citrate could be attributed to the diffusion of the soluble complex into the cell periplasm and its reduction by other *c*-type cytochromes (such as FccA or Stc). Alternatively, it could be that MtrA in Δ OMC, with its solvent exposed terminal heme in absence of MtrC⁸⁷, reduces Fe(III)-citrate as Edward et al. suggested. As for Δ ccmG, cell death and lysis could account for the reduction of Fe(III), as the cell viability assay shows that cell concentration decreased from about 10^8 to 10^4 (Figure 3:2.C.). In summary, both Δ OMC and Δ ccmG showed impairment in the reduction of solid and aqueous phase Fe(III) substrates for 48 and 24 hours, respectively and, by extension, are hypothesized to do the same for U.

3.3.2 Reduction of solid phase U(VI)-dpaea proceeds via dissolution followed by reduction

3.3.2.1 Solid phase U(VI)-dpaea

The WT, Δ OMC and Δ ccmG strains were incubated with either 1mM solid phase U(VI)-dpaea (Figure 3:3.A.) or $\sim 23 \mu\text{M}$ aqueous phase U(VI)-dpaea (corresponding to the solubility limit of U(VI)-dpaea³²) (Figure 3:3.B.), at a cell concentration of OD₆₀₀ of 0.1. We chose to incubate the cells at a lower OD₆₀₀ (it is usually OD₆₀₀ 1) to enhance any differences in reduction rates between strains. Both the WT and Δ OMC strains displayed rapid reduction rates of solid phase U(VI)-dpaea in the first 11h as the aqueous concentrations of U increased from about 100 μM to 1.27 mM and 1.1mM, respectively (Figure 3:3.A.). This rapid rise of aqueous U concentrations was followed by a phase of slower increase, up to 1.97mM for WT incubations and up to 1.73mM for Δ OMC incubations. Based on our previous study, we infer that the aqueous U released in the incubation supernatants corresponds to U(V)-dpaea³². As for Δ ccmG, it was fully impaired in solid phase U(VI)-dpaea reduction as the aqueous U concentration remained stable over the experimental time, oscillating between 97 μM and 130 μM (Figure 3:3.A.). Furthermore, we observed a similar trend in the no-cell control, for which aqueous U concentrations oscillated from 101 μM to 123 μM , the solubility limit of the solid U(VI)-dpaea stock used in these experiments (variability in the solubility of U(VI)-dpaea has been reported depending on the stock). The fact that Δ ccmG could not reduce solid phase U(VI)-dpaea confirms the involvement of *c*-type cytochromes in solid phase U(VI)-dpaea reduction. In addition, Δ OMC, lacking outer-membrane *c*-type cytochromes, could reduce solid phase U(VI)-dpaea at a similar rate as compared to the WT. Therefore, it implies that U(VI)-dpaea can access another pool of *c*-type cytochromes, likely that located in the periplasm. This result points to the dissolution of solid phase U(VI)-dpaea as a prerequisite for the reduction of U(VI)-dpaea, prior to migrating through the outer membrane and being reduced in the periplasm.

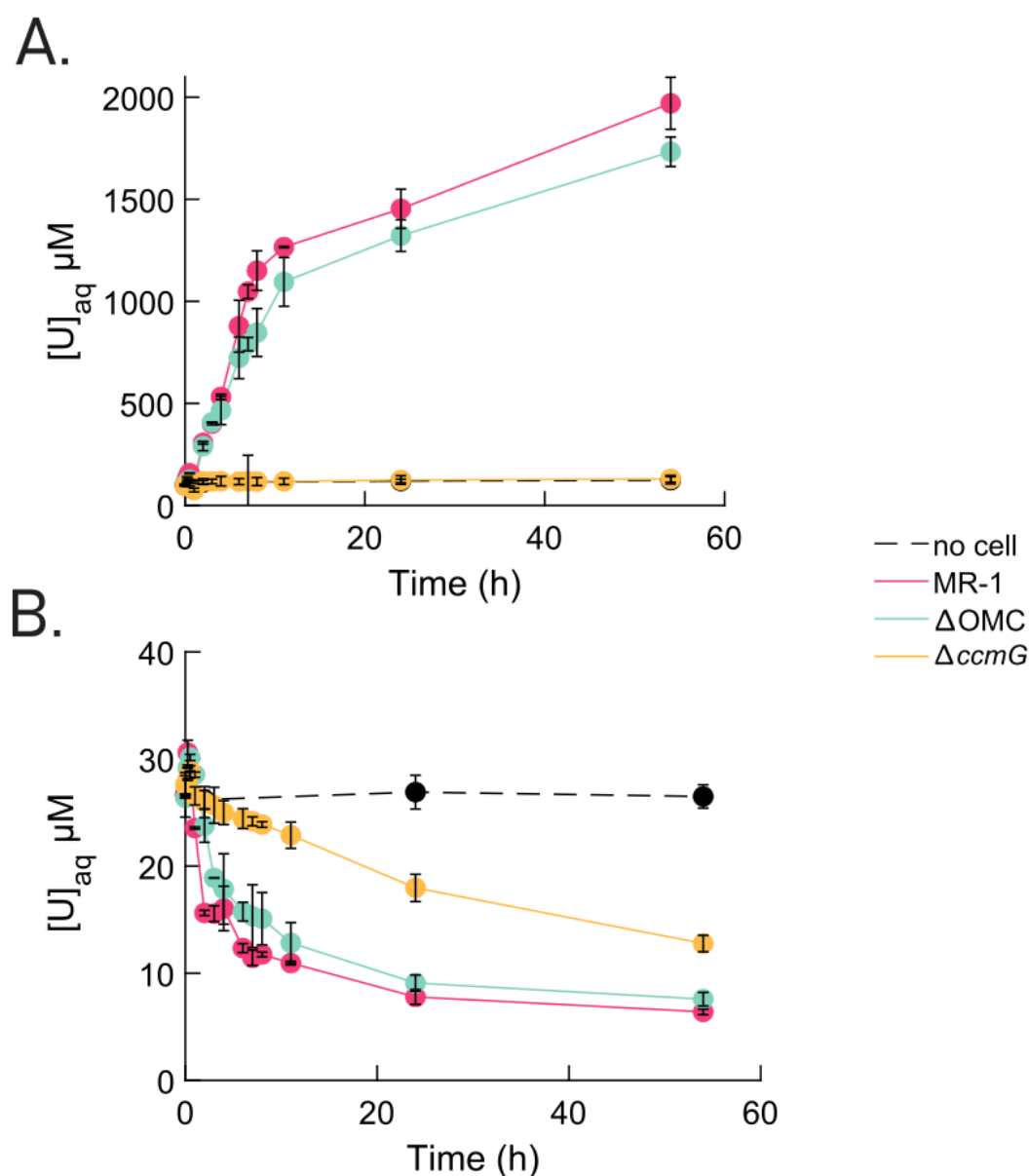


Figure 3:3. Incubation of MR-1, Δ OMC and Δ ccmG with U(VI)-dpaea. Aqueous $[U]_{aq}$ concentration in the incubation supernatants of MR-1 (pink dots), Δ OMC (blue dots), Δ ccmG (yellow dots) and a no-cell control (black dots) from 0h to 54h of incubation with A. solid phase U(VI)-dpaea; B. aqueous phase U(VI)-dpaea.

3.3.2.2 Aqueous U(VI)-dpaea

To confirm that soluble U(VI)-dpaea could be reduced by our set of strains, we incubated them with the soluble fraction of U(VI)-dpaea, which arises from its limited solubility in water at pH 7³². As observed for solid phase U(VI)-dpaea, both the WT and Δ OMC strains reduced aqueous U(VI)-dpaea by two third after 54h (Figure 3:3.B). In fact, the aqueous U concentrations decreased from about 26 μ M to 6.4 μ M in incubations with the WT, and to 7.6 μ M in incubations with Δ OMC. Surprisingly, Δ ccmG also showed reductive activity, as the aqueous U concentration decreased from 27.6 μ M to 12.8 μ M after 54h (Figure 3:3.B). Analysis of aliquots of 2-week-old Δ ccmG cell suspensions by ion exchange chromatography revealed that 50% of the total U was eluted in the U(IV) fraction. Hence, Δ ccmG could reduce about 15 μ M of

aqueous U(VI)-dpaea to U(IV) albeit at a slower rate than the WT or Δ OMC strains. As reported above, a similar behavior was observed in presence of Fe(III) substrates. Δ ccmG was impaired in solid phase Fe(III) reduction, but could reduce aqueous phase Fe(III) after 24h (Figures 3:2.A. and 3:2.B.). We attribute this activity towards soluble substrates to the presence of intracellular redox metabolites released when cells lyse. We will investigate this point in future experiments consisting of incubating lysed Δ ccmG cells with soluble Fe(III) and soluble U(VI)-dpaea. Alternatively, this observation could be explained by the existence of non-cytochrome reducing agents that are ordinarily overshadowed by the activity of *c*-type cytochromes. This activity may only be evidenced when low concentrations of U are considered, as is the case here.

Overall, these results indicate that solid phase U(VI)-dpaea reduction proceeds first via dissolution of solid phase U(VI)-dpaea to an aqueous U(VI)-dpaea species, followed by its subsequent reduction to U(V)-dpaea and then U(IV)-dpaea by both outer-membrane and periplasmic *c*-type cytochromes. These results are congruent with the findings obtained with the mineral sodium boltwoodite ($\text{NaUO}_2\text{SiO}_3\text{OH}\cdot 1.5\text{H}_2\text{O}$)¹⁴⁷ and hydrogen uranyl phosphate crystals¹⁴⁸. However, Yang et al. proposed that three uranyl(VI) borate and boronate crystals can be reduced directly by strain MR-1 cells and does not necessarily need dissolution¹⁵⁰. They calculated the maximum amount of U(VI) dissolved which could be reduced over the experimental time and observed that it was lower than the experimentally recovered amount of reduced U.

3.3.3 Role of *c*-type cytochromes in U(V)-dpaea reduction

3.3.3.1 At the cellular level

We incubated the WT, Δ OMC, and Δ ccmG strains at a cell density of OD₆₀₀ 1 with 550 μM of U(V)-dpaea. We increased the cell density compared to the reactions with U(VI)-dpaea as the kinetics of reduction are known to be slower³². After 74h, the concentration of U(V)-dpaea showed a 12.3% decrease in the incubations with the WT, and of 3% in the incubations with Δ OMC (Figure 3:4.A.). In comparison, in the no cell control, the U(V)-dpaea concentration remained stable over the experimental time, which ensures that U(V)-dpaea did not undergo spontaneous disproportionation (Figure 3:4.A.). As previously published, we observed a 2% of U(V)-dpaea concentration in the incubations with Δ ccmG³². These observations hint at the involvement of outer-membrane *c*-type cytochromes in the reduction of U(V)-dpaea.

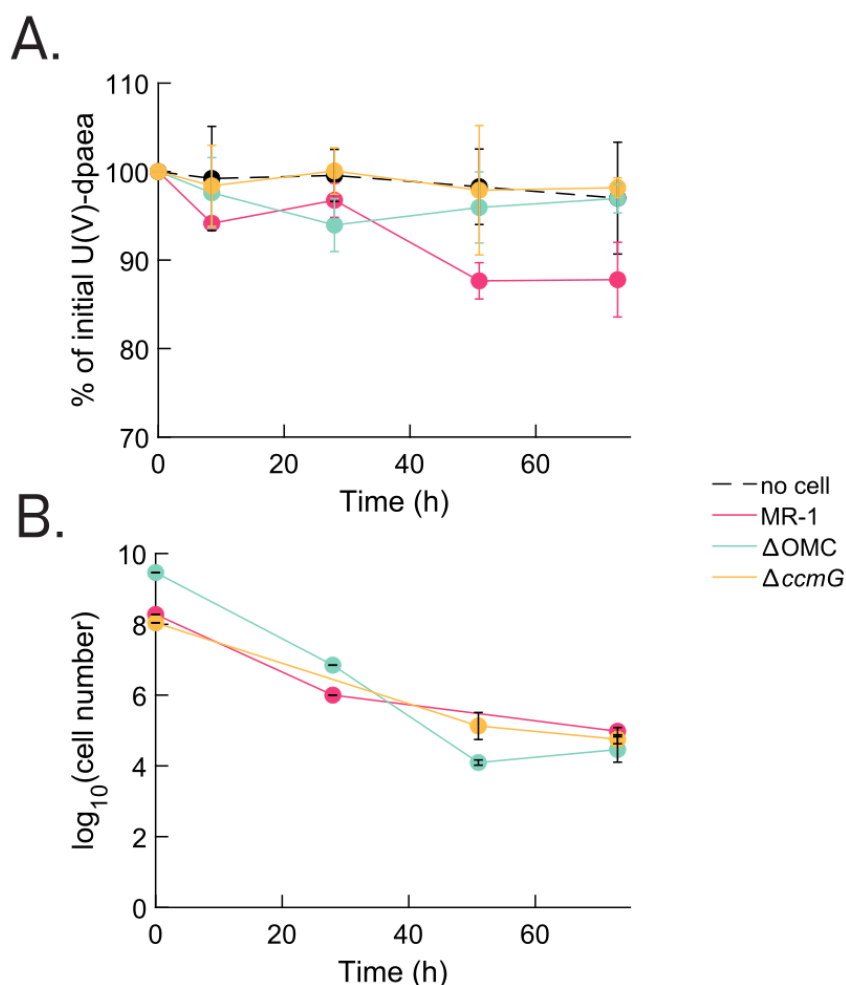


Figure 3:4. Incubation of MR-1, Δ OMC and Δ ccmG with U(V)-dpaea. A. U concentration in the incubation supernatants of MR-1 (pink dots), Δ OMC (blue dots), Δ ccmG (yellow dots) and a no-cell control (black dots) from 0h to 72h of incubation with U(V)-dpaea; C. cell viability of MR-1, Δ OMC and Δ ccmG over the experimental time in incubations with U(V)-dpaea.

3.3.3.2 At the molecular level

To further decipher the involvement of MHC in the reduction of U(V)-dpaea, we investigated the reactions between U(V)-dpaea and the purified *c*-type cytochrome MtrC from *S. oneidensis* MR-1. We studied MtrC in both its oxidized state, i.e., when all hemes are in the Fe^{3+} form, and in its reduced state, i.e., all hemes are in the Fe^{2+} form. MtrC protrudes from the surface of MR-1 cells and was shown to be a terminal reductase⁹². Therefore, MtrC is likely to transfer electrons to electron acceptors such as U. The reaction between U(V)-dpaea and either oxidized or reduced MtrC was monitored by ion exchange chromatography, to resolve the oxidation state of U after reaction. In addition, the redox state of the MtrC hemes was probed by UV-vis spectroscopy, in order to assess potential electron transfer. The no-protein control consisted of U(V)-dpaea only and thus, upon ion-exchange chromatography treatment (with acid) is expected to yield 50% U(IV) and 50% U(VI), as a result of disproportionation. Any deviation from this ratio is attributable to the reaction with MtrC.

For the reaction between U(V)-dpaea and oxidized MtrC, we observed a 14% decrease in the U(IV) fraction (corresponding to an equal increase in the U(VI) fraction) after 2min, relative to the no-protein control (Figure 3:5.A., Table 3:1.) and the same result after the reaction proceeded for 4 hours (Figure 3:6, Table 3:2).

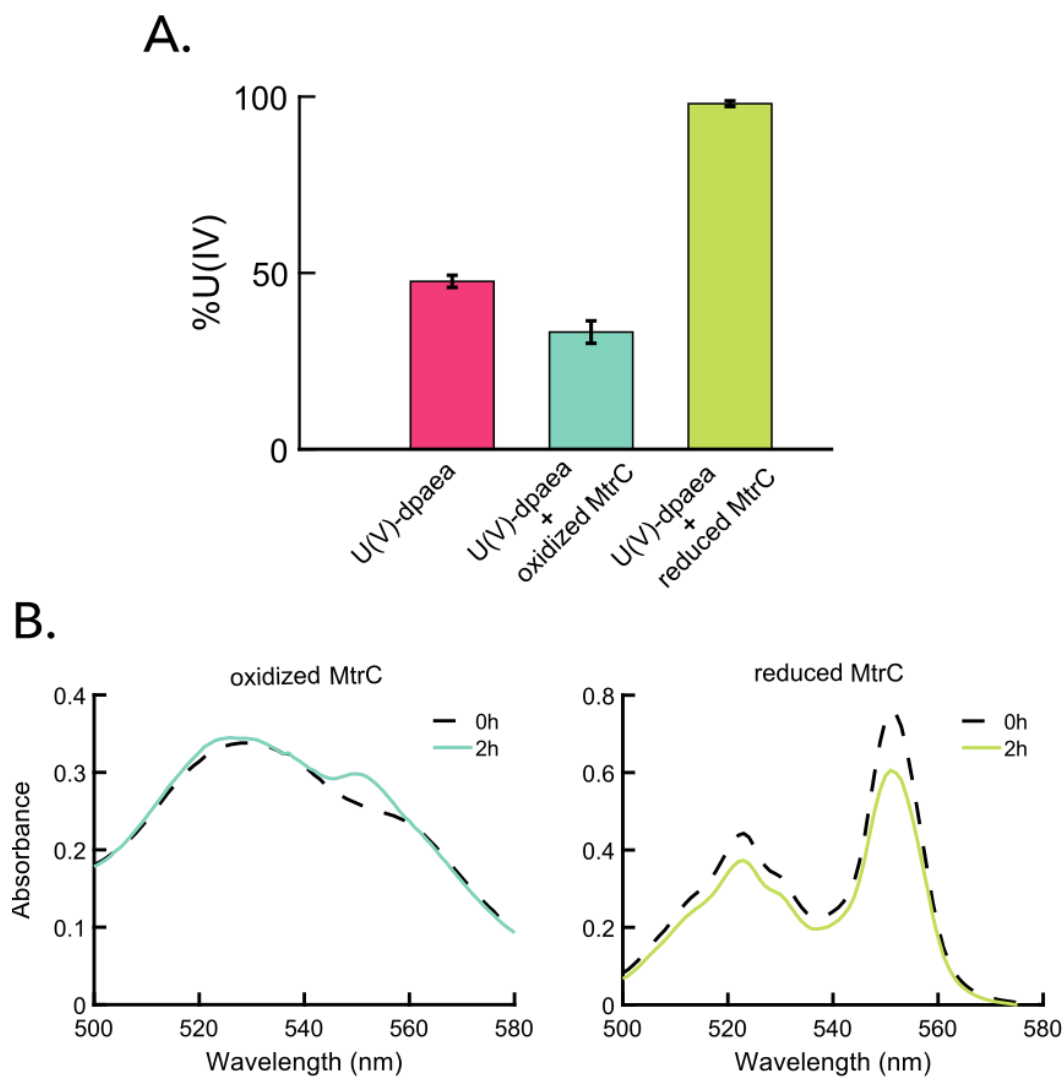


Figure 3:5. MtrC reacted with U(V)-dpaea. A. Percentage of U(IV) obtained by ion exchange chromatography for the reaction between U(V)-dpaea and either oxidized (light blue) or reduced (green) MtrC after 2 min of reaction. U(V)-dpaea in buffer (raspberry pink) was used as a control for acid induced disproportionation which is expected for the ion chromatography separation. B. UV-vis spectra of the hemes of MtrC before (dotted black) and after (solid line) reaction with U(V) dpaea for 2 hours.

Reaction mixture	%U(IV)	Standard deviation	[U] (μM)	[MtrC] (μM)	[U]/[MtrC]
U(V)-dpaea - 2min					
U(V)-dpaea	47.62	1.72	117.70	/	/
Oxidized MtrC	33.24	3.19	116.78	166.26	0.70
Reduced MtrC	98.02	0.81	120.51	155.70	0.77
dialysis control	49.59	2.55	119.52	/	/
U(IV)-citrate - 2min					
U(IV)-citrate	99.02	0.56	113.391	/	/
Oxidized MtrC	98.78	3.97	113.713	102.20	1.15
solid U(VI)-dpaea					
no protein control	4.32	4.25	137.78	/	/
Reduced MtrC	57.6	2.27	153.873	166.06	0.7
soluble U(VI)-dpaea					
no protein control	18.27	1.88	22.07	/	/
Reduced MtrC	76.21	0.46	23.1	115.24	0.2

Table 3:1. Summary of the experimental results describing the reactions of U(V)-dpaea with either oxidized or reduced MtrC after 2 min, and also with the dialysis control obtained by dialyzing the amount of sodium dithionite used to reduce MtrC. Additionally, the reaction of U(IV)-citrate with oxidized MtrC is reported as well. We also included the results from the reaction between reduced MtrC and solid or soluble U(VI)-dpaea. The %U(IV) was obtained by ion exchange chromatography separation. The ion exchange chromatography separation cannot directly identify U(V), because the samples are acidified prior to loading onto the column. Acid treatment is known to disproportionate uranyl(V) to produce equal proportions of U(V) and U(IV). Therefore, here in the case of U(V)-dpaea, about 50% U(IV) is a proxy for U(V) (result demonstrated by U M_{4-} edge HR-XANES). The table also reports the concentration of U and the concentration of MtrC, and also their ratio.

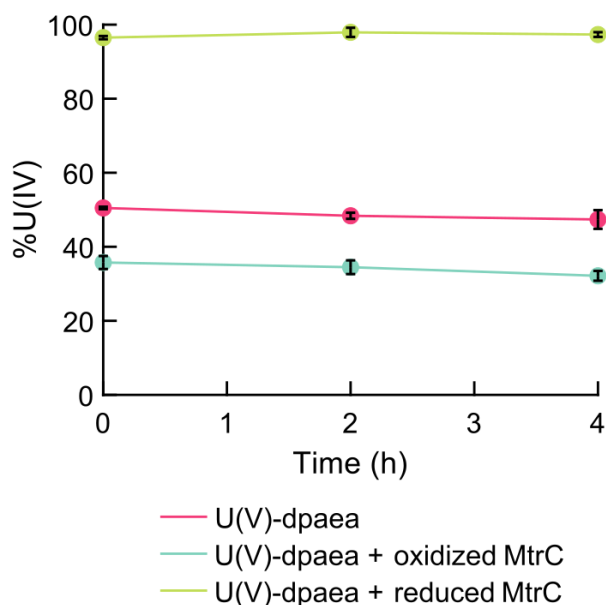


Figure 3:6. Timeline of the reaction between MtrC and U(V)-dpaea. Percentage of U(IV) obtained by ion exchange chromatography of the reaction between U(V)-dpaea and either oxidized (blue) or reduced (green) MtrC after 20s, 2h and 4h of reaction. U(V)-dpaea (pink) was used as a control to ensure that no spontaneous disproportionation occurred during the experimental time. The ion exchange chromatography separation cannot directly identify U(V), because the samples are acidified prior to loading onto the column. Acid treatment is known to disproportionate uranyl(V) to produce equal proportions of U(VI) and U(IV). Therefore, here, the equal proportions observed for U(VI) and U(IV) in the supernatant are a proxy for U(V) (result demonstrated by U M_{4-} edge HR-XANES).

Reaction mixture	Time	%U(IV)	Standard deviation	[U] (uM)	[MtrC] (uM)	[U]/[MtrC]
U(V)-dpaea	20s	50.48	0.33	129.33	/	/
	2h	48.37	0.82			
	4h	47.37	2.53			
Oxidized MtrC	20s	35.75	1.76	126.01	175.84	0.72
	2h	34.48	1.85			
	4h	32.15	1.33			
Reduced MtrC	20s	96.49	0.43	124.54	161.46	0.77
	2h	97.92	1.24			
	4h	97.32	0.64			

Table 3:2. Summary of the experimental results describing the reactions of U(V)-dpaea with either oxidized or reduced MtrC over 4h. The %U(IV) was obtained by ion exchange chromatography separation. The ion exchange chromatography separation cannot directly identify U(V), because the samples are acidified prior to loading onto the column. Acid treatment is known to disproportionate uranyl(V) to produce equal proportions of U(V) and U(IV). Therefore, here in the case of U(V)-dpaea, about 50% U(IV) is a proxy for U(V) (result demonstrated by U M4-edge HR-XANES). The table also report the concentration of U(V)-dpaea and the concentration of MtrC, and also their ratio.

Furthermore, MtrC hemes were slightly reduced. Indeed, the local absorption maximum at 530nm (oxidized hemes) shifted to 522nm and a second peak increased at 552nm. These spectral features are characteristic of reduced hemes in MtrC (Figure 3:5.B. left panel).

This result can be interpreted in one of two ways: (i) 28% of U(V)-dpaea was oxidized to U(VI)-dpaea while the hemes were reduced, suggesting an electron transfer from U(V)-dpaea to MtrC; or (ii) U(V)-dpaea has fully disproportionated, and a part of the resulting U(IV) product was re-oxidized by MtrC to U(VI)-dpaea. To distinguish between these two scenarios, we studied the reaction between soluble U(IV)-citrate and oxidized MtrC (Figure 3:7, Table 3:1.).

We did not observe any change in U oxidation state (Figure 3:7.A.), nor heme redox status (Figure 3:7.B.). Hence, we concluded that no electron transfer occurred from U(IV)-citrate to oxidized MtrC. Such a result suggests that the interaction between U(V)-dpaea and the *c*-type cytochrome MtrC does not trigger the disproportionation of U(V)-dpaea and that U(V)-dpaea was oxidized by transferring one electron to MtrC.

In parallel, we probed the reaction of U(V)-dpaea with reduced MtrC to confirm that U(V)-dpaea can be transformed to U(IV) by a one-electron transfer. We noted a transformation of 98.8% of U(V)-dpaea to U(IV) species (Figure 3:5.A.), and the hemes of MtrC were slightly oxidized (Figure 3:5.B. right panel), suggesting that MtrC donated electrons to U(V)-dpaea. Thus, these findings support the previous report of the reduction of U(V)-dpaea in *S. oneidensis* MR-1 being mediated by *c*-type cytochromes³².

We ruled out the possibility that U(V)-dpaea could be reduced by sodium dithionite left over from MtrC reduction step. The details of the test are provided in the experimental methods and the results of the test in Table 3:1.

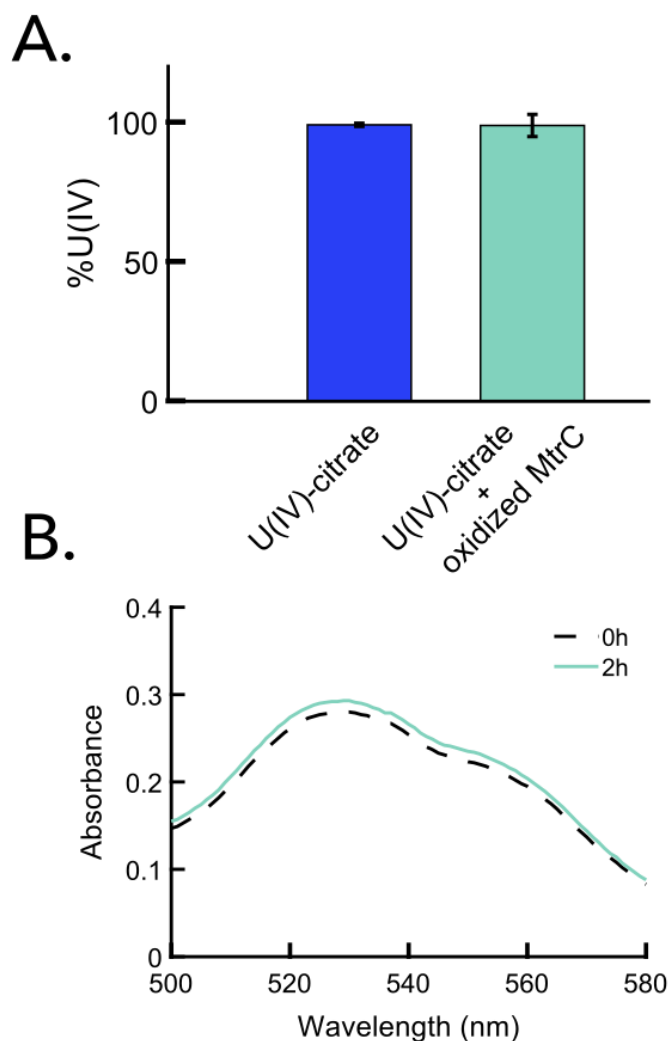


Figure 3:7. MtrC reacted with U(IV)-citrate. A. Percentage of U(IV) obtained by ion exchange chromatography of the reaction between U(IV)-citrate and oxidized MtrC (light blue) after 2 min of reaction. U(IV)-citrate in buffer A (dark blue) was used as a control for the U oxidation state. B. UV-vis spectra of the hemes of MtrC before (dotted black) and after (light blue) reaction (2 hours) with U(IV) citrate.

To further support the fact that we did not observe *c*-type cytochrome-mediated disproportionation followed by reduction of the U(VI)-dpaea moiety, we set-up the reaction between either solid or aqueous phase U(VI)-dpaea and reduced MtrC. We observed that 60% and 80% of U(VI) could be reduced by MtrC, respectively, after 2 min (Figure 3:8.A. and B. and Table 3:1). In addition, in both reactions, we observed that the hemes of MtrC underwent slight oxidation (Figure 3:8.C. and D.), suggesting that electron transfer from the hemes occurred. Furthermore, the rate of reduction was slower than that of U(V)-dpaea reacted with reduced MtrC (98.8% after 2 min). In fact, when reacting purified MtrC with aqueous U(VI)-dpaea, ~17 μ M of aqueous U(VI)-dpaea (76% of the initial U(VI)) was reduced in 2 min, whereas 118.6 μ M U(V)-dpaea (98.8% of initial U(V)) were reduced in 2min.-As the reduction from U(V)-dpaea to U(IV) is faster than that from U(VI)-dpaea to U(IV), this experiment provides conclusive evidence that U(V) does not undergo disproportionation followed by reduction of the oxidized fraction.

The reduction rate of U(V)-dpaea and U(VI)-dpaea by the purified protein was observed to be much larger than that in whole cells. We propose that isolated MtrC is more accessible to substrates because it presents additional electron exits than MtrC embedded in the MtrCAB complex. In the MtrCAB structure, four out of the 10 MtrC hemes are solvent-exposed. Namely, hemes 5 and 10 are located at opposite ends of the structure and hemes 2 and 7 are oriented towards β -barrel domains that scaffold the two pentaheme domains^{93,95}. When embedded in *S. oneidensis* MR-1 cell membranes, heme 5 receives electron from MtrA, whereas heme 10 is a favorable electron exit^{94,106}. Hemes 2 and 7 on the sides are potential binding sites for the outer membrane c-type cytochrome OmcA⁹² or flavin shuttles. It is possible that, in purified MtrC, electrons can be transferred in and out of all four hemes, accelerating the reaction with electron acceptors. Moreover, it is likely that the redox potential of isolated MtrC differs from that of MtrC when the MtrCAB complex is embedded in the cell membrane.

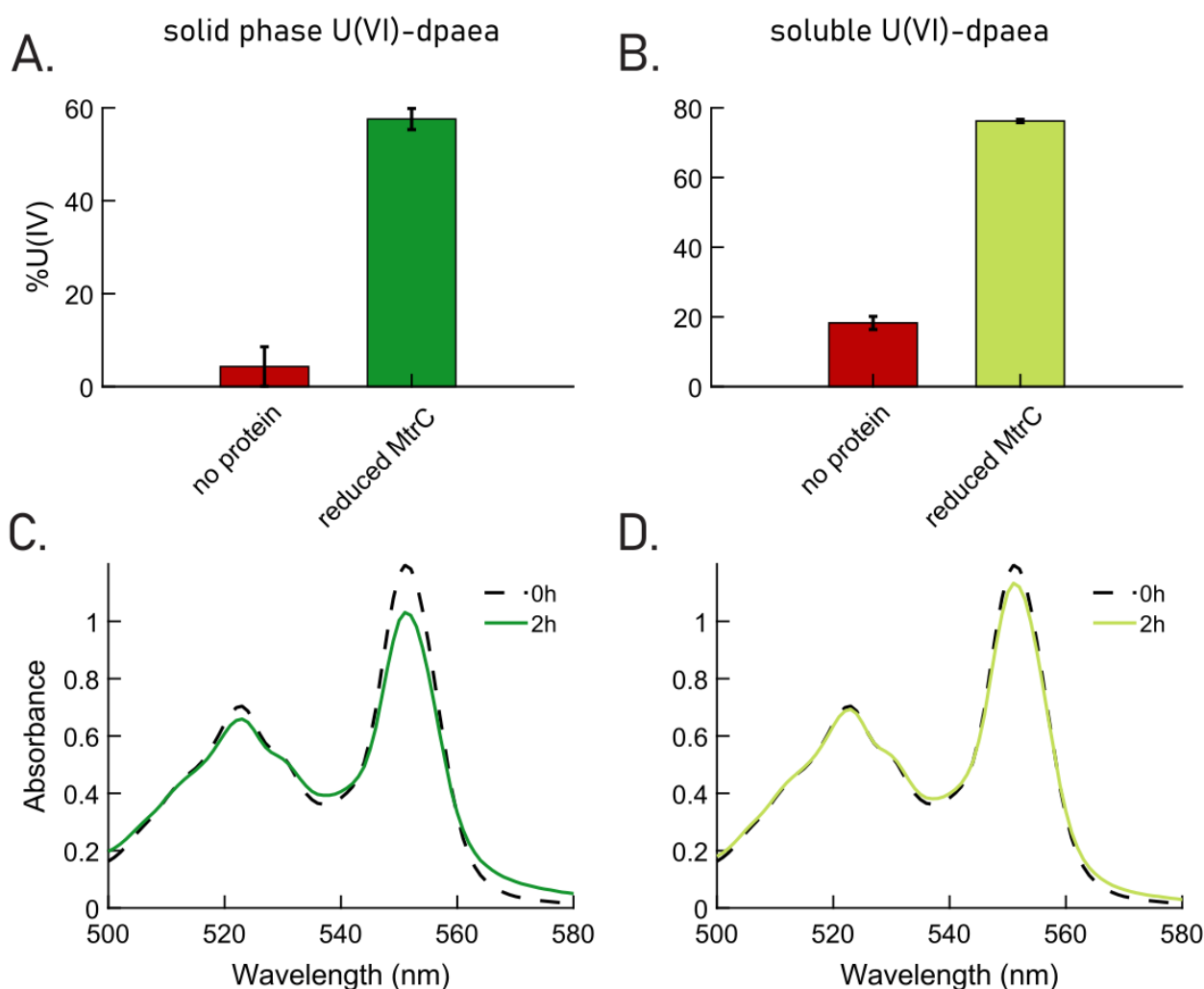


Figure 3:8. MtrC reacted with U(VI)-dpaea. A. Percentage of U(IV) obtained by ion exchange chromatography for the reaction between reduced MtrC and either (A) solid U(VI)-dpaea or (B) soluble U(VI)-dpaea after 2 min. C. and D. UV-vis spectra of MtrC hemes before (dotted black) and after (solid U(VI)-dpaea: dark green, soluble U(VI)-dpaea: light green) reaction with U(VI)-dpaea.

3.4 Conclusion

As expected, the construct lacking *c*-type cytochromes ($\Delta ccmG$) was severely impaired in the reduction of solid phase Fe(III) (for 48h) or aqueous phase Fe(III) (for 24h). Additionally, it was also impaired in the reduction of solid phase U(VI)-dpaea and aqueous U(V)-dpaea. As for the reduction of aqueous U(VI)-dpaea, $\Delta ccmG$'s reducing activity was lower than that of the WT and ΔOMC strains. Therefore, we can infer that *c*-type cytochromes are key mediators of the reduction of U solid and aqueous phase substrates. Additionally, comparison of the reductive activities of WT and ΔOMC suggests that not all pools of *c*-type cytochromes are required for U reduction. Indeed, ΔOMC reduced solid phase U(VI)-dpaea at a rate and an extent similar to those of the WT, which supports the potential involvement of periplasmic *c*-type cytochromes in the reduction of solid phase U(VI). Likely, periplasmic MHC can carry out to reduction of aqueous U(VI)-dpaea in the absence of outer-membrane MHC. Finally, this study provides direct evidence that U(V)-dpaea can be biologically reduced to U(IV) species by *c*-type cytochromes and that solid phase U(VI)-dpaea reduction is dissolution controlled. The findings are summarized in Figure 3:9.

Nevertheless, the ability of a microorganism relies also on external parameters. In fact, we investigated two solid phases (i) ferrihydrite whose solubility is $\sim 2 \times 10^{-9} \text{ M}^{151}$ and whose electrochemical potential is +0.012 V (SHE) and (ii) U(VI)-dpaea whose solubility is $\sim 3 \times 10^{-6} \text{ M}^{32}$ and electrochemical potential is -0.312 V (SHE). Thermodynamics suggest that ferrihydrite reduction by *S. oneidensis* MR-1, whose electron donating capability spans a window of redox potentials from 0 to -400mV⁹⁰, would be more favorable. Nevertheless, ferrihydrite was scarcely reduced by ΔOMC after 48h (Figure 3:2.A.) whereas the same strain reduced U(VI)-dpaea at about the same rate as the WT. This difference may be explained by the difference in solubility, hence the availability of the solid substrates in the aqueous phase, and suggests that the reduction of U(VI)-dpaea is controlled by dissolution. Thus, limited direct electron transfer to solid phase U(VI)-dpaea takes place. These results underline that dissolution of a solid phase substrate is a crucial step for reduction.

As a follow-up, it would be judicious to study additional environmentally relevant aminocarboxylate ligands, as they may also stabilize pentavalent U. It would provide a more complete overview of the fate of U(V) intermediates in the environment and of the mechanistic paths and the kinetics of their biological reduction (i.e., disproportionation or reduction). In addition, the impact of U speciation on the mechanism of electron transfer remains to be explicated. This would be key to studies of U isotopic fractionation during reduction, used as a marker to trace redox conditions across geological time.

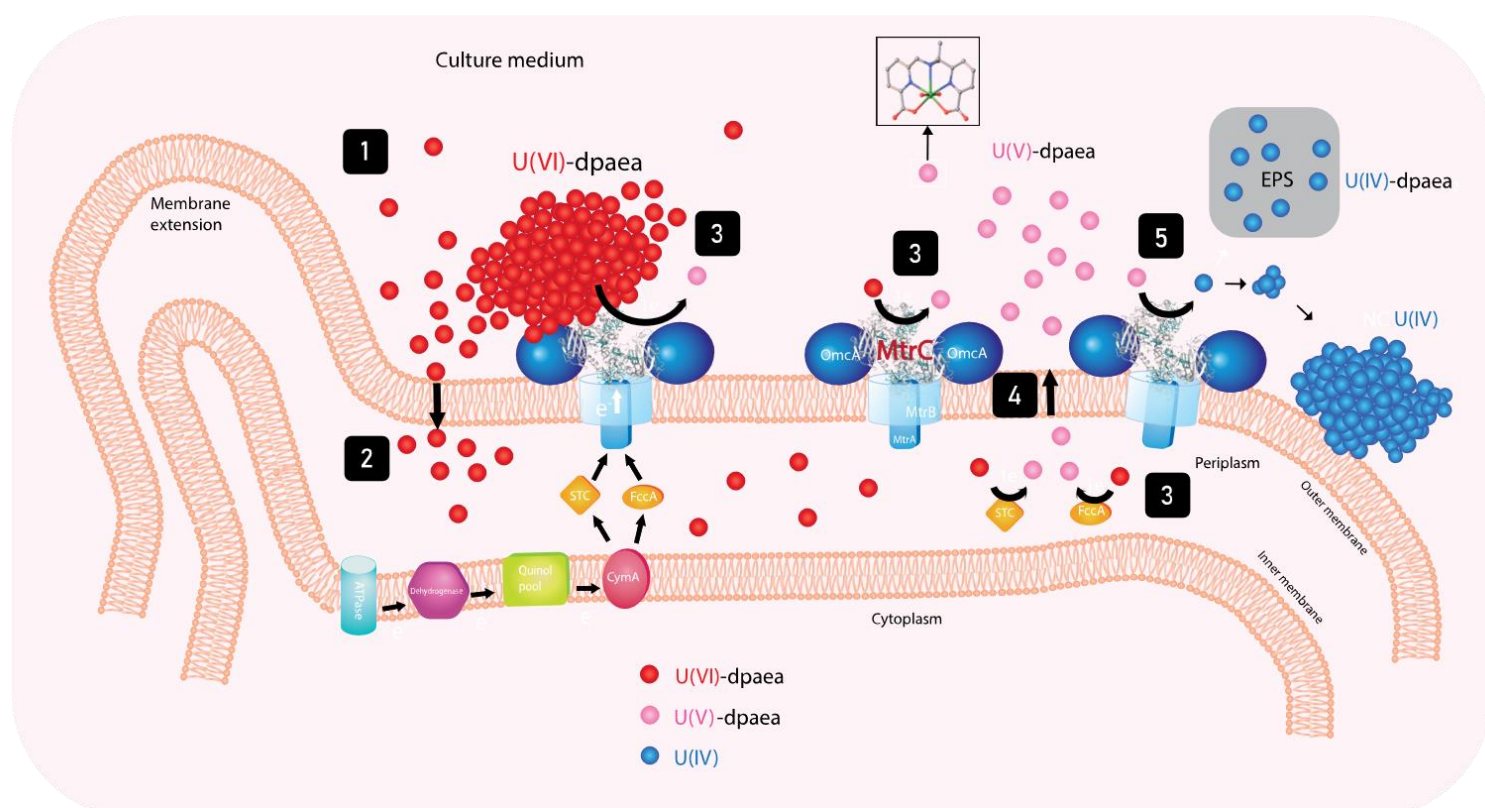


Figure 3:9. Schematic representation of the evidenced mechanisms taking place in *S. oneidensis* MR-1 when incubated with solid phase U(VI)-dpaea (red) and aqueous U(V)-dpaea (pink). 1- U(VI)-dpaea dissolution; 2- diffusion of dissolved U(VI)-dpaea; 3- reduction of dissolved or solid U(VI)-dpaea by periplasmic and outer-membrane c-type cytochromes; 4- release of U(V)-dpaea in the culture medium; 5- reduction of U(V)-dpaea by the outer-membrane c-type cytochrome MtrC to U(IV) (blue).

3.5 References

- (1) Lovley, D. R.; Phillips, E. J. P. Bioremediation of Uranium Contamination with Enzymatic Uranium Reduction. *Environ. Sci. Technol.* **1992**, *26* (11), 2228–2234. <https://doi.org/10.1021/es00035a023>.
- (2) Ribera, D.; Labrot, F.; Tisnerat, G.; Narbonne, J. F. Uranium in the Environment: Occurrence, Transfer, and Biological Effects. *Rev. Environ. Contam. Toxicol.* **1996**, *146*, 53–89.
- (3) Markich, S. J. Uranium Speciation and Bioavailability in Aquatic Systems: An Overview. *ScientificWorldJournal* **2002**, *2*, 707–729. <https://doi.org/10.1100/tsw.2002.130>.
- (4) Bernier-Latmani, R.; Veeramani, H.; Vecchia, E. D.; Junier, P.; Lezama-Pacheco, J. S.; Suvorova, E. I.; Sharp, J. O.; Wigginton, N. S.; Bargar, J. R. Non-Uraninite Products of Microbial U(VI) Reduction. *Environ. Sci. Technol.* **2010**, *44* (24), 9456–9462. <https://doi.org/10.1021/es101675a>.
- (5) Lovley, D. R.; Phillips, E. J. P.; Gorby, Y. A.; Landa, E. R. Microbial Reduction of Uranium. *Nature* **1991**, *350* (6317), 413–416. <https://doi.org/10.1038/350413a0>.
- (6) Gorby, Y. A.; Lovley, D. R. Electron Transport in the Dissimilatory Iron Reducer, GS-15. *Appl. Environ. Microbiol.* **1991**, *57* (3), 867–870.
- (7) Subramanian, P.; Pirbadian, S.; El-Naggar, M. Y.; Jensen, G. J. Ultrastructure of *Shewanella Oneidensis* MR-1 Nanowires Revealed by Electron Cryotomography. *Proc. Natl. Acad. Sci. U. S. A.* **2018**, *115* (14), E3246–E3255. <https://doi.org/10.1073/pnas.1718810115>.
- (8) White, G. F.; Shi, Z.; Shi, L.; Wang, Z.; Dohnalkova, A. C.; Marshall, M. J.; Fredrickson, J. K.; Zachara, J. M.; Butt, J. N.; Richardson, D. J.; Clarke, T. A. Rapid Electron Exchange between Surface-Exposed Bacterial Cytochromes and Fe(III) Minerals. *Proc. Natl. Acad. Sci.* **2013**, *110* (16), 6346–6351. <https://doi.org/10.1073/pnas.1220074110>.
- (9) Hartshorne, R. S.; Reardon, C. L.; Ross, D.; Nuester, J.; Clarke, T. A.; Gates, A. J.; Mills, P. C.; Fredrickson, J. K.; Zachara, J. M.; Shi, L.; Beliaev, A. S.; Marshall, M. J.; Tien, M.; Brantley, S.; Butt, J. N.; Richardson, D. J. Characterization of an Electron Conduit between Bacteria and the Extracellular Environment. *Proc. Natl. Acad. Sci.* **2009**, *106* (52), 22169–22174. <https://doi.org/10.1073/pnas.0900086106>.
- (10) White, G. F.; Shi, Z.; Shi, L.; Dohnalkova, A. C.; Fredrickson, J. K.; Zachara, J. M.; Butt, J. N.; Richardson, D. J.; Clarke, T. A. Development of a Proteoliposome Model to Probe Transmembrane Electron-Transfer Reactions. *Biochem. Soc. Trans.* **2012**, *40* (6), 1257–1260. <https://doi.org/10.1042/BST20120116>.
- (11) Wang, Z.; Shi, Z.; Shi, L.; White, G. F.; Richardson, D. J.; Clarke, T. A.; Fredrickson, J. K.; Zachara, J. M. Effects of Soluble Flavin on Heterogeneous Electron Transfer between Surface-Exposed Bacterial Cytochromes and Iron Oxides. *Geochim. Cosmochim. Acta* **2015**, *163*, 299–310. <https://doi.org/10.1016/j.gca.2015.03.039>.
- (12) Edwards, M. J.; White, G. F.; Norman, M.; Tome-Fernandez, A.; Ainsworth, E.; Shi, L.; Fredrickson, J. K.; Zachara, J. M.; Butt, J. N.; Richardson, D. J.; Clarke, T. A. Redox Linked Flavin Sites in Extracellular Decaheme Proteins Involved in Microbe-Mineral Electron Transfer. *Sci. Rep.* **2015**, *5*, 11677. <https://doi.org/10.1038/srep11677>.
- (13) Cherkouk, A.; Law, G. T. W.; Rizoulis, A.; Law, K.; Renshaw, J. C.; Morris, K.; Livens, F. R.; Lloyd, J. R. Influence of Riboflavin on the Reduction of Radionuclides by *Shewanella Oneidensis* MR-1. *Dalton Trans.* **2016**, *45* (12), 5030–5037. <https://doi.org/10.1039/C4DT02929A>.

- (14) Okamoto, A.; Hashimoto, K.; Nealson, K. H.; Nakamura, R. Rate Enhancement of Bacterial Extracellular Electron Transport Involves Bound Flavin Semiquinones. *Proc. Natl. Acad. Sci. U. S. A.* **2013**, *110* (19), 7856–7861. <https://doi.org/10.1073/pnas.1220823110>.
- (15) Marshall, M. J.; Beliaev, A. S.; Dohnalkova, A. C.; Kennedy, D. W.; Shi, L.; Wang, Z.; Boyanov, M. I.; Lai, B.; Kemner, K. M.; McLean, J. S.; Reed, S. B.; Culley, D. E.; Bailey, V. L.; Simonson, C. J.; Saffarini, D. A.; Romine, M. F.; Zachara, J. M.; Fredrickson, J. K. C-Type Cytochrome-Dependent Formation of U(IV) Nanoparticles by *Shewanella Oneidensis*. *PLoS Biol.* **2006**, *4* (8). <https://doi.org/10.1371/journal.pbio.0040268>.
- (16) Sundararajan, M.; Campbell, A. J.; Hillier, I. H. Catalytic Cycles for the Reduction of [UO₂]²⁺ by Cytochrome C7 Proteins Proposed from DFT Calculations. *J. Phys. Chem. A* **2008**, *112* (19), 4451–4457. <https://doi.org/10.1021/jp800209p>.
- (17) Sundararajan, M.; Campbell, A. J.; Hillier, I. H. Catalytic Cycles for the Reduction of [UO₂]²⁺ by Cytochrome C7 Proteins Proposed from DFT Calculations. *J. Phys. Chem. A* **2008**, *112* (19), 4451–4457. <https://doi.org/10.1021/jp800209p>.
- (18) Faizova, R.; Scopelliti, R.; Chauvin, A.-S.; Mazzanti, M. Synthesis and Characterization of a Water Stable Uranyl(V) Complex. *J. Am. Chem. Soc.* **2018**, *140* (42), 13554–13557. <https://doi.org/10.1021/jacs.8b07885>.
- (19) Molinas, M.; Faizova, R.; Brown, A.; Galanzew, J.; Schacherl, B.; Bartova, B.; Meibom, K. L.; Vitova, T.; Mazzanti, M.; Bernier-Latmani, R. Biological Reduction of a U(V)–Organic Ligand Complex. *Environ. Sci. Technol.* **2021**, *55* (8), 4753–4761. <https://doi.org/10.1021/acs.est.0c06633>.
- (20) Setlow, B.; Atluri, S.; Kitchel, R.; Koziol-Dube, K.; Setlow, P. Role of Dipicolinic Acid in Resistance and Stability of Spores of *Bacillus Subtilis* with or without DNA-Protective α/β -Type Small Acid-Soluble Proteins. *J. Bacteriol.* **2006**, *188* (11), 3740–3747. <https://doi.org/10.1128/JB.00212-06>.
- (21) Takahashi, M.; Terada, Y.; Nakai, I.; Nakanishi, H.; Yoshimura, E.; Mori, S.; Nishizawa, N. K. Role of Nicotianamine in the Intracellular Delivery of Metals and Plant Reproductive Development. *Plant Cell* **2003**, *15* (6), 1263–1280. <https://doi.org/10.1105/tpc.010256>.
- (22) Song, Y.; Ammami, M.-T.; Benamar, A.; Mezazigh, S.; Wang, H. Effect of EDTA, EDDS, NTA and Citric Acid on Electrokinetic Remediation of As, Cd, Cr, Cu, Ni, Pb and Zn Contaminated Dredged Marine Sediment. *Environ. Sci. Pollut. Res.* **2016**, *23* (11), 10577–10586. <https://doi.org/10.1007/s11356-015-5966-5>.
- (23) Lapka, J. L.; Paulenova, A.; Alyapyshev, M. Y.; Babain, V. A.; Herbst, R. S.; Law, J. D. Extraction of Uranium(VI) with Diamides of Dipicolinic Acid from Nitric Acid Solutions. *Radiochim. Acta* **2009**, *97* (6), 291–296. <https://doi.org/10.1524/ract.2009.1588>.
- (24) Brown, M. A.; Paulenova, A.; Gelis, A. V. Aqueous Complexation of Thorium(IV), Uranium(IV), Neptunium(IV), Plutonium(III/IV), and Cerium(III/IV) with DTPA. *Inorg. Chem.* **2012**, *51* (14), 7741–7748. <https://doi.org/10.1021/ic300757k>.
- (25) Knepper, T. P. Synthetic Chelating Agents and Compounds Exhibiting Complexing Properties in the Aquatic Environment. *TrAC Trends Anal. Chem.* **2003**, *22* (10), 708–724. [https://doi.org/10.1016/S0165-9936\(03\)01008-2](https://doi.org/10.1016/S0165-9936(03)01008-2).
- (26) Bucheli-Witschel, M.; Egli, T. Environmental Fate and Microbial Degradation of Aminopolycarboxylic Acids. *FEMS Microbiol. Rev.* **2001**, *25* (1), 69–106. <https://doi.org/10.1111/j.1574-6976.2001.tb00572.x>.

- (27) Liu, C.; Jeon, B.-H.; Zachara, J. M.; Wang, Z.; Dohnalkova, A.; Fredrickson, J. K. Kinetics of Microbial Reduction of Solid Phase U(VI). *Environ. Sci. Technol.* **2006**, *40* (20), 6290–6296. <https://doi.org/10.1021/es0608601>.
- (28) Rui, X.; Kwon, M. J.; O'Loughlin, E. J.; Dunham-Cheatham, S.; Fein, J. B.; Bunker, B.; Kemner, K. M.; Boyanov, M. I. Bioreduction of Hydrogen Uranyl Phosphate: Mechanisms and U(IV) Products. *Environ. Sci. Technol.* **2013**, *47* (11), 5668–5678. <https://doi.org/10.1021/es305258p>.
- (29) Meibom, K. L.; Cabello, E. M.; Bernier-Latmani, R. The Small RNA RyhB Is a Regulator of Cytochrome Expression in *Shewanella Oneidensis*. *Front. Microbiol.* **2018**, *9*. <https://doi.org/10.3389/fmicb.2018.00268>.
- (30) Edwards, M. J.; White, G. F.; Butt, J. N.; Richardson, D. J.; Clarke, T. A. The Crystal Structure of a Biological Insulated Transmembrane Molecular Wire. *Cell* **2020**, *181* (3), 665–673.e10. <https://doi.org/10.1016/j.cell.2020.03.032>.
- (31) Yang, Y.; Wang, S.; Albrecht-Schmitt, T. E. Microbial Dissolution and Reduction of Uranyl Crystals by *Shewanella Oneidensis* MR-1. *Chem. Geol.* **2014**, *387*, 59–65. <https://doi.org/10.1016/j.chemgeo.2014.08.020>.
- (32) Shi, L.; Chen, B.; Wang, Z.; Elias, D. A.; Mayer, M. U.; Gorby, Y. A.; Ni, S.; Lower, B. H.; Kennedy, D. W.; Wunschel, D. S.; Mottaz, H. M.; Marshall, M. J.; Hill, E. A.; Beliaev, A. S.; Zachara, J. M.; Fredrickson, J. K.; Squier, T. C. Isolation of a High-Affinity Functional Protein Complex between OmcA and MtrC: Two Outer Membrane Decaheme c-Type Cytochromes of *Shewanella Oneidensis* MR-1. *J. Bacteriol.* **2006**, *188* (13), 4705–4714. <https://doi.org/10.1128/JB.01966-05>.
- (33) Edwards, M. J.; Fredrickson, J. K.; Zachara, J. M.; Richardson, D. J.; Clarke, T. A. Analysis of Structural MtrC Models Based on Homology with the Crystal Structure of MtrF. *Biochem. Soc. Trans.* **2012**, *40* (6), 1181–1185. <https://doi.org/10.1042/BST20120132>.
- (34) Edwards, M. J.; Baiden, N. A.; Johs, A.; Tomanicek, S. J.; Liang, L.; Shi, L.; Fredrickson, J. K.; Zachara, J. M.; Gates, A. J.; Butt, J. N.; Richardson, D. J.; Clarke, T. A. The X-Ray Crystal Structure of *Shewanella Oneidensis* OmcA Reveals New Insight at the Microbe–Mineral Interface. *FEBS Lett.* **2014**, *588* (10), 1886–1890. <https://doi.org/10.1016/j.febslet.2014.04.013>.
- (35) Hartshorne, R. S.; Reardon, C. L.; Ross, D.; Nuester, J.; Clarke, T. A.; Gates, A. J.; Mills, P. C.; Fredrickson, J. K.; Zachara, J. M.; Shi, L.; Beliaev, A. S.; Marshall, M. J.; Tien, M.; Brantley, S.; Butt, J. N.; Richardson, D. J. Characterization of an Electron Conduit between Bacteria and the Extracellular Environment. *Proc. Natl. Acad. Sci. U. S. A.* **2009**, *106* (52), 22169–22174. <https://doi.org/10.1073/pnas.0900086106>.
- (36) Kraemer, S. M. Iron Oxide Dissolution and Solubility in the Presence of Siderophores. *Aquat. Sci.* **2004**, *66* (1), 3–18. <https://doi.org/10.1007/s00027-003-0690-5>.

Chapter 4 Speciation-dependent electron transfer from the c-type cytochrome MtrC to U(VI)-ligand complexes

Chapter 4 seeks to determine factors which may influence the kinetics of reaction and the nature of the interaction between the c-type cytochrome MtrC of *S. oneidensis* MR-1 and soluble U(VI)-aminocarboxylate complexes.

This work is intended for publication.

Author Contributions:

Margaux Molinas, Ashley Brown, Tim Prüßmann, Tonya Vitova, Rizlan Bernier-Latman

The manuscript was written through contributions from all authors. RBL conceived of the research. MMO performed the experiments, TP and TV helped with the M₄-edge XANES, AB developed the ion-exchange chromatography method.

Abstract

The metal-reducing bacteria *Shewanella oneidensis* MR-1 transfers electrons to metal electron acceptors such as U via c-type cytochromes. The intracellular mechanism of electron transfer is well studied but the delivery of electrons to external electron acceptors less well so. MtrC, a decaheme c-type cytochrome located on the outer-membrane of *S. oneidensis* MR-1 transfers electrons to U(VI), both when embedded in the bacterial membrane and when purified. However, it is unclear how the electron transfer between the terminal heme of the protein and extracellular U(VI) occurs. There remain uncertainties regarding the type of interaction, but also the parameters controlling the electron transfer. We sought to shed light on some aspects of this process. We investigated the reduction kinetics of soluble U(VI) complexes with four ligands: carbonate, nitrilotriacetic acid (NTA), ethylenediaminetetraacetic acid (EDTA), and diethylenetriaminepentaacetic acid (DTPA) by reduced MtrC and strain MR-1 cells. With MtrC, we observed two reaction rates, one more rapid for U-EDTA and U-DTPA, and another slower for U-NTA and U-carbonate. We attributed these differences to the type of interaction with MtrC, i.e., electrostatic interactions with U-EDTA and DTPA and hydrogen bonds with U-NTA and U-carbonate as there was no evidence of strong docking of U(VI) to MtrC.

4.1 Introduction

Uranium is a metal that is encountered in the environment mainly in two stable oxidation states: U(VI) under oxidized conditions and U(IV) under reduced conditions. The electron transfer allowing U(VI) to be reduced to U(IV) can be performed either abiotically^{3,4,6,119}, by a wide range of iron or sulfur-bearing minerals, or biologically^{10,11,13,19,118}. Dissimilatory metal-reducing bacteria (DMRB) are capable of delivering electrons to extracellular electron acceptors, often metals such as U. In particular, *Shewanella oneidensis* MR-1 transfers electrons to U(VI) via c-type cytochromes¹⁷. In c-type cytochromes, iron (Fe) centers surrounded by a porphyrin ring, designated as hemes, are embedded in the amino acid structure. The Fe centers exist as one of two oxidation states in the hemes, either reduced Fe²⁺ or oxidized Fe³⁺. By switching from one to the other oxidation state, the hemes can transfer electrons.

MtrC, a decaheme c-type cytochrome located in the outer membrane of *S. oneidensis* MR-1, is a terminal reductase that delivers electrons directly to electron acceptors^{17,92,106}. MtrC receives electrons via a chain of c-type cytochromes linking the cytoplasm to the external medium^{84,89,152,153}. When embedded in the outer-membrane, three out of ten MtrC hemes are exposed to the extracellular medium^{95,154}. These are hemes 2, 7 and 10. Heme 2 and 7 are binding sites for a second outer-membrane decaheme c-type cytochrome, OmcA⁹², or binding sites for flavin molecules^{95,154,155}, that shuttle electrons to electron acceptors. Heme 5 is expected to be a favorable site for the transfer of electrons to extracellular electron acceptors. In strain MR-1, extracellular electron transfer is the last step of a series of electron transfers along a chain of c-type cytochrome, and is likely the rate limiting step in the overall mechanism of electron transfer¹⁴³. Several studies have described the electron flow in multiheme c-type cytochromes and characterized the process step by step. For instance, scanning tunneling spectroscopy, which is imaging of a surface at the molecular level by probing with a sharp metallic tip to which a voltage is applied, or its extension, tunneling spectroscopy¹⁵⁶ were applied to measure the conductance of MtrC and OmcA¹⁵⁷. In addition, quantum and molecular mechanics were applied to unveil the step by step electron transfer in MtrF, a homologue protein to MtrC, giving insights into the redox properties of each heme¹⁵⁸. Furthermore, an alternative method to describe electron transfer within c-type cytochromes was derived from Marcus

theory for redox reactions¹⁵⁹. Marcus theory describes the parameters which may influence electron transfer during redox reactions, which enable, in particular, the mathematical computation of the electron tunneling rates in biological systems, i.e., rates at which electrons hop from one redox center to the other¹⁶⁰. These parameters include ΔG^0 , the free energy of the reaction, ΔG^\ddagger the free activation energy, λ the nuclear reorganization energy upon electron transfer, H_{DA} the electronic coupling of the redox couple donor/acceptor, and the temperature. The free energy of activation can be influenced by solvent polarization. Indeed, as the electron transfer is a rearrangement of charges, the electron transfer rates strongly depend on the dielectric properties of the surrounding medium¹⁵⁶.

Yet, it is unclear how electrons are delivered to the electron acceptor. Several types of interactions have been reported between various substrates and c-type cytochromes. Motifs have been identified for the binding of MtrC and OmcA to solid iron substrates such as iron oxides (Fe_2O_3)¹⁶¹, and hydrogen interactions invoked as the binding mechanism. In MtrF, a homologue protein of MtrC, also located on the outer-membrane of *S. oneidensis* MR-1, a positively charged pocket around heme 6 and 7 was identified, and found to be likely to interact electrostatically with the negatively charged surface of Fe_2O_3 ¹⁶². As for soluble iron substrates, hydrogen bonds were also involved in Fe(III)-NTA binding to the undecaheme c-type cytochrome of *Shewanella* species HRCR-6¹⁶³. In the case of U, the only evidence of interaction with a c-type cytochrome was demonstrated theoretically by density functional theory calculations¹²¹. In that study, U(VI) binds covalently to the carboxylic group of an amino acid residue, likely aspartate or glutamate. Based on this limited evidence, the emerging view is that c-type cytochromes are versatile proteins that can interact electrostatically, via hydrogen or covalent bonds, with various substrates.

Here, we study the interaction between U(VI) and MtrC, in particular, what controls the electron transfer rate and whether U(VI) speciation impacts this rate. To that end, we chose to investigate a series of aminocarboxylate ligands that are environmentally relevant, nitrilotriacetic acid (NTA), ethylenediaminetetraacetic acid (EDTA) and diethylenetriaminepentaacetic acid (DTPA). These ligands are used to extract heavy metals and radionuclides, due to their strong binding to metal ions¹²⁸. Additionally, NTA, EDTA and DTPA exhibit increasing denticity, i.e., an increasing number of atoms that can bind to a central atom such as uranyl. They are quadridentate, hexadentate, and octadentate ligands, consisting of one to three basic amino nitrogen donors, and three to five carboxylic acid groups. In addition, we also investigated U complexed to carbonate. We first reacted the four U complexes with reduced MtrC, i.e., with all hemes in their Fe^{2+} configuration, and followed the kinetics. We noticed that the reduction rates clustered in two groups. Hence, we studied the binding extent of the U(VI)-ligand complexes with oxidized MtrC and the binding extent of U with reduced MtrC. Under oxidized conditions, we observed a similar binding extent for all selected complexes of U. Under reduced conditions, binding occurred only with the product of U(VI)-carbonate reduction, likely a mixture of U(V) and U(IV) species, as M_4 -edge HR-XANES measurements suggested. We suggest that the type and strength of interaction of MtrC with the U-ligand complexes correlates with the reduction rates. In addition, with MR-1, we report the rates of reduction of the three U aminocarboxylate complexes as we could follow U(IV) increases in solution. Similar reduction rates were observed for U-NTA and U-EDTA, but the reduction rates were slower for U-DTPA and U-carbonate.

4.2 Experimental methods

4.2.1 MtrC purification and reduction

MtrC was purified, reduced, and dialyzed as described previously in paragraphs 3.2.6, 3.2.7, and 3.2.8.

4.2.2 Preparation of the stock solutions

For the aminocarboxylate stock solutions, appropriate amount of NTA, EDTA, DTPA were dissolved in buffer A (composed of 100mM HEPES and 50mM NaCl) to a final concentration of 30mM. The solutions were either kept oxic for the oxic tests or flushed with N₂ to remove the O₂ and kept under anoxic conditions in a N₂ MBraun glovebox. The oxic carbonate stock was prepared by dissolving HCO₃⁻ in buffer A to a concentration of 1M, minimizing the headspace of the stock vial. For the anoxic carbonate stock, the HCO₃⁻ powder was first degassed with N₂, then introduced inside the glovebox, dissolved in buffer A. Equilibration was allowed for 48h.

4.2.3 Kinetics of reaction

4.2.3.1 Purified MtrC

In the glovebox, working solutions of reduced MtrC or U(VI)-ligand were prepared to a concentration of 300μM. The U(VI)-ligand working solutions were prepared by diluting the appropriate volume of U(VI)-Cl in the freshly prepared ligand stock solutions. The redox status of the hemes was confirmed before the experiments by UV-vis spectroscopy. Equal volumes of the working solutions of reduced MtrC and U(VI)-ligand were mixed, so the initial concentration of reduced MtrC and U(VI)-ligand are equal to 150 μM. The sampling consisted of collecting a volume of the reaction mixture after 5s, 15s, 30s and 60s and loading it immediately onto the ion-exchange chromatography resins to separate U(VI) from U(IV). U was subsequently measured in each fraction by ICP-MS. The concentration of MtrC was controlled by BCA assay in the reaction mixture. For each ligand, these reactions were performed in duplicates.

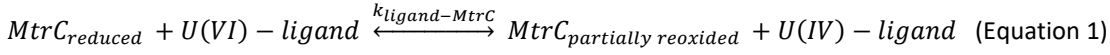
4.2.3.2 Strain MR-1

S. oneidensis MR-1 was incubated as previously described³², under non-growth conditions, in anoxic modified WLP medium (Table S1), in the presence of 400 μM U(VI)-ligand, along with 20 mM of lactate as the electron donor. The starting OD₆₀₀ of the incubations was measured to be 1. The incubations were maintained in the dark at room temperature, inside the anaerobic chamber. At several time points, an aliquot of the supernatant was further filtered through 0.2 μm PTFE filters (Whatman, Maidstone, United Kingdom). For NTA, EDTA, and DTPA, the U(IV) product is soluble^{64,164}, complicating the quantification of U(VI) reduced. As for carbonate, the product forms a solid precipitate associated with the biomass, filtration is sufficient to separate aqueous U(VI) and quantify its concentration over time. Thus, for NTA, EDTA and DTPA experiments, the filtered aliquot was acidified with 4.5M HCl (final concentration). Hexavalent and tetravalent U were then separated by ion-exchange chromatography³², as described below, to resolve the U oxidation state.

4.2.3.3 Kinetics modelling

To model the kinetics of reaction between MtrC or MR-1 and the U(VI)-ligand complexes, we used first order or second order kinetics models.

For the reaction between MtrC and U(VI)-ligand complexes, both concentrations of MtrC and U(VI)-ligand are set to be equal when the reaction starts, and both reactants are transformed in the course of the reaction. The reaction does not follow the Michaelis-Menten model, for which the enzyme should be in large excess compared to the substrate. The equation of the reaction between reduced MtrC and U bound to the different organic ligands is:



The first order kinetic model for this reaction is expressed as:

$$\frac{d[U(VI)-ligand](t)}{dt} = -k_{ligand-MtrC}[U(VI) - ligand](t) \quad (\text{Equation 2})$$

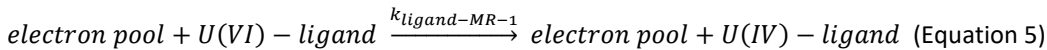
The second order kinetic model for this reaction can be written as:

$$\frac{d[U(VI)-ligand](t)}{dt} = -k_{ligand-MtrC}[U(VI) - ligand](t)[MtrC_{reduced}](t) \quad (\text{Equation 3})$$

However, in our experimental set-up: $[U(VI) - ligand](t = 0) = [MtrC_{reduced}](t = 0)$. and both reactants are transformed simultaneously by the transfer of an electron from MtrC to U(VI)-ligand complexes so Equation 3 becomes:

$$\frac{d[U(VI)-ligand](t)}{dt} = -k_{ligand-MtrC}[U(VI) - ligand]^2(t) \quad (\text{Equation 4})$$

For the reaction between MR-1 cells and U(VI)-ligand under non-growing conditions, a first order reaction model was used to described the data. The bacteria behave as a pool of electrons, which are in excess compared to the U(VI)-ligand reactant. We will consider here that the electron pool is constant over the experimental time. In fact, the electron donor, lactate is in large excess (20mM lactate for 400 μ M U(VI)). The equation of the reaction can be written as:



The first order kinetic applied to this reaction is expressed as:

$$\frac{d[U(VI)-ligand](t)}{dt} = -k_{ligand-MR-1}[U(VI) - ligand](t) \quad (\text{Equation 6})$$

A second order kinetic model was also applied to the data, with a similar expression as Equation 3 for comparison purposes.

By integrating Equation 2, 4, 5 and 6, we obtained a linear relationship between $[U(VI) - ligand](t)$ and the time t. The slope of the linear relationship corresponds to k_{ligand_MtrC} or k_{ligand_MR-1} .

4.2.4 Binding tests

4.2.4.1 Principle of the experiment

In order to investigate whether the U complexes bind to the purified protein, we used size-exclusion desalting columns that are ordinarily employed to remove ions from a protein solution or to exchange a protein buffer. In our case, the size exclusion columns allowed the separation of the protein fraction from the rest of the reaction mixture. The size

exclusion column pores trap all components smaller than the exclusion size (40kDa in our case) and allow the elution of the protein (MtrC, size of 74.5kDa) by centrifugation in a first fraction (called F1). In particular, once we reacted MtrC with the U complexes, this technique allowed us to remove the free U from the reaction mixture and collect MtrC. If any U is detected in the fraction F1, then it is likely bound to the protein, otherwise it would have remained in the pores of the size exclusion column. Once the protein has been eluted, the trapped U is stripped from the columns by washing the beads in 6M HCl. We determined that 6 washes, from fraction F2 to F7 in this work, usually permit a recovery of 90 to 95% of the total U applied to the size exclusion columns.

4.2.4.2 Binding of U to oxidized MtrC

40kDa size-exclusion desalting columns (Zeba® Spin Desalting Columns, Thermofisher Scientific, Waltham MA USA) were conditioned by 3 washes with buffer A. Working solutions of oxidized MtrC and U(VI)-ligand were prepared to a concentration of 300µM each. The U(VI)-ligand working solutions were prepared by diluting the appropriate volume of U(VI)-Cl in the freshly prepared oxic ligand stock solutions. The reaction was initiated by mixing equal volumes of oxidized MtrC and the U-ligand complex solutions, and allowed to proceed for 30min. No protein controls were set up by mixing equal volumes of the U-ligand working solution with buffer A. Then, 100µl of the reaction mixtures were loaded onto the size-exclusion columns and spun for 1.5min at 3500xg. The first fraction eluted, fraction F1, contains the protein. Then, 6 successive washes were performed by adding 350µL of 6M HCl and spinning for 1.5min at 3500xg and fractions F2 to F7 recovered. U was quantified by ICP-MS and the concentration of MtrC evaluated in both the reaction mixtures and the fractions F1 by the BCA assay.

4.2.4.3 Binding of U to reduced MtrC

A week ahead of the reaction, the 40kDa size-exclusion resins were degassed and introduced in the glovebox. They were conditioned as described above, in anoxic buffer A. Working solutions of reduced MtrC and U-ligand were prepared as mentioned above but using anoxic ligand stock solutions. The experimental steps are similar to those followed for oxidized MtrC. Once the 7 fractions were recovered from the no-protein controls and the reaction mixtures with reduced MtrC, ion-exchange chromatography was performed on fraction F1 and on a combined mixture of F2 to F7 to separate U(VI) and U(IV). U was measured by ICP-MS and the concentration of MtrC was evaluated by BCA in the whole reaction mixture and in the fraction F1.

4.2.5 Uranium quantification

U concentration was measured by Inductively Coupled Plasma Mass Spectrometry (ICP-MS 7900, Agilent, Santa Clara, California, US) for both filtered supernatants and samples eluted from the ion-exchange chromatography test. Dilutions to a range of 1 to 10 ppb of U were performed in a matrix of 1% HNO₃ prior to analysis. All samples were measured in technical duplicates.

4.2.6 M₄-edge HR-XANES on U(VI)-carbonate reacted with reduced MtrC

4.2.6.1 Reaction

In the glovebox, a solution of 1.2mM of U(VI) and 10 mM carbonate was combined and mixed with an equal volume of a solution of 600 µM of reduced MtrC were reacted by mixed to initiate the reaction. Consequently, the initial

concentrations were 600 μM of U(VI)-carbonate and 300 μM of MtrC. Aliquots were collected at distinct time points (30s, 1min, 2min, 5min and 20min) and placed in sample holders designed to fit into a N_2 -flushed cryostat. The sample holders were sealed anoxically, snap frozen in a cold trap in the glovebox and kept frozen until measured.

4.2.6.2 U M_4 -edge HR-XANES

U M_4 -edge (3.726 keV) HR-XANES was used to elucidate the oxidation state of U as a function of time in the reaction between U(VI)-carbonate and reduced MtrC. Spectra were collected at the station for actinide science (ACT) at the CAT-ACT beamline at the Karlsruhe Research Accelerator (KARA), Karlsruhe, Germany. The CAT-ACT beamline is equipped with a Johann type X-ray emission spectrometer¹³⁵. The incident beam was monochromatized by a Si(111) double crystal monochromator (DCM) and focused onto the sample to a spot size of about 500 μm x 500 μm . The X-ray emission spectrometer consists of four Si (110) crystals with 1 m bending radius and a single diode VITUS silicon drift detector (Ketek, Germany), which together with the sample are arranged in a vertical Rowland circle geometry. A UO_2 reference was used to calibrate the spectra. The main absorption maximum was set to 3.275 keV. The sample cells were placed in a cryostat flushed with N_2 , maintaining anoxic conditions. The X-ray spectrometer was inside a He flushed box in order to minimize intensity loss due to absorption or scattering of photons.

Data processing consisted of normalization and linear combination fits (LCF) using the ATHENA software¹³⁶. The spectra obtained were modeled using the references U(VI)-carbonate, U(V)-iodide and U(IV)O_2 , for which spectra were also collected and analyzed in the same manner. The goodness of fit was evaluated with two statistical parameters, the R-factor and the reduced χ^2 , which were minimized by the fitting algorithm.

4.3 Results

4.3.1 Kinetics of reduction

4.3.1.1 Reaction of MtrC with U complexed with NTA, EDTA, DTPA or carbonate.

Reduced MtrC, with all hemes in the Fe^{2+} valence state, was reacted with U bound to the following series of aminocarboxylate ligands: NTA, EDTA, DTPA as well as to carbonate (Figure 4.1). The starting ratio of protein to U is reported for each reaction mixture in Table 4.1, along with their respective concentrations. Experiments with the aminocarboxylate ligands were performed in duplicate, and the values in Table 4.1 correspond to the average of the measurements for both experiments, except for carbonate that represents a single experiment. The ratio U:MtrC was adjusted to be close to 1, for consistency across reactions (0.98 for NTA, 1.36 for EDTA, 1.29 for DTPA and 0.91 for carbonate). In addition,

the ligand concentration was adjusted to tune the speciation for a 1:1 U:ligand complex to prevail with the series of aminocarboxylate ligands and to obtain the bi- and tri-carbonato complexes with carbonate (Table 4.2).

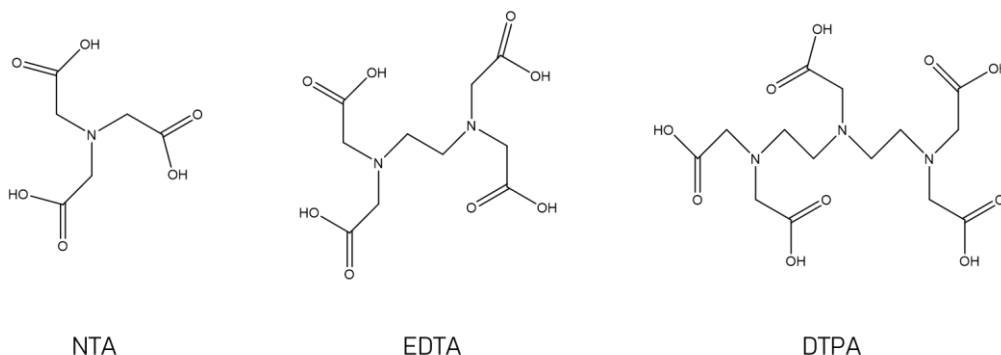


Figure 4:1. Molecular structures of protonated aminocarboxylate ligands NTA, EDTA, and DTPA

Ligand	[MtrC] (uM)	std dev [MtrC]	[U] (uM)	std dev [U]	[U]/[MtrC]	std dev [U]/[MtrC]
NTA	138.87	24.06	134.60	10.63	0.98	0.09
EDTA	115.6	11.37	157.3	11.4	1.36	0.01
DTPA	121.06	0.59	156.12	2.27	1.29	0.03
carbonate	150	/	137	/	0.91	/

Table 4:1. Average concentrations in U and MtrC, and their ratio for duplicate reactions between MtrC and U-ligand (ligand = NTA, EDTA, DTPA, carbonate) under oxic (MtrC oxidized) and reduced (MtrC reduced) conditions (described in Figure 6).

Carbonate - [U] = 150uM, [HCO ₃ ⁻] = 15mM			
Species	UO ₂ (CO ₃) ₂ ²⁻	UO ₂ (CO ₃) ₃ ⁴⁻	
Speciation (%)	56.3	43.5	
NTA - [U] = 150uM, [NTA] = 15mM			
Species	UO ₂ NTA ⁻	UO ₂ (OH)NTA ²⁻	(UO ₂) ₃ (OH) ⁵⁺
Speciation (%)	2.38	90.3	7.27
EDTA - [U] = 150uM, [EDTA] = 15mM with De Stefano et al. 2006			
Species	UO ₂ EDTA ²⁻	UO ₂ (OH)EDTA ³⁻	UO ₂ (H)EDTA ⁻
Speciation (%)	6.31	93.3	0.06
EDTA - [U] = 150uM, [EDTA] = 15mM with Hummel et al. 2005			
Species	UO ₂ EDTA ²⁻	UO ₂ (HEDTA) ⁻	
Speciation (%)	100	0.06	
DTPA - [U] = 150uM, [DTPA] = 15mM			
Species	UO ₂ DTPA ³⁻	UO ₂ (H)DTPA ²⁻	UO ₂ (H ₂)DTPA ⁻
Speciation (%)	91.1	4.28	4.58

Table 4:2. U speciation calculated using Mineql for U(VI)-ligand complexes at pH 7.5, with 50mM NaCl, and 100mM HEPES

The speciation was evaluated under the conditions of reaction (pH 7.5 in a buffer containing 100mM HEPES and 50mM NaCl) using the software Mineql (Tables 4.2 and 4.3). For NTA and DTPA, the predominant species is the 1:1 U:ligand hydroxo complex, $\text{UO}_2(\text{OH})\text{NTA}^{2-}$ (90.3%) and $\text{UO}_2\text{DTPA}^{3-}$ (91.1%). Regarding EDTA, we ran the speciation calculations using two sets of thermodynamics constants. With the logK values published in De Stefano et al.¹⁶⁵, we obtained $\text{UO}_2(\text{OH})\text{EDTA}^{3-}$ (93.3%) as the dominant species. However, a recent study suggested that the dominant species for EDTA would be $\text{UO}_2\text{EDTA}^{2-}$. Hence, using thermodynamic data published by Hummel et al.¹⁶⁶, we also obtained $\text{UO}_2\text{EDTA}^{2-}$ as the dominant species (100%). Finally, with carbonate, a mixture of the bi-carbonato $\text{UO}_2(\text{CO}_3)_2^{2-}$ (56.3%) and tri-carbonato $\text{UO}_2(\text{CO}_3)_3^{4-}$ (43.5%) was observed.

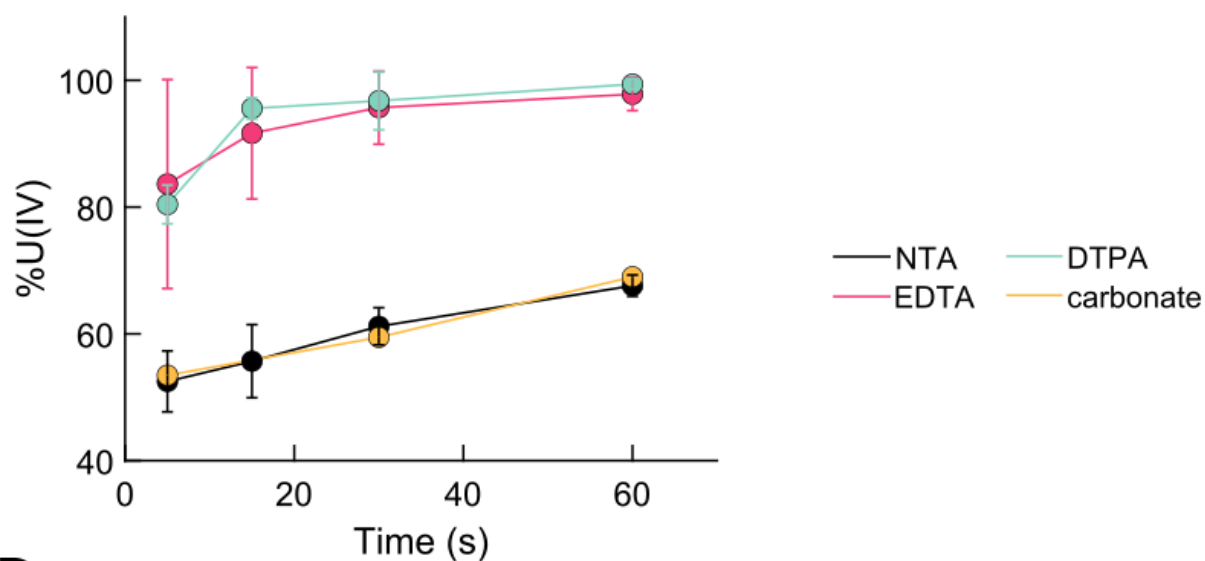
Compound	LogK	Reference
U(VI)		
$\text{U(VI)O}_2(\text{CO}_3)_2^{2-}$	16.94 ± 0.12 *	Grenthe et al. 1992 ⁶¹
$\text{U(VI)O}_2(\text{CO}_3)_3^{4-}$	21.60 ± 0.05 *	Pashalidis et al 1997 ¹⁶⁷
$\text{U(VI)O}_2\text{NTA}^-$	8.21 ± 0.02	De Stefano et al. 2006 ¹⁶⁵
$\text{U(VI)O}_2(\text{OH})\text{NTA}^{2-}$	2.39 ± 0.04	De Stefano et al. 2006
$\text{U(VI)O}_2\text{EDTA}^{2-}$	9.81 ± 0.015	De Stefano et al. 2006
$\text{U(VI)O}_2(\text{OH})\text{EDTA}^{3-}$	3.58 ± 0.03	De Stefano et al. 2006
$\text{U(VI)O}_2(\text{H})\text{EDTA}^-$	15.19 ± 0.02	De Stefano et al. 2006
$\text{U(VI)O}_2(\text{H})\text{EDTA}^-$	6.9 ± 0.3 *	Hummel et al. 2005 ¹⁶⁶
$\text{U(VI)O}_2\text{EDTA}^{2-}$	11.4 ± 0.3 *	Hummel et al. 2005
$\text{U(VI)O}_2\text{DTPA}^{3-}$	11.789 ± 0.01	De Stefano et al. 2006
$\text{U(VI)O}_2(\text{H})\text{DTPA}^{2-}$	17.861 ± 0.01	De Stefano et al. 2006
$\text{U(VI)O}_2(\text{H}_2)\text{DTPA}^-$	22.144 ± 0.01	De Stefano et al. 2006
U(IV)		
U(IV)EDTA	29.5 ± 0.2 *	Hummel et al. 2007 ¹⁶⁸
U(IV)NTA	15.6 ± 0.8	Bonin et al. 2009 ¹⁶⁹
U(IV)NTA_2	28.6 ± 1.6	Bonin et al. 2009
U(IV)DTPA	32.3 ± 0.1	Brown et al. 2012 ¹³¹

*Thermodynamic constants extracted from OECD Nuclear Energy Agency Data Bank

Table 4:3. LogK of aqueous complexes of interest in this work.

Once the reactions between reduced MtrC and the abovementioned complexes were initiated, four time points were obtained: at 5s, 15s, 30s and 60s, and analyzed for the U oxidation state to resolve the rate of reduction (Figure 4.2.A). Interestingly, we observed two groups of reaction rates. On the one hand, complexes of U with EDTA and DTPA presented very rapid reaction rates, with 80% completion reached within 5s. On the other hand, complexes of U with NTA and carbonate were reduced at slower rates. A second-order kinetic model was used to describe the kinetics of reaction, and the regression model (Figure 4.2.B). The kinetic constants for each reaction were extracted from the slope of the regression line. The kinetic constants of the reduction of U complexes with EDTA and DTPA are $k_{\text{EDTA_MtrC}} = 7.2 \text{ nM}^{-1} \cdot \text{s}^{-1}$ and $k_{\text{DTPA_MtrC}} = 9.948 \text{ nM}^{-1} \cdot \text{s}^{-1}$, respectively (Table 4.4). These are greater than what was derived for U complexes with NTA and carbonate, $k_{\text{NTA_MtrC}} = 0.181 \text{ nM}^{-1} \cdot \text{s}^{-1}$ and $k_{\text{carbonate_MtrC}} = 0.198 \text{ nM}^{-1} \cdot \text{s}^{-1}$, respectively. According to the R^2 values, second-order kinetics result in a good fit for these reactions (Table 4. 4). The fit for DTPA has a slightly lower R^2 , which is certainly related to an outlier point at 10s, but overall, it does not affect dramatically the model.

A.



B.

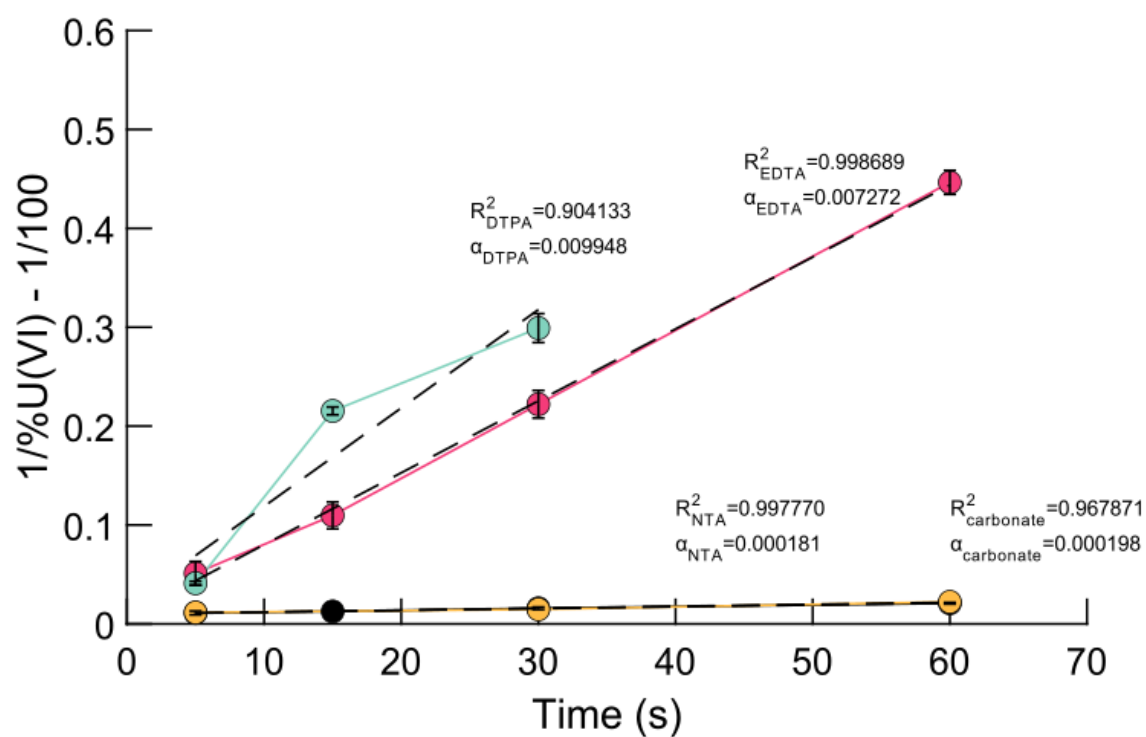


Figure 4.2: Kinetics of reaction between MtrC and the U-ligands complexes. A. Timeline of the reactions between reduced MtrC and U-NTA (black), U-EDTA (pink), U-DTPA (blue) and U-carbonate (yellow). B. Second-order kinetic models of the reactions between reduced MtrC and U-NTA (black), U-EDTA (pink), U-DTPA (blue) and U-carbonate (yellow). The linear regression for each U-ligand complex is displayed in dotted black line, along with R^2 and the coefficient of the line, corresponding to the kinetic constant of these reactions. The obtained equations are $y_{\text{NTA}}=0.000181x+0.010092$; $y_{\text{EDTA}}=0.007272x+0.07351$; $y_{\text{DTPA}}=0.009948x+0.019372$; $y_{\text{carbonate}}=0.000198x+0.009881$.

MtrC			MR-1		
ligand	k (uM ⁻¹ .s ⁻¹)	R ²	ligand	k (uM ⁻¹ .h ⁻¹)	R ²
NTA	0.000181	0.997	NTA	0.093	0.86
EDTA	0.007272	0.998	EDTA	0.161	0.85
DTPA	0.009948	0.904	DTPA	0.021	0.95
carbonate	0.000198	0.97	carbonate	0.000033	0.97

Table 4:4. Second-order rates for the kinetics of reactions between the U-ligand complex (ligand = NTA, EDTA, DTPA, carbonate) and MtrC (right), and MR-1 (left).

4.3.1.2 Reaction of strain MR-1 cells with U complexed with NTA, EDTA, DTPA or carbonate.

S. oneidensis MR-1 cells were incubated with the four abovementioned U complexes. The reactions with U complexed to aminocarboxylate ligands were followed by ion-exchange chromatography (Figure 4.3.A-C.). Thus, we observed that as aqueous phase U(VI) decreases, aqueous U(IV) increases. In addition, the U(VI) concentration remained stable in the no-cell controls over the experimental time, suggesting active reduction of the abovementioned complexes. As for incubations of MR-1 with carbonate, we observed a decrease in aqueous U(VI) concentration while it remained constant in the no-cell control (Figure 4.3D.). The kinetics of all reactions were evaluated by fitting a first-order kinetic model. In our set of experiments, a first-order reaction resulted (Table 4.5) in a better fit than a second-order model (Table 4.4). The reaction rates extracted from the regression model were ordered as follow from the lowest to the highest: $k_{\text{carbonate-MR-1}} = 0.013 \text{ h}^{-1} < k_{\text{DTPA-MR-1}} = 0.224 \text{ h}^{-1} < k_{\text{NTA-MR-1}} = 2.3 \text{ h}^{-1} < k_{\text{EDTA-MR-1}} = 2.6 \text{ h}^{-1}$ (Figure 4.4).

A comparison of the rates of reduction of complexed U by MtrC and strain MR-1 cells reveal significant differences in the values of the rates but also the relative rates across ligands. In both cases, the EDTA complex displays a rapid reaction rate and the carbonate complex a slow rate. Specifically, for carbonate, the rate constant is the lowest amongst ligands considered for both MtrC and strain MR-1 cells. DTPA displays the most rapid rate with MtrC but it is slower than EDTA and NTA with strain MR-1. In contrast, for NTA, we observed a slow reduction rate with MtrC comparable to that of carbonate, but rapid reduction with strain MR-1, at a rate comparable to that of the EDTA complex.

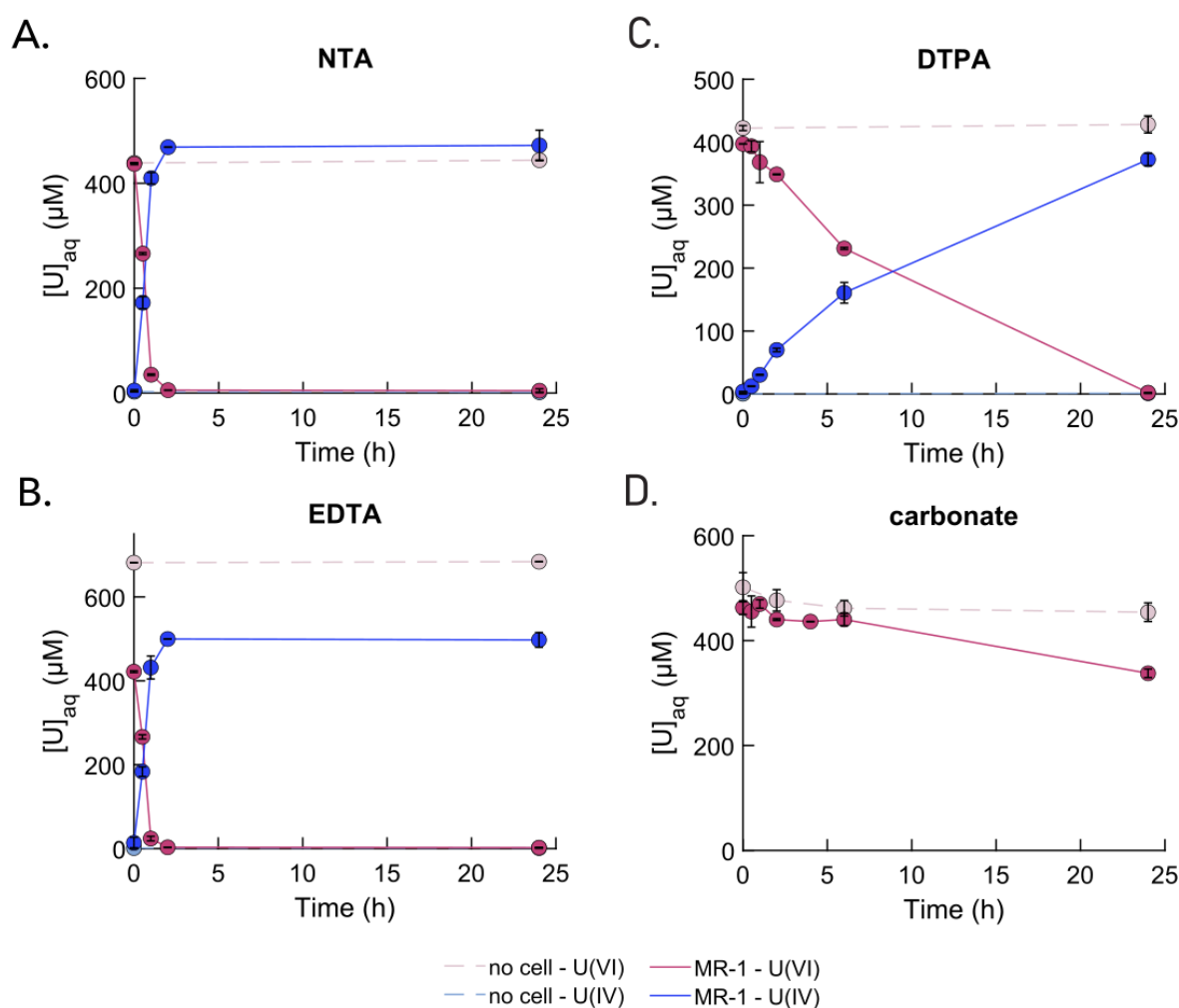


Figure 4:3. Incubations of strain MR-1 cells with the U-ligand complexes. U(VI) and U(IV) aqueous concentrations over 24h in incubations of *S. oneidensis* MR-1 and no cell controls with A. U-NTA, B. U-EDTA, C. DTPA and D. carbonate (no U(IV) line as the U(IV) product with U-carbonate is not soluble).

MtrC			MR-1		
ligand	k (s ⁻¹)	R ²	ligand	k (h ⁻¹)	R ²
NTA	0.007	0.99	NTA	2.3	0.97
EDTA	0.035	0.94	EDTA	2.6	0.96
DTPA	0.057	0.93	DTPA	0.224	0.98
carbonate	0.0074	0.98	carbonate	0.013	0.97

Table 4:5. First-order rates for the kinetics reactions between the U-ligand complex (ligand = NTA, EDTA, DTPA, carbonate) and MtrC (right), and MR-1 (left).

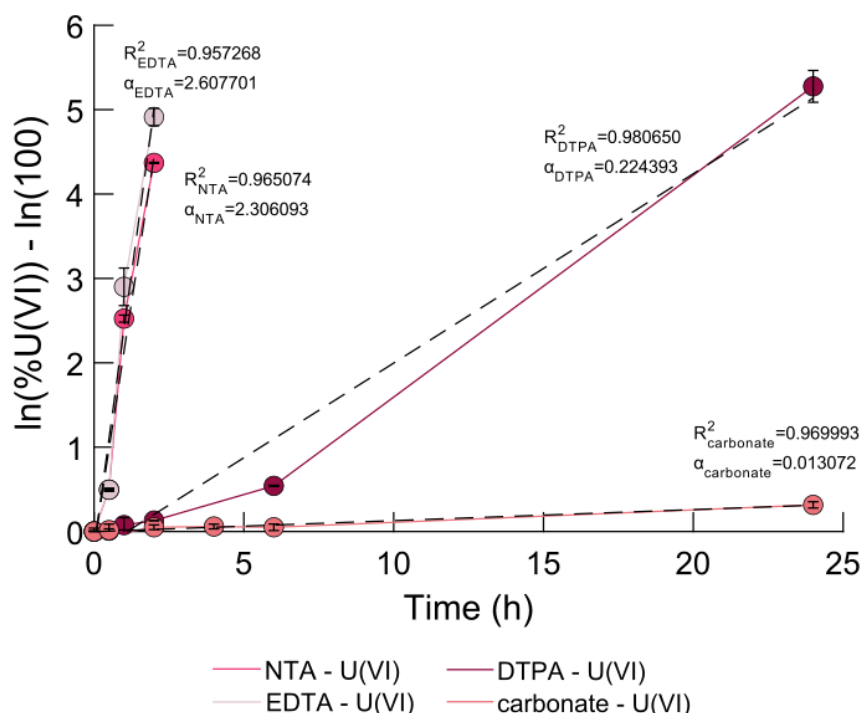


Figure 4.4: Kinetics of reaction between strain MR-1 cells and the U-ligands complexes. First-order kinetic models of the reactions between MR-1 and U-NTA (fuchsia pink), U-EDTA (light pink), U-DTPA (burgundy red) and U-carbonate (salmon pink). The linear regression for each U-ligand complex is displayed in dotted black line, along with R^2 and the coefficient of the line, corresponding to the kinetic constant of these reactions. The obtained equations are $y_{\text{NTA}} = 2.306x - 0.171$; $y_{\text{EDTA}} = 2.607x - 0.074$; $y_{\text{DTPA}} = 0.224x - 0.247$; $y_{\text{carbonate}} = 0.013x - 0.009$.

4.3.2 Binding of U complexed with NTA, EDTA, DTPA or carbonate to MtrC

Based on the observation that U(VI)-ligand complex reduction rates fall into two groups when the reaction is catalyzed by reduced MtrC, we propose that there may be distinct U-MtrC interactions depending on U speciation. For instance, we hypothesized that in the case of slow reduction kinetics (i.e., carbonate and NTA), the U complex interacts more closely with the protein, prior to electron transfer, whereas in the case of rapid kinetics (i.e., EDTA and DTPA), the U atom may come close enough to the heme to allow electron hopping from MtrC to the complex, with little or no binding. We investigated whether U complexes bind to the purified protein by using size-exclusion columns. MtrC reacted with one of the U complexes was placed on a size-exclusion column (40 kDa pore size) to trap unbound U and to collect MtrC along with any U bound to the protein. These experiments were carried out with oxidized MtrC under oxic conditions to establish the binding of U(VI) to the protein and with reduced MtrC under anoxic conditions to quantify the binding of the U(IV) product of reduction to the protein.

4.3.2.1 Binding to oxidized MtrC

The results for the oxic binding tests are summarized in Figure 4.5, Tables 4.6 and 4.7. Fraction F1 includes the protein and subsequent fractions do not. In the experiment without MtrC, little U was eluted in the first fraction through the size exclusion columns, suggesting that the majority of free U was efficiently trapped into the pores of the resin beads (Figure 4.5.A.). The six following washes allowed the recovery of >95% of the total U initially loaded. This confirmed that we can use this size-exclusion technique to quantify U associated with MtrC. In the case with MtrC, limited binding was

observed with U(VI) bound in the range of 11% for NTA, EDTA, and DTPA and 14% for carbonate. (Figure 4.5.B, Table S1).

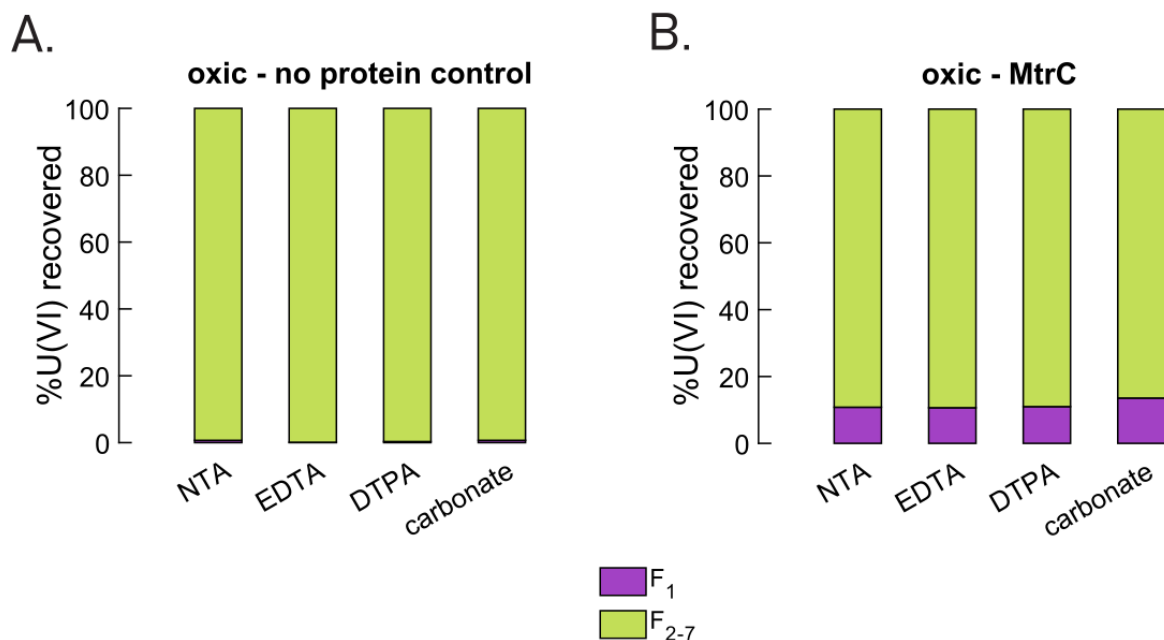


Figure 4.5: Oxidic binding tests. Distribution of U in the fractions recovered from 40kDa size-exclusion columns in the absence of protein or after reaction with oxidized MtrC. A. In control reactions without protein with U(VI)-NTA, U(VI)-EDTA, U(VI)-DTPA, and U(VI)-carbonate; and B. In reactions between oxidized MtrC and U(VI)-NTA, U(VI)-EDTA, U(VI)-DTPA, and U(VI)-carbonate for 30min, if present, proteins elute in the first fraction F₁ (purple). Fractions F₂ to F₇ (green) corresponds to successive washes with 6M HCl aiming at washing remaining U out of the size exclusion columns.

Ligand	[MtrC] (uM)	[U] (uM)	[U]/[MtrC]
oxic conditions			
NTA	129.14	126.6	0.98
EDTA	123.4	120.84	0.98
DTPA	125.79	128.5	1.02
carbonate	135.38	124.40	0.92
reduced conditions			
NTA	220.71	171.69	0.78
EDTA	234.13	173.42	0.74
DTPA	155.42	192.09	1.24
carbonate	147.74	171.69	1.16

Table 4:6. Concentrations in U and MtrC, and the ratio between them for the reactions between MtrC and U-ligand (ligand = NTA, EDTA, DTPA, carbonate) under oxic (MtrC oxidized) and reduced (MtrC reduced) conditions described in Figure 7 and 8, in the whole reaction mixtures.

Ligand	[MtrC] (uM)	[U] (uM)	[U]/[MtrC]
oxic conditions			
NTA	115.72	13.65	0.12
EDTA	104.7	13.17	0.13
DTPA	116.2	14.13	0.12
carbonate	121.48	18.85	0.16
reduced conditions			
NTA	224.54	4.74	0.02
EDTA	217.83	1.90	0.01
DTPA	157.33	4.45	0.03
carbonate	153.02	4.74	0.03

Table 4:7. Concentrations in U and MtrC, and the ratio between them for the reactions between MtrC and U-ligand (ligand = NTA, EDTA, DTPA, carbonate) under oxic (MtrC oxidized) and reduced (MtrC reduced) conditions described in Figure 7 and 8, in the first fraction F1 eluted from the size-exclusion desalting columns.

4.3.2.2 Binding to reduced MtrC

Reactions identical to the ones described with oxidized MtrC were performed under anoxic conditions with reduced MtrC. In addition to probing the U concentration eluted in each fraction, ion-exchange chromatography was performed on fraction F1 (the one corresponding to MtrC) and on combined fractions F2 to F7. This allowed determination of the speciation of U upon reaction with MtrC, and of the oxidation state of U bound to MtrC. The tests without protein gave similar results to those performed with oxidized MtrC (Figure 4.6 and Table S2). Indeed, most of the U was retained in the size exclusion column and eluted with the six following washes (Figure 4.6.A.). However, a small amount of U was eluted in the first fraction, particularly for DTPA and carbonate, probably due to negative charge repulsion with the resin beads, as DTPA and carbonate complexes have charges -3 and -4, respectively. In the presence of reduced protein, we observed that, with carbonate, 72% of the U was eluted in F1, suggesting that it was associated with the protein (Figure 4.6.B.). In contrast, the U recovered upon reaction of U aminocarboxylate ligand complexes with reduced MtrC was not bound to the protein and corresponded overwhelmingly to U(IV) (Figure 4.6.C., Table 4.8). For the carbonate system, the MtrC-associated U consists of 84% U(IV) (60.5% of the total U) and 16% U(VI) (11.5% of the total U) (Table 8). We hypothesize that U(VI) found in association with MtrC actually corresponds to U(V) that is disproportionated due to acidification prior to ion-exchange chromatography separation. If that is correct, U(V) would actually represent 32% of MtrC-associated U (23% of total U) and U(IV) ~68% of MtrC-associated U (49% of total U). Additionally, ~24% of U recovered in fraction F2 to F7 was U(VI), suggesting incomplete reduction of U(VI).

Ligand	F1		F2 to F7	
	%U(VI)	%U(IV)	%U(VI)	%U(IV)
NTA	0.46	3.07	1.78	94.69
EDTA	0.22	1.17	1.63	96.97
DTPA	1.26	1.47	1.93	95.34
carbonate	11.51	60.46	23.69	4.34

Table 4:8. Percent of the total U recovered identified as U(VI) or U(IV) in both the first fraction F1 (in which MtrC elutes) and in the combined subsequent fractions F2 to F7 post reaction of reduced MtrC and the U-ligand complexes under reduced conditions. The U(VI) and U(IV) fractions were obtained by ion exchange chromatography.

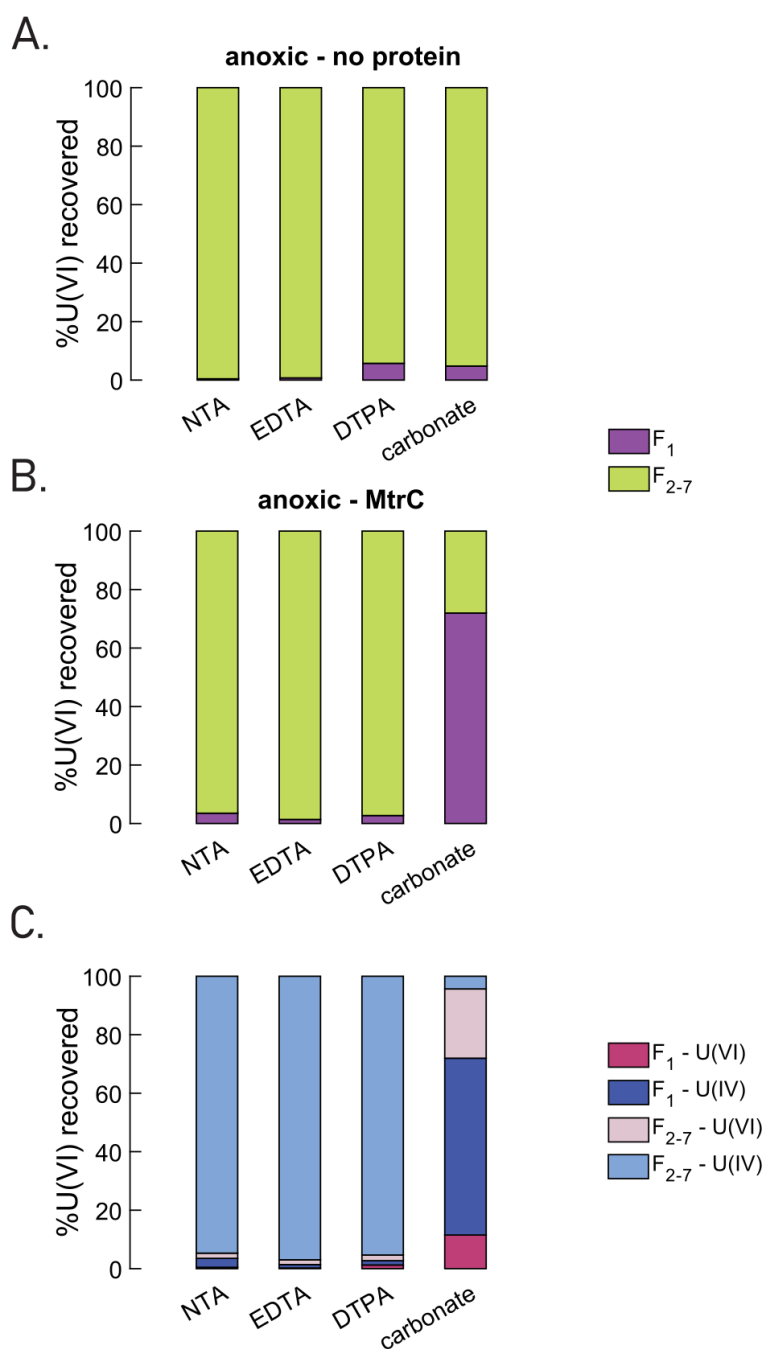


Figure 4:6. Anoxic binding tests. Distribution of U in the fractions recovered from 40kDa size-exclusion columns under anoxic conditions. A. Control reactions without protein with U(VI)-NTA, U(VI)-EDTA, U(VI)-DTPA, or U(VI)-carbonate; and B. Reaction of reduced MtrC with U(VI)-NTA, U(VI)-EDTA, U(VI)-DTPA, or U(VI)-carbonate for 30min. If present, proteins elute in the first fraction F₁ (purple). Fractions F₂ to F₇ (green) corresponds to successive washes with 6M HCl aiming at washing the remaining U out of the size exclusion columns. C. represents the oxidation states of U in fraction F₁ and in fractions F₂ to F₇ gathered for the reaction shown in B. with MtrC. The U(VI) and U(IV) fractions were obtained by ion exchange chromatography.

4.3.3 Speciation of U during reaction of U(VI)-carbonate with reduced MtrC

U(VI)-carbonate was reacted with reduced MtrC and the U speciation measured after 30s, 1min, 2 min, 5min and 20 min of reaction. The speciation was analyzed by M₄-edge High Resolution X-ray Absorption Near Edge Structure

spectroscopy under cryogenic conditions in order to minimize beam damage. As the reaction progressed, the spectra shifted to lower energies, towards the U(IV)O₂ standard white line (Figure 4.7, Table 4.9). In fact, the average white line is at 3,726.81 eV at 30s and shifts to lower energies, down to 3,726.34 eV at 20min, displaying a downward shift of ~0.5 eV. Additionally, two features indicated by the black arrows at 3,732.6 eV and 3,729.4 eV on the 30s spectra faded as the reaction time progressed. These spectra were modelled using linear combination fitting (LCF) (Table 4.9). The references selected were U(VI)-carbonate, U(IV)O₂ and U(V)-iodide as a proxy for U(V) species. The fits revealed $51.2 \pm 2.1\%$ U(V) and $46.9 \pm 1.2\%$ U(IV) for the 1-min timepoint and $33.4 \pm 2.0\%$ U(V) and $64.1 \pm 1.2\%$ U(IV) at 20 min (Figure 4.8A&B, Table 4.9). Moreover, to ensure that the model fits are robust, a model using only U(VI) and U(IV) as references was evaluated (Figure 4.8.C.) and the goodness of fit obtained compared to that (ii) using U(V) and U(IV) as references (Table 4.10). The model with U(VI) and U(IV) as references does not properly reproduce the data, as the edge of the fit is shifted to lower energies and the uranyl characteristic feature at 3,732.4 eV is accentuated compared to the data. (Figure 4.8.C.). In addition, the reduced χ^2 of the U(VI) and U(IV)-only model was calculated to be 0.3309, whereas that with U(V) and U(IV) had a reduced χ^2 of 0.095, pointing to a better fit (Table 4.10). We conclude that U(V) species persist for up to 20 min upon reaction between U(VI)-carbonate and reduced MtrC. Thus, the results suggest that U(VI) found in association with MtrC in the carbonate system could well correspond to bound U(V) species.

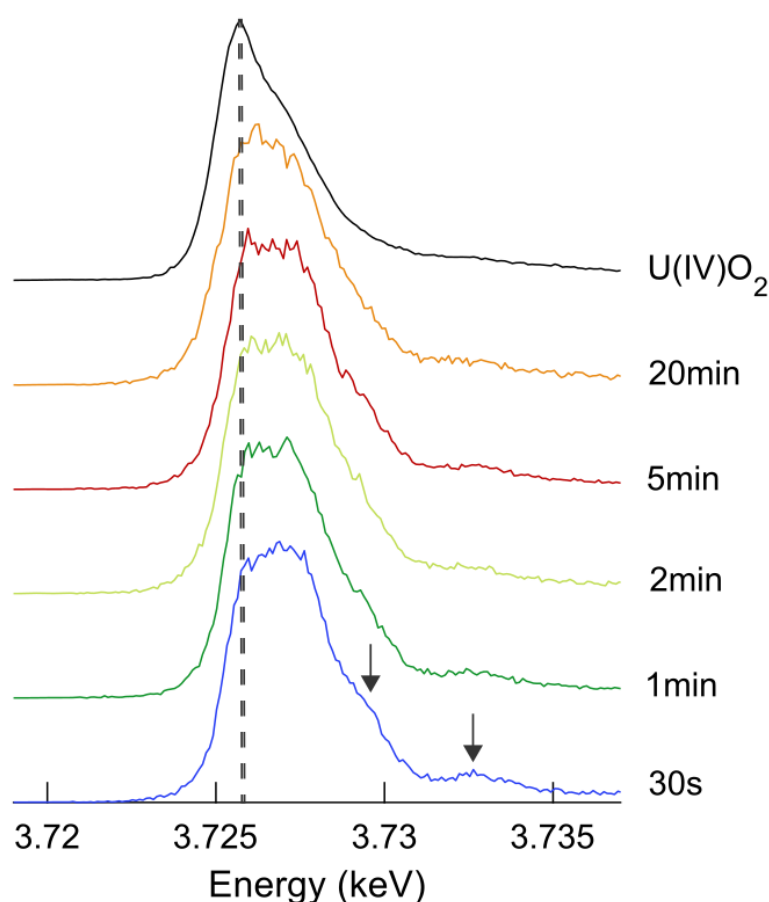


Figure 4.7: U M₄-edge HR-XANES spectra of a time course reduction experiment between U(VI)-carbonate and reduced MtrC from 30s to 20min. The dotted line marks the white line of U(IV)O₂ at 3.7255 keV as a reference. The two black arrows on the spectra for 30s show features at 3,732.6 eV and 3,729.4 eV, which fade overtime as the reaction proceeds.

Sample	white line (keV)	standard deviation
30s	3.72681	0.00022
1min	3.72666	0.00014
2min	3.72656	0.00018
5min	3.72657	0.00004
20min	3.72634	0.00014
U(IV)O ₂	3.72555	0.00004

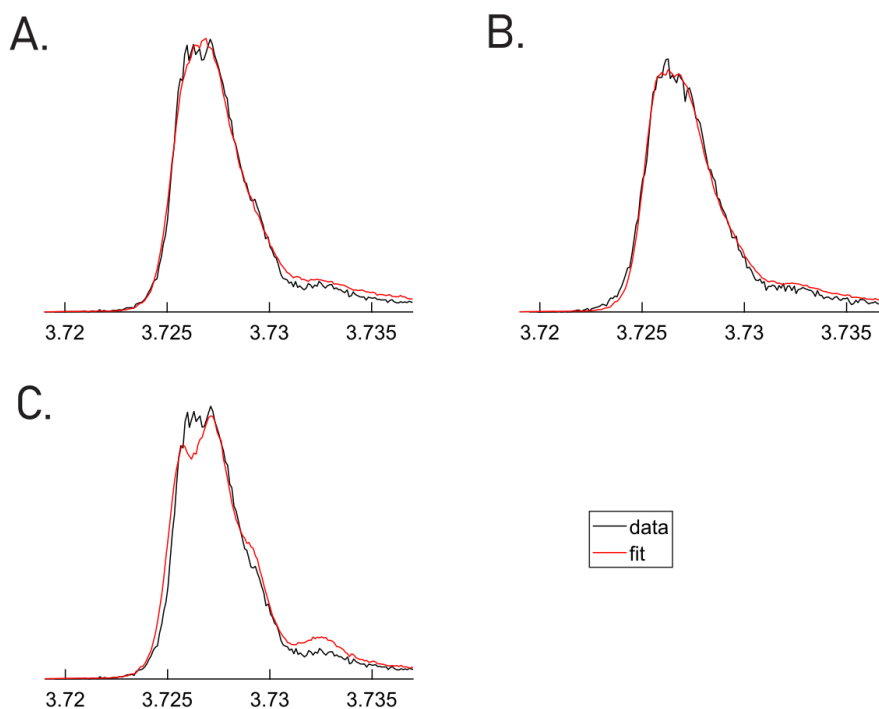
Table 4.9. Average white line of the U M₄-edge HR-XANES spectra measured in this study

Figure 4.8. LCF fitting results (red) compared to the data (black) for the M₄-edge HERFD-XANES spectra measured on the reaction mixture of U(VI)-carbonate and MtrC at A. 1 min, and B. 20 min using U(IV)O₂ and U(V)-iodine (as a proxy for U(V) species) components; at C. 1min using U(IV)O₂ and U(VI)-carbonate components.

Sample	%U(VI) carbonate	%U(V) iodine	%U(IV)O ₂	R factor	Reduced χ^2
Figure 4.7 and 4.8					
30s	4.1 ± 1.2	53.0 ± 2.2	42.9 ± 1.1	0.0061	0.0895
1min	1.9 ± 1	51.2 ± 2.1	46.9 ± 1.2	0.0059	0.0953
2min	6.5 ± 1	40.8 ± 2.1	52.7 ± 1.2	0.0059	0.0855
5min	0.2 ± 1.2	52.2 ± 2.4	47.6 ± 1.4	0.0078	0.1163
20min	2.5 ± 1	33.4 ± 2.0	64.1 ± 1.2	0.0058	0.0754
Figure 4.8					
1min	26 ± 0.7	/	74 ± 1.2	0.02063	0.3309

Table 4.10. LCF of the M₄-edge HR-XANES spectra for samples described in Figure 4.7 and Figure 4.8 using the references U(VI)-carbonate, U(V)-iodine, U(IV)O₂. We interpret these figures as supportive indicators for the presence of a given U oxidation state, providing qualitative information about the distribution of the oxidation U states in the samples. The error bars are derived from the linear combination fit algorithm.

4.4 Discussion

4.4.1 There is no obvious correlation between U-complex stability and reaction rate.

We chose to work with the selected aminocarboxylate ligands NTA, EDTA, and DTPA. Along the aminocarboxylate series the formation constant of the calculated dominant ligand-U complex increases with denticity, and likely with the coordination number with U equatorial plane (Figure 4.9). In fact, the stability constants of the aminocarboxylate series for the dominant species is ordered as $\text{NTA} < \text{EDTA} < \text{DTPA}$, more precisely $\log K_{\text{NTA}} = 2.39 \pm 0.04^{165} < \log K_{\text{EDTA}} = 11.4 \pm 0.3^{166} < \log K_{\text{DTPA}} = 11.89 \pm 0.01^{165}$. As for carbonate, the $\log K$ of the bi- and tri-carbonato complexes are higher than that of U(VI) complexed with DTPA. Our initial hypothesis was that the greater the $\log K$, the more stable the U(VI)-ligand complex and the slower the reduction by strain MR-1 cells and MtrC. Indeed, Brooks et al. observed that U bioreduction is less favorable when U is complexed with Ca, probably because of a higher complexation constant compared to a similar species lacking Ca ($\text{Ca}_2\text{UO}_2(\text{CO}_3)_3$ has a $\log K$ of 30.55 ± 0.25^{170} , whereas that of $[\text{U(VI)O}_2(\text{CO}_3)_3]^{4-}$ is 16.94 ± 0.12^{61}). With strain MR-1 cells, we indeed observed a trend in the reduction rate as follows: $k_{\text{EDTA_MR-1}} \approx k_{\text{NTA_MR-1}} > k_{\text{DTPA_MR-1}} > k_{\text{carbonate_MR-1}}$. In addition, as previously demonstrated, the presence of strong organic ligands such as NTA, EDTA and DTPA inhibited the precipitation of U(IV) ^{64,164,171}, likely due to their high $\log K$ values (Table 3). However, in those studies, the rate of reduction was not reported as the separation of aqueous U(VI) and U(IV) was not performed.

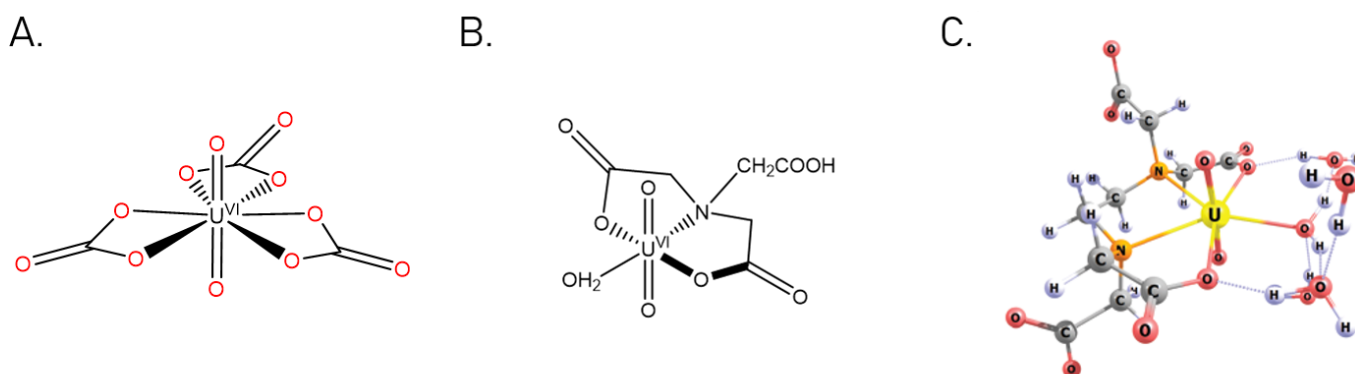


Figure 4.9: Structure of some U(VI)-aminocarboxylate ligand complexes. A. B. Structure of $[\text{U(VI)O}_2(\text{CO}_3)]^{4-}$. B. Structure of $\text{UO}_2(\text{H}_2\text{O})\text{NTA}^-$ (Teleb et al. 2004). C. Structure of $\text{UO}_2\text{EDTA}^{2-}$ complex dominant at $\text{pH} > 6$ (Kim et al. 2021)¹⁷²

Moreover, our results suggest that the complexes of U(VI) with NTA and EDTA showed similar reduction rates, and this finding is comparable to what was observed by Ross et al., but with Fe(III)-ligand complexes¹⁰². However, despite a larger difference between the U(VI)-NTA and U(VI)-EDTA $\log K$ values than between those of U(VI)-DTPA and U(VI)-EDTA, the rates of reaction of U(VI)-NTA and U(VI)-EDTA are almost similar, and both greater than that of U-DTPA. Hence, the correlation between $\log K$ values and reduction rates is not sufficient to explain the strain MR-1 cells data.

With MtrC, within the experimental conditions set, we identified two clusters of reaction rates ordered as follows $k_{\text{EDTA_MtrC}} \approx k_{\text{DTPA_MtrC}} > k_{\text{NTA_MtrC}} \approx k_{\text{carbonate_MtrC}}$. Intriguingly, the two bulkier complexes, U bound to EDTA and to DTPA, reacted more rapidly than U-NTA and U-carbonate. Therefore, with the purified protein, there is no obvious correlation between formation constant and reaction rate.

The results observed with the cells could be explained by the combination of electrostatics and compound bulk. In fact, both $\text{UO}_2(\text{OH})\text{NTA}^{2-}$ and $\text{UO}_2\text{EDTA}^{2-}$ complexes have two negative charges while the $\text{UO}_2\text{DTPA}^{3-}$, $\text{UO}_2(\text{CO}_3)^{4-}$ complexes exhibit respectively, 3 and 4 negative charges. The bacterial cell surface is generally negatively charged, hence electrostatic repulsion may reduce the rate of reaction. In addition, the octadentate DTPA ligand likely forms a bulkier complex with U than the other two aminocarboxylate ligands, and may be inhibited in its access to the enzyme embedded in the outer-membrane. As for carbonate, the formation of a stabilized U(V) intermediate in association with the outer-membrane c-type cytochromes could explain why the reaction is slower than that with aminocarboxylate ligands for which the reduction may happen without binding^{28,30,31}. Nevertheless, the hypothesis of the role of electrostatic interactions and bulkiness cannot explain the results with purified MtrC.

4.4.2 Interaction between MtrC and the soluble U substrates

Next, we hypothesized that the four U-ligand complexes may vary in the strength of their interaction with MtrC. Hence, we studied the binding extent of the selected U(VI) complexes with either oxidized or reduced MtrC. Oxidized MtrC served to delineate the binding of U(VI)-complexes to the enzyme while reduced MtrC was used to establish the extent of association of reduced U with the enzyme.

We observed no significant difference in the binding of the four U(VI)-ligand complexes under oxic conditions as they ranged between 10% to 13.6% of U(VI) bound to oxidized MtrC. These results raise the possibility that the interaction of oxidized MtrC with soluble U substrates is weak, and it is possible that they cannot be identified by size-exclusion. We could envisage that the strength of the interaction between MtrC and the complexes of U correlates with the reaction rates. Hence, we would expect a weaker interaction with U-DTPA and U-EDTA, which showed the most rapid reduction rates, and stronger interaction with U-NTA and U-carbonate.

Interestingly, the results reported above for U(VI) were also observed for the reduction of Fe(III)-aminocarboxylate ligand complexes with the purified undecaheme c-type cytochrome UndA¹⁷³. The rate of reduction of Fe(III)-EDTA by UndA was about 100x more rapid than that of Fe(III)-NTA¹⁷³. In addition, two iron complexes, Fe(III)-NTA and Fe(III)-citrate were shown to interact with the same region around the heme 7 of UndA¹⁶³. Moreover, Fe(III)-EDTA could not be crystallized with UndA, whereas Fe(III)-NTA and Fe(III)-citrate were¹⁶³. In this study, Edwards et al. observed that a Fe(III)-NTA dimer associates with UndA close to heme 7, with the two Fe(III) atoms localized at 6.2 Å and 8.3 Å from the heme center, respectively. Both dimer NTA molecules interacting via hydrogen bonds between one of a carboxylic group and the guanidinium group of an Arginine and the backbone nitrogen of a Serine and a Lysine. Thus, the more rapid reaction of UndA with Fe(III)-EDTA than Fe(III)-NTA could be hypothesized to be linked to weaker electrostatic interactions between the protein and Fe(III)-EDTA as compared to Fe(III)-NTA. This is possibly inherent to the ligand properties when bound to the metal center.

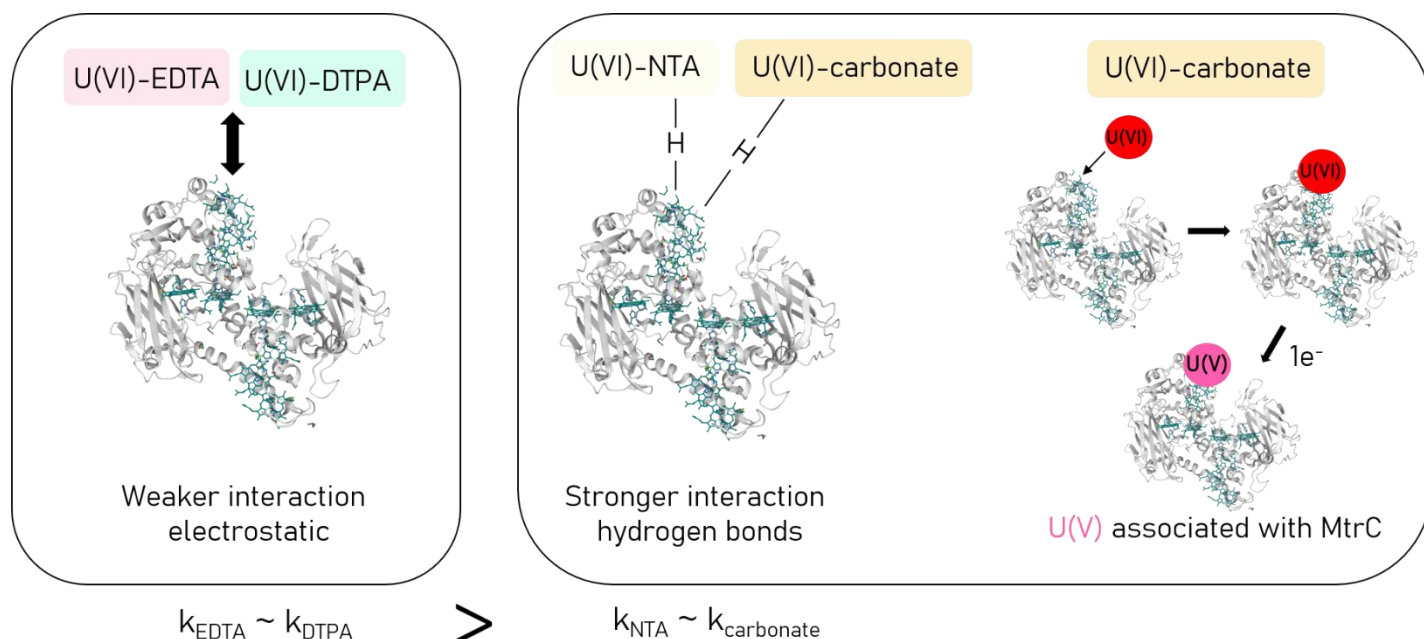
Electrostatic interactions between protein and substrate were also reported by Fukushima et al.¹⁶². They studied the interaction of MtrF with the surface of $\alpha\text{-Fe}_2\text{O}_3$ nanoparticles by protease foot-printing. They identified a positively charged pocket at the surface of MtrF, close to hemes 6 and 7 where the negatively charged surface of $\alpha\text{-Fe}_2\text{O}_3$ nanoparticles likely interacts. Moreover, Edwards et al. found that the overall electrostatic charge near heme 7 was positive, likely attracting negatively charged substrates¹⁶³. These findings further underscore the importance of substrate charge as one of the parameters influencing the type and locus of protein-complex, and therefore the rate of reaction.

All considered, we propose that the rapid reaction rates observed for U(VI)-EDTA or U(VI)-DTPA, stemmed from weaker interactions. We suppose that these two complexes can approach one terminal heme via electrostatic interaction. In contrast, in the case of U(VI)-NTA or U(VI)-carbonate complexes, exhibiting slower reduction rates, we propose that binding to a site close to a terminal heme occurs via hydrogen bonding, as reported by Edwards et al. for Fe(III)-NTA and UndA. Indeed, covalent binding to MtrC can be excluded as a major factor in the reduction of these four U(VI) complexes as there were no significant differences in the binding extent of the four U species to MtrC. This assumption is that hydrogen bonds did not withstand the separation process by size-exclusion chromatography.

With reduced MtrC, U(IV) remained in solution for all three aminocarboxylate ligands while U complexed with carbonate remained largely bound to MtrC after reaction. We confirm that the strong complexation constant of U(IV) with the aminocarboxylate ligands (Table 3) ensures the retention of reduced U in solution^{131,166,169}. In contrast, for carbonate, we hypothesize that while U(VI) binding is limited, pentavalent U may bind to the protein. Indeed, M₄-edge HR-XANES data evidence the formation and persistence of U(V) in association with the protein. This U(V) intermediate must have a close interaction with MtrC otherwise, it would spontaneously disproportionate in carbonate buffer at pH 7.5¹²². The formation of subsequent U(IV) may proceed as Sundararajan et al. described: two U(V) nuclei bound to the protein disproportionate to U(VI) and U(IV)¹²¹. We propose that the U(IV) formed remains associated with the protein (Figure 6). The formation of a stabilized U(V) intermediate may also be a parameter that contributes to slow down the reduction rate of U(VI) to U(IV).

4.5 Conclusion

In this study, we interested ourselves to the parameters which may influence the reduction rate of U(VI) by *S. oneidensis* MR-1 and the purified c-type cytochrome MtrC. We first concluded that the reduction mechanism for both strain MR-1 cells and MtrC is highly dependent on speciation. In fact, with strain MR-1 cells, we observed that U(VI)-NTA and U(VI)-EDTA complexes displayed more rapid reduction rates than U(VI)-DTPA and U(VI)-carbonate. We attribute this difference to electrostatic, bulkiness, and diffusion limitations. Moreover, with isolated MtrC, reaction rates are grouped in two clusters, one with more rapid rates observed with U(VI)-EDTA and U(VI)-DTPA, and one with slower comprising U(VI)-NTA and U(VI)-carbonate. Clearly, the hypothesis of a correlation between logK and reduction rates does not hold here, since U(VI)-EDTA and U(VI)-DTPA were reduced more rapidly and have the higher logK of the series. However, we propose that hydrogen bonds may form between U(VI)-NTA or U(VI)-carbonate and MtrC, whereas, electrostatic interactions governed the interaction between U(VI)-EDTA or U(VI)-DTPA and MtrC. Stronger interaction between MtrC and U(VI)-complexes would slow down the reaction. Other parameters which could substantially influence are the U(VI)-complexes and MtrC surface charges, the formation of a pentavalent intermediate, observed in the system with MtrC and U(VI)-carbonate, or structural rearrangement required from U(V) to U(IV) (Figure 4:10).



Electron transfer rate is speciation dependent: type of interaction, U(V) intermediates, steric hindrance

Figure 4:10. Schematic representation of the factors which could influence electron transfer rate from MtrC to U(VI)-ligand complexes

4.6 Limits of the experimental study and outlooks

We chose to work with purified MtrC, and performed enzymatic assays between MtrC and soluble U complexes. This system allows us to study specifically the interaction between two molecules, however, the experimental conditions are far from *in vivo* conditions, under which the protein receives a continuous flow of electrons when embedded within the outer membrane of bacterial cells. Hence, MtrC may display distinct redox potentials and redox properties when isolated or when embedded in the outer-membrane. In addition, several electron exits may be available and energetically accessible in the isolated MtrC, as there are four solvent-exposed hemes in the structure of MtrC, heme 2,7 and heme 5,10¹⁵⁴. These may not be as readily accessible in the membrane-embedded protein, and may have distinct redox potential when exposed to the solvent. Moreover, we lack information on thermodynamic parameters, namely the redox potential of the selected U complexes, for U(VI)/U(V) and the U(V)/U(IV) redox couples. These would allow us to estimate the free energy of the redox reactions between the U-ligand complexes and the terminal hemes. The redox potential of the terminal hemes are already modeled for MtrF, a homologue of MtrC^{174,175}.

A more in-depth study of the binding strength will be undertaken, namely by investigating the crystallization of the four U-complexes with MtrC, in order to identify binding regions of U soluble substrates, but also the nature of their interaction with MtrC. Alternative methods include Atomic Force Microscopy (AFM) to probe the strength of interaction between the U-complexes and MtrC, or investigating engineered proteins lacking terminal hemes or electrostatically altered putative hydrogen bonding region to better grasp the mechanism of electron transfer.

4.7 References

- (1) Veeramani, H.; Alessi, D. S.; Suvorova, E. I.; Lezama-Pacheco, J. S.; Stubbs, J. E.; Sharp, J. O.; Dippon, U.; Kappler, A.; Bargar, J. R.; Bernier-Latmani, R. Products of Abiotic U(VI) Reduction by Biogenic Magnetite and Vivianite. *Geochim. Cosmochim. Acta* **2011**, 75 (9), 2512–2528. <https://doi.org/10.1016/j.gca.2011.02.024>.
- (2) Veeramani, H.; Scheinost, A. C.; Monsegue, N.; Qafoku, N. P.; Kukkadapu, R.; Newville, M.; Lanzirotti, A.; Pruden, A.; Murayama, M.; Hochella, M. F. Abiotic Reductive Immobilization of U(VI) by Biogenic Mackinawite. *Environ. Sci. Technol.* **2013**, 47 (5), 2361–2369. <https://doi.org/10.1021/es304025x>.
- (3) O'Loughlin, E. J.; Kelly, S. D.; Cook, R. E.; Csencsits, R.; Kemner, K. M. Reduction of Uranium(VI) by Mixed Iron(II)/Iron(III) Hydroxide (Green Rust): Formation of UO₂ Nanoparticles. *Environ. Sci. Technol.* **2003**, 37 (4), 721–727. <https://doi.org/10.1021/es0208409>.
- (4) Scott, T. B.; Allen, G. C.; Heard, P. J.; Randell, M. G. Reduction of U(VI) to U(IV) on the Surface of Magnetite. *Geochim. Cosmochim. Acta* **2005**, 69 (24), 5639–5646. <https://doi.org/10.1016/j.gca.2005.07.003>.
- (5) Lovley, D. R.; Phillips, E. J. P.; Gorby, Y. A.; Landa, E. R. Microbial Reduction of Uranium. *Nature* **1991**, 350 (6317), 413–416. <https://doi.org/10.1038/350413a0>.
- (6) Bernier-Latmani, R.; Veeramani, H.; Vecchia, E. D.; Junier, P.; Lezama-Pacheco, J. S.; Suvorova, E. I.; Sharp, J. O.; Wigginton, N. S.; Bargar, J. R. Non-Uraninite Products of Microbial U(VI) Reduction. *Environ. Sci. Technol.* **2010**, 44 (24), 9456–9462. <https://doi.org/10.1021/es101675a>.
- (7) Lovley, D. R.; Roden, E. E.; Phillips, E. J. P.; Woodward, J. C. Enzymatic Iron and Uranium Reduction by Sulfate-Reducing Bacteria. *Mar. Geol.* **1993**, 113 (1–2), 13.
- (8) Francis, A. J.; Dodge, C. J.; Lu, Fulong.; Halada, G. P.; Clayton, C. R. XPS and XANES Studies of Uranium Reduction by *Clostridium* Sp. *Environ. Sci. Technol.* **1994**, 28 (4), 636–639. <https://doi.org/10.1021/es00053a016>.
- (9) Bargar, J. R.; Bernier-Latmani, R.; Giammar, D. E.; Tebo, B. M. Biogenic Uraninite Nanoparticles and Their Importance for Uranium Remediation. *Elements* **2008**, 4 (6), 407–412. <https://doi.org/10.2113/gselements.4.6.407>.
- (10) Marshall, M. J.; Beliaev, A. S.; Dohnalkova, A. C.; Kennedy, D. W.; Shi, L.; Wang, Z.; Boyanov, M. I.; Lai, B.; Kemner, K. M.; McLean, J. S.; Reed, S. B.; Culley, D. E.; Bailey, V. L.; Simonson, C. J.; Saffarini, D. A.; Romine, M. F.; Zachara, J. M.; Fredrickson, J. K. C-Type Cytochrome-Dependent Formation of U(IV) Nanoparticles by *Shewanella Oneidensis*. *PLoS Biol.* **2006**, 4 (8). <https://doi.org/10.1371/journal.pbio.0040268>.
- (11) Hartshorne, R. S.; Reardon, C. L.; Ross, D.; Nuester, J.; Clarke, T. A.; Gates, A. J.; Mills, P. C.; Fredrickson, J. K.; Zachara, J. M.; Shi, L.; Beliaev, A. S.; Marshall, M. J.; Tien, M.; Brantley, S.; Butt, J. N.; Richardson, D. J. Characterization of an Electron Conduit between Bacteria and the Extracellular Environment. *Proc. Natl. Acad. Sci. U. S. A.* **2009**, 106 (52), 22169–22174. <https://doi.org/10.1073/pnas.0900086106>.
- (12) Shi, L.; Chen, B.; Wang, Z.; Elias, D. A.; Mayer, M. U.; Gorby, Y. A.; Ni, S.; Lower, B. H.; Kennedy, D. W.; Wunschel, D. S.; Mottaz, H. M.; Marshall, M. J.; Hill, E. A.; Beliaev, A. S.; Zachara, J. M.; Fredrickson, J. K.; Squier, T. C. Isolation of a High-Affinity Functional Protein Complex between OmcA and MtrC: Two Outer Membrane Decaheme c-Type Cytochromes of *Shewanella Oneidensis* MR-1. *J. Bacteriol.* **2006**, 188 (13), 4705–4714. <https://doi.org/10.1128/JB.01966-05>.

- (13) Ross, D. E.; Ruebush, S. S.; Brantley, S. L.; Hartshorne, R. S.; Clarke, T. A.; Richardson, D. J.; Tien, M. Characterization of Protein-Protein Interactions Involved in Iron Reduction by *Shewanella Oneidensis* MR-1. *Appl. Environ. Microbiol.* **2007**, *73* (18), 5797–5808. <https://doi.org/10.1128/AEM.00146-07>.
- (14) Schuetz, B.; Schicklberger, M.; Kuermann, J.; Spormann, A. M.; Gescher, J. Periplasmic Electron Transfer via the C-Type Cytochromes MtrA and FccA of *Shewanella Oneidensis* MR-1. *Appl. Environ. Microbiol.* **2009**, *75* (24), 7789–7796. <https://doi.org/10.1128/AEM.01834-09>.
- (15) Schwalb, C.; Chapman, S. K.; Reid, G. A. The Membrane-Bound Tetrahaem c-Type Cytochrome CymA Interacts Directly with the Soluble Fumarate Reductase in *Shewanella*. *Biochem. Soc. Trans.* **2002**, *30* (4), 658–662. <https://doi.org/10.1042/>.
- (16) Richardson, D. J.; Edwards, M. J.; White, G. F.; Baiden, N.; Hartshorne, R. S.; Fredrickson, J.; Shi, L.; Zachara, J.; Gates, A. J.; Butt, J. N.; Clarke, T. A. Exploring the Biochemistry at the Extracellular Redox Frontier of Bacterial Mineral Fe(III) Respiration. *Biochem. Soc. Trans.* **2012**, *40* (3), 493–500. <https://doi.org/10.1042/BST20120018>.
- (17) Edwards, M. J.; Fredrickson, J. K.; Zachara, J. M.; Richardson, D. J.; Clarke, T. A. Analysis of Structural MtrC Models Based on Homology with the Crystal Structure of MtrF. *Biochem. Soc. Trans.* **2012**, *40* (6), 1181–1185. <https://doi.org/10.1042/BST20120132>.
- (18) Edwards, M. J.; White, G. F.; Norman, M.; Tome-Fernandez, A.; Ainsworth, E.; Shi, L.; Fredrickson, J. K.; Zachara, J. M.; Butt, J. N.; Richardson, D. J.; Clarke, T. A. Redox Linked Flavin Sites in Extracellular Decaheme Proteins Involved in Microbe-Mineral Electron Transfer. *Sci. Rep.* **2015**, *5* (1), 11677. <https://doi.org/10.1038/srep11677>.
- (19) Watanabe, H. C.; Yamashita, Y.; Ishikita, H. Electron Transfer Pathways in a Multiheme Cytochrome MtrF. *Proc. Natl. Acad. Sci.* **2017**, *114* (11), 2916–2921. <https://doi.org/10.1073/pnas.1617615114>.
- (20) White, G. F.; Shi, Z.; Shi, L.; Wang, Z.; Dohnalkova, A. C.; Marshall, M. J.; Fredrickson, J. K.; Zachara, J. M.; Butt, J. N.; Richardson, D. J.; Clarke, T. A. Rapid Electron Exchange between Surface-Exposed Bacterial Cytochromes and Fe(III) Minerals. *Proc. Natl. Acad. Sci.* **2013**, *110* (16), 6346–6351. <https://doi.org/10.1073/pnas.1220074110>.
- (21) Wigginton, N. S.; Rosso, K. M.; Lower, B. H.; Shi, L.; Hochella, M. F. Electron Tunneling Properties of Outer-Membrane Decaheme Cytochromes from *Shewanella Oneidensis*. *Geochim. Cosmochim. Acta* **2007**, *71* (3), 543–555. <https://doi.org/10.1016/j.gca.2006.10.002>.
- (22) Wigginton, N. S.; Rosso, K. M.; Hochella, M. F. Mechanisms of Electron Transfer in Two Decaheme Cytochromes from a Metal-Reducing Bacterium. *J. Phys. Chem. B* **2007**, *111* (44), 12857–12864. <https://doi.org/10.1021/jp0718698>.
- (23) Breuer, M.; Rosso, K. M.; Blumberger, J. Electron Flow in Multiheme Bacterial Cytochromes Is a Balancing Act between Heme Electronic Interaction and Redox Potentials. *Proc. Natl. Acad. Sci. U. S. A.* **2014**, *111* (2), 611–616. <https://doi.org/10.1073/pnas.1316156111>.
- (24) Pirbadian, S.; El-Naggar, M. Y. Multistep Hopping and Extracellular Charge Transfer in Microbial Redox Chains. *Phys. Chem. Chem. Phys.* **2012**, *14* (40), 13802–13808. <https://doi.org/10.1039/C2CP41185G>.
- (25) Marcus, R. A.; Sutin, N. Electron Transfers in Chemistry and Biology. *Biochim. Biophys. Acta BBA - Rev. Bioenerg.* **1985**, *811* (3), 265–322. [https://doi.org/10.1016/0304-4173\(85\)90014-X](https://doi.org/10.1016/0304-4173(85)90014-X).

- (26) Lower, B. H.; Shi, L.; Yongsunthon, R.; Droubay, T. C.; McCready, D. E.; Lower, S. K. Specific Bonds between an Iron Oxide Surface and Outer Membrane Cytochromes MtrC and OmcA from *Shewanella Oneidensis* MR-1. *J. Bacteriol.* **2007**, *189* (13), 4944–4952. <https://doi.org/10.1128/JB.01518-06>.
- (27) Fukushima, T.; Gupta, S.; Rad, B.; Cornejo, J. A.; Petzold, C. J.; Chan, L. J. G.; Mizrahi, R. A.; Ralston, C. Y.; Ajo-Franklin, C. M. The Molecular Basis for Binding of an Electron Transfer Protein to a Metal Oxide Surface. *J. Am. Chem. Soc.* **2017**, *139* (36), 12647–12654. <https://doi.org/10.1021/jacs.7b06560>.
- (28) Edwards, M. J.; Hall, A.; Shi, L.; Fredrickson, J. K.; Zachara, J. M.; Butt, J. N.; Richardson, D. J.; Clarke, T. A. The Crystal Structure of the Extracellular 11-Heme Cytochrome UndA Reveals a Conserved 10-Heme Motif and Defined Binding Site for Soluble Iron Chelates. *Structure* **2012**, *20* (7), 1275–1284. <https://doi.org/10.1016/j.str.2012.04.016>.
- (29) Sundararajan, M.; Campbell, A. J.; Hillier, I. H. Catalytic Cycles for the Reduction of [UO₂]²⁺ by Cytochrome C7 Proteins Proposed from DFT Calculations. *J. Phys. Chem. A* **2008**, *112* (19), 4451–4457. <https://doi.org/10.1021/jp800209p>.
- (30) Tandy, S.; Bossart, K.; Mueller, R.; Ritschel, J.; Hauser, L.; Schulin, R.; Nowack, B. Extraction of Heavy Metals from Soils Using Biodegradable Chelating Agents. *Environ. Sci. Technol.* **2004**, *38* (3), 937–944. <https://doi.org/10.1021/es0348750>.
- (31) Molinas, M.; Faizova, R.; Brown, A.; Galanzew, J.; Schacherl, B.; Bartova, B.; Meibom, K. L.; Vitova, T.; Mazzanti, M.; Bernier-Latmani, R. Biological Reduction of a U(V)–Organic Ligand Complex. *Environ. Sci. Technol.* **2021**, *55* (8), 4753–4761. <https://doi.org/10.1021/acs.est.0c06633>.
- (32) Suzuki, Y.; Tanaka, K.; Kozai, N.; Ohnuki, T. Effects of Citrate, NTA, and EDTA on the Reduction of U(VI) by *Shewanella Putrefaciens*. *Geomicrobiol. J.* **2010**, *27* (3), 245–250. <https://doi.org/10.1080/01490450903456764>.
- (33) Haas, J. R.; Northup, A. Effects of Aqueous Complexation on Reductive Precipitation of Uranium by *Shewanella Putrefaciens*. *Geochem. Trans.* **2004**, *5* (3), 41. <https://doi.org/10.1186/1467-4866-5-41>.
- (34) Zimina, A.; Dardenne, K.; Denecke, M. A.; Doronkin, D. E.; Huttel, E.; Lichtenberg, H.; Mangold, S.; Pruessmann, T.; Rothe, J.; Spangenberg, Th.; Steininger, R.; Vitova, T.; Geckeis, H.; Grunwaldt, J.-D. CAT-ACT—A New Highly Versatile x-Ray Spectroscopy Beamline for Catalysis and Radionuclide Science at the KIT Synchrotron Light Facility ANKA. *Rev. Sci. Instrum.* **2017**, *88* (11), 113113. <https://doi.org/10.1063/1.4999928>.
- (35) Ravel, B.; Newville, M. ATHENA, ARTEMIS, HEPHAESTUS: Data Analysis for X-Ray Absorption Spectroscopy Using IFEFFIT. *J. Synchrotron Radiat.* **2005**, *12* (Pt 4), 537–541. <https://doi.org/10.1107/S0909049505012719>.
- (36) De Stefano, C.; Gianguzza, A.; Milea, D.; Pettignano, A.; Sammartano, S. Sequestering Ability of Polyaminopolycarboxylic Ligands towards Dioxouranium(VI) Cation. *J. Alloys Compd.* **2006**, *424* (1), 93–104. <https://doi.org/10.1016/j.jallcom.2006.01.003>.
- (37) Hummel, W.; Anderegg, G.; Rao, L.; Puigdomenech, I.; Tochiyama, O. *Chemical Thermodynamics of Compounds and Complexes of U, Np, Pu, Am, Tc, Se, Ni and Zr with Selected Organic Ligands*; 2005; Vol. 9.
- (38) Grenthe, I.; Fuger, J.; Lemire, R. J.; Muller, A. B.; Nguyen-Trung Cregu, C.; Wanner, H. Chemical Thermodynamics of Uranium. **1992**.

- (39) Pashalidis, I.; Czerwinski, K. R.; Fanghänel, T.; Kim, J. I. Solid-Liquid Phase Equilibria of Pu(VI) and U(VI) in Aqueous Carbonate Systems. Determination of Stability Constants. *Radiochim. Acta* **1997**, *76* (1–2), 55–62. <https://doi.org/10.1524/ract.1997.76.12.55>.
- (40) Hummel, W.; Puigdomènech, I.; Rao, L.; Tochiyama, O. Thermodynamic Data of Compounds and Complexes of U, Np, Pu and Am with Selected Organic Ligands. *Comptes Rendus Chim.* **2007**, *10* (10), 948–958. <https://doi.org/10.1016/j.crci.2007.03.012>.
- (41) Bonin, L.; Guillaumont, D.; Jeanson, A.; Den Auwer, C.; Grigoriev, M.; Berthet, J.-C.; Hennig, C.; Scheinost, A.; Moisy, Ph. Thermodynamics and Structure of Actinide(IV) Complexes with Nitrilotriacetic Acid. *Inorg. Chem.* **2009**, *48* (9), 3943–3953. <https://doi.org/10.1021/ic801453w>.
- (42) Brown, M. A.; Paulenova, A.; Gelis, A. V. Aqueous Complexation of Thorium(IV), Uranium(IV), Neptunium(IV), Plutonium(III/IV), and Cerium(III/IV) with DTPA. *Inorg. Chem.* **2012**, *51* (14), 7741–7748. <https://doi.org/10.1021/ic300757k>.
- (43) Bernhard, G.; Geipel, G.; Reich, T.; Brendler, V.; Amayri, S.; Nitsche, H. Uranyl(VI) Carbonate Complex Formation: Validation of the $\text{Ca}_2\text{UO}_2(\text{CO}_3)_3(\text{Aq.})$ Species. *Radiochim. Acta* **2001**, *89* (8), 511–518. <https://doi.org/10.1524/ract.2001.89.8.511>.
- (44) Ganesh, R.; Robinson, K. G.; Reed, G. D.; Saylor, G. S. Reduction of Hexavalent Uranium from Organic Complexes by Sulfate- and Iron-Reducing Bacteria. *Appl. Environ. Microbiol.* **1997**, *63* (11), 4385–4391.
- (45) Kim, S.; Bender, W. M.; Becker, U. Exploring the Kinetics of Actinyl–EDTA Reduction by Ferrous Iron Using Quantum-Mechanical Calculations. *Phys. Chem. Chem. Phys.* **2021**, *23* (9), 5298–5314. <https://doi.org/10.1039/D0CP05179A>.
- (46) Ross, D. E.; Brantley, S. L.; Tien, M. Kinetic Characterization of OmcA and MtrC, Terminal Reductases Involved in Respiratory Electron Transfer for Dissimilatory Iron Reduction in *Shewanella Oneidensis* MR-1. *Appl. Environ. Microbiol.* **2009**, *75* (16), 5218–5226. <https://doi.org/10.1128/AEM.00544-09>.
- (47) Renshaw, J. C.; Butchins, L. J. C.; Livens, F. R.; May, I.; Charnock, J. M.; Lloyd, J. R. Bioreduction of Uranium: Environmental Implications of a Pentavalent Intermediate. *ResearchGate* **2005**, *39* (15), 5657–5660. <https://doi.org/10.1021/es048232b>.
- (48) Jones, D. L.; Andrews, M. B.; Swinburne, A. N.; Botchway, S. W.; Ward, A. D.; Lloyd, J. R.; Natrajan, L. S. Fluorescence Spectroscopy and Microscopy as Tools for Monitoring Redox Transformations of Uranium in Biological Systems. *Chem. Sci.* **2015**, *6* (9), 5133–5138. <https://doi.org/10.1039/C5SC00661A>.
- (49) Vettese, G. F.; Morris, K.; Natrajan, L. S.; Shaw, S.; Vitova, T.; Galanzew, J.; Jones, D. L.; Lloyd, J. R. Multiple Lines of Evidence Identify U(V) as a Key Intermediate during U(VI) Reduction by *Shewanella Oneidensis* MR1. *Environ. Sci. Technol.* **2020**. <https://doi.org/10.1021/acs.est.9b05285>.
- (50) Shi, L.; Belchik, S. M.; Wang, Z.; Kennedy, D. W.; Dohnalkova, A. C.; Marshall, M. J.; Zachara, J. M.; Fredrickson, J. K. Identification and Characterization of UndAHR-6, an Outer Membrane Endecaheme c-Type Cytochrome of *Shewanella* Sp. Strain HRCR-6. *Appl. Environ. Microbiol.* **2011**, *77* (15), 5521–5523. <https://doi.org/10.1128/AEM.00614-11>.

- (51) Kern, D. M. H.; Orlemann, E. F. The Potential of the Uranium (V), Uranium (VI) Couple and the Kinetics of Uranium (V) Disproportionation in Perchlorate Media. *J. Am. Chem. Soc.* **1949**, *71* (6), 2102–2106. <https://doi.org/10.1021/ja01174a055>.
- (52) Breuer, M.; Zarzycki, P.; Blumberger, J.; Rosso, K. M. Thermodynamics of Electron Flow in the Bacterial Decaheme Cytochrome MtrF. *J. Am. Chem. Soc.* **2012**, *134* (24), 9868–9871. <https://doi.org/10.1021/ja3027696>.
- (53) Edwards, M. J.; Gates, A. J.; Butt, J. N.; Richardson, D. J.; Clarke, T. A. Comparative Structure-Potential-Spectroscopy of the Shewanella Outer Membrane Multiheme Cytochromes. *Curr. Opin. Electrochem.* **2017**, *4* (1), 199–205. <https://doi.org/10.1016/j.coelec.2017.08.013>.

Chapter 5 Conclusion

5.1 Achieved results

This thesis focused on the reduction mechanism of U(VI), and in particular that of U(V) by the metal-reducing bacterium *S. oneidensis* MR-1 and its outer-membrane *c*-type cytochrome MtrC. We sought to provide better insights into the molecular underpinnings of U reduction. The motives of such a quest are: (i) probing the relevance of U(V) in the environmental systems, poorly documented because of its ephemerality; (ii) having better understanding of the processes underway during the implementation of remediation strategies in U contaminated sites; (iii) paving the way for the study of the isotope fractionation mechanism of U when undergoing biological reduction at the molecular scale. In fact, ratios of ^{238}U vs ^{235}U are employed to evaluate and date anoxic events in geological times; (iv) satisfying some enthusiastic scientific curiosity.

As we moved through the observations, we increased the magnification, starting from a bacterial system, transitioning through a genetically-modified bacterial system, to end with a specific enzyme. This journey allowed us to confirm some of our hypothesis, to demonstrate some facts, but above all to raise additional questions.

The initial start to our work was the synthesis, achieved by our co-workers at the Group of Complex Chemistry at EPFL, Radmila Faizova and Marinella Mazzanti, of an aminocarboxylate ligand (dpaea) with the propensity to stabilize uranyl(V) in water at pH 7. In fact, dpaea surrounds the equatorial plan of the U atom, preventing that cation-cation interactions that provoke U(V) disproportionation. As a result of their work, we had access to a compound to carry out further investigations.

We initiated our work by investigating the reduction of (i) solid-phase U(VI)-dpaea and (ii) aqueous phase U(V)-dpaea by *S. oneidensis* MR-1. Using M4-edge XANES, we observed (i) that solid-phase U(VI)-dpaea was being reduced to aqueous U(V)-dpaea. Then, we noticed (ii) a 20% decrease in aqueous U(V)-dpaea concentration over 336h upon incubation with *S. oneidensis*-MR-1. To discern whether it resulted from disproportionation or from an additional one-electron transfer, we used a mutant strain of *S. oneidensis* MR-1, ΔccmG , lacking the full maturation system for *c*-type cytochromes. ΔccmG was impaired in reducing U(V)-dpaea, as its concentration remained stable in solution over the experimental time. Hence, we ruled out the possibility of cell-mediated disproportionation of U(V)-dpaea and concluded that U(V)-dpaea was reduced by a one-electron transfer. The slow reduction rate of U(V)-dpaea may be attributed to important structural rearrangements upon reduction. Furthermore, the U(IV) products formed were studied by STEM and two types of non-crystalline U(IV) associated with *S. oneidensis* MR-1 were identified. Morphology type 1 corresponded to U dispersed at the surface of the bacteria, which we attributed to non-crystalline U(IV). Morphology type 2 coincides with U clusters associated to the EPS matrix of the cells. The presence of N in morphology 2 suggests that it may contain

U(IV)-dpaea₂. To better comprehend the formed U(IV) products, EXAFS analysis was recently performed at the Mars beamline in SOLEIL, but data still require appropriate processing.

We then investigated solid phase U(VI)-dpaea and aqueous phase U(V)-dpaea reduction using two mutant strains of *S. oneidensis* MR-1, which we constructed. These strains, Δ OMC lacking the outer-membrane *c*-type cytochromes MtrC, OmcA and MtrF, and Δ ccmG were incubated along with the wild type (WT) on both substrates. Δ ccmG could not reduce solid-phase U(VI)-dpaea, however Δ OMC exhibited similar reduction rate as that of the WT. As Δ OMC lacks outer-membrane *c*-type cytochromes, we proposed that reduction of soluble U(VI)-dpaea could occur within the cell periplasm of Δ OMC. As the rates of reduction were very similar, we deduced that dissolution of U(VI)-dpaea occurs prior to its reduction, and that it is the limiting step in the reaction. However, we cannot also exclude that MtrA, which terminal heme is exposed to the extracellular medium in absence of MtrC, could reduce solid phase U(VI)-dpaea. Additional tests using a mutant strain lacking the outer-membrane *c*-type cytochromes and MtrA will be investigated to better elucidate this point. Regarding incubations with U(V)-dpaea, we observed over 74h that U(V)-dpaea concentrations decreased by 12.3% in the WT incubations, 3% with Δ OMC and 2% with Δ ccmG. These results imply that outer-membrane *c*-type cytochromes are involved in U(V)-dpaea reduction to U(IV) species. In addition, when reacting the isolated outer-membrane *c*-type cytochrome MtrC with U(V)-dpaea, we observed direct electron transfer from MtrC to U(V)-dpaea, confirming that outer-membrane *c*-type cytochromes are involved in U(V)-dpaea reduction. Moreover, when reacting isolated MtrC with aqueous U(VI)-dpaea, about 15 μ M aqueous U(VI)-dpaea (80% of the initial U(VI)) were reduced in 2 min, whereas 118.6 μ M U(V)-dpaea (98.8% of initial U(V)) were reduced in 2min. If U(V) had disproportionated, we would not have observed that extent of U(V)-dpaea reduction based on the slower rate of aqueous U(VI)-dpaea reduction. Therefore, we confirmed that U(V)-dpaea is not transformed to U(IV) via disproportionation, but undergoes reduction by outer-membrane *c*-type cytochromes.

Last but not least, we undertook investigations of the reactions between the isolated *c*-type cytochrome MtrC and four U(VI) complexes: U(VI)-NTA, U(VI)-EDTA, U(VI)-DTPA, and U(VI)-carbonate. Along the aminocarboxylate ligands series, the ligand denticity, increases with the logK of the U-ligand complex and their bulkiness as follows U(VI)-NTA < U(VI)-EDTA < U(VI)-DTPA. We hypothesized first that U(VI)-EDTA and U(VI)-DTPA would display slower reactions rates compared to the smaller U(VI)-NTA and U(VI)-carbonate complexes. Indeed, we conjectured that logK and complex size were parameters which could influence the reduction mechanism. Interestingly, we observed two clusters of reaction rates: U(VI)-EDTA and U(VI)-DTPA were almost completely reduced after 15s with comparable reaction rates, whereas U(VI)-NTA and U(VI)-carbonate reached 50% of reduction after 15s, with similar rates. Therefore, we proposed that there may be differences in the nature of the interaction between MtrC and these two groups of complexes. Our second hypothesis was that U(VI)-NTA and U(VI)-carbonate interact via covalent or hydrogen bonding with MtrC, likely close to one solvent-exposed heme, whereas U(VI)-EDTA and U(VI)-DTPA interact via electrostatic forces. To test our hypothesis, we ran size-exclusion columns experiments, to separate MtrC from the reaction mixture. For oxidized MtrC under oxic conditions, we did not observe significant differences between the binding extent of the four U(VI)-ligand complexes. However, under anoxic conditions, we observed that 72% of the U(IV) product was associated with MtrC. We interpreted these results as follows: (i) for oxidized MtrC, the similarities observed between the different ligands could be

linked to an experimental artefact. It is possible that hydrogen bonds formed between MtrC and U(VI)-NTA or U(VI)-carbonate broke during the separation process; (ii) the binding of U(IV) products to MtrC upon U(VI)-carbonate reduction suggests that there must be a stronger interaction between U(VI)-carbonate and MtrC compared to the other complexes; (iii) probably, U(VI)-NTA also interacts strongly with MtrC, however, U(IV)-NTA or U(IV)-NTA₂ have high formation constants, hence it may be more favorable for the soluble U(IV) complexes to form rather than U(IV) remaining bound to MtrC; (iv) in addition, we captured the formation of a U(V) intermediate by M₄-edge HR-XANES in the carbonate system upon reduction of U(VI). It could also be that the U(V) intermediates formed in the carbonate and NTA systems have longer half-lives than those of U(V) formed in the EDTA and DTPA systems. Overall, our results hint at the fact that the reduction of U by *c*-type cytochromes depends on the U species, and that various types of interactions exist between the protein and U-ligand complexes. In particular, it could be that hydrogen bonding slows down the reaction rates, and weaker electrostatic interactions enable fast reduction. This would also match the complexes' sizes and bulkiness. The bulkier the complex is, the harder it could be to come into close interaction with a binding site in MtrC.

5.2 Future development

This thesis has opened questions that will require more investigation. It has been a wonderful and captivating journey which does not have an end yet!

Regarding the work presented in chapter 3, we seek to repeat the mutant experiments to strengthen the data. In addition, we are intrigued by the reducing power of $\Delta ccmG$ after 48h of incubation with iron oxides and 24h with Fe(III)-citrate, which we attributed to cell lysis. Hence, we plan to incubate lysed cells of $\Delta ccmG$ along with the WT with either iron substrates but also with U(VI)-dpaea (aqueous and solid-phase) to confirm the hypothesis.

As for chapter 4, additional experiments will be set to bring additional evidence regarding the question of the binding of U(VI) to the protein. First, series of binding tests with the size-exclusion columns will be carried out with the four abovementioned complexes, varying the speciation, in order to better grasp the role of U speciation in the U-MtrC interaction. Moreover, in parallel to the experiments discussed in this manuscript, we started to work on the crystallization of MtrC reacted with U(VI)-carbonate. Ideally, we would like to crystallize MtrC with the four U-ligand complexes studied to obtain deeper insights into the molecular interactions between U and MtrC. This could shed light on the potential binding area for U in MtrC. We managed to crystallize MtrC with U-carbonate, however the resolution of the diffraction patterns was not high enough (about 5Å) for the data to be interpreted. Other strategies to probe the U-MtrC interactions involve Atomic Force Microscopy, to probe the binding strength between MtrC and the U-ligands complexes. Alternatively, we could engineer MtrC by modifying the distal ligands of some hemes to increase their redox potential, rendering less thermodynamically favorable the reduction of U by these engineered hemes. We could hence envision to engineer heme 2 and 7, involved in electron transfer to flavin molecules, and react the resulting engineered MtrC with the U-ligand complexes. This would enable us to refine the electron transfer rates and binding interactions. A variant of this tack is to vary the electrostatics of the region around hemes 6 and 7 to determine whether this modification alters the reduction rate of U(VI)-ligands. Further, we would like to probe to U(IV) products structure by EXAFS.

We are looking forward to progressing in these directions, and further elucidating some of the underpinnings of the molecular mechanism of the enzymatic reduction of U

Annexes

Annex 1 – Supplementary information for chapter 2

This supporting information contains:

Text S1. Experimental method for UV-vis spectroscopy and for the evaluation of cell viability in incubations of *S. oneidensis* MR-1.

Text S2. Experimental method for the control experiment of U(V)-dpaea incubations.

Text S3. Correction for the ion exchange chromatography separation test of U(V)-dpaea.

Text S4. Experimental method for the incubation experiments of inactivated *S. oneidensis* MR-1 cells with U(VI)-acetate and then with U(V)-dpaea.

Text S5. Comparison of the inactivated cells versus active cells incubated with U(V)-dpaea reduction.

Figure S1. UV-vis spectra of the incubations with U(VI)-dpaea and incubations with U(V)-dpaea through time.

Figure S2. Aqueous Fe(II) concentration (A) and cell viability (B) through time in incubations with *S. oneidensis* MR-1, the deletion mutant ΔCcmG and a no-cell control with ferrihydrite.

Figure S3. Solubility of solid phases U(VI)-dpaea and of U(IV)-dpaea₂ measured in WLP medium.

Figure S4. LCF fitting results compared to the data for the 96h supernatant using U(VI)-dpaea and U(IV)-dpaea₂ as fitting components.

Figure S5. U M₄-edge HR-XANES spectra of the 150h solid phase shown in black during reduction U(VI)-dpaea.

Figure S6. Ratio of U(VI) and U(IV) recovered after ion-exchange chromatography elution of eight solutions with varying concentrations of U(V)-dpaea.

Figure S7. Linear regression showing the correlation between the amount of U eluted as U(IV) and the initial concentration of U(V)-dpaea prior the ion-exchange chromatography elution.

Figure S8. U speciation after ion-exchange chromatography separation of a set of six solutions containing the same starting ratio of U(IV) and U(VI) but different concentrations, with or without addition of dpaea ligand.

Figure S9. Cell viability in incubations of *S. oneidensis* MR-1 with A. U(VI)-dpaea over 720h (30 days) and U(V)-dpaea over 648h (27 days).

Figure S10. Energy dispersive spectroscopy (EDS) performed by scanning electron microscopy (SEM) on the two types of morphologies described for the U(IV) product obtained upon U(V)-dpaea reduction.

Figure S11. Selected area electron diffraction (SAED) collected for the morphology type 1 of the U(VI) product, which corresponds to dispersed small U clusters at the surface of the bacteria.

Figure S12. Selected area electron diffraction (SAED) collected for the morphology type 2 of the U(VI) product, which describes U clusters associated with cells.

Figure S13. U speciation in the solid phase (cell pellet) and in the aqueous phase (supernatant) of the controls and cultures incubated with 'synthetic' U(V)-dpaea.

Figure S14. A. U concentration in the inactivated-cells culture supernatants and in the cell-free controls incubated with U(VI)-acetate. B. U speciation in the solid phase and in the aqueous phase of both the inactivated-cells incubations and the cell-free controls after 69h.

Figure S15. Distribution of aqueous U(V)-dpaea and solid phase U overtime in incubations with *S. oneidensis* MR-1, incubations with inactivated cells of *S. oneidensis* MR-1 and cell-free controls with 'synthetic' U(V)-dpaea.

Figure S16. U speciation in the solid phase (cell pellet) and in the aqueous phase (supernatant) of (A) incubations with inactivated cells of *S. oneidensis* MR-1 and (B) cell-free controls, in presence of 'synthetic' U(V)-dpaea.

Table S1. Primers used for PCR and sequencing.

Table S2. Bacterial strains and plasmids used for this study.

Table S3. Composition of Widdel low phosphate (WLP) modified.

Table S4. Measurements and associated standard deviations for the ion-exchange chromatography separations of U from aqueous and solid phase samples.

TextS1. Experimental method for UV-vis spectroscopy and for the evaluation of cell viability in incubations of *S. oneidensis* MR-1.

Resting cell experiment with U(VI)-dpaea and U(V)-dpaea were set up as described in the Experimental methods section. In these batches of experiment, we chose to work with [U(VI)-dpaea]=1mM and [U(V)-dpaea]=0.8mM for UV-vis detection. For both U(VI)-dpaea and U(V)-dpaea, incubations with cells were done in triplicates and the no-cell controls in duplicates.

For UV-vis measurements, in an N₂-atmosphere, aliquots of about 250μL of the incubation supernatant were placed into an air-tight semi-macro screw cap UV quartz cuvette with a light path of 10mmx1mm (Msscientific, Berlin, Germany). The UV-vis spectra were acquired with a Shimadzu spectrophotometer (Shimadzu UV-2501PC, Suzhou Instruments Manufacturing Co. Ltd., Suzhou, China) in ambient atmosphere, while samples were kept anoxic in the air-tight cuvette. The wavelengths ranged from 400nm to 800nm. The results are shown in figure S1A. for incubations with U(VI)-dpaea and on figure S1.B. for incubation with U(V)-dpaea. As for cell viability evaluation, at selected times, aliquots of 200μL of the incubation supernatant were taken from 2 replicates. 6 dilutions of each samples were prepared in WLP medium (0x, 10x, 100x, 1000x, 10000x and 100000x). 50μL of each dilution were streaked on LB agar plates. The plates were incubated overnight at 30°C. Single colonies were counted manually on each plate. The average calculated at each time point in both the incubations with and without cells are displayed on figure S9.

Text S2. Experimental method for the control experiments of U(V)-dpaea incubations.

Prior to be incubated on U, the *ΔccmG* strain was characterized and compared to the WT strain using ferrihydrite. Fresh ferrihydrite was prepared by titrating 0.5M Fe(III)-Cl with 10M NaOH until the pH reached 7. After 30 minutes of equilibration, the precipitate was centrifuged and washed 5 times with deionized water (8000 g, 10 min). The total Fe concentration was measured by ICP-OES. *S. oneidensis* MR-1 and *ΔccmG* were prepared as described in the first paragraph of the Experimental method section before being incubated with 5mM anoxic ferrihydrite for 72h. The starting OD₆₀₀ of the incubations was calculated to be 1. The incubations were maintained in the dark at room temperature, inside the anaerobic chamber. Fe(II) was measured by the ferrozine assay and cell viability of both strains was followed by streaking an aliquot of culture on LB agar plates. The results of *ΔccmG* characterization with ferrihydrite are shown on Figure S2. We did not observe reduction of Fe(III) by *ΔccmG* in the first 48h. The slight reduction observed at 72h can be explained by potential cell lysis and release of reducing metabolites.

Then, *S. oneidensis* MR-1 and *ΔccmG* were incubated using 550 μM U(V)-dpaea as described in the first paragraph of the Experimental method section, at a starting cell OD of 1, and with 20 mM lactate in triplicate. All incubations were kept in the dark for the duration of the experiments.

Text S3. Correction for the ion exchange chromatography separation test of U(V)-dpaea.

In an N₂-atmosphere, a solution of U(V)-dpaea at 220 µM in 1 mL of deionized was diluted to the following concentrations: 110 µM, 58 µM, 31 µM, 19 µM, 11 µM, 6 µM 4.2 µM. The eight solutions were acidified and eluted through the ion-exchange chromatography columns following the protocol described in the Experimental methods section. In addition, four different volumes of the acidified solution prepared with 31 µM of U(V)-dpaea were eluted. The aim was to test whether the mass of U loaded post-acid treatment for a given concentration of U(V)-dpaea had an effect on the elution of U(VI) and U(IV).

The results of these tests showed that the mass of U loaded does not affect the amount of U recovered in the U(VI) and U(IV) fractions. However, we observed that for decreasing U(V)-dpaea initial concentrations, we recovered decreasing amount of U in the U(IV) fraction after elution (Figure S6). We then established the correlation linking U(V)-dpaea initial concentrations to the amount of U recovered in the U(IV) fraction, and we obtained the linear regression to extract the equation expressing %U(IV) as a function of initial mass of U(V)-dpaea (Figure S7). The best correlation was found using the natural logarithm of %U(IV) and the natural logarithm of (1-1/(1+ initial concentration of U(V)-dpaea)) as follow :

$$\ln(\%U(IV)) \propto \ln\left(1 - \frac{1}{1 + \text{initial concentration of } U(V)\text{dpaea}}\right)$$

We used the latter equation to correct for U(V)-dpaea behavior in ion-exchange chromatography analyses performed in the reduction experiment of 'biological U(V)' (Figure 5) and 'synthetic U(V)' (Figure S13) and the inactive cell experiment (Figure S16) with starting U(V) concentrations of 60µM and 30µM respectively. We attributed these shifts to residual oxidant (impurities or residual oxygen) in the HCl used for acid-treatment of the sample prior to ion exchange chromatography elution. We observed that, independently from the initial [U(V)-dpaea], the same mass of U is oxidized (2-3 µg) and eluted with the U(VI) fraction. It would explain why the effect is exacerbated at lower concentrations. Additionally, we established that the dpaea ligand does not influence the separation of U(VI) and U(IV) by ion-exchange chromatography (Figure S8).

Text S4. Experimental method for the incubation experiments of inactivated *S. oneidensis* MR-1 cells with U(VI)-acetate and then with U(V)-dpaea.

Preparation of inactive cells. *S. oneidensis* MR-1 was first grown as described in the first paragraph of the Experimental methods section. The cells harvested after the second incubation step were washed three times in aerobic modified WLP medium. The washed cells were then incubated in modified WLP medium aerobically for 48h (at 30°C and 140 rpm shaking speed). This step had the purpose to exhaust the cells of

electrons, which they deliver to O_2 as the electron acceptor. After 48h of aerobic incubation, the cells were autoclaved (20min at 121°C) and further washed three times in anoxic modified WLP.

Incubations with U(VI)-acetate. Inactivated *S. oneidensis* MR-1 cells were incubated in anoxic modified WLP medium in the presence of 400 μ M aqueous phase U(VI)-acetate, along with 20 mM of lactate as the electron donor (in triplicate). A cell-free control was conducted in parallel (in duplicate). The starting OD_{600} of the incubations was calculated to be 1. The incubations were maintained in the dark at room temperature, inside the anaerobic chamber. Aliquots of the supernatants were obtained at different incubation times and were filtered through 0.2 μ m PTFE filters (Whatman, Maidstone, United Kingdom). U concentrations were determined as described before by ICP-MS. An entire culture was sacrificed after 69h of incubation as described in the experimental methods for ion-exchange chromatography separation of U(VI) and U(IV) in the aqueous and the solid phases.

Incubations with U(V)-dpaea. Inactivated *S. oneidensis* MR-1 cells (not incubated with U(VI)-acetate) were also incubated in anoxic modified WLP medium in the presence of 50 μ M aqueous phase ‘synthetic’ U(V)-dpaea as described in the paragraph ‘Reduction of U(V)-dpaea’ in the Experimental methods section. Similarly, at specific times, entire cultures and associated cell-free controls were sacrificed, and separation of U(VI) and U(IV) was performed by ion exchange chromatography. Results are shown in Figures S14, S15, and S16, and described in the Results section of the article.

Text S5. Comparison of the inactivated cells versus active cells incubated with U(V)-dpaea reduction.

In order to confirm that the solid phase U(IV) observed in the incubations of *S. oneidensis* MR-1 with U(V)-dpaea was the product of an active reduction mechanism, we substituted active cells with cells lacking reducing power (inactivated cells), in an experiment similar to the one described above. The inactivated cells were first incubated in presence of 400 μ M U(VI)-acetate to ensure they lacked the ability to reduce (method in Text S4). We noticed a 25% decrease in the U concentration in the incubations compared to the no-cell controls (Figure S14.A.), which we could explain by sorption of U(VI) onto the biomass (Figure S14.B.). We concluded that the inactivated cells were impaired in their reducing activity. Identical inactivated cells were then incubated for 312 h (~ 2 weeks) in the presence of U(V)-dpaea as described in Text S4. Even though we detected a 5% decrease of U(V)-dpaea in the aqueous phase, the extent of that decrease is significantly lower than that observed in incubations with active cells (about 30-35%) (Figures S15 and S16). The presence of a very small amount of U(VI) and U(IV) in the solid phase (Figure S16.A.) is attributed to biomass-associated U(V)-dpaea, likely as an adsorbed species, which undergoes disproportionation upon acidification, prior to ion exchange chromatography. Therefore, we can exclude disproportionation as a significant contributor to U(V)-dpaea reduction. This is because spontaneous disproportionation of U(V)-dpaea does not occur in absence of active cells in either system ‘biological’ and ‘synthetic’. Additionally, the U(VI)/U(IV) ratio is close to

50:50 after separation of the aqueous phase in the no-cell controls for the 'biological' and 'synthetic' U(V)-dpaea experiments, suggesting stable aqueous U(V)-dpaea (Figure 2:5.B. and Figure S14.B.). Finally, we did not observe a significant accumulation of U(IV) when U(V)-dpaea was incubated with inactive cells (Figure S15 and Figure S16.A.). In contrast, we observed the substantial accumulation of U(IV) in the presence of active cells, providing evidence for microbial U(V)-dpaea reduction. Thus, we conclude that *S. oneidensis* MR-1 cells are able to reduce U(V)-dpaea to U(IV).

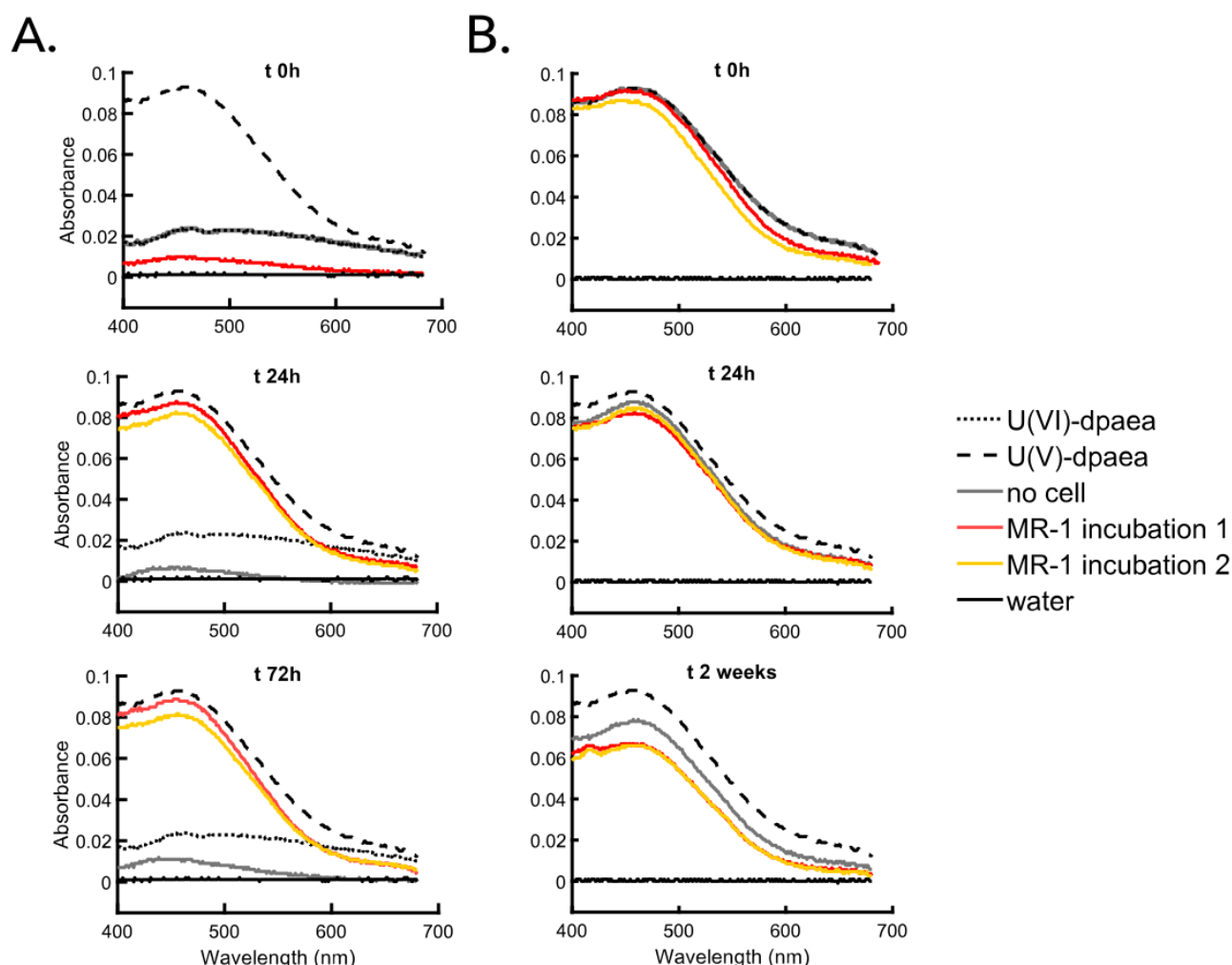


Figure S1. UV-vis spectra of duplicate incubations (1 and 2) of *S. oneidensis* MR-1 with either U(VI)-dpaea or synthetic U(V)-dpaea and associated no-cell controls as a function of time (incubation times indicated in graphic title). Column A: incubations with U(VI)-dpaea ([U(VI)-dpaea]=1mM); column B: incubations with U(V)-dpaea ([U(V)-dpaea]=0.8mM). U(VI)dpaea and U(V)-dpaea references are included in the relevant panels but are obscured by the no-cell controls in figures in column A and at t=0h for column B. For the incubations with U(VI)-dpaea (column A), no absorbance is detected at t=0h, but a spectrum with a maximum at about 460nm (corresponding to the maxima observed in the U(V)-dpaea reference) is observed at t=24h and t=72h. This confirms the formation of U(V)-dpaea in the incubation supernatants. In Column B, incubations with U(V)-dpaea, we observed a slight decrease of the absorbance at 460 nm in the incubations after two weeks, suggesting consumption of U(V)-dpaea during that time.

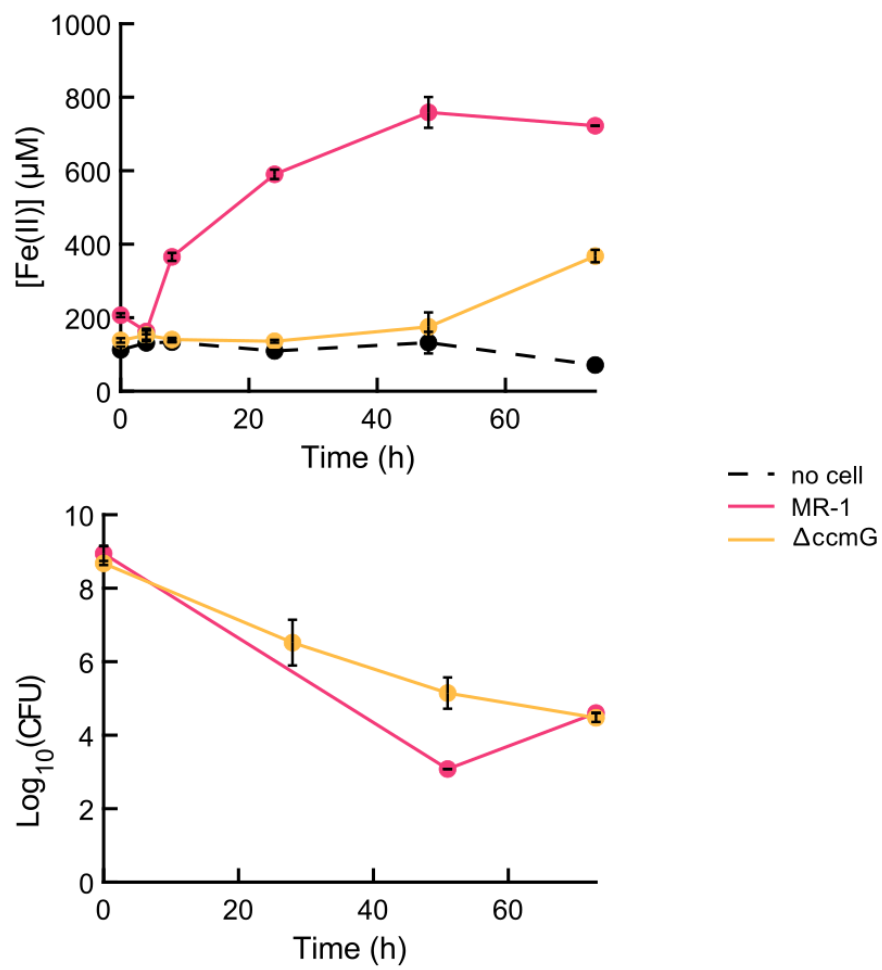


Figure S2. Aqueous Fe(II) concentration (A) and cell viability (B) through time in incubations with *S. oneidensis* MR-1, the deletion mutant $\Delta ccmG$ and a no-cell control with ferrihydrite. CFU stands for colony-forming units.

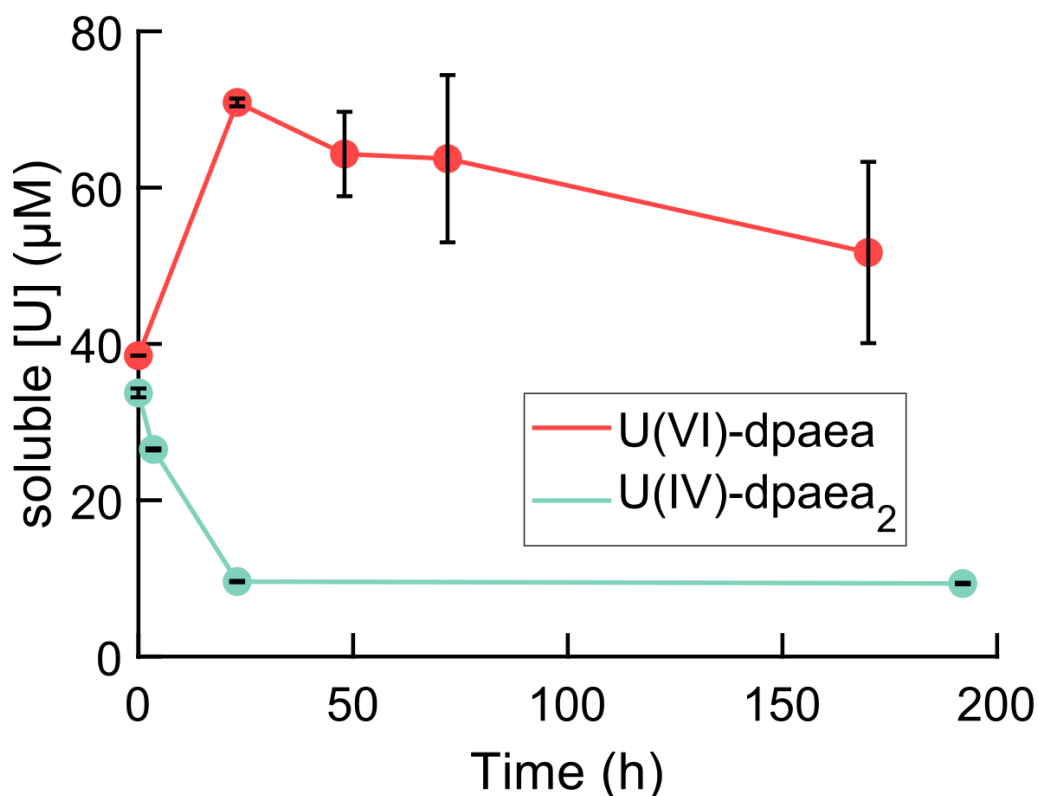


Figure S3. Solubility of solid phases U(VI)-dpaea (in red) and of U(IV)-dpaea₂ (in light blue) measured in WLP medium (used for the bacterial incubations) over 7 and 8 days, respectively. Solubility measurements were obtained by dissolving either U(VI)-dpaea or U(IV)-dpaea₂ powder in WLP medium and measuring the aqueous [U] over time by ICPMS. These measurements were initiated with [U(VI)-dpaea]=0.583 g.L⁻¹ (equivalent to 1 mM aqueous U if fully dissolved) and [U(IV)-dpaea₂]=0.432 g.L⁻¹ (equivalent to 0.5 mM aqueous U if fully dissolved).

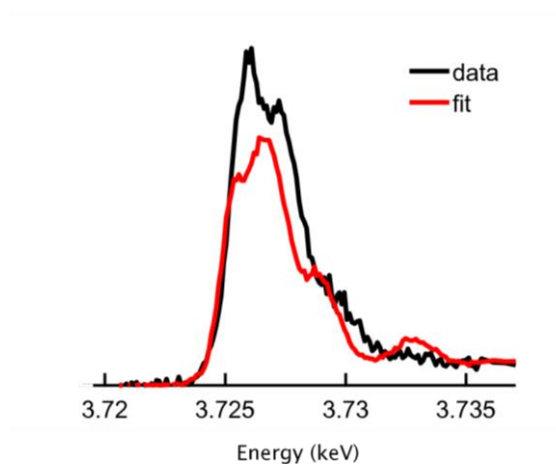


Figure S4. LCF fitting results (red) compared to the data (black) for the 96h supernatant using U(VI)-dpaea and U(IV)-dpaea₂ as fitting components. We provided this option of fitting to confirm that the spectra observed for the aqueous U intermediate do not result from a mixture of U(VI) and U(IV) valence states. The fit above describes poorly the data, with a R factor of 0.119638 and a Reduced χ^2 of 2.248364 compared to a R factor of 0.0061 and a Reduced χ^2 of 0.1196 for the fit using U(V)-dpaea as principal component (Figure 2:3.B.).

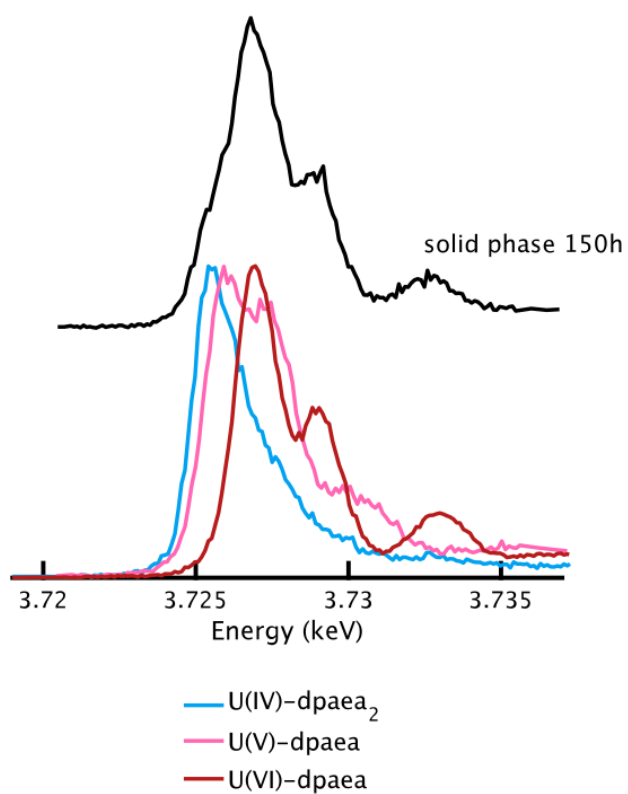


Figure S5. U M₄-edge HR-XANES spectra of the 150h solid phase shown in black during reduction U(VI)-dpaea. The references are U(VI)-dpaea (in red), U(V)-dpaea (in pink) and U(IV)-dpaea₂ (in blue). U(IV)-dpaea₂ was used as a reference and likely does not characterize fully the U(IV) phases produced.

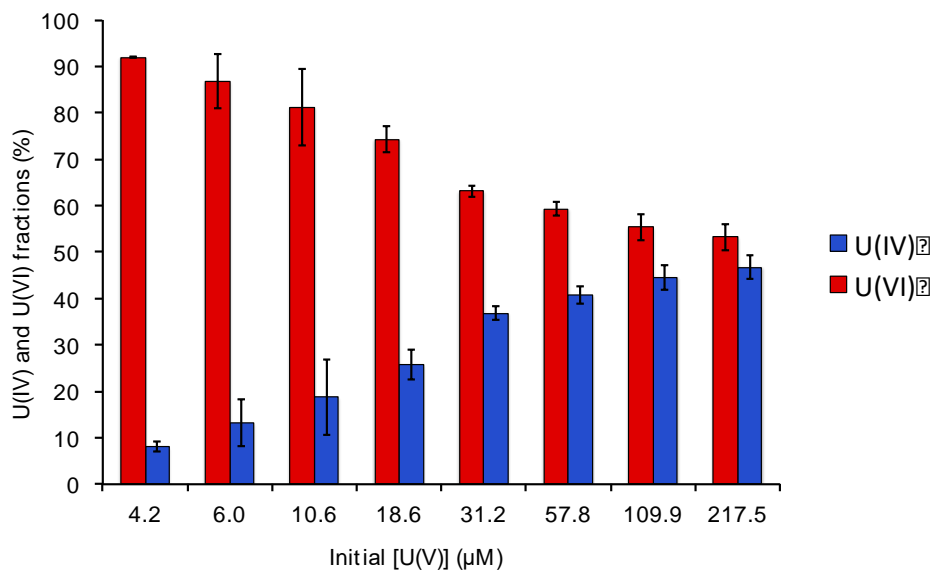


Figure S6. Ratio of U(VI) (red) and U(IV) (blue) recovered after ion-exchange chromatography elution of eight solutions with varying initial concentrations of U(V)-dpaea. As the concentration of U(V)-dpaea decreases, the amount of U eluted in the U(IV) fraction decreases.

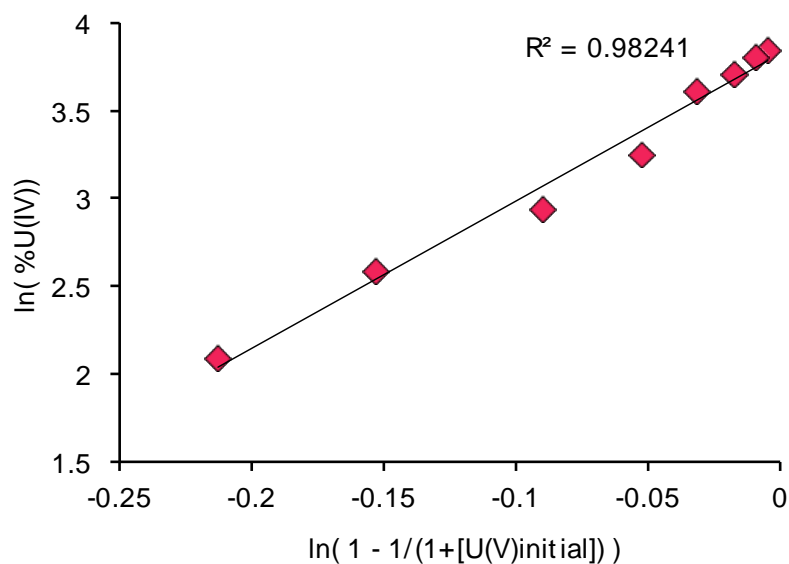


Figure S7. Linear regression showing the correlation between the amount of U eluted as U(IV) and the initial concentration of U(V)-dpaea prior to ion-exchange chromatography. The linear equation shown was used to correct the data obtained for the reduction experiments of 'biological U(V)' (Figure 4) and 'synthetic U(V)' (Figure S14), but also the incubation of inactivated cells with U(V)-dpaea (Figure S17).

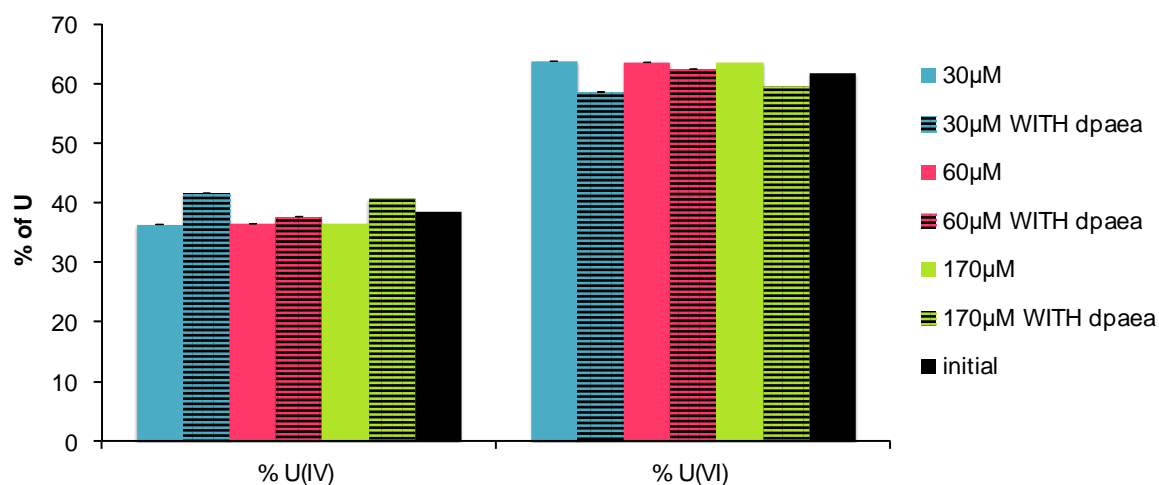


Figure S8. U speciation after ion exchange chromatography separation of a set of six solutions containing the same initial ratio of aqueous U(IV)-citrate and U(VI)-acetate (shown in black, labeled 'initial'). Three concentrations of U were investigated (30 μM in blue, 60 μM in red and 170 μM in green) and for each concentration selected, two solutions were tested, one amended with dpaea ligand and the other one without amendment. We observed that the dpaea ligand did not have an effect on the U(IV) and U(VI) fractions collected after resin elution.

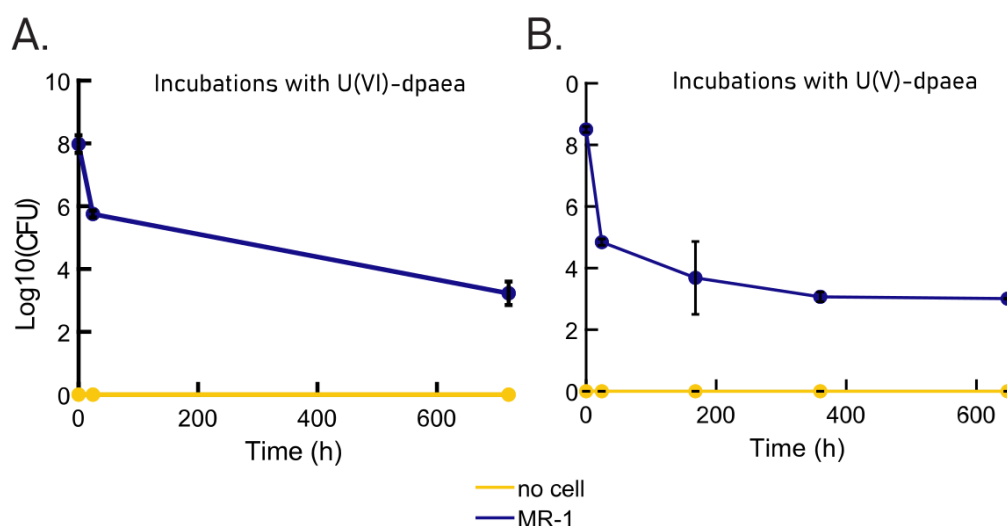


Figure S9. Cell viability in incubations of *S. oneidensis* MR-1 with A. U(VI)-dpaea over 720h (30 days) and U(V)-dpaea over 648h (27 days). The experimental conditions are described in Text S1.

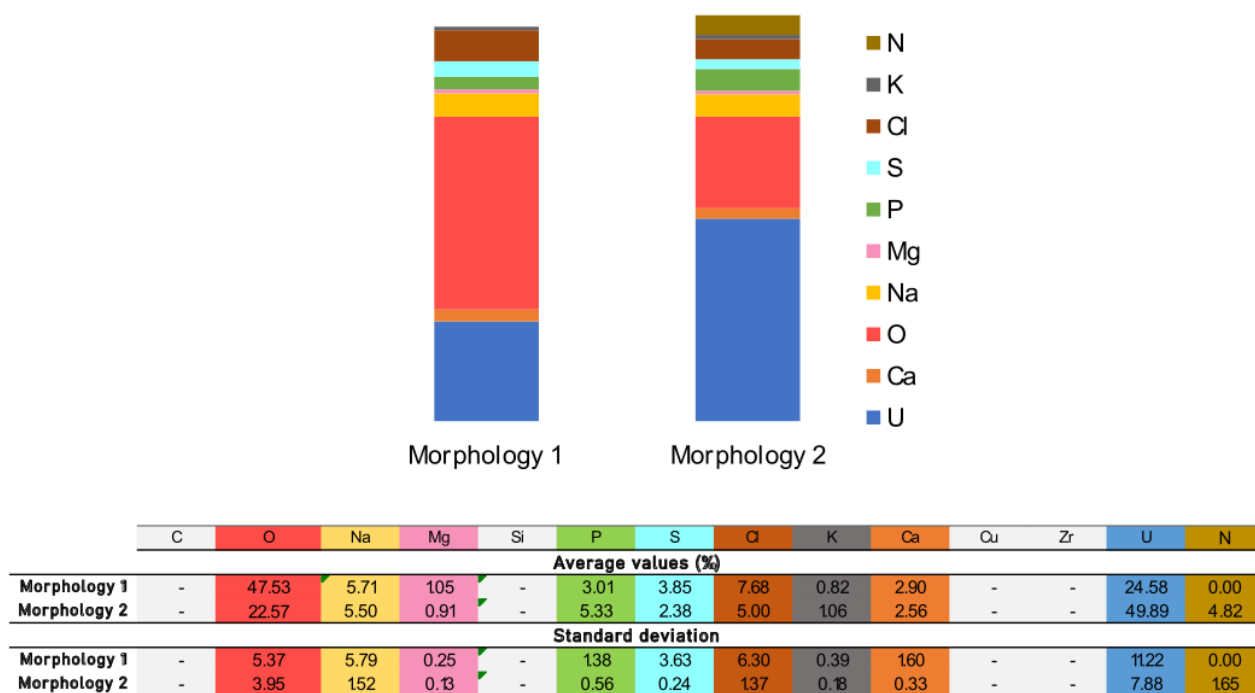


Figure S10. Energy dispersive spectroscopy (EDS) performed by scanning transmission electron microscopy (STEM) on the two types of morphologies described for the U(IV) product obtained upon U(V)-dpaea reduction. The values of elemental composition are displayed in the table below the histograms. The average values were obtained by averaging the measurements of the two morphology types for two samples incubated for 2 months and 3 months. The standard deviations for these average values are also displayed in the latter table. The color code matches columns to their corresponding element in the histogram.

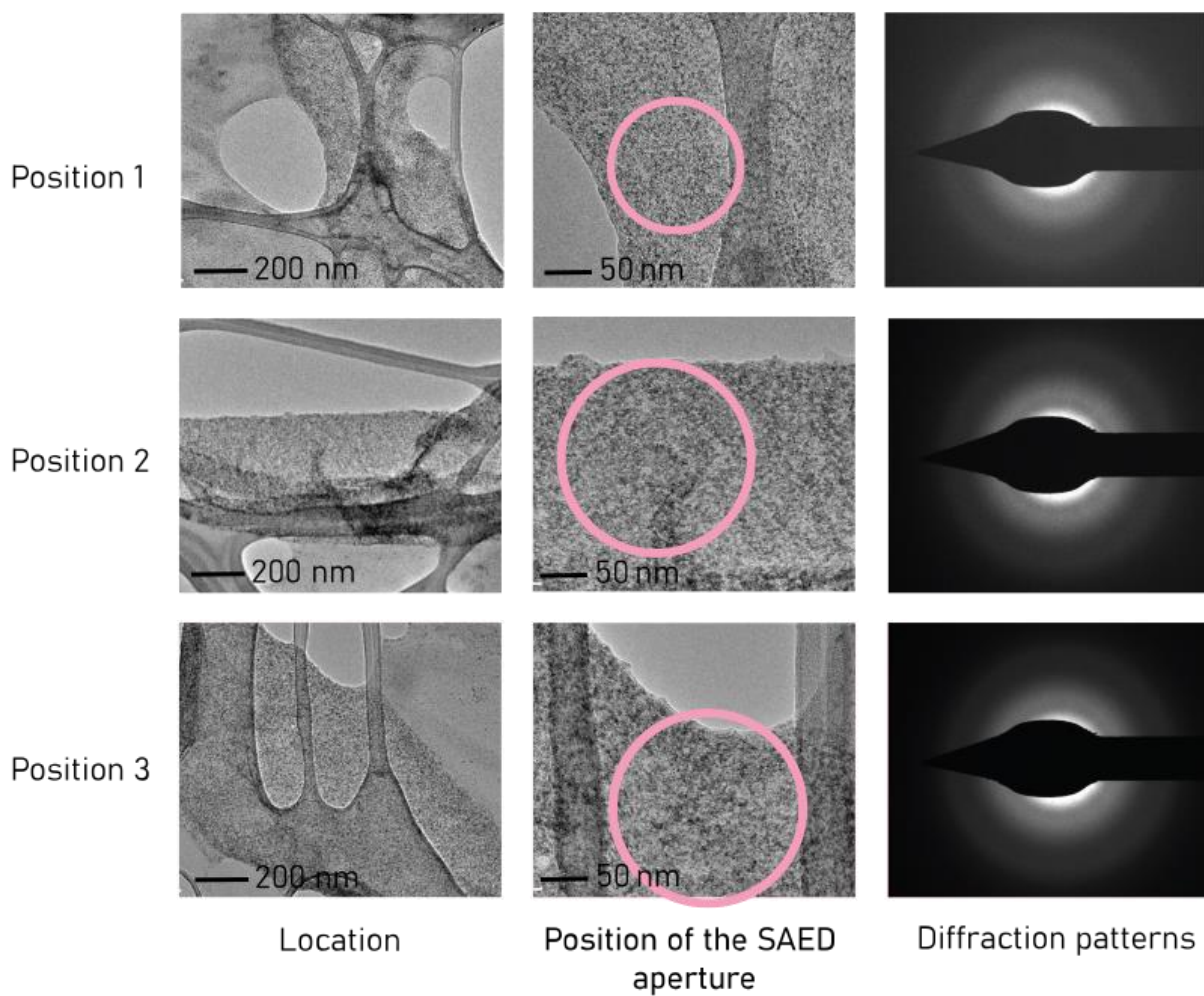


Figure S11. Selected area electron diffraction (SAED) collected for morphology type 1 of the U(IV) product, which corresponds to dispersed small U clusters, <200nm, at the surface of the bacteria. Three positions were selected to perform diffraction analysis and are represented by pink circles. The diffraction patterns display diffuse rings suggesting that morphology type 1 of the U(IV) product is not crystalline.

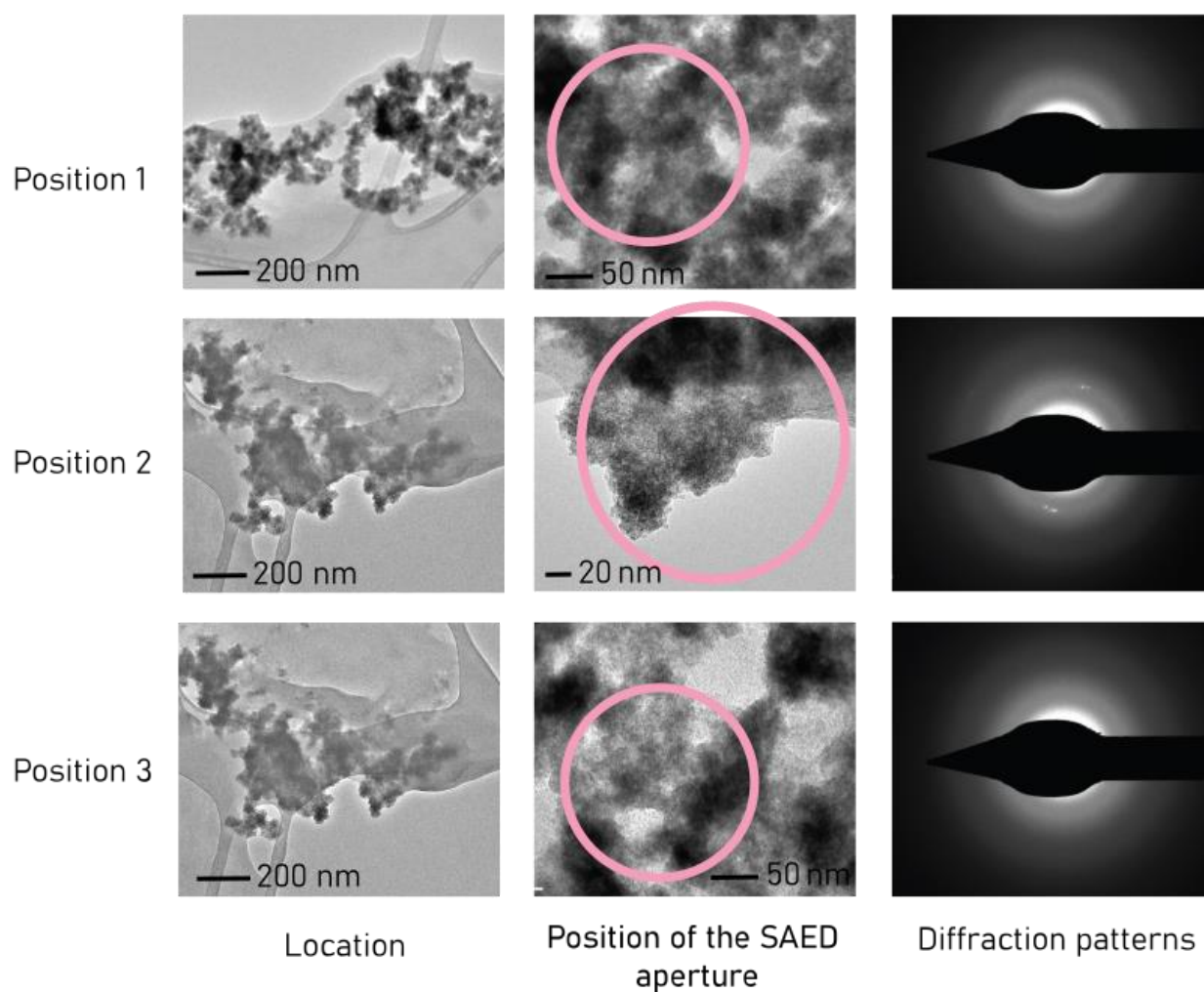


Figure S12. Selected area electron diffraction (SAED) collected for morphology type 2 of the U(VI) product, which describes U clusters of $> 1 \mu\text{m}$ associated with cells. Three positions were selected to perform diffraction and are represented by pink circles. The diffraction patterns display diffuse rings suggesting that morphology 2 of the U(IV) product is not crystalline.

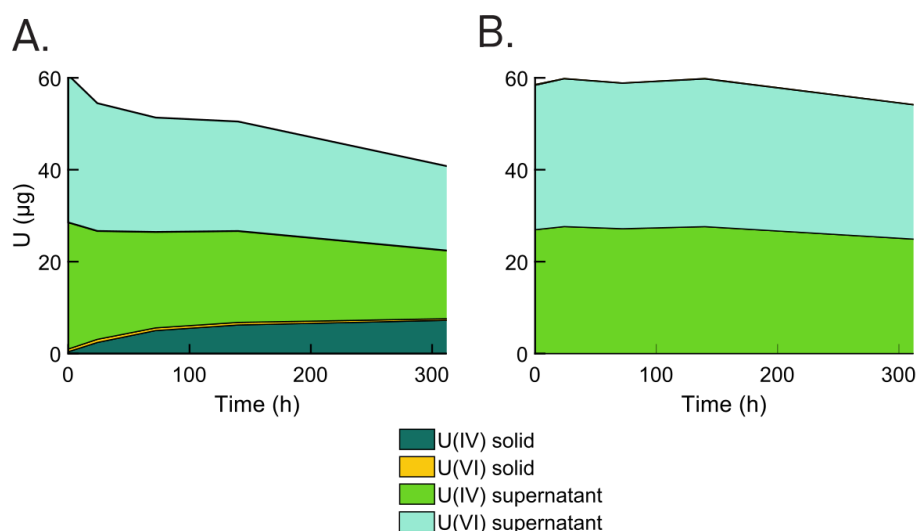


Figure S12. U speciation in the solid phase (cell pellet) and in the aqueous phase (supernatant) of (A) incubations with *S. oneidensis* MR-1 and (B) no-cell controls, in presence of 'synthetic' U(V)-dpaea. The U(VI) and U(IV) fractions were obtained by ion exchange chromatography separation.

The ion exchange chromatography separation cannot directly identify U(V), because the samples are acidified prior to loading onto the column. Acid treatment is known to disproportionate uranyl(V) to produce equal proportions of U(VI) and U(IV). Therefore, here, the equal proportions observed for U(VI) and U(IV) in the supernatant are a proxy for U(V) (result demonstrated by U $M_{4\text{-edge}}$ HR-XANES).

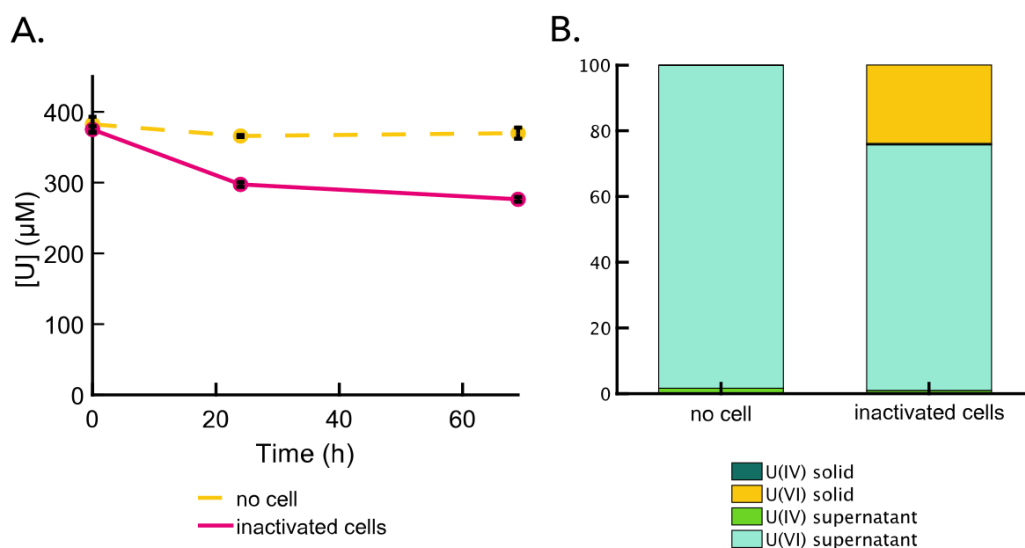


Figure S14. Incubations of lysed and autoclaved cells with U(VI)-acetate (in duplicate) to confirm their inactivation. A. Aqueous U concentration in the inactivated-cells incubations (pink dots) and in the no-cell controls (yellow dots), measured by ICP-MS from 0 to 69h. B. U speciation in the solid phase and in the aqueous phase for both the inactivated-cells incubations and the no-cell controls after 69h. The U(VI) and U(IV) fractions were obtained by ion exchange chromatography.

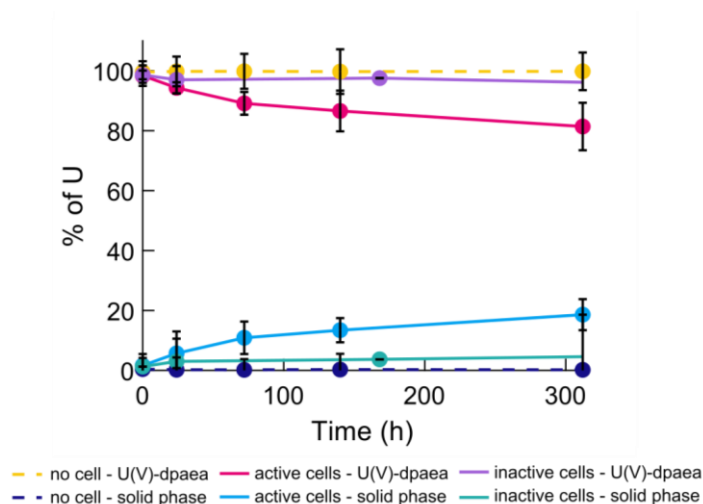


Figure S15. Distribution of aqueous U(V)-dpaea and solid phase U through time in incubations with *S. oneidensis* MR-1 (in pink and blue), incubations with inactivated cells of *S. oneidensis* MR-1 (in purple and blue green), and no-cell controls (in yellow and dark blue) with 'synthetic' U(V)-dpaea.

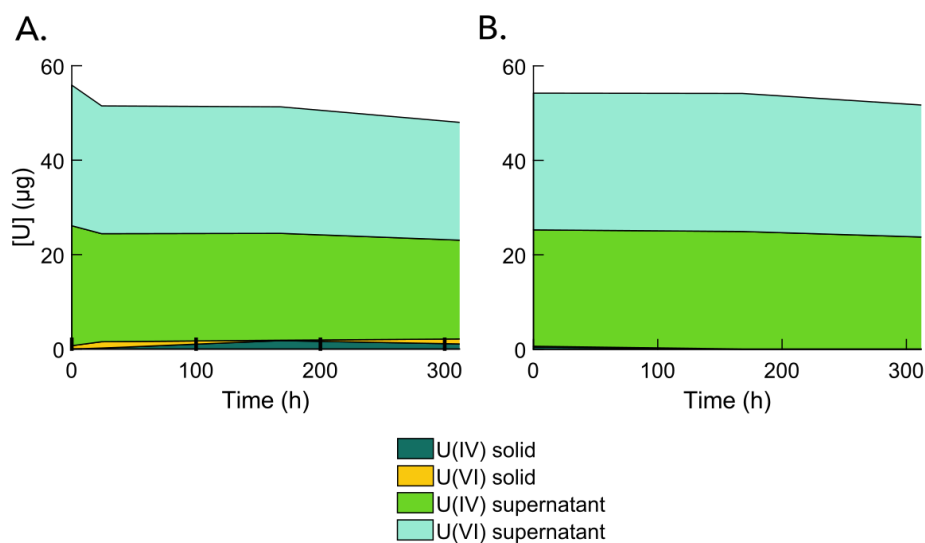


Figure S16. U speciation in the solid phase (cell pellet) and in the aqueous phase (supernatant) of (A) incubations with inactivated cells of *S. oneidensis* MR-1 and (B) no-cell controls, in presence of 'synthetic' U(V)-dpaea. The U(VI) and U(IV) fractions were obtained by ion exchange chromatography separation. The ion exchange chromatography separation cannot directly identify U(V), because the samples are acidified prior to loading onto the column. Acid treatment is known to disproportionate uranyl(V) to produce equal proportions of U(V) and U(IV). Therefore, here the equal proportions observed for U(VI) and U(IV) in the supernatant are a proxy for U(V) (result demonstrated by U $M_{4\text{-edge}}$ HR-XANES).

Primer name	Nucleotide sequence (5'-3') ^a
ccmG_FO	GCCGTTTATCGTCGATGGG
ccmG_RO	AGTCGATAGGCTTGCCATTG
ccmG_5'O	CGGGGT <u>ACCG</u> CCAACTCGGTATGATCATC
ccmG_5'I	CTTCTTCATACATTCCCCAATT
ccmG_3'I	AATTGGGGAATGTATGAAGAAGGCAGCATGAGAACACTGACA
ccmG_3'O	CGC <u>GGATCC</u> AACTTGCGAGAATTACAGCC

^a restriction sites used for cloning are underlined.

Table S1. Primers used for PCR and sequencing.

Strains and plasmids	Description	Reference
<i>Shewanella oneidensis</i>		
MR-1	Manganese-reducing strain (Lake Oneida, NY)	[1]
ΔccmG	MR-1 with deletion of <i>ccmG</i>	This study
<i>Escherichia coli</i>		
WM3064	Host strain for conjugation (<i>thrB1004 pro thi rpsL hsdS lacZΔM15</i> RP-4-1360 Δ(<i>araBAD</i>)567 Δ <i>dapA</i> 1341:[<i>erm pir</i> (wt)])	Lab collection
Plasmids		
pMQS	Mobilizable suicide vector, Kan ^R (<i>sacB oriT R6K nptII cen6</i>)	[2]
pMQS-ccmG	pMQS with <i>ccmG</i> deletion construct	This study

[1] Myers CR, Nealson KH (1988) Bacterial manganese reduction and growth with manganese oxide as the sole electron acceptor. *Science* 240: 1319–1321.

[2] Meibom KL, Cabello EM, Bernier-Latmani R (2018) The small RNA RyhB Is a regulator of cytochrome expression in *Shewanella oneidensis*. *Front Microbiol* 9:268.

Table S2. Bacterial strains and plasmids used for this study.

Compounds	Molar mass (g.mol ⁻¹)	WLP (mM)
CaCl ₂ .2H ₂ O	147.01	0.68
KCl	74.55	6.71
MgCl ₂ .6H ₂ O	203.3	2.46
NaCl	58.44	85.56
NH ₄ Cl	53.49	4.67
PIPES buffer (6.1-7.5)	302.37	20
pH		7.3

Table S3. Composition of modified Widdel low phosphate (WLP) medium.

	Time (h)	% U(IV) aqueous	% U(VI) aqueous	% U(IV) solid	% U(VI) solid
Reduction of U(VI)-dpaea - Figure 2:1.B.					
Measurements (%)	0	0.09	0.69	0.83	98.39
	14	18.70	19.85	2.81	58.63
	24	24.06	25.95	3.01	46.99
	48	33.12	34.05	4.02	28.81
	72	31.43	35.54	4.48	28.55
	96	37.70	40.53	6.31	15.47
Standard deviation (%)	0	5.46	1.98	2.08	2.00
	14	1.44	2.09	3.23	1.70
	24	5.92	5.84	4.99	3.76
	48	2.13	5.53	2.46	1.92
	72	6.12	17.74	6.83	8.12
	96	2.51	6.32	2.99	6.14
Reduction of 'biological' U(V)-dpaea - Figure 2:5.A. and 2:5.B.					
No-cell samples – 2:5.B.					
Measurements (%)	0	47.01	52.90	0.03	0.06
	24	47.01	52.90	0.05	0.04
	72	47.06	52.85	0.03	0.06
	144	47.04	52.90	0.03	0.04
	312	47.01	52.93	0.03	0.04
	600	46.95	53.01	0.01	0.03

	984	46.51	52.55	0.40	0.56
Standard de- viations (%)	0	0.99	1.97	4.76	0.94
	24	0.22	0.34	1.30	3.15
	72	0.75	1.47	1.45	1.48
	144	0.3 1	0.52	0.69	1.92
	312	1.23	2.46	2.17	1.38
	600	0.62	1.16	0.65	1.02
	984	1.13	2.21	2.67	2.05
Incubations with <i>S. oneidensis</i> MR-1- 2:5.A.					
Measure- ments (%)	0	46.67	52.51	0.39	0.43
	24	44.90	50.80	3.33	0.97
	72	43.25	49.13	6.74	0.89
	144	41.50	47.19	10.35	0.95
	312	38.41	44.30	15.75	1.85
	600	34.91	40.60	23.40	1.09
	984	33.54	39.16	25.12	2.18
Standard de- viations (%)	0	0.84	1.65	1.75	0.97
	24	1.10	2.23	1.95	4.75
	72	0.49	0.84	1.99	3.91
	144	1.56	1.94	13.62	2.21
	312	0.84	1.5	2.36	1.63
	600	0.15	0.15	0.12	4.17
	984	1.87	2.97	5.87	2.68
Reduction of 'synthetic' U(V)-dpaea - Figure S12.A. et S12.B.					
No-cell samples – S12.B.					
Measure- ments (%)	0	45.96	53.61	0.23	0.20
	24	46.11	53.69	0.10	0.11
	72	46.09	53.73	0.09	0.1
	144	46.07	53.65	0.12	0.15
	312	45.91	53.90	0.08	0.10
	600	46.05	53.82	0.06	0.07
	984	45.43	53.83	0.30	0.44
Standard de- viations (%)	0	1.63	3.23	2.05	3.11
	24	2.24	4.42	3.37	2.34
	72	2.63	5.20	2.58	2.49
	144	3.36	6.65	3.22	4.15
	312	2.85	5.59	17.01	7.03
	600	3.51	6.92	4.07	4.11
	984	0.50	0.98	8.16	4.11
Incubations with <i>S. oneidensis</i> MR-1 – S12.A.					
	0	45.44	52.93	0.66	0.98

	24	43.28	51.04	4.43	1.25
Measurements (%)	72	40.65	48.48	9.75	1.13
	144	39.38	47.20	12.32	1.10
	312	36.36	45.04	17.73	0.87
	600	31.09	38.91	29.26	0.74
	984	27.68	35.67	34.72	1.93
Standard deviations (%)	0	1.53	3.05	2.18	3.14
	24	0.82	1.65	2.36	4.30
	72	1.66	3.41	2.89	4.58
	144	2.93	6.13	2.65	3.05
	312	3.45	7.13	2.96	4.23
	600	0.50	0.98	1.00	1.82
	984	3.90	8.56	3.11	3.92
Inactivated cells and U(V)-dpaea - Figure S16.A. and S16.B.					
No-cell samples – S16.B.					
Measurements (%)	0	45.44	53.40	0.84	0.32
	168	45.97	53.97	0.03	0.03
	528	45.66	54.21	0.05	0.08
Standards deviations (%)	0	0.00	2.12	0.00	0.00
	168	0.00	1.83	0.00	0.00
	528	1.00	1.43	0.00	0.00
Incubations with inactivated <i>S. oneidensis</i> MR-1 – S16.A.					
Measurements (%)	0	45.40	53.21	0.00	1.26
	24	44.44	52.55	0.41	2.60
	168	44.67	52.88	3.51	0.17
	528	42.61	51.49	0.08	5.82
Standards deviations (%)	0	0.00	1.45	0.00	0.00
	24	2.18	4.02	6.77	7.34
	168	0.01	0.00	0.00	0.00
	528	1.43	0.88	3.24	1.98

Table S4. Measurements (entries in blue) and associated standard deviations (entries in black) for the ion-exchange chromatography separations of U from aqueous and solid phase samples. The corresponding experiment is indicated in the red box along with the figure number.

Annex 2 – Supplementary information for chapter 3

This supporting information contains:

Table S1. Primers used for PCR and sequencing for the $\Delta ccmG$ construct

Table S2. Primers used for PCR and sequencing for the $\Delta mtrC/omcA/mtrF$ construct.

Primer name	Nucleotide sequence (5'-3') ^a
ccmG_FO	GCCGTTTATCGTCGATGGG
ccmG_RO	AGTCGATAGGCTTGCCATTG
ccmG_5'O	CGGGGT <u>ACCG</u> CCAACTCGGTATGATCATC
ccmG_5'I	CTTCTTCATACATTCCCCAATT
ccmG_3'I	AATTGGGGAATGTATGAAGAAGGCAGCATGAGAACACTGACA
ccmG_3'O	CGC <u>GGATCC</u> AACTTGCGAGAATTACAGCC

^a restriction sites used for cloning are underlined.

Table S1. Primers used for PCR and sequencing for the Δ ccmG construct

Primer name	Nucleotide sequence (5'-3') ^a	Use
mtrF_5'I	CGAGTTAGTTTATTGGATGGACTGCAAACCTT ATTCATAATTCTATCC	Deletion construct
mtrF_5'O	CCGGAATTCTCAACGCCTGATTGGTATAGTAC	Deletion construct
mtrF_3'O(DD) ^b	GGAAATAGAATTCCCCAAGG	Deletion construct
mtrF_3'I	CTTCTTCATACATTCCCCAATT	Deletion construct
mtrF_FO	TAACCATACATCTGTCGGAC	Verification construct
mtrF_RO(DD)	GGCTTCCCAATTTGTCCCAA	Verification construct

^a *Eco*RI sites used for cloning are underlined.

^b *Eco*RI site in primer mtrF_3'O(DD) and used for cloning is naturally occurring in the genomic sequence amplified

Table S2. Primers used for PCR and sequencing for the Δ mtrC/omcA/mtrF construct.

Annex 3 – Supplementary information for chapter 4

This supporting information contains:

Table S1. Percentages of U eluted in the different fractions from 40kDa size-exclusion desalting in oxic conditions.

Table S2. Percentages of U eluted from 40kDa size-exclusion desalting columns in the different fractions in reduced conditions.

No protein control		
Ligand	F1	F2 to F7
NTA	0.114	99.886
EDTA	0.325	99.675
DTPA	0.691	99.309
carbonate	0.693	99.307

oxidized MtrC		
Ligand	F1	F2 to F7
NTA	10.663	89.337
EDTA	10.989	89.011
DTPA	10.814	89.186
carbonate	13.552	86.448

Table S1. Percentages of U eluted in the different fractions from 40kDa size-exclusion desalting **in oxix conditions**, in no protein control (above part of the table) and in reaction between MtrC and the different U-ligand complexes studied. The last column sums the U in the fractions F2 to F7.

no protein control								
Ligand	F1	F2	F3	F4	F5	F6	F7	F2 to F7
NTA	0.44	24.93	47.14	20.31	5.33	1.53	0.31	99.56
EDTA	0.75	24.56	40.57	26.26	6.54	1.09	0.23	99.25
DTPA	5.73	65.67	23.15	4.46	0.87	0.10	0.02	94.27
carbonate	4.80	57.32	26.49	9.18	1.87	0.34	0.02	95.20

MtrC								
Ligand	F1	F2	F3	F4	F5	F6	F7	F2 to F7
NTA	3.52	60.25	21.99	10.54	2.67	0.76	0.26	96.48
EDTA	1.39	33.25	26.06	23.42	12.18	3.08	0.63	98.61
DTPA	2.73	54.65	19.62	15.65	4.90	1.85	0.60	97.27
carbonate	71.97	11.35	10.08	4.88	1.29	0.31	0.11	28.03

Table S2. Percentages of U eluted from 40kDa size-exclusion desalting columns in the different fractions **in reduced conditions**, in no protein control (above part of the table) and in reaction between MtrC and the different U-ligand complexes studied. The last column sums the U in the fractions F2 to F7.

Curriculum Vitae



Margaux MOLINAS

margaux.molinas@epfl.ch

+33 6 87 44 05 25

Allée du Tilleul 4, 1022, Suisse

Nationality: French

Birth date: 02/09/1993

Status: single

Permis de résidence B

Permis de conduire B

LANGUAGES

French: native

English: current

Italian: B1

Spanish: working proficiency

EDUCATION

- 2016-2021 **PhD in Environmental Science – EPFL, Switzerland**
 Prof. Rizlan Bernier-Latmani
 Fields of research: environmental microbiology, protein-metal interaction, actinide chemistry, biochemistry
- 2013-2016 **Master of Science in Chemical Science and Chemical Engineering**
 Chimie ParisTech – www.chimie-paristech.fr
 Coursework: Microbiology, Biochemistry, Polymer chemistry, Organic and Inorganic chemistry, Spectroscopy, Analytical and Physics Chemistry, Entrepreneurship
- 2011-2013 **Physics, Chemistry, Mathematics Classes Préparatoires – College Stanislas, Paris**
 GPA: 3,95, intensive and advanced preparation for nationwide selective entrance to French engineering schools.

EXPERIENCE

- 2016-2021 **PhD thesis – EPFL, Lausanne, Switzerland**
 Environmental Microbiology Laboratory (EML)
Thesis: Insights into the microbial reduction of pentavalent and hexavalent uranium species by *Shewanella Oneidensis* MR-1
- March-Sept. 2016 **Master thesis – LBNL, Berkeley, California USA**
 Joint BioEnergy Institute, Jay Keasling laboratory, Microbial communities Group
Project: Proposed solutions to overcome bottlenecks met toward lignin bio-depolymerization and valorization using *Acinetobacter baylyi* ADP1
- 2015-2016 **Entrepreneurship project manager – Chimie ParisTech, Paris, France**
Project: Developed an eco-friendly innovation for bathroom furniture and cosmetics
- March-Aug. 2015 **Research Assistant – LBNL, Berkeley, California USA**
 Joint BioEnergy Institute, Fuel synthesis division, supervisor Dr. Taek Lee Soon
Project: Engineering and optimizing of the 1,8-cineole pathway in *Escherichia coli* for biofuel additives production
- July 2014 **Laboratory Technician – ARKEMA, Verneuil-en-Halatte, France**
Project: Development of a novel thickener for textile coating, formulation and physicochemical tests
- 2013-2014 **Consultant – Altran Research Company, Paris, France**

Co-Author of the report: "What is the economic strategy which could be implemented on the market of recycling of organic composite materials?"

PUBLICATIONS

- 2021 Molinas, M.; Faizova, R.; Brown, A.; Galanzew, J.; Schacherl, B.; Bartova, B.; Meibom, K. L.; Vitova, T.; Mazzanti, M.; Bernier-Latmani, R. Biological Reduction of a U(V)–Organic Ligand Complex. *Environ. Sci. Technol.* **2021**, *55* (8), 4753–4761. <https://doi.org/10.1021/acs.est.0c06633>.
- 2017 Mendez-Perez, D.; Alonso-Gutierrez, J.; Hu, Q.; Molinas, M.; Baidoo, E. E. K.; Wang, G.; Chan, L. J. G.; Adams, P. D.; Petzold, C. J.; Keasling, J. D.; Lee, T. S. Production of Jet Fuel Precursor Monoterpenoids from Engineered Escherichia Coli. *Biotechnol. Bioeng.* **2017**, *114* (8), 1703–1712. <https://doi.org/10.1002/bit.26296>.

ORAL PRESENTATIONS

- 2021 Molinas M., Faizova R., Brown A., Meibom K., Prüßmann T., Vitova T., Mazzanti M., Bernier-Latmani R., Microbial reduction of a U(V) complex with an organic ligand, August 2021, Goldschmidt, Lyon, France
- 2019 Molinas M.; Faizova R., Mazzanti M., Schacherl B., Galanzew J., Vitova T., Bernier-Latmani R., U(V) is an intermediate in the reduction of U(VI) by *Shewanella oneidensis* MR-1, Goldschmidt, August 2019, Barcelona, Spain
- 2018 Molinas M., Faizova R., Mazzanti M., Bernier-Latmani R., Mechanism of biotic reduction of U(VI)-DPAEA by *Shewanella oneidensis* MR-1 and the c-type cytochrome MtrC, Uranium Biogeochemistry meeting, August 2018, Ascona, Switzerland
- 2017 Molinas M.; Bacteria have a crush for Uranium, Pitch your impact contest, 2017, EPFL, Lausanne, Switzerland
Jury prize winner.

SKILLS

- Expertise Biochemistry, Environmental microbiology, Actinide chemistry, X-ray synchrotron-based spectroscopy (XANES, EXAFS), Analytical chemistry (HPLC, ICP-MS), Molecular biology (protein expression and purification), C-lab management.
- Soft skills Creativity, Enthusiasm, Attentiveness, Flexibility, Communication, Teamwork.

PERSONAL INTERESTS

- Sports Dancing, Cycling, Swimming, Yoga
- Mountain Ski touring, Alpinism, Climbing
- Music Guitar, Piano, and singing =-
- Gastronomy Cooking and Baking
- Interests Geology, Neurobiology of behavior